



HAL
open science

Photodegradation of contaminants of emerging concern in environmental matrices : a new holistic perspective to complete the laboratory modeling approach

Zsuzsanna Varga

► To cite this version:

Zsuzsanna Varga. Photodegradation of contaminants of emerging concern in environmental matrices : a new holistic perspective to complete the laboratory modeling approach. Analytical chemistry. Institut Polytechnique de Paris, 2021. English. NNT : 2021IPPAX036 . tel-03450185

HAL Id: tel-03450185

<https://theses.hal.science/tel-03450185>

Submitted on 25 Nov 2021

HAL is a multi-disciplinary open access archive for the deposit and dissemination of scientific research documents, whether they are published or not. The documents may come from teaching and research institutions in France or abroad, or from public or private research centers.

L'archive ouverte pluridisciplinaire **HAL**, est destinée au dépôt et à la diffusion de documents scientifiques de niveau recherche, publiés ou non, émanant des établissements d'enseignement et de recherche français ou étrangers, des laboratoires publics ou privés.

Photodegradation of contaminants of emerging concern in environmental matrices: a new holistic perspective to complete the laboratory modeling approach

Thèse de doctorat de l'Institut Polytechnique de Paris
préparée à l'École Polytechnique

École doctorale n°626 École Doctorale de l'Institut Polytechnique de Paris
(ED IP Paris)
Spécialité de doctorat: Chimie

Thèse présentée et soutenue à Palaiseau, le 10/06/2021, par

Zsuzsanna Varga

Composition du Jury :

Corinne Gosmini Research director, École Polytechnique, Laboratoire de Chimie Moléculaire, France	Présidente
Vasilios A. Sakkas Professor, University of Ioannina, Department of Chemistry, Greece	Rapporteur
Olivier Chapleur Researcher, INRAE, Procédés biotechnologiques au Service de l'Environnement, France	Rapporteur
Claire Richard Research director, Université Clermont Auvergne, ICCF - Photochimie, France	Examineur
Antonio Arques Research director, Universitat Politècnica de València, Dpto. de Ingeniería Textil y Papelera, Spain	Examineur
Stéphane Bouchonnet Research engineer, École Polytechnique, Laboratoire de Chimie Moléculaire, France	Directeur de thèse

Acknowledgement

Firstly, I would like to express my eternal gratitude to my supervisor Stéphane, who always supported me tremendously and brought many insightful viewpoints into the project. From him, I have learned what it means to lead with empathy, trust your co-workers, and never be afraid to ask questions. I would like to offer Anne-Flo my heartfelt thanks for her kindness and for helping me navigate this demanding project's administrations at the highest level. I would like to thank Edith for being a generous co-worker (and a great baker) and for her mentorship on the FT-ICR instrument. I am very grateful for Adrien and Christophe, as they were always eager to help me around the lab. I would like to thank the other members of LCM, especially Louis, Céline, Ding, Thibault, Valeriu, and Pauline, as they were always great companions and made working at LCM really easy and enjoyable.

I would like to thank all the members of AQUALity for the fruitful collaborations and the scientific exchange that we did in these 3 years. I would like to thank my secondment supervisors, Claire, Fran, Elisa, and Rita, for accommodating me at their institutes. The highlight of this project was working together with the other ESRs and getting to know them, especially Dimitra, Iván, Masho, and Nuno, with whom we shared great travels and fantastic experiences.

I would like to express my sincere gratitude to my father, who has always been my role model and my moral compass, my mother, who always does everything for us and for her unconditional love; and my sister, who is the coolest sister ever and I admire her intelligence, compassion, and resilience deeply. I would like to thank all my friends who were there for me in this journey and offered me their encouragements, especially Mateusz, Zsolt, Edina, Dóri, Benedek, and Zouhair, who helped me become a better person. Last but not least, I am grateful for having Max in my life and for all the love and support he gives me every day.

Besides scientific achievements, I have learned so much in these three years, on a personal level. I have embarked on a journey of self-knowledge and self-improvement, thanks to all the wonderful people around me. I am fortunate to have such circles of friends, co-workers, and family, who made these three years a great adventure and with whom we have created beautiful and deep connections.

Abstract

Contaminants of emerging concern (CECs) show great environmental concern due to their potential toxicity and persistence. More and more are detected every year; they became ubiquitous as anthropogenic activities increase. Their harmful effects were shown on aquatic organisms and human health. Conventional wastewater treatment plants do not fully remove CECs, as they were not designed to eliminate these pollutants. Developing and understanding novel water treatment approaches is essential to improve water quality and protect the environment. Processes based on irradiation with light are very promising in this way. It is of high interest to evaluate the formation of potential photoproducts and their related toxicity; this also helps understanding sunlight-induced transformation mechanisms of contaminants in the environment.

The aim of this project was to apply different approaches to study the photodegradation of contaminants. Firstly, a laboratory modeling approach was employed to five contaminants: benzisothiazolinone, naproxen, perfluorooctanoic acid, maprotiline, and enrofloxacin. Direct photolysis and advanced oxidation processes, such as peroxide/UV, photocatalysis, photosensitizers, and Fenton reactions were employed. They were either carried out under laboratory conditions in ultrapure water or on a pilot plant scale in secondary treated wastewater to model realistic conditions and study the matrix effect. The photodegradation efficiencies were studied using LC-MS analysis and UV-Vis spectroscopy. As mineralization is rarely achieved, LC-MS measurements were performed for the untargeted detection of photoproducts on an ultrahigh-resolution FT-ICR mass spectrometer. This made the accurate identification of molecular formulae possible; structural elucidation of numerous photoproducts was achieved owing to MS² experiments. Based on these structures, *in silico* toxicity calculations were performed to obtain information on their potential toxic effects. In parallel, *in vitro* bioassays were used to study the mixture's toxicity at each step of the photodegradation reaction. Through this approach, the scientific achievements include assessing the fate of contaminants, proposing and optimizing viable photodegradation processes, and elucidating photochemical reaction pathways.

In parallel with the modeling approach, a non-targeted analytical approach was used to study complex mixtures. Direct infusion mass spectrometry was employed to detect thousands of molecular ions and assess their formulae accurately. To better process these datafiles, SPIX software was developed. One of its features is to find all the ions that undergo changes between two conditions. The other feature includes comparing a series of conditions, proposing kinetic models for each of them individually. The exportation of statistically relevant changes and further data processing was carried out. The software's application and mathematical background are presented through the analysis of contaminants in complex matrices, such as secondary treated wastewater and natural organic matter. The extension of the software to process 3D LC-MS datasets represents the latest developments. This software helped with rapid data processing; it is innovative and unique in studying molecules' kinetics in complex samples. The holistic approach provided by SPIX constitutes a complementary tool to modeling approaches; it allows to detect and monitor relevant reactions in very complex media and contributes to reducing operator-related subjectivity during results interpretation.

Résumé

Les activités humaines entraînent la contamination des ressources en eau et les usines conventionnelles de traitement des eaux usées n'éliminent malheureusement pas complètement les contaminants d'intérêt émergent. Nous avons étudié les effets de procédés d'oxydation avancés, en particulier induits par la lumière, sur la dégradation de ces polluants en matrices aqueuses. Ces procédés dégradent efficacement les contaminants d'intérêt mais engendrent des sous-produits potentiellement toxiques. Les structures des produits de dégradation ont été élucidées et des tests de toxicité ont été menés, dans le but d'évaluer l'intérêt d'approches photochimiques pour éliminer certains contaminants. La deuxième partie de cette thèse présente le logiciel SPIX, développé dans le cadre de ces travaux, qui aide au traitement des données complexes issues de spectrométrie de masse à très haute résolution. Celui-ci a été appliqué avec succès à l'étude d'échantillons environnementaux complexes ayant subi des réactions induites par la lumière.

Les contaminants d'intérêt émergent (CECs) constituent une source importante de préoccupation en raison de leurs effets toxiques potentiels et de leur persistance dans l'environnement. Leurs effets nocifs ont été démontrés sur les organismes aquatiques et la santé humaine. D'avantage de CECs sont détectés chaque année ; ils deviennent omniprésents à mesure que les activités anthropiques augmentent. Les CECs sont mal éliminés par les usines conventionnelles de traitement des eaux usées, celles-ci n'ayant pas été conçues pour gérer ces polluants. Il est ainsi essentiel d'élaborer de nouvelles approches de traitement pour améliorer la qualité des eaux et protéger l'environnement. Les procédés basés sur l'irradiation par la lumière sont très prometteurs dans ce domaine. Il convient néanmoins de considérer la formation de photoproduits potentiels et la toxicité de ces derniers. Ce type d'étude vise également à comprendre les mécanismes photoinduits de transformation des contaminants en matrices environnementales.

Un des objectifs de ce projet était de comparer différentes approches pour étudier la photodégradation des CECs. Une approche de modélisation en laboratoire a d'abord été appliquée à cinq contaminants. La photolyse directe et certains procédés avancés d'oxydation, tels que l'irradiation UV en présence de peroxyde ou de photo-sensibilisants, la photocatalyse hétérogène ou des réactions de Fenton, ont été employés. Les expériences ont été réalisées en conditions de laboratoire dans de l'eau ultrapure, ou à l'échelle d'une

usine pilote dans des eaux usées traitées secondaires, afin de modéliser des conditions réalistes et d'étudier l'effet matriciel sur la dégradation. L'efficacité de la photodégradation a été suivie par LC-MS et spectroscopie UV-Visible. La minéralisation des polluants étant rarement atteinte, des analyses non ciblées ont été réalisées sur un spectromètre de masse FT-ICR à très haute résolution. Cela a rendu possible l'identification précise des formules moléculaires alors que l'élucidation des structures des photoproduits a été conduite par MS2. Des calculs *in silico* ont été effectués à partir des structures des photoproduits pour évaluer leurs effets toxiques potentiels. Parallèlement, des tests *in vitro* ont permis d'étudier la toxicité du mélange à chaque étape de la réaction de photodégradation. Cette approche a permis d'évaluer le devenir des contaminants, de proposer et optimiser des procédés de photodégradation efficaces et d'élucider les mécanismes réactionnels associés.

Parallèlement à la modélisation, une approche analytique non ciblée a été utilisée pour étudier des mélanges complexes. La spectrométrie de masse a été employée en introduction directe pour détecter des milliers d'ions moléculaires et déterminer leurs formules avec précision. Le logiciel SPIX a été développé pour extraire les informations pertinentes de ces données complexes. Une de ses caractéristiques est d'extraire les ions qui subissent des changements d'intensité significatifs entre deux conditions. Il permet par ailleurs de révéler l'évolution d'une série de conditions, proposant des modèles cinétiques associés. L'exportation de données statistiquement pertinentes et leur traitement ont été réalisés. L'application du logiciel et les principes mathématiques associés sont présentés au travers de l'analyse des contaminants dans les matrices complexes, telles que les eaux usées traitées secondaires et la matière organique naturelle. Le traitement de jeux de données 3D LC-MS constitue le dernier développement du logiciel. Ce dernier est innovant et unique pour l'étude de la cinétique de réactions inconnues dans des échantillons complexes. L'approche holistique fournie par SPIX constitue un outil complémentaire aux approches de modélisation; il permet de détecter et de surveiller les réactions pertinentes dans des média très complexes et contribue significativement à réduire la subjectivité de l'opérateur.

List of publications in the thesis

- [1] Z Varga, E Nicol, and S Bouchonnet. “Photodegradation of benzisothiazolinone: Identification and biological activity of degradation products”. In: *Chemosphere* 240 (2020), p. 124862. DOI: 10.1016/j.chemosphere.2019.124862.
- [2] I Sciscenko, A Arques, Z Varga, S Bouchonnet, O Monfort, M Brigante, and G Mailhot. “Significant role of iron on the fate and photodegradation of enrofloxacin”. In: *Chemosphere* 270 (2021), p. 129791. DOI: 10.1016/j.chemosphere.2021.129791.
- [3] E Nicol, Y Xu, Z Varga, S Kinani, S Bouchonnet, and M Lavielle. “SPIX: A new software package to reveal chemical reactions at trace amounts in very complex mixtures from high-resolution mass spectra dataset”. In: *Rapid Commun Mass Spectrom* 35.6 (2021), e9015. DOI: 10.1002/rcm.9015.
- [4] NPF Gonçalves, Z Varga, S Bouchonnet, V Dulio, N Alygizakis, F Dal Bello, C Medana, and P Calza. “Study of the photoinduced transformations of maprotiline in river water using liquid chromatography high-resolution mass spectrometry.” In: *Sci Total Environ* 755.2 (2020), p. 143556. DOI: 10.1016/j.scitotenv.2020.143556.
- [5] N Cazzaniga, Z Varga, E Nicol, and S Bouchonnet. “UV-visible photodegradation of naproxen in water - Structural elucidation of photoproducts and potential toxicity”. In: *Eur J Mass Spectrom* 26.6 (2020), pp. 400–408. DOI: 10.1177/1469066720973412.

Additional collaborative works

- [1] NPF Gonçalves, Z Varga, E Nicol, P Calza, and S Bouchonnet. “Comparison of advanced oxidation processes for the degradation of maprotiline in water — Kinetics, degradation products and potential ecotoxicity”. In: *Catalysts* 11.2 (2021). DOI: 10.3390/catal11020240.
- [2] E Nicol, Z Varga, S Vujovic, and S Bouchonnet. “Laboratory scale UV–visible degradation of acetamiprid in aqueous marketed mixtures – Structural elucidation of photoproducts and toxicological consequences.” In: *Chemosphere* 248 (2020), p. 126040. DOI: 10.1016/j.chemosphere.2020.126040.

Contents

Introduction	22
1 Bibliography	25
1.1 Context and molecules	26
1.1.1 The concept of contaminants of emerging concern	26
1.1.2 Guidelines and regulations on water quality	28
1.1.3 Compounds selected for the present study	31
1.2 Photochemistry	38
1.2.1 Generalities on photochemistry	38
1.2.2 Photolysis of contaminants	42
1.2.3 Advanced oxidation processes	46
1.2.4 Applications and limitations of AOPs	49
2 Materials and methods	68
2.1 Photodegradation set-ups and parameters	69
2.2 <i>In vitro</i> and <i>in silico</i> toxicity estimations	69
2.3 HRMS and non-targeted analysis	71
2.4 ESI and FT-ICR MS	74
2.5 Direct infusion mass spectrometry (DI-MS)	77
2.6 Data processing	78
3 Modeling approach - Results on direct photochemical reactions	84
3.1 General approach	85
3.2 Photolysis of benzisothiazolinone	87
3.3 Photolysis of naproxen	111
4 Modeling approach - Results on indirect photochemical experiments	128
4.1 General approach	129
4.2 Photodegradation experiments on perfluorooctanoic acid	130
4.3 Photoinduced transformation of maprotiline	134
4.4 Role of iron in the photodegradation of enrofloxacin	181
4.5 Photodegradation of enrofloxacin in a pilot plant	213

5	Untargeted approach using SPIX	226
5.1	Introduction of Spix	227
5.2	SPIX software	233
5.3	Latest developments of SPIX - 3D approach	261
	Conclusions	264

List of Figures

1.1.1	Molecular structure of benzisothiazolinone	32
1.1.2	Molecular structure of naproxen	32
1.1.3	Molecular structure of maprotiline	33
1.1.4	The lifecycle of perfluorinated compounds	34
1.1.5	Molecular structures of perfluorooctanoic acid and perfluorooctane sul- fonate	35
1.1.6	Molecular structure of enrofloxacin	36
1.2.1	Reaching an excited state by radiation absorption	38
1.2.2	Franck-Condon principle and its translation to absorption/emission spectra	39
1.2.3	Pathways of electronic excitation loss	39
1.2.4	Jablonski diagram	40
1.2.5	Norrish reaction type I	42
1.2.6	Norrish reaction type II	42
1.2.7	Proposed levels of identification	45
1.2.8	Mechanism of hydroxyl radical generation by photocatalysis	47
1.2.9	Possible hydroxylation sites of toluene	49
1.2.10	Subsequent reaction mechanisms after the addition of hydroxyl radical onto a double bond	49
2.3.1	Mass defects of common elements and their isotopes	72
2.3.2	Number of ions that can be detected at the nominal m/z 191 using ultrahigh resolution MS	73
2.3.3	Number of contaminants lost at each sample preparation and analysis step	74
2.4.1	Principle of operation of an electrospray ionization source	75
2.4.2	Image of the FT-ICR SolarixXR at the LCM	76
2.4.3	Schematic representation of an ICR cell	76
2.6.1	Interface of the Bruker Compass DataAnalysis software, showing the pa- rameters for manual formula assessment	79
3.2.1	UV-Vis absorption spectrum of BIT in ultrapure water at different ir- radiation times	92

3.2.2	Suggested pathways for the photodegradation of BIT	97
S3.2.1	UV-Vis absorption spectrum of BIT in ultrapure water	101
S3.2.2	Consecutive CO eliminations from hydroxylated isomers of BIT and PP1 (a)	102
S3.2.3	Consecutive CO eliminations from hydroxylated isomers of BIT and PP1 (b)	103
S3.2.4	Dissociation pathways of [PP5 - H] ⁻ under collisional activation	104
S3.2.5	Dissociation pathways of PP6 isomers	105
S3.2.6	Relative amount of BIT as a function of irradiation time	106
3.3.1	Relative abundances of naproxen and its photoproducts over time	116
3.3.2	Mechanisms proposed for the photodegradation of naproxen in water	119
S3.3.1	Dissociations of molecular ions of the photoproducts detected by GC- EI-MS	123
S3.3.2	Dissociations of the pseudomolecular ions (MH ⁺) of the photoproducts detected by LC-ESI-MS	124
4.2.1	UV-Vis absorption spectrum of PFOA in ultrapure water.	130
4.3.1	Numbering of maprotiline carbon atoms	137
4.3.2	Maprotiline degradation and mineralization in the presence of TiO ₂	142
4.3.3	Inhibition on <i>Vibrio fischeri</i> bioluminescence in the presence of TPs	143
4.3.4	Suggested fragmentation pathways for protonated maprotiline in CID experiments	144
4.3.5	Suggested dissociation pathways for photoproducts resulting from hy- droxylation of maprotiline on an aromatic ring	145
4.3.6	Maprotiline removal over time in a river water sample, in the dark and under UVA irradiation	148
4.3.7	Profile over time of maprotiline degradation products observed in a river water sample over time	150
4.3.8	Proposed maprotiline degradation pathways in river water in the dark and under irradiation	151
S4.3.1	Schematic view of the workflow for maprotiline degradation pathway	152
S4.3.2	Profiles over time of maprotiline TPs observed in ultrapure water in the presence of TiO ₂	153
S4.3.3	HPLC/HRMS chromatogram of maprotiline and m/z 294	169
S4.3.4	Specific CID mechanisms for the compound 294-D	169
S4.3.5	Specific CID mechanisms for the compound 294-E	169
S4.3.6	Specific CID mechanisms for the compound 294-B	170
S4.3.7	CID mechanisms for the compound 292-B issued from dehydrogenation of 294-E	170

S4.3.8	CID mechanism for the compound 292-E	170
S4.3.9	Dehydrogenation of species with MH^+ at m/z 294	171
S4.3.10	Suggested dissociation pathways for m/z 310 photoproducts	172
S4.3.11	CID mechanisms for the compound 310-F	173
S4.3.12	CID mechanisms for the compound 310-E	173
S4.3.13	CID mechanisms for the compound 310-B	174
S4.3.14	CID mechanisms for the compound 284-A	174
S4.3.15	CID mechanisms for the compound 284-B	175
S4.3.16	CID mechanisms for the compound 284-C	175
S4.3.17	CID mechanisms for the compound 258	175
4.4.1	Absorption spectra and Iron(III) concentration at different pH values	185
4.4.2	Photolytic rate constants and relaxation kinetics	186
4.4.3	Time-course absorbance spectra changes during irradiation experiments at pH 3.0.	189
4.4.4	Degradation percentages after 60 min at both studied pH in aerated conditions	190
4.4.5	Summary of the studied reactions and photoproduct formation mecha- nism proposal.	192
4.4.6	Obtained photoproducts formation after 120 min for ENR and Fe^{III} -ENR ₃	193
S4.4.1	ENR pKa determination	196
S4.4.2	Effect of ROS scavenger addition at aerated conditions	196
S4.4.3	FFA removal by 1O_2 generation at different tested conditions	197
S4.4.4	ENR laser flash photolysis measurements	198
S4.4.5	$Fe(II)$ formation from Fe^{III} -ENR ₃	202
S4.4.6	Changes on absorbance spectra during direct photolysis at pH 7.0	203
S4.4.7	All detected photoproducts for ENR and Fe^{III} -ENR ₃	204
S4.4.8	Photoproduct formation kinetics when H_2O_2 was added at pH 3.0	205
4.5.1	Efficiency of AOPs on the decoloration of Rhodamine B	213
4.5.2	Degradation kinetics of Rhodamine B under three different AOPs	218
4.5.3	LC-MS monitoring of enrofloxacin removal using a peroxide/UV AOP	219
S4.5.1	UV-Vis absorption spectrum of Rhodamine B	219
S4.5.2	Pilot plant	221
S4.5.3	Degradation of enrofloxacin in wastewater with UV-VIS spectroscopy	222
5.1.1	Interface displaying the parameters of SPIX: the comparison of two con- ditions	230
5.1.2	Interface displaying the parameters of SPIX: kinetic modeling	230
5.1.3	Change in the intensity of the BIT pseudomolecular ion	231
5.1.4	Kinetic model of benzisothiazolinone, exponential fit	231

5.2.1	Chemical structures of maprotiline and acetamiprid	240
5.2.2	Protonated maprotiline signal	241
5.2.3	m/z 294.18552 signal extracted for each irradiation time and associated kinetic model	244
5.2.4	Mass spectra of acetamiprid in mixture with fulvic acid.	246
5.2.5	Visual result provided by the SPIX software	247
S5.2.1	Current kinetic models in SPIX	251
5.3.1	LC-MS dataset in SPIX	261
5.3.2	Modeling the behavior of the parent compound, exponential fit	262
5.3.3	Modeling the behavior of an isomer of the parent compound, exponential fit	262
5.3.4	Modeling the behavior of a photoproduct, exponential fit	263

List of Tables

3.2.1	Photoproducts of BIT detected in LC-MS and GC-MS couplings	92
3.2.2	Toxicity values estimated by the T.E.S.T. software for BIT and its photoproducts except PP6b	98
S3.2.1	Exact m/z values and corresponding formulae of collision-induced product ions from $[M+H]^+$ and $[M-H]^-$ ions in LC-MS/MS	100
3.3.1	Retention times, main ions, and elucidated structures of the photoproducts PP4 to PP7 detected by LC-ESI-MS	117
3.3.2	Retention times, main ions, and elucidated structures of the photoproducts PP1 to PP3 detected in GC-MS/MS (electron ionization)	118
3.3.3	Toxicity values estimated by the T.E.S.T. software for BIT and its photoproducts	120
S3.3.1	Collision-induced ESI ⁺ mass spectra of naproxen and photoproducts . .	122
4.2.1	Added photosensitizer molecules and local maximum absorbance	131
4.2.2	LC-MS measurement results	132
4.3.1	Ions detected in CID experiments for maprotiline main degradation products	146
S4.3.1	Summary of $[M+H]^+$ ions and main product ions from CID experiments	153
S4.3.2	Ions in common detected in CID experiments for m/z 310 transformation products	158
S4.3.3	Maprotiline TPs observed in river water in the dark and under irradiation; (+) observed, (-) non observed	158
S4.3.4	Investigation of maprotiline and its TPs in digitally archived wastewater and river water samples	159
S4.3.5	Description of the river water and wastewater samples used in the retrospective analysis	160
S4.4.1	Elucidated major photoproducts in both systems ENR and Fe ^{III} -ENR ₃ and at both studied pHs	198
S4.5.1	Wastewater characterization	220
5.1.1	Available exporting formats with Bruker DataAnalysis software	228
5.1.2	Describing the data files in a .csv file	229
5.1.3	Available exponential kinetic model types in the SPIX library	230

5.2.1	Ions extracted and associated kinetic models related to the photodegradation of maprotiline in wastewater	242
5.2.2	m/z values for which the intensity significantly varied between series of spectra recorded before and after 30 min of irradiation	245
S5.2.1	Current kinetic models in SPIX - equations	250
S5.2.2	Exported data from the SPIX software after assignation of a kinetic model to a m/z ratio.	252
5.3.1	Exporting the simulated data for the 3D dataset	263

Abbreviations

ACN	Acetonitrile
AOP	Advanced oxidation process
API	Active pharmaceutical ingredient
BIT	Benzisothiazolinone
BOD	Biological oxygen demand
CAS	Chemical abstract service
CEC	Contaminant of emerging concern
CI	Chemical ionization
CID	Collision-induced dissociation
CMAP	Centre de Mathématiques Appliquées
COD	Chemical oxygen demand
DI	Direct infusion
DSFP	Digital Sample Freezing Platform
EC	European Commission
EI	Electron impact
ENR	Enrofloxacin
EPA	Environmental Protection Agency
EQS	Environmental quality standards
ESI	Electrospray ionization
EU	European Union
FA	Formic acid
FFA	Furfuryl alcohol
FoA	Frequency of appearance
FQ	Fluoroquinolone
FT-ICR	Fourier-transform ion cyclotron resonance
GC	Gas chromatography
HPLC	High-performance liquid chromatography
HRMS	High-resolution mass spectrometry
ICCF	Institut de Chimie de Clermont-Ferrand
IN	Inorganic carbon
INERIS	Institut national de l'environnement industriel et des risques
LC	Liquid chromatography



LC50	Lethal concentration 50
LD50	Lethal dose 50
LCM	Laboratoire de Chimie Moléculaire
LOD	Limit of detection
LTQ	Linear ion trap
MS	Mass spectrometry
MS²	Tandem mass spectrometry
MS/MS	Tandem mass spectrometry
NAP	Naproxen
NOM	Natural organic matter
NSAID	Non-steroidal anti-inflammatory drugs
PAH	Polycyclic aromatic hydrocarbons
PBT	Persistent, Bioaccumulative, Toxic
PNEC	Provisional No Effect Concentration
PFAS	Per- and polyfluoroalkyl substances
PFOA	Perfluorooctanoic acid
PFOS	Perfluorooctanesulfonic acid
PP	Photoproduct
PPCP	Pharmaceuticals and personal care product
QSAR	Quantitative Structure-Activity Relationship
REACH	Registration, Evaluation, Authorization, and Restriction of Chemicals
RhB	Rhodamine B
ROS	Reactive oxygen species
RT	Retention time
T.E.S.T.	Toxicity Estimation Software Tool
TN	Total nitrogen
TOC	Total organic carbon
TP	Transformation product
UHPLC	Ultra-high-performance liquid chromatography
UNEP	United Nations Environment Programme
UV	Ultraviolet
UV-Vis	Ultraviolet-Visible
WHO	World Health Organization
WWTP	Wastewater treatment plant



Introduction

This PhD project is part of the AQUALity project, a Marie Skłodowska Curie Actions (MSCA) –Innovative Training Network (Call: H2020-MSCA-ITN-2017), project n. 765860. Various European research institutes, universities, and industrial partners participate in this project with a common goal: developing innovative approaches for the abatement of contaminants of emerging concern (CECs). The first aspect was to bring interdisciplinary expertise regarding their detection, toxicity, and photochemical fate and perform risk assessment. Secondly, photochemical approaches applicable for removing CECs, such as advanced oxidation processes, were studied, considering complex environmental matrices. Thirdly, novel membrane technologies were developed for their removal. These viewpoints will help in the global understanding of the issues of CECs and propose viable solutions for their abatement while minimizing risks of toxic by-products generation. Hopefully, this project will impact regulations and the implementation of novel decontamination solutions on an industrial scale.

Fifteen early stage researchers (ESRs) were enrolled in the project and worked in close collaboration that resulted in numerous scientific publications. During the dynamic PhD, secondments were carried out to bring a cross-sectoral approach involving universities, research centers, and industrial partners. For efficient information exchange, seven project meetings were organized within the consortium. These were also connected to workshops and summer schools to ensure scientific training of the ESRs.

The core of this work was performed at École Polytechnique, aiming at studying the photodegradation of contaminants of emerging concern. Firstly, a modeling approach was employed, where the goal was not only to assess the photodegradation efficiency but also to assess photochemical transformation mechanisms. The photochemical reactions were followed by LC-MS and GC-MS analysis, and tandem MS experiments were performed to elucidate the structures of the formed photoproducts. While this resulted in accurate structural information and mechanistic pathways, it is a time-consuming method, and it is challenging to consider all the parameters impacting photochemical reactions, such as the influence of complex matrices. To obtain a holistic overview of these processes, the capabilities of high-resolution mass spectrometry were utilized, and a software was developed to extract relevant information from the resulting big data. This was a novel approach

that works by analyzing highly complex datasets and finding statistically relevant changes that occur throughout a reaction.

During the project, my first secondment was carried out at the Institut de Chimie de Clermont-Ferrand (ICCF), France, under the supervision of Dr. Claire Richard. Their expertise is mainly in the field of photochemistry; therefore, it laid down the basis for good practices in carrying out photochemical experiments. This is essential as different factors, like pH, solvent, contaminant concentration, irradiation wavelength, highly influence the photochemical reaction outcomes. It helped to understand how to select and optimize photochemical reaction parameters and monitor them using various analytical techniques, such as UV-Vis spectroscopy, ion chromatography, and pH measurements.

Three months were spent at FACSA, a company in charge of water management in Spain. The secondment was conducted at a wastewater treatment plant (Alhama de Murcia), under the supervision of Francisco Valero, who is the plant's leading engineer. The task was to focus on applying advanced oxidation processes under realistic conditions in a pilot plant and understanding how conventional wastewater treatment plants operate. This showed the industrial approach for the removal of contaminants and viable applications on a large scale. By performing the reactions in a pilot plant, the effect of secondary treated wastewater was studied. This is important as many advanced oxidation processes work well on a laboratory scale but fail under realistic conditions, as reaction hindrance can occur, primarily due to the complexity of the water matrix. Robust analytical methods are necessary that can be easily used and rapid to assess the quality of wastewater effluents.

The third secondment was carried out at Università degli Studi del Piemonte Orientale "Amedeo Avogadro" (UPO) in Alessandria, Italy. The scope of this secondment was to become familiarized with data processing methods, basic programming skills, and statistical analysis in Matlab, thanks to the mentorship of Dr. Elisa Robotti. These are key competencies, as the modern, highly performant analytical instruments generate large amounts of complex datasets, and it is essential to extract relevant information from them.

The last secondment was conducted at Società Metropolitana Acque Torino S.p.A (SMAT) in Turin, Italy, in a research center connected to a drinking water treatment plant under Rita Binetti's supervision. The aim was to understand drinking water treatment processes and carry out a sampling campaign. The sample extractions were performed using multiple extraction methods, thus minimizing the loss of compounds for non-targeted analysis. The samples were analyzed by LC-MS, and some potential disinfection by-products were found. At the time of writing this thesis, the data analysis was not completed; therefore, the results of the secondment are not presented in the thesis, but future scientific publication is planned.

This thesis is divided into five chapters. The core of the results is presented through scientific articles. The first chapter provides a general overview of the issue of contaminants of emerging concern and their regulations. This is followed by the introduction of the concept of photochemistry. The photochemical reactions of organic molecules and the applicability of photodegradation processes are discussed as a possible way to remove contaminants. The second chapter is devoted to materials and methods; photochemical setups and toxicity tests are presented. The performance of high-end mass spectrometry for non-targeted analysis and its capabilities to generate high-resolution datasets from complex environmental samples is discussed.

The presentation of the results is divided into three chapters (3 to 5), based on differences in photochemical or analytical approaches. The third and fourth chapters cover the modeling approach, which consists of submitting the studied molecules to light-induced irradiation or advanced oxidation processes under laboratory or pilot plant conditions. This allows working with micropollutant concentrations higher than under environmental conditions, which reduces matrix effects and favors the detection of potential degradation products. The purpose of such studies is to obtain information on the photodegradation efficiency and the formation of photoproducts and intermediates. By elucidating the phototransformation products' structures and determining their persistence, it is possible to assess their potential risks and toxic effects. In these two chapters, considerations are discussed regarding the photochemical and analytical parameters, and light-induced degradation of five different molecules from various micropollutant families is reported. These compounds were selected based on recommendations by the NORMAN network, frequent detection, potential harmful effect, and previous expertise of the LCM, considering different families of compounds. Most of these studies were part of collaborations within the AQUALity consortium institutes, with a common goal to improve knowledge on the photochemical reactions of CECs and their consequences. Throughout the whole study, non-targeted analytical approaches have been employed to extract a maximum amount of information. The third and fourth chapters, however, encompass commonly employed data analysis approaches: characterizing the photoproducts one by one owing to HRMS measurements and tandem mass spectrometry experiments. The fifth chapter introduces an innovative data analysis approach that aims to gain a holistic overview of the changes occurring in a complex matrix with a new software developed by our group. In this work, the vast majority of the analytical information was obtained from an ultrahigh-resolution FT-ICR mass spectrometer, thus gaining a large amount of high-quality analytical information that had to be processed methodically. Overall, important advances were achieved in understanding photodegradation mechanisms, assessing potential harmful effects of photoproducts, and extracting relevant information from non-targeted datasets.



Chapter 1

Bibliography



1.1 Context and molecules

1.1.1 The concept of contaminants of emerging concern

Water management is one of the most pressing societal challenges of the 21st century. Clean water is essential for human life, agriculture, and a healthy ecosystem. The following part contains a short overview regarding contaminants of emerging concern, their number, nature, and the pursuit for their regulations, focusing on the aspects relevant to this project. Increased human consumption, overuse of aquifers, natural calamities, and climate change are reasons behind water scarcity. It is essential to value the existing water resources and recycle wastewater to attain sustainability goals.

Contaminants of emerging concern are defined as anthropogenic chemicals or substances of natural origin, which are currently not regulated but might be submitted to future regulations because they can pose risks to human health or the environment, as their persistence or toxicity might alter the metabolism of a living being [1]. These are not necessarily new contaminants; emerging data on legacy compounds can also introduce new regulations or make the existing ones stricter. It is an extremely complex field of study, as 100 million chemicals are registered in the Chemical Abstract Services (CAS) database, and this number increases each year.

The occurrence of emerging pollutants is an important subject of investigation worldwide. Many surveys and studies have been conducted on the topic to better understand their presence and environmental impact [2–6].

More than one-third of Earth’s accessible renewable freshwater is exploited for agricultural, industrial, and domestic use, these activities leading to water pollution. Every year around 300 million tons of synthetic compounds of industrial origin and consumer products end up in natural waters. This number is 140 million tons for agricultural chemicals [7]. A considerable quantity and variety of pollutants are transferred to wastewater, originating from hospitals, households, and industries. As conventional wastewater treatment plants (WWTPs) were not designed to remove persistent organic pollutants, they represent an important environmental contamination source [8]. In the European Union, 30,000 to 70,000 chemicals are in daily use (EINECS, European Inventory of Existing Chemical Substances) [9]. More than 700 contaminants, their metabolites, and transformation products were detected in the European aquatic environment, assessed into 20 categories based on their function and origin [10].

Contaminants of emerging concern encompass a wide range of compounds with different physical and chemical properties. The use/function of these contaminants also covers a broad range of products: pharmaceutical and personal care products, illicit drugs, hor-

mones, steroids, perfluorinated chemicals, disinfection by-products, flame retardants, artificial sweeteners, nanomaterials, pesticides, veterinary products, industrial compounds and by-products, food additives, UV filters... Their sources can be either point-sources (spatially discrete, constrained spatial extent: industrial effluents, municipal sewage treatment plants, and combined sewage- storm-water overflows, resource extraction, waste disposal sites, buried septic tanks, etc.) or diffuse sources of pollution (poorly defined, broad geographical scale: agricultural runoff from bio-solids and manure sources, storm-water and urban runoff, leakage from reticulated urban sewerage systems, diffuse aerial deposition, etc.). Usually, the concentrations of emerging pollutants are not too high, although in some cases, it can be significant (> 100 ng/l) [11, 12].

The large number and variety of CECs are challenging in terms of regulations, as there is a need for prioritization which itself raises many questions: what kind of quality criteria should be followed - especially in the cases where only limited information is available, which compounds should be targeted, how to take into account spatiotemporal factors and so on. There are “true or really new” contaminants that recently appeared in the scientific literature, contaminants of emerging interest, previously described but whose environmental impact is not fully understood, and emerging issues appearing about existing chemicals. CECs emerged as epidemiology has improved, and harmful effects have been demonstrated at lower concentration levels, leading to a dynamically changing field [13]. For instance, organophosphate pesticides have been replaced by glyphosate, neonicotinoid, and pyrethroid pesticides in the early 2000s. Since then, neonicotinoid pesticides have been banned in the EU due to their harmful effect on pollinators, particularly honey bees. The scientific community is extensively studying the toxic effects of glyphosate; restrictions or bans were recommended and implemented against its use in some European countries [14–16]. When a compound starts raising concerns, data is acquired on its environmental effects, ecotoxicity, and human toxicity. As sufficient evidence and data are accumulated about harmful effects, governments establish or re-evaluate guidelines, criteria, or regulations. CECs should remain emerging until there is not sufficient scientific data and documentation about potential problems. Not all the CECs will be harmful, but the aim is to gather conclusive data to accurately evaluate and assess risks.

Richardson et al. publish biennial reviews titled “Emerging Contaminants and Current Issues.” These reviews cover the emerging contaminants, regulations, toxicological data, and advances in analytical chemistry; the last one covers the period between 2017-2019. At the beginning of the 2000s, pesticides were the most studied organic environmental contaminants and, despite regulations, continue to pose a relevant risk due to their employment in large quantities [17]. There are more than 3000 pharmaceutical substances, such as painkillers, antibiotics, lipid regulators, antidepressants, and a substantial amount are entering the water bodies [18]. The testing of their specific environmental effects is still

limited due to their high number, but estrogenic effects [19], renal alterations [20], and behavioral changes [21] in aquatic animals were reported in the literature. An unintended consequence of eliminating pathogens from drinking water is the formation of disinfection byproducts, bearing potential harmful effects for human health, such as carcinogenicity and inducing miscarriage [22]. Every year more and more contaminants emerge as data is becoming available, antibiotics leading to the formation of antibiotic-resistant genes being the most recent addition. It is indisputable that the field of contaminants of emerging concern is extremely dynamic, caused by the continuous increase in chemical manufacturing, together with the advances in highly sensitive, accurate instrumentation and toxicological assessment methodologies, and the expanding availability of monitoring data [23].

1.1.2 Guidelines and regulations on water quality

In the following section, a brief introduction to the timeline of European regulations regarding water quality and contaminants of emerging concern is presented, as it is of particular interest for the AQUAlity project. National agencies, such as the USA Environmental Protection Agency (EPA), and global organizations, for example, the United Nations Environment Programme (UNEP) and the World Health Organization (WHO), exist to provide guidelines and regulations regarding water quality. European regulations are generally more advanced and complex, taking into account contaminants of emerging concern, despite the fact that their detection and removal requires state-of-the-art technologies and are costly.

EU water framework directive was established in 2000. Under the directive 2000/60/EC, different goals were set as a summary of previously held seminars, communications, written policies to ensure the water quality and avoid long-term deterioration of the European water bodies. The aim is sustainable management and protection of freshwater sources. The primary approach should be preventive in nature. Early and long-term protective measures should be implemented, considering their economic viability and the achievement of the environmental quality standards. Scientific and technical environmental data should be used for monitoring, risk assessment, elimination of priority hazardous substances, and ultimately ensuring the progressive reduction of pollutants. Hazardous substances are defined as *'substances or groups of substances that are toxic, persistent and liable to bio-accumulate, and other substances or groups of substances which give rise to an equivalent level of concern'* [24].

Decision No 2455/2001/EC of the European Parliament and of the Council provided the first list of 33 priority substances based on combined monitoring-based and modeling-based priority setting (COMMPS) scheme, introduced in Directive 2000/60/EC. This method takes into account the intrinsic hazard of the compounds (ecotoxicity, human

toxicity), presence in the environment, and other factors such as production and consumption. The list includes both contaminants of anthropogenic origins, like pesticides, flame-retardants, industrial precursors, and naturally occurring compounds, such as metals and polycyclic aromatic hydrocarbons (PAHs). Emissions, discharges, and losses into water bodies should be phased out for the priority substances originating from human activities. For the naturally occurring substances, background values should be achieved [25].

The Directive 2008/105/EC endorsing and amending the previous Directives gives a higher focus on pollution control, environmental quality standards (EQS), and the effects of chemical pollution, which should be halted at the source. Acute and chronic toxicity to aquatic organisms, biodiversity loss, accumulation of pollutants in the ecosystem, and human health risk are considered. In Annex II of the directive, EQS are listed for 33 priority substances, including their annual average and maximum allowable concentrations. The need is recognized for high-quality monitoring data on the contaminants in the European Union's aquatic environment [26].

The directive 2013/39/EU highlights the high cost of wastewater treatment, indicating that the development and implementation of innovative treatment technologies should be supported. In a review of the priority substances, new substances were identified, for which the EQS values were set, and some of the existing EQS values were revised; pesticides and perfluorooctane sulfonic acid and its derivatives were added to the list. Pharmaceuticals in water and soils were considered as contaminants of emerging concern. The minimum performance criteria for analytical instruments are discussed to obtain relevant environmental data. Persistent, bioaccumulative, and toxic substances (PBTs) are among the priority substances, as they are present at levels of significant risk, capable of long-range transport, and ubiquitous in the environment. Additional monitoring of substances with PBT-like behavior is encouraged, including spatial and temporal parameters in the monitoring. High-quality monitoring data and toxicity tests are required for the prioritization of suspect substances [27]. Under the directive of 2013, a dynamic watch-list was proposed to facilitate future prioritization that should include between 10 and 14 substances or groups of substances and be updated every 24 months. Diclofenac, 17-beta-estradiol (E2), and 17-alpha-ethinylestradiol (EE2) were selected for the first list together with 7 other pollutants or classes of pollutants; the description of their identification procedure was presented in a Joint Research Center technical report. This procedure includes data collection, predicted no-effect concentration calculations, and risk characterization. The selected substances pose a significant risk to the aquatic environment (hazard and exposure) and lack monitoring data. Compounds belonging to the classes of neonicotinoid and carbamate pesticides, fungicides, fire retardants, and antibiotics were identified as potentially hazardous [28].

According to Article 8c of the Priority Substances Directive (2008/105/EC), as amended by Directive (2013/39/EU), the European Commission proposes a strategic approach on microbial resistance caused by pharmaceutical substances. This is similar to the commitment made in 2017 by the Assembly of the United Nations and WHO. It refers to pharmacovigilance legislation to assess the extent of the water and soil pollution problem regarding pharmaceuticals and personal care products (PPCPs) [29].

Another noteworthy regulation of the European Union, REACH (Registration, Evaluation, Authorization, and Restriction of Chemicals), entered into force in 2007, aiming at lowering the risks posed by chemicals for human health and the environment [30]. It encompasses industrial chemicals but also substances used in households. REACH establishes protocols for risk assessment by collecting information on the properties and hazards of substances. Their databases contain valuable information on many compounds. This will influence future regulations to improve water quality, preserve biota, and protect human health.

The French regulations on water quality for human consumption and raw water are governed by the public health code CSP (Articles L. 1321-1 to 1321-10 and R. 1321-1 to 1321-68). France applies European directives into its national law regarding the water and sanitation field. The quality limits of water intended for human consumption are the same as those proposed in the council directive 98/83/EC. As an example, the directive indicates an individual pesticide quality limit value of 0.1 $\mu\text{g/L}$. Exceptions are aldrin, dieldrin, heptachlor, and heptachlor epoxide, with a lower parametric value of 0.03 $\mu\text{g/L}$. For the sum of pesticides and their relevant metabolites, the quality limit is 0.5 $\mu\text{g/L}$ [31].

Financed by the European Commission, the NORMAN network was established in 2005, being a network of reference laboratories, research centers and related organisations for monitoring of emerging environmental substances. The network aims to improve data collection, enhance information exchange on emerging substances, and standardize measurement methods. Problem-oriented research has to be ensured with a focus on tailored solutions for specific needs. INERIS is a partner of the AQUALity project and is part of the NORMAN network. In the framework of the 3rd AQUALity winterschool and meeting, INERIS organized a workshop on substance prioritization. As a result of this fruitful event, a report was drafted to identify challenges and solutions, titled “Contaminants of Emerging Concern in Urban Wastewater Joint NORMAN and Water Europe Position Paper” [32]. It encompasses a series of recommendations for the Urban Waste Water Treatment Directive of the European Commission.

It is important to highlight that these lists have to be remarkably dynamic, as the number of existing substances and their detection in the environment follows an increasing trend and new information regarding their risk and toxic effects continuously comes to light. This results from scientific expertise, advances in analytical and toxicological experiments,

and an intensified interest from stakeholders. To achieve the water quality goals, provide clean water to all, and protect the environment, large-scale collaborations are essential.

1.1.3 Compounds selected for the present study

The modeling approach consists of performing in-lab photodegradation reactions on individual compounds or on a limited number of molecules (e.g., a marketed product containing the active ingredient), therefore a few compounds had to be selected from the myriad of existing contaminants of emerging concern. For this reason, the NORMAN list of CECs was examined; it contains 1036 compounds, including the most frequently discussed emerging substances and pollutants.

In the framework of the AQUALity project, 41 contaminants of emerging concern were selected to study their presence in the environment, photochemistry, potential advanced elimination technologies, and toxicity. These contaminants were chosen based on a prioritization performed by INERIS. This was a simplified version of the NORMAN approach; the substances were ranked using a score calculated from key indicators such as exposure, hazard, persistency, bioaccumulation, and mobility [33, 34]. Furthermore, during the Workshop on the Prioritization of CECs in Urban Wastewaters, organized within the AQUALity project, additional CECs were suggested to be studied. In the framework of this PhD project, the studied compounds from the proposed NORMAN list were: perfluorooctanoic acid, perfluorononanoic acid, imidacloprid, acetamiprid, and maprotiline. Other studied CECs were selected based on their relevant environmental concentrations, risk or toxic effects: naproxen, benzisothiazolinone, enrofloxacin, amitryptiline, and gemfibrozil. Five contaminants were selected for detailed photochemical studies and are introduced below. Extensive information and literature review about benzisothiazolinone, naproxen, and maprotiline is presented in the results chapter within the published articles.

In addition to their relevance in terms of environmental presence and potentially harmful effects, these molecules were also selected to increase our group's level of expertise in photodegradation mechanism elucidation. The compounds were selected to represent different classes of compounds with a variety of functional groups. Understanding the formation of the photoproducts was challenging and helped us deepen our knowledge in photochemistry and interpretation of MS fragmentation patterns. They also show different kinds of biological activity, therefore adequate toxicity testing approaches were essential.

Benzisothiazolinone

Benzisothiazolinone (Figure 1.1.1), a preservative and antimicrobial agent, was the first compound selected, as it is of high interest for our working group due to an obvious lack of information regarding its photodegradation mechanism. The LCM plans future works on

benzothiazolinone photodegradation in mixture with other pesticides, as this compound is often marketed in solution with active substances. Being in a mixture could alter the photodegradation kinetics of the present compounds or the nature of the photodegradation products.

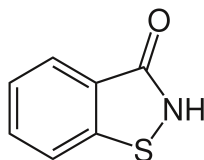


Figure 1.1.1: Molecular structure of benzothiazolinone

Naproxen

Naproxen (Figure 1.1.2), another candidate molecule on the NORMAN list of emerging pollutants, is a nonsteroidal anti-inflammatory drug. This compound was selected due to its extensive consumption and high detection frequency in the environment. The photodegradation of naproxen was previously studied, although only a simplified mechanistic pathway was suggested for the reaction that was mainly focused on the degradation kinetics, without in-depth structural elucidation of photoproducts [35].

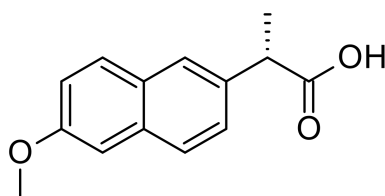


Figure 1.1.2: Molecular structure of naproxen

Maprotiline

The latest update of the NORMAN list was in 2016. Since then, an additional 40 000 compounds are being investigated and prioritized. Maprotiline (Figure 1.1.3), an anti-depressant drug, is one of these compounds, and it was classified with “Sufficient frequency of appearance.” The description of its prioritization process will be presented in one of the publications presented in this manuscript. Besides being a new CEC, with a limited amount of information regarding its behavior and potential risks, it was also chosen due to its symmetrical structure, making the elucidation of photoproducts more challenging.

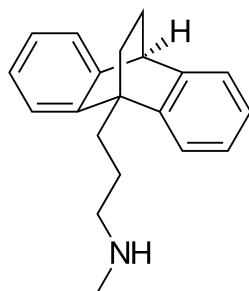


Figure 1.1.3: Molecular structure of maprotiline

Perfluorinated compounds

Perfluorinated compounds, also known as per- and polyfluoroalkyl substances (PFAS), consist of a hydrophobic carbon backbone to which fluorine atoms are bound, and a hydrophilic end group. Since the carbon-fluorine bond is the strongest covalent bond, these substances show high thermal, chemical, and biological inertness; moreover, fluorochemicals are resistant to many photodegradation processes, bacteria, oxidants, acids, and bases [36]. They are high-temperature and fire-resistant, non-wetting, non-stick, inert, and surface-active chemicals. Due to their attractive properties, this class of compounds is widespread in the industry as intermediates or additives in manufacturing processes (Figure 1.1.4). Furthermore, they are commonly found in consumer products and household utensils (cookware, clothes, carpets, etc.) and professional equipment (military uniforms, fire-fighting foams, etc.) as they provide great water and grease repellent characteristics. They are also used as additives in paints, ink, water-repellent products, and motor oil [37].

These perfluorinated organic molecules are used in the industry since the 1950s, but due to a lack of sensitive instrumentation and toxicological data, they have been recognized as contaminants only in the 2000s. Since they are polar or have high molecular weight, the development of ESI-MS, advances in LC-MS, and improved sensitivity of these analytical techniques, largely helped in their detectability. Due to their hydrophobic/hydrophilic nature and the aforementioned carbon-fluorine bond strength, they are extremely stable in the environment, resulting in their persistence and bioaccumulation.

The two most commonly studied and detected compounds are perfluorooctanoic acid (PFOA) and perfluorooctane sulfonate (PFOS) (Figure 1.1.5) [39]. An early investigation of the analysis of perfluorinated surfactants was conducted in Germany, in which these substances were detected in surface and drinking waters, with a maximum of 519 ng/L of PFOA in drinking water [40]. In France, a national screening study carried out on raw and tapwater samples of ten different perfluorinated compounds concluded that out of the

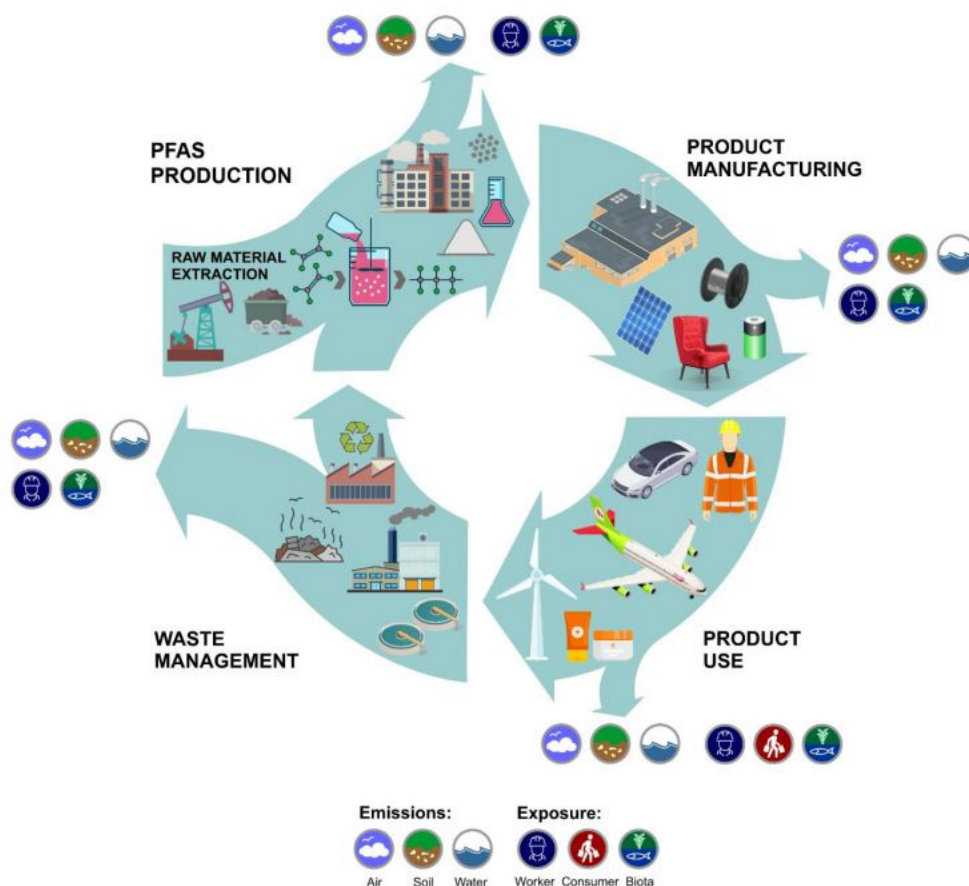


Figure 1.1.4: The lifecycle of perfluorinated compounds [38]

441 samples, 27% of them contained PFOS, but the investigation did not conclude any heavily contaminated site [41]. Other European countries reported as well the presence of perfluorinated compounds in various water body samples, notably in drinking water [42–46]. A study was conducted on the riverine discharge of perfluorinated carboxylates from 14 major European rivers; the Po river was accounted for the majority of the PFOA discharge [47]. Besides their detection in water, perfluorinated compounds were also detected in a wide diversity of matrices such as fish [45, 48], human blood [49, 50], and human breast milk [51]. The detection of these compounds, especially PFOS and PFOA, from various media and locations, indicates their bioaccumulation in the ecosystems and the global nature of the contamination.

Data on toxicity related to human health is sparse because, until the 1980s, chemically inert molecules were wrongly considered as certainly benign and biologically inactive. Evidence of toxic effects in humans arises mainly from epidemiologic and observational studies, but these are limited as long-term adverse effects are difficult to determine [52, 53]. Cyto- and potential developmental toxicity was shown for shorter chain perfluorinated substances in human stem cells [54]. A review of the wide range of toxicological

studies performed mainly on rats summarized the multitude of potential adverse effects such as developmental toxicity, carcinogenicity, hepatotoxicity, neurotoxicity, endocrine disruption, and immunotoxicity [55].

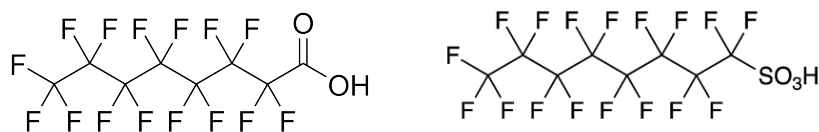


Figure 1.1.5: Molecular structure of perfluorooctanoic acid (left) and perfluorooctane sulfonate (right)

Due to their ubiquity, persistence, and potentially harmful effects, perfluorinated compounds are being progressively regulated both on the international and EU levels. In the European Union, perfluorooctane sulfonic acid and its derivatives are considered persistent organic pollutants, and their content in the waste cannot exceed 50 mg/kg [56]. A review of the directive 98/83/EC proposed a limit value of 0.1 µg/L for a sum of 20 individual PFAS in water and a value of 0.5 µg/L for total PFAS concentration [38]. According to the Water Framework Directive, only PFOS and its derivatives are currently listed as priority hazardous substances concerning surface water bodies [57]. Stricter regulations are envisaged as more evidence of toxicological data is prevailing, although the multitude of compounds in the family of perfluorinated substances impedes a comprehensive regulatory system.

Numerous studies indicate that conventional WWTPs do not remove these substances. This is a prominent issue, especially in industrial wastewater, where the concentrations are higher than in raw waters [43, 45, 58]. Due to their chemistry, very few removal methods proved to be efficient, as they required harsh conditions, elevated costs, and difficulties arose in the up-scaling from laboratory to industrial scales. Another issue is that most of the studies report partial defluorination and break down of precursors, but complete mineralization is rarely achieved. Advanced oxidation approaches with promising efficiency include removal by vacuum ultraviolet light (at 185 nm) [59], photocatalysis [60], and UV-Fenton system [61]. In the framework of the secondment conducted under the supervision of Dr. Claire Richard at Institut de Chimie de Clermont Ferrand (ICCF), PFOA was subjected to degradation under UV-Vis light in a mixture with molecules that can act as photosensitizers. Due to the abovementioned extreme persistence and stability of this class of compounds, irradiation at wavelengths above 300 nm proved inefficient in their decomposition, even when potential photosensitizer molecules were added to the mixture.

Enrofloxacin

Around 3000 compounds exist as pharmaceutical ingredients [62]. A subset of these compounds are antibiotics, which show, among other potential adverse effects, a specific en-

vironmental and human health issue, namely the development of antibiotic-resistant bacteria and antibiotic-resistant genes. This was not only the result of their intensive use in humans but also of their common application for livestock as a preventative approach. [23] Antibiotic resistance becomes an issue when antimicrobial drugs are no longer efficient in treating infectious diseases, leading to approximately 33 000 deaths per year in Europe alone [63].

Enrofloxacin (Figure 1.1.6) is a fluoroquinolone antibiotic used for veterinary purposes; it achieves its biological activity by inhibiting the bacterial DNA gyrase. 3,6 tons of fluoroquinolone antibiotics are sold every year in France only, as they are broad-spectrum bactericides, effective against Gram-positive and Gram-negative bacteria [64]. Compounds from this class of antibiotics were detected in wastewater effluents in France, Italy, Germany, Switzerland, the USA, and Canada [65–67]. Enrofloxacin was detected in animal farm effluent, river, and pond water in China [68]. It was also present in tap water at 96 ng/L concentrations [69]. In Japan, fluoroquinolone-resistant genes were discovered in aquatic media. They are contributors to the development of antimicrobial resistance, besides metals and general waste discharges [70, 71]. Besides the risk of inducing antibiotic resistance, enrofloxacin demonstrated toxic effects on photoautotrophic aquatic organisms, such as green algae [72]. Phytotoxic effects of enrofloxacin were shown in crop plants, and their monitoring should be implemented due to potentially damaging effects on genetic structures of non-target populations [73].

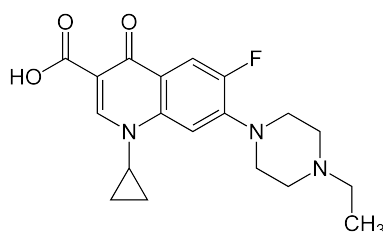


Figure 1.1.6: Molecular structure of enrofloxacin

The photodegradation of enrofloxacin ($550 \mu\text{g L}^{-1}$ starting concentration) by sunlight was studied in natural waters, and it has been established that the parent compound degraded within 1 hour under such conditions. Moreover, some of the structures of the main photoproducts were elucidated. The photodegradation was the most efficient at pH 8, where the molecule is in zwitterionic form [74]. Another study confirmed this rapid degradation in river water and synthetic wastewater matrices and reported that the photodegradation pathway was pH-dependent [75]. Therefore natural irradiation-induced degradation is a potential method of remediation in surface waters. The question is whether mineralization is achieved; if not, the extensive characterization of photoproducts in terms of structure, persistence, and toxicity is necessary. Indeed, when enrofloxacin was submitted

to photoirradiation under simulated sunlight conditions, only 13% of mineralization was achieved, and toxicity testing on *Vibrio fischeri* indicated the formation of phototransformation products with higher toxicity than the parent molecule [76]. On the other hand, when an advanced oxidation process involving UV/persulfate system was applied to the degradation of enrofloxacin, a degree of mineralization of 60% was achieved [77].

Enrofloxacin is part of the NORMAN list of emerging contaminants. In the framework of this project, it was selected to be submitted to degradation via various advanced oxidation processes. A scientific article was published as a result of a collaboration between our group, Universitat Politecnica de Valencia (Spain), and ICCF, to study the interaction between enrofloxacin and iron and its effect on the photodegradation mechanism. Enrofloxacin was also used as one of the probe molecules in a pilot plant set up at a wastewater treatment plant operated by FACSA (Alhama de Murcia, Spain). The results regarding the optimization of the plant and photodegradation effectiveness are presented in chapter 3.

1.2 Photochemistry

1.2.1 Generalities on photochemistry

Photochemical reactions constitute an important part of physical, chemical, and biological transformations of compounds in the environment and they are indispensable for the evolution of life on Earth. Inspired by natural processes, the study of photochemistry has become an important field, where the fate of molecules submitted to artificial or natural light is being studied. In photochemistry, light is usually defined as electromagnetic radiation in the ultraviolet and visible spectrum, with a wavelength range from 100 to 700 nm [78]. In photochemical reactions, molecules reach electronically excited states by absorbing photons during irradiation, yielding specific activation routes and transformation pathways; however, it does not necessarily result in a chemical change. It is essential to understand the possible competing physical processes and the different ways a molecule can return to its ground state. Reaching an electronically excited state means that one electron from one of the lowest energy ground states of the molecule is promoted to a vacant higher energy orbital (Figure 1.2.1).

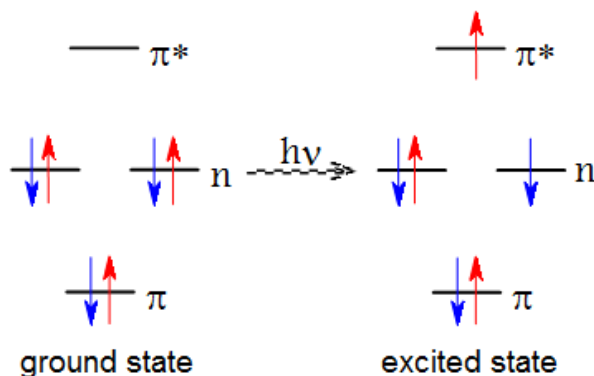


Figure 1.2.1: Reaching an excited state by radiation absorption [79]

The condition of light interacting with a specific molecule is that the wavelength of the incident radiation corresponds to the energy difference between the ground and excited states; therefore, the concept of energy quantization is essential. According to the Stark and Einstein law, the photochemical reaction is caused by the absorption of one photon by one particle. A photochemical process's efficiency is estimated through the quantum yield, defined as the number of molecules consumed for each photon of light absorbed. The Franck-Condon principle states that vertical transitions are the most probable, the ones that do not cause changes in the momentum or geometrical structure. It explains the spectral intensity distribution and reflects the probability of vibrational transitions (Figure 1.2.2) [80].

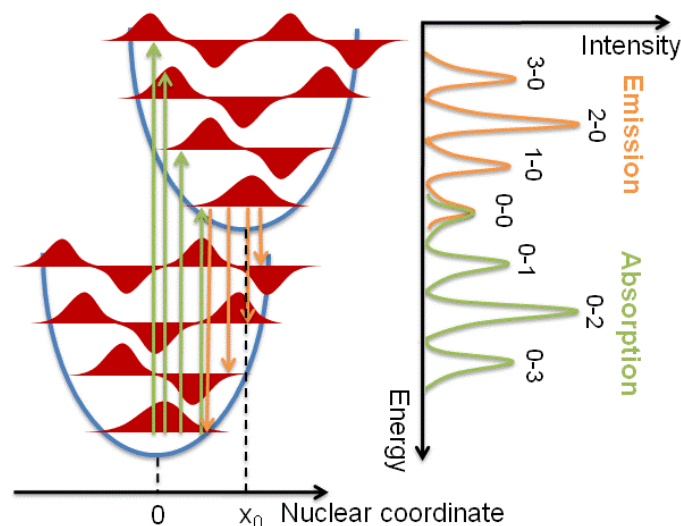


Figure 1.2.2: Franck-Condon principle and its translation to absorption/emission spectra [80]

According to the aforementioned principles, after a molecule reaches its excited state, it will return to its ground state by losing the electronic excitation. This can be achieved through various concurrent mechanisms, and it is important to study them to reach a deeper understanding of photochemical reactions. (Figure 1.2.3)

One of these processes is the intramolecular energy transfer. This will lead to new excited species, that can further undergo loss of electronic excitation. In this case, the sum of electronic and vibrational energies will be constant. Intramolecular energy transfer can occur between states with the same multiplicity of spins (internal conversion) or states with different spin multiplicities (intersystem crossing).

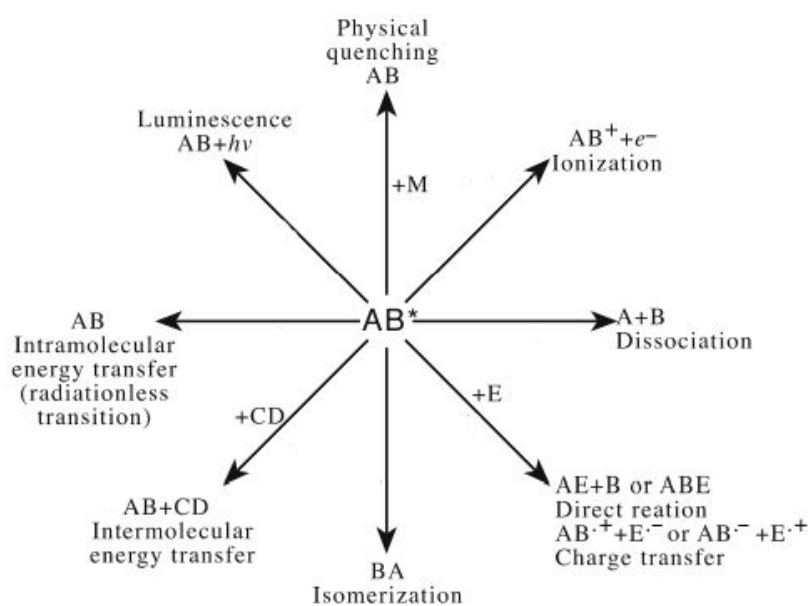


Figure 1.2.3: Pathways electronic excitation loss [81]

Radiative loss results in the emission of a photon and it is known as luminescence. This can be either fluorescence or phosphorescence, depending on the mechanism of relaxation to the ground state. While fluorescence halts when the radiation source is stopped, phosphorescence continues, characterized by a so-called “afterglow.” The reason is that fluorescence does not involve spin change and is, therefore, a short-lived process ($10^{-9} - 10^{-5}$ s), while phosphorescence involves spin change and is a less probable transition ($10^{-3} - 10$ s). The Jablonski diagram (Figure 1.2.4) was proposed to visualize and describe luminescence phenomena of organic molecules and illustrates these possible electronic transitions [82]. Fluorescence occurs from the lowest energy excited state, which is reached via internal conversion; it is a transition between the same multiplicity states ($S_1 \rightarrow S_0$). In phosphorescence, the excited state involves a change in the spin state through intersystem crossing; the long life-time is caused by the forbidden transition between the excited triplet state to the ground state ($T_1 \rightarrow S_0$). Therefore, it is characteristic of every molecule, based on its energy gap, and it is not dependent on the wavelength of irradiation, as long as excitation occurs.

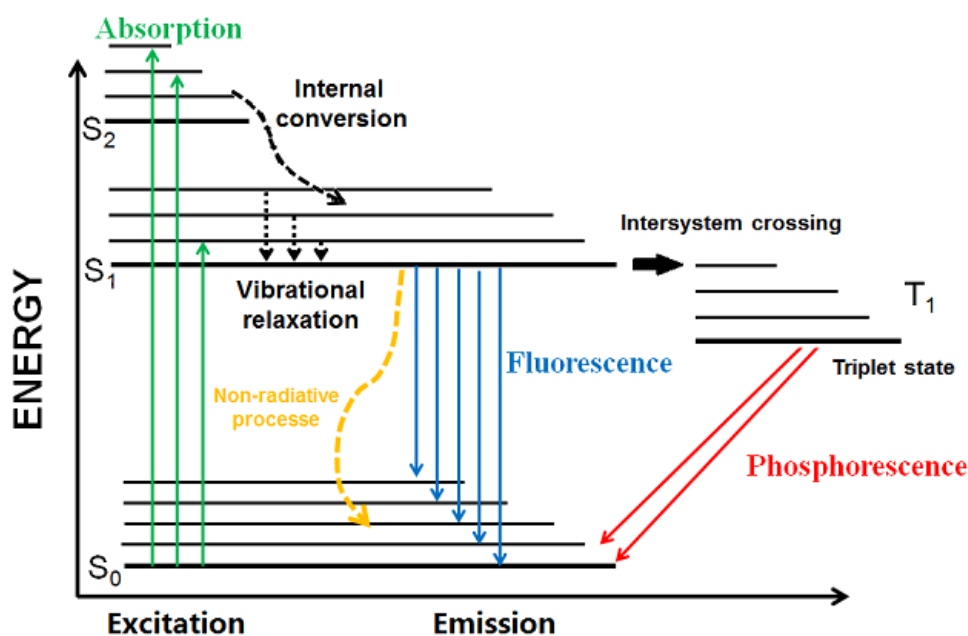


Figure 1.2.4: Jablonski diagram [83]

In terms of understanding organic photochemical reactions, pathways of the highest interest are those involving chemical changes. This can be the dissociation of the molecule (including ionization), isomerization, or the direct reaction of the excited species. Intermolecular energy transfer is also relevant: when a different molecule will uptake the excess energy, this can result in the phenomenon of photosensitization, where photochemical changes will occur in a molecule other than the irradiated one. When there is no chemical change in the molecule that uptakes the excess energy, physical quenching takes

place; this is often used to stop photochemical reactions. When studying photochemical reactions, it is important to take into consideration the aforementioned competing deactivation mechanisms.

Photodegradation reactions

The previously discussed chemical changes show specific reaction pathways that can occur during photochemical reactions. As previously discussed, when molecules are irradiated, they reach an excited state (eq. 1.1). From the excited state, an electron can be transferred to molecular dioxygen, which is naturally dissolved in water (eq. 1.2). The organic radical can also recombine with other radical species. Hydrolysis or homolysis of radical cation can form radicals (eq. 1.3) that react with oxygen radicals (eq. 1.4). The rate of photo-oxidation will thus depend on the concentration of dissolved oxygen [84]. Other possible photochemical reactions of the excited state include the abstraction of electron from an electron donor, energy transfer or deactivation.



Organic photochemical reactions show some particular mechanistic pathways because a significantly higher number of molecules will reach excited states compared to thermal reactions. These can go through an intermediate singlet or triplet state, leading to a wide range of reactions. Some previously described photochemical reaction mechanisms are isomerization, addition reactions, photo-oxidation, cyclization reactions, bond cleavage, intramolecular rearrangement, hydrogen abstraction, dehalogenation, photohydrolysis, decarboxylation [78]. Well described photochemical mechanisms are the Norrish reactions involving organic molecules with carbonyl groups [85]. Norrish type I reaction consists of photochemical cleavage of aldehydes and ketones. Here the homolytic cleavage of the bond occurs between the carbonyl group and the alpha carbon atom (Figure 1.2.5) [86].

A classic example of hydrogen abstraction is the Norrish type II reaction, typical for carbonyl compounds and consists of intramolecular hydrogen transfer (Figure 1.2.6) [86].

The well-studied Norrish reactions can appear as the “wood for the trees” to photochemistry specialists as these reactions suggest a good knowledge of the scientific community regarding the photodegradation of organic molecules. The truth is Norrish reactions are

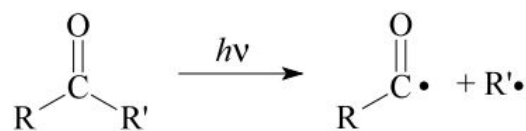


Figure 1.2.5: Norrish reaction type I

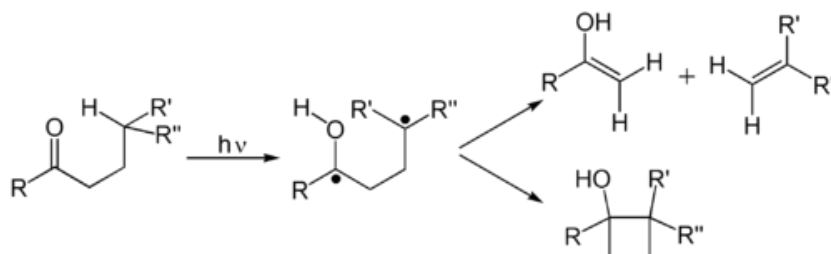


Figure 1.2.6: Norrish reaction type II

exceptions: most photochemical pathways occurring on mid- and big-size systems are less or not known at all, and most importantly, they are currently not predictable. This will be discussed in more detail in chapters 3 and 4.

1.2.2 Photolysis of contaminants

Direct photolysis of contaminants

The photochemical fate of contaminants is of high interest, both due to natural environmental processes involving photo-induced transformations by sunlight and the application of UV-light for disinfection and degradation of contaminants in water treatment.

The photodegradation of various emerging contaminants under natural sunlight has been previously investigated. Direct photolysis proved to be efficient for the degradation of, inter alia, non-steroidal anti-inflammatory drugs, endocrine disrupting chemicals, fluoroquinolone antibiotics, and disinfection by-products [87–89].

For water treatment, a variety of photodegradation studies were performed under laboratory, pilot plant, and industrial conditions. The wavelength of irradiation will highly influence the photodegradation efficiency and the phototransformation pathways. Irradiation with a germicidal Hg lamp in the short wave UV-C region (254 nm) was widely investigated due to its high energy and the absorption of light by many molecules at this wavelength. Efficient removal of pharmaceuticals, biocides, pesticides, corrosion inhibitors was achieved [90–95]. A number of these studies were conducted on the pilot plant level. On an industrial scale, most of the UV systems are used for disinfection, as they reduce microbiological growth in water through DNA damaging.

As the carbon-halogen bond, especially C-F, is very strong, high energies are needed to

break them down. Perfluorinated molecules represent an important class of highly persistent emerging contaminants, and it was shown that using Vacuum UV process can cause the defluorination of these compounds [96]. This process consists of a light source emitting at wavelengths below 200 nm. Water absorbs in this region, which causes its homolysis and photochemical ionization, thus generating hydroxyl radicals that can further react with the contaminants [97]. Since oxygen strongly absorbs in this region, the reactions have to be conducted under vacuum or non-absorbing gases [84]. Because of this general absorption, only smaller volumes of water can be treated at a time, so its application is not widespread on the industrial scale.

Medium pressure Hg arcs provide polychromatic irradiation that emit between 254 and 400 nm [98]. They can cause electronic transitions in a large number of organic pollutants. The induced chemical reactions include fragmentation reactions, rearrangements, and electron-transfer reactions [84]. The removal of antibiotics and endocrine disrupting chemicals was carried out using these light sources [99–101].

A considerable percentage of the studies discuss not only the removal efficiency but also the photodegradation mechanisms and formation of photoproducts. Based on our group's experience and the existing literature, it can be said that photochemical reactions are very complex. Due to the wide variety of possible activation/deactivation mechanisms, a large number of possible activation sites within the same molecule, the external parameters, such as irradiation wavelength, presence of reactive species, catalyst, pH value, type of the solvent and matrix components, it is arduous to find a comprehensive overview on photochemical reactions. For example, a study carried out on fluoroquinolones showed that, while direct irradiation caused fluorine substitution and reductive elimination, the presence of photocatalyst caused oxidative degradation [88]. Some theoretical photochemistry studies include performing the reaction in other solvents, such as acetonitrile. In such instances, the purpose is to either achieve higher solubility of the parent molecule or study the effect of various concentrations of dissolved oxygen, which differs from solvent to solvent. Furthermore, it has been demonstrated that the hydrogen donor character of the solvent plays a strong role in the degradation pathways involved in the process [102].

Our working group's long-term aim is to acquire sufficient expertise to predict the outcome of photodegradation reactions for individual compounds. This includes the determination of degradation kinetics and elucidation of the structures of photoproducts. An example of a common mechanism is the primary homolysis of a carbon-halogen bond. UV photolysis is used to eliminate chlorinated aromatics, and it was shown that the mineralization of organic chlorides to chloride ions occurs at 254 nm [103]. This mechanism was observed by our group in the case of the photolysis of chlorine-containing pesticides, where dehalogenation was a primary step [104]. However, a recent study about the photodegradation of boscalid fungicide contradicted these observations, as most of the photoproducts con-

served at least one of the chloride atoms on the aromatic ring [105]. This shows that despite ambitions to predict photodegradation pathways based on the molecular structures accurately, photochemical reactions' complexity makes this a great challenge.

The nature of photoproducts

When organic molecules are irradiated, they rarely reach mineralization unless harsh reaction conditions are applied. Instead, these processes lead to the formation of phototransformation products. Many studies indicate that these can be more toxic and persistent than the parent compound [106]. This phenomenon is known as photo-induced or –enhanced toxicity and it can occur during direct photolysis and advanced oxidation processes. It was previously shown that some of the photoproducts of aromatic hydrocarbons, pesticides, biocides exhibit higher potential toxicity than the parent molecule [92, 107, 108]. *In silico* and *in vitro* toxicity testing are powerful tools to show their potential toxic effects [104, 109]. Besides inducing toxicity, other potentially dangerous processes were described, such as forming antibacterially active transformation products that can induce antibiotic resistance [110]. It was also demonstrated that if chlorination is applied, the additional UV/H₂O₂ treatment can further increase the disinfection by-product formation [111]. It is important to understand the structures of these photoproducts to be able to perform risk assessment.

Often these photoproducts are in low concentration and might be under detection limits; thus, high-performance analytical instruments are required to detect them. On the other hand, expertise in non-targeted analysis and structural elucidation based on mass spectrometry is needed, which can pose great scientific challenges and is time-consuming [112]. The lack of standards for photoproducts also makes it difficult to confirm structures. Figure 1.2.7 shows proposed confidence levels of identification for unknown compounds, based on analytical data, such as exact molecular formula, retention time matching, mass spectrometry fragmentation patterns. In the present work, most of the structures proposed are highly probable structures. For some of them for which reference standards were available, or the suspect compounds were synthesized for reference, the confirmation of the exact structure was achieved. Our laboratory group greatly contributed to the understanding of photochemical degradation mechanisms of contaminants of emerging concern and assessment of their potential toxicity. However, there are recommendations to reduce further the knowledge gap, including the development of photodegradation reaction study protocols, prioritization of data generation for known toxic photoproducts, and performing more toxicity testing.

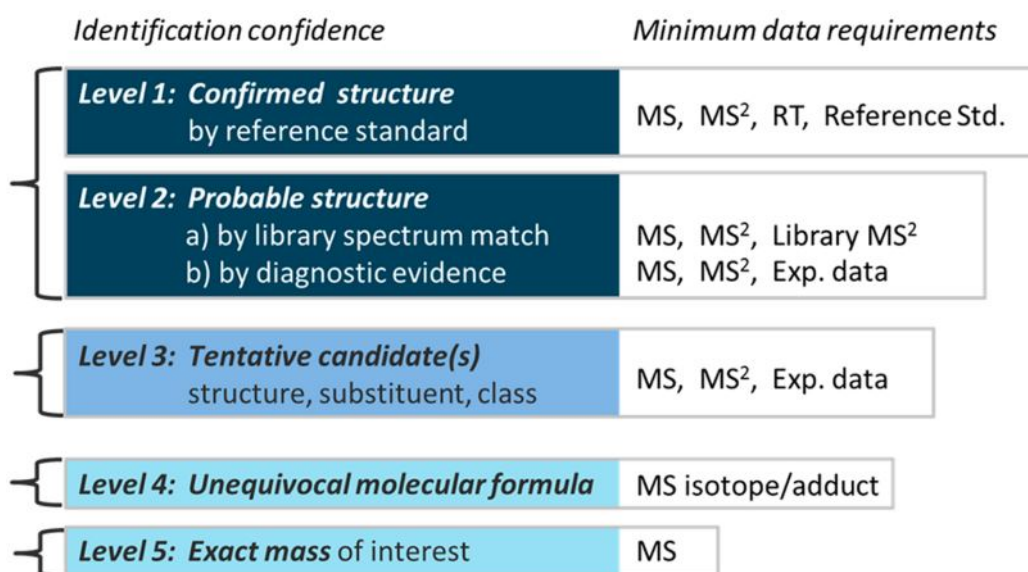


Figure 1.2.7: Proposed levels of identification [113]

Matrix effect

Several studies are carried out on laboratory scale in ultrapure water; this, however, does not accurately reflect the processes that occur in the environment or wastewater treatment. The main reason is related to the complexity of the matrix the reactions take place in. In a natural environment, many components can either enhance, hinder or even modify the photochemical reactions of the contaminants present in water.

Natural organic matter (NOM) is an important part of the mixture; it consists of various organic compounds present in all types of freshwater. NOM encompasses a wide range of compounds from aliphatic to aromatic, including phenolic structures, conjugated double bonds, nitrogenous compounds, proteins, sugars. Hydrophobic acids represent a large part of NOM; they are called humic substances and represent half of the dissolved organic matter [114, 115]. Other water components that can influence photochemical reactions include inorganic ions and metals. They can lead to indirect chemical reactions induced by reactive species such as, for example, carbonate radicals or chromophoric organic species in triplet state. This phenomenon referred to as “photosensitization,” can improve the degradation of contaminants.

On the other hand, dissolved organic matter and carbonate ions can scavenge hydroxyl radicals [116]. In denitrified water, nitrite can also act as an $\cdot\text{OH}$ scavenger [117]. NOM can also have a filtering effect during irradiation reactions. These processes will all reduce the efficiency of photodegradation reactions. A worrying aspect of the presence of NOM in water during treatment processes is that it can increase the formation of harmful disinfection by-products [118]. Thus, it is important to characterize the water matrix, to understand the natural environmental processes and achieve efficient water treatment.

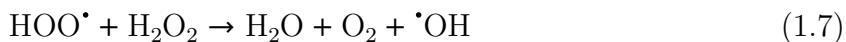
1.2.3 Advanced oxidation processes

As pioneers of advanced oxidation processes, Glaze et al. defined them as processes involving free radical formation at considerable quantities to improve water treatment [119]. Free radicals contain one or more unpaired electrons, such as superoxide radical ($\cdot\text{O}_2^-$), hydroperoxyl radical ($\text{HO}_2\cdot$), hydroxyl radical ($\cdot\text{OH}$), peroxy radical ($\text{ROO}\cdot$) and alkoxy radical ($\text{RO}\cdot$) [120]. The hydroxyl radical is one of the strongest oxidizing agents; it represents the basis of these AOPs due to its favourable properties, like high reactivity and low selectivity. It reacts with organic compounds at high rates, and the reaction is usually controlled by diffusion. Furthermore, $\cdot\text{OH}$ is naturally present in the environment as a result of solar irradiation of chromophoric dissolved organic matter, dissolved metals, nitrate, and nitrite ions [121].

Advanced oxidation processes are coupled techniques that involve an irradiation source, for instance, UV-Vis irradiation or vacuum-UV radiation, and a chemical or physical system, like peroxide, Fe(II), Fe(III), ozone, or a photocatalyst. These techniques can be used alone or in combination [121]. Besides processes involving $\cdot\text{OH}$, other viable techniques are persulfate-based and electrochemical AOPs [122, 123]. This literature review will focus on the description of photocatalysis/UV, peroxide/UV, and Fenton/photo-Fenton processes, as these were the techniques used throughout the project.

Hydroxyl radical generation

One of the ways to achieve the efficient formation of hydroxyl radicals, hydrogen peroxide has to be activated by UV light, metals, catalysts, or ozone. The activation can occur through homogeneous or heterogeneous processes. Hydrogen peroxide interacts with light in the wavelength range of 185- 400 nm, with the highest yields in the range of 200 – 280 nm; therefore UV irradiation is an efficient method of activation [124]. Upon radiation, the $\cdot\text{OH}$ are formed through the cleavage of the oxygen – oxygen bond (eq. 1.5); they react in an aqueous medium as presented below (eq. 1.6 to 1.8) [125]:



Another widely studied way to produce hydroxyl radicals is through photocatalysis. TiO_2

is the most widely used material due to its mechanical, chemical, and thermal stability, commercial availability, high photocatalytic activity, bandgap properties, non-toxicity, and low price [126]. In this method, irradiation of the photocatalyst causes an electron's ejection from the valence to the conduction band (Figure 1.2.8). The energy of irradiation has to be equal to or higher than the energy of the bandgap, therefore, a suitable wavelength is needed. Before the phenomenon of recombination of holes and electrons, these charge carriers cause charge transfer reactions at the surface of the catalyst. The valence band hole (h^+) has a high redox potential and oxidizes water, thus generating hydroxyl radicals. This phenomenon can also directly oxidize organic compounds. Conversely, the electrons from the conduction band have the ability to reduce compounds, and oxygen usually acts as electron scavenger. This can further produce hydroxyl radicals [127].

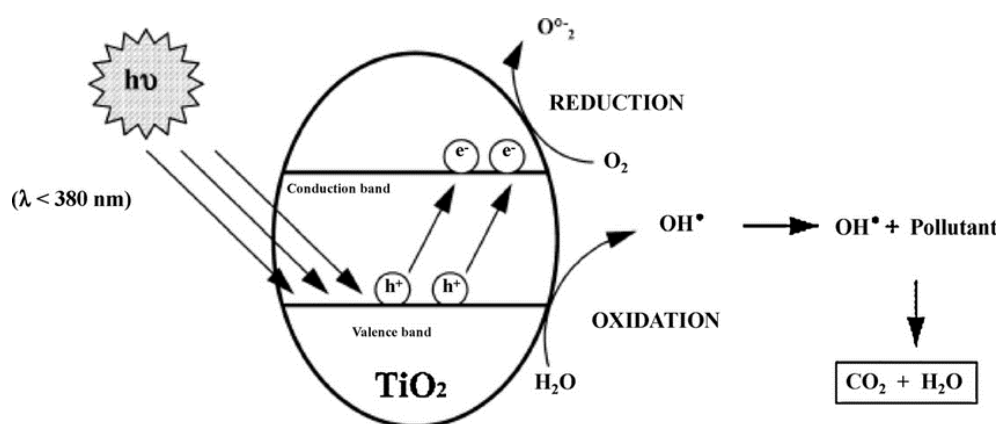
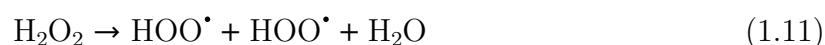
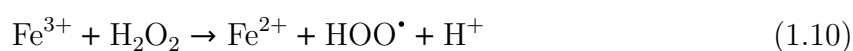
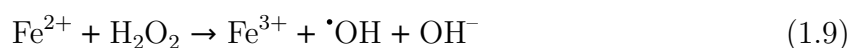


Figure 1.2.8: Mechanism of hydroxyl radical generation by photocatalysis [126]

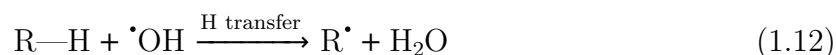
The ability of iron combined with H₂O₂ to oxidize organic molecules was first described in 1893 by H.J.H Fenton [128]. Due to the subsequent generation of hydroxyl radicals, it gained popularity in the field of water treatment. In the Fenton reaction, iron(II) (typically in the form of FeSO₄) acts as a catalyst and is oxidized by H₂O₂ to form iron(III), a hydroxyl ion, and the desired hydroxyl radical; iron(III) is then reduced back to iron(II) in addition to the formation of hydroperoxyl radical and a proton (eq. 1.9 to 1.11). The pH of the solution has to be acidic, the best operating condition being around pH 3; at higher pH values, the iron will precipitate in the form of Fe(OH)₃ [129].



Compared to the dark Fenton reaction, the photo-Fenton reaction shows an improvement in the efficiency of degradation of organic compounds. Three parallel processes explain the mechanism of this increased reaction rate: the light-induced H_2O_2 photolysis, the reduction of Fe(III) to Fe(II) with simultaneous hydroxyl radical production, and the direct activation of the organic molecules by radiation [130].

Reaction of hydroxyl radical with organic compounds

The hydroxyl radical can react with the organic compounds, initiate a radical chain reaction, or recombine with other species. The activation of organic compounds by the hydroxyl radical occurs through hydrogen atom abstraction or electron abstraction, where the radical acts as an electrophile (eq. 1.13 and 1.12) [131, 132]. Electron transfer reactions are not very common, as they occur mainly with easily oxidizable organic molecules. Furthermore, the reaction step after the formation of an organic radical is often the subtraction of a hydrogen atom to reach a more stable form. Direct hydrogen abstraction results in a more stable radical through lower activation energy and a more favourable pathway; therefore, this is the main reaction of hydroxyl radical with aliphatic compounds and carboxylic acids. The organic radical can react with dissolved oxygen or another hydroxyl radical. On the other hand, ground state organic molecules do not react readily with dissolved oxygen [121, 132, 133]. Due to these possible reaction pathways, it is interesting to characterize the water in terms of dissolved oxygen concentration. Moreover, mechanistic studies of photochemical reactions are often performed in different solvents, or water under oxygen-rich and oxygen-poor conditions. For example, the solubility of oxygen in acetonitrile is 8-fold higher than in water [134]. As a consequence, photoproducts may differ depending on which medium is used for irradiation; acetonitrile will promote mechanisms involving dissolved O_2 while water will more likely promote direct mechanisms.



Molecules with unsaturated bonds, such as alkenes and aromatic compounds, undergo $\cdot\text{OH}$ addition to the double bond. In the case of an aromatic compound, this addition leads to many isomeric transformation products (Figure 1.2.9) [135]. After the addition reaction, different reactions can occur, such as substitution reactions, addition of O_2 , and reduction (Figure 1.2.10) [132]. Hydroxyl radicals in the reaction mixtures will further complicate the photodegradation mechanisms and possibly yield a greater variety of photoproducts. This is evidenced by results presented in this work, reflected by the photodegradation of

enrofloxacin and maprotiline by AOPs.

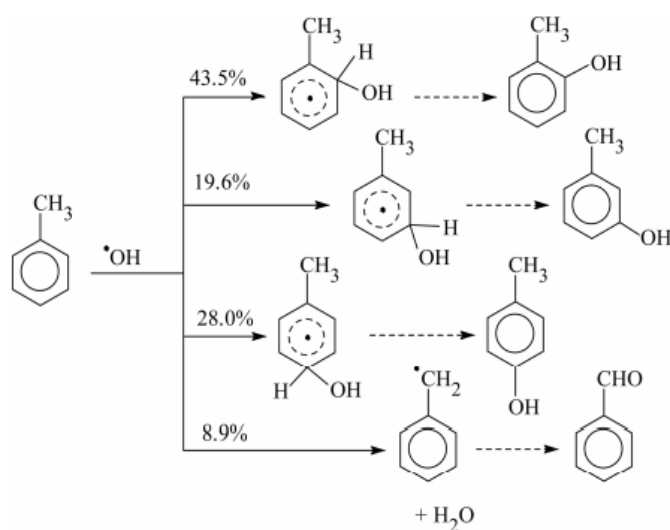


Figure 1.2.9: Possible hydroxylation sites of toluene and their probability, based on quantum mechanical calculations and experimental data

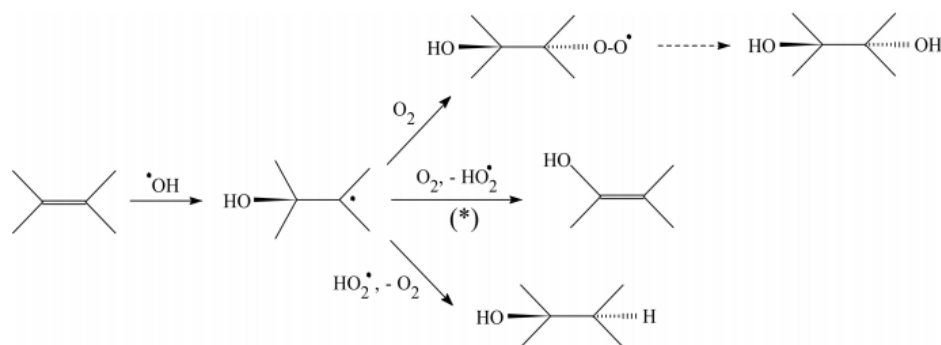


Figure 1.2.10: Subsequent reaction mechanisms after the addition of hydroxyl radical onto a double bond

1.2.4 Applications and limitations of AOPs

On the laboratory scale, AOPs are an efficient way to remove contaminants of emerging concern, and examples of studies will be presented in this section. However, scaling up the processes can present several technical issues that will also briefly be discussed.

The UV/peroxide method was successfully applied to remove volatile organic compounds [136] and contaminants of emerging concern (pharmaceuticals, herbicides, insecticides), where it presented a significant improvement in comparison with direct photolysis [137–139]. The application of this method was successful for the disinfection and the removal of natural organic matter in seawater [140]. The molar extinction coefficient of hydrogen peroxide is quite low ($19.6 \text{ M}^{-1} \text{ s}^{-1}$) at 254 nm [119]. This poses applicability issues of the

method on the industrial scale as it requires long irradiation times or a high dose of hydrogen peroxide. The reaction can be improved by exposure to lower wavelength radiation or by altering the pH, which was shown to impact the molar absorption coefficient [141]. It is important to note that increasing the dose of H_2O_2 can yield to filtering effect, meaning that the incidence of direct photolysis of contaminants will decrease, and the scavenging of hydroxyl radicals by peroxide will increase [142].

There are thousands of studies revolving around the photocatalytic degradation of pollutants. As previously mentioned, the most common catalyst is TiO_2 , but other catalysts are being developed and employed to improve the reaction rates and applicabilities, for example, ZnO , WO_3 , MgO , CdS , Fe_2O_3 , CaBi_2O_4 [143, 144]. The requirements for these materials are stability, inertness, photoactivity, low cost, and non-toxicity. One of the aims of the development of novel photocatalysts is to decrease the bandgap energy. As TiO_2 has a relatively high bandgap energy (3.2 eV), light sources above 400 nm do not interact with it, limiting its application in the visible region (380–700 nm) [144]. Nevertheless, TiO_2 remains one of the cheapest catalysts, which is of major importance considering water treatment at the industrial scale.

Photocatalysis is widely applied on the laboratory scale and shows success in the degradation of various contaminants of emerging concern: pesticides [145, 146], phenolic pollutants [147, 148], pharmaceuticals [145, 149, 150]. Notable efforts are made at Plataforma Solar de Almería (Spain), one of the partner institutes of the AQUAlity project, for the upscaling of photocatalysis and photo-Fenton reactions. They developed pilot plant prototypes for the degradation of contaminants of emerging concern using solar light activation, thus making it an affordable and sustainable option [151].

The limitations of catalyst application are related to the adsorption of compounds on the surface of the catalyst [152]. On the one hand, pollutants have to adsorb on the catalyst to interact with short-lived hydroxyl radicals forming on their surface. On the other hand, carbonate ions and natural organic matter can adsorb on the catalyst and reduce the availability of active sites for the degradation of pollutants and acting as radical scavengers [153]. Adsorption is pH-dependent and differs from molecule to molecule [127]. The pH value also influences the charge on the catalyst, and any variation in the pH impacts the oxidation performance [154]. Another issue related to the water matrix is the filtering effect that affects all the AOPs. When designing the process, it is important to consider the composition and pH of the water and its variability.

Photo-Fenton reaction operates up to a wavelength of 600 nm; this makes it applicable with solar light, thus making it a sustainable option in terms of energy use. The degradation of pesticides [155–157], pharmaceuticals [158–161], and bisphenol A [162] was achieved with a satisfactory efficiency (50 - 100% removal depending on the compound). In terms of contaminants degradation efficiency, photo-Fenton proved to be a superior method to

TiO₂ photocatalysis when applied under realistic conditions in wastewater matrix in pilot plants [163, 164]. However, the biggest technical issue of photo-Fenton reaction is that the reaction medium has to be at acidic pH (around pH value of 3), and pH rectification is costly. To overcome this, photo-Fenton processes at circumneutral pH are a feasible option, and they work by the addition of chelating agents [165]. The presence of ions in water also affects the Fe(II)/Fe(III) equilibrium [154].

Another aspect to consider is the reuse of the catalyst. First of all, the recovery of the catalyst is easier when heterogeneous catalysis is applied. When catalyst particles are in solution, especially in the form of nanoparticles, their recovery can pose problems, although novel solutions are suggested, such as their suspension on magnetic particles and recovery by using magnets [166]. The use of magnetic photocatalysts and peroxide/UV treatment in a pilot plant will be presented in chapter 4 in the framework of the work performed during the secondment at FACSA (Spain).

Ultimately, the goal is to find cost-effective solutions applicable on industrial scales to eliminate contaminants of emerging concern from water. This results in improved drinking water quality and the safe reuse of water, thus protecting the environment, improving human health and achieving sustainability goals.

References

- [1] V Dulio, B van Bavel, E Brorström-Lundén, J Harmsen, J Hollander, M Schlabach, J Slobodnik, K Thomas, and J Koschorreck. “Emerging pollutants in the EU : 10 years of NORMAN in support of environmental policies and regulations”. In: *Environ Sci Eur* 30.5 (2018). DOI: 10.1186/s12302-018-0135-3.
- [2] KY Bell, MJM Wells, KA Traexler, M Pellegrin, A Morse, and J Bandy. “Emerging Pollutants”. In: *Water Environ Res* 83.10 (2011), pp. 1906–1984. DOI: 10.2175/106143011X13075599870298.
- [3] G Vandermeersch, HM Lourenço, D Alvarez-Muñoz, S Cunha, J Diogène, G Cano-Sancho, JJ Sloth, C Kwadijk, D Barcelo, W Allegaert, K Bekaert, JO Fernandes, A Marques, and J Robbens. “Environmental contaminants of emerging concern in seafood–European database on contaminant levels”. In: *Environ Res* 143.Pt B (2015), pp. 29–45. DOI: 10.1016/j.envres.2015.06.011.
- [4] MCVM Starling, CC Amorim, and MMD Leão. “Occurrence, control and fate of contaminants of emerging concern in environmental compartments in Brazil”. In: *J Hazard Mater* 372 (2019), pp. 17–36. DOI: 10.1016/j.jhazmat.2018.04.043.
- [5] C Qi, J Huang, B Wang, S Deng, Y Wang, and G Yu. “Contaminants of emerging concern in landfill leachate in China: A review”. In: *Emerg Contam* 4.1 (2018), pp. 1–10. DOI: 10.1016/j.emcon.2018.06.001.
- [6] KA Maruya, NG Dodder, A Sengupta, DJ Smith, JM Lyons, AT Heil, and JE Drewes. “Multimedia screening of contaminants of emerging concern (CECS) in coastal urban watersheds in southern California (USA)”. In: *Environ Toxicol Chem* 35.8 (2016), pp. 1986–1994. DOI: 10.1002/etc.3348.
- [7] RP Schwarzenbach, BI Escher, K Fenner, TB Hofstetter, CA Johnson, U Gunten, and B Wehrli. “The challenge of micropollutants in aquatic systems”. In: *Science* 313.5790 (2006), pp. 1072–1077. DOI: 10.1126/science.1127291.
- [8] MJ Focazio, DW Kolpin, KK Barnes, ET Furlong, MT Meyer, SD Zaugg, LB Barber, and ME Thurman. “A national reconnaissance for pharmaceuticals and other organic wastewater contaminants in the United States–II) untreated drinking water sources”. In: *Sci Total Environ* 402.2-3 (2008), pp. 201–216. DOI: 10.1016/j.scitotenv.2008.02.021.
- [9] R Loos, BM Gawlik, G Locoro, E Rimaviciute, S Contini, and G Bidoglio. “EU-wide survey of polar organic persistent pollutants in European river waters”. In: *Environ Pollut* 157.2 (2009), pp. 561–568. DOI: 10.1016/j.envpol.2008.09.020.

- [10] Network of reference laboratories research centres and related organisations for monitoring of emerging environmental substances (NORMAN Association). *Emerging substances. Why do we need to address emerging substances?* 2016. URL: <https://www.norman-network.net/?q=node/19>.
- [11] NS Thomaidis, AG Asimakopoulos, and AA Bletsou. “Emerging contaminants: A tutorial mini-review”. In: *Glob NEST* 14.1 (2012), pp. 72–79. DOI: 10.30955/gnj.000823.
- [12] SD Richardson and TA Ternes. “Water Analysis : Emerging Contaminants and Current Issues”. In: *Anal Chem* 83.12 (2011), pp. 4614–4648. DOI: 10.1021/ac200915r.
- [13] S Sauvé and M Desrosiers. “A review of what is an emerging contaminant”. In: *Chem Cent J* 8.15 (2014). DOI: 10.1186/1752-153X-8-15.
- [14] K Kozawa, Y Aoyama, S Mashimo, and H Kimura. “Toxicity and actual regulation of organophosphate pesticides”. In: *Toxin Reviews* 28.4 (2009), pp. 245–254. DOI: 10.3109/15569540903297808.
- [15] F Sgolastra, P Medrzycki, L Bortolotti, S Maini, C Porrini, N Simon-Delso, and J Bosch. “Bees and pesticide regulation: Lessons from the neonicotinoid experience”. In: *Biol Conserv* 241 (2020), p. 108356. DOI: 10.1016/j.biocon.2019.108356.
- [16] A Szekacs and B Darvas. “Re-registration Challenges of Glyphosate in the European Union”. In: *Front Environ Sci* 6.78 (2018). DOI: 10.3389/fenvs.2018.00078.
- [17] SD Richardson. “Environmental Mass Spectrometry: Emerging Contaminants and Current Issues”. In: *Anal Chem* 74.12 (2002), pp. 2719–2742. DOI: 10.1021/ac020211h.
- [18] SD Richardson and TA Ternes. “Water analysis: emerging contaminants and current issues”. In: *Anal Chem* 77.12 (2005), pp. 3807–3838. DOI: 10.1021/ac058022x.
- [19] EJ Routledge, D Sheahan, C Desbrow, GC Brighty, M Waldock, and JP Sumpter. “Identification of Estrogenic Chemicals in STW Effluent. 2. In Vivo Responses in Trout and Roach”. In: *Environ Sci Technol* 32.11 (1998), pp. 1559–1565. DOI: 10.1021/es970796a.
- [20] R Triebkorn, H Casper, A Heyd, R Eikemper, HR Köhler, and J Schwaiger. “Toxic effects of the non-steroidal anti-inflammatory drug diclofenac. Part II: cytological effects in liver, kidney, gills and intestine of rainbow trout (*Oncorhynchus mykiss*)”. In: *Aquat Toxicol* 68.2 (2004), pp. 151–166. DOI: 10.1016/j.aquatox.2004.03.015.

- [21] R-L Bachour, O Golovko, M Kellner, and J Pohl. “Behavioral effects of citalopram, tramadol, and binary mixture in zebrafish (*Danio rerio*) larvae”. In: *Chemosphere* 238 (2020), p. 124587. DOI: 10.1016/j.chemosphere.2019.124587.
- [22] SD Richardson and SY Kimura. “Water Analysis: Emerging Contaminants and Current Issues”. In: *Anal Chem* 88.1 (2016), pp. 546–582. DOI: 10.1021/acs.analchem.5b04493.
- [23] SD Richardson and S Kimura. “Water Analysis: Emerging Contaminants and Current Issues”. In: *Anal Chem* 92.1 (2020), pp. 473–505. DOI: 10.1021/acs.analchem.9b05269.
- [24] *Directive 2000/60/EC of the European Parliament and of the Council*. 2000. URL: <https://eur-lex.europa.eu/legal-content/en/ALL/?uri=CELEX%3A32000L0060>.
- [25] *Decision No 2455/2001/EC of the European Parliament and of the Council*. 2001. URL: <https://eur-lex.europa.eu/legal-content/EN/TXT/?uri=CELEX%3A32001D2455>.
- [26] *Directive 2008/105/EC of the European Parliament and of the Council*. 2008. URL: <https://eur-lex.europa.eu/legal-content/EN/ALL/?uri=CELEX%3A32008L0105>.
- [27] *Directive 2013/39/EU of the European Parliament and of the Council*. 2013. URL: <https://eur-lex.europa.eu/legal-content/EN/ALL/?uri=CELEX%3A32013L0039>.
- [28] RN Carvalho, L Ceriani, and A Ippolito. *Development of the first Watch List under the Environmental Quality Standards Directive water policy*. EC - JRC Technical Report, 2015. DOI: 10.2788/238541.
- [29] *European Union Strategic Approach to Pharmaceuticals in the Environment*. 2019. URL: <https://eur-lex.europa.eu/legal-content/EN/ALL/?uri=COM:2019:128:FIN>.
- [30] *Registration, Evaluation, Authorisation and Restriction of Chemicals (REACH)*. 2007. URL: <https://echa.europa.eu/regulations/reach/understanding-reach>.
- [31] Ministry of Health. *Arrêté du 11 janvier 2007 relatif aux limites et références de qualité des eaux brutes et des eaux destinées à la consommation humaine mentionnées aux articles R. 1321-2, R. 1321-3, R. 1321-7 et R. 1321-38 du code de la santé publique*. 2007. URL: <https://www.legifrance.gouv.fr/loda/id/JORFTEXT000000465574/>.

- [32] *Contaminants of Emerging Concern in Urban Wastewater Joint NORMAN and Water Europe Position Paper*. 2019. URL: https://www.normandata.eu/sites/default/files/files/Publications/Position%20paper_CECs%20UWW-NORMAN_WE_2019_Final_20190910_public.pdf.
- [33] Network of reference laboratories research centres and related organisations for monitoring of emerging environmental substances (NORMAN Association). *Prioritisation of emerging substances in groundwater*. 2009. URL: <https://www.norman-network.net/?q=node/50>.
- [34] V Dulio and PC von der Ohe. *NORMAN Prioritisation Framework for Emerging Substances*. 2013. URL: https://www.norman-network.com/sites/default/files/norman_prioritisation_manual_15%20April2013_final_for_website.pdf.
- [35] R Marotta, D Spasiano, I Di Somma, and R Andreozzi. “Photodegradation of naproxen and its photoproducts in aqueous solution at 254 nm: a kinetic investigation”. In: *Water Res* 47.1 (2013), pp. 373–383. DOI: 10.1016/j.watres.2012.10.016.
- [36] JR Parsons, M Sáez, J Dolfing, and P de Voogt. “Biodegradation of perfluorinated compounds”. In: *Rev Environ Contam Toxicol* 196 (2008), pp. 53–71. DOI: 10.1007/978-0-387-78444-1_2.
- [37] S Posner. “Perfluorinated Compounds: Occurrence and Uses in Products”. In: *Polyfluorinated Chemicals and Transformation Products. The Handbook of Environmental Chemistry*. Ed. by Knepper T and Lange F. Vol. 17. Berlin, Heidelberg: Springer, 2012. DOI: 10.1007/978-3-642-21872-9_2.
- [38] *Commission Staff Working Document on Poly- and perfluoroalkyl substances (PFAS)*. 2020. URL: <https://op.europa.eu/en/publication-detail/-/publication/2614f1f2-0f02-11eb-bc07-01aa75ed71a1/language-en>.
- [39] SD Richardson and SY Kimura. “Emerging environmental contaminants: Challenges facing our next generation and potential engineering solutions”. In: *Environ Technol Innov* 8 (2017), pp. 40–56. DOI: 10.1016/j.eti.2017.04.002.
- [40] M Exner and H Färber. “Perfluorinated surfactants in surface and drinking waters”. In: *Environ Sci Pollut Res Int* 13.5 (2006), pp. 299–307. DOI: 10.1065/espr2006.07.326.
- [41] V Boiteux, X Dauchy, C Rosin, and J-F Munoz. “National Screening Study on 10 Perfluorinated Compounds in Raw and Treated Tap Water in France”. In: *Arch Environ Contam Toxicol* 63 (2012), pp. 1–12. DOI: 10.1007/s00244-012-9754-7.

- [42] CJAF Kwadijk, P Korytár, and AA Koelmans. “Distribution of Perfluorinated Compounds in Aquatic Systems in The Netherlands”. In: *Environ Sci Technol* 44.10 (2010), pp. 3746–3751. DOI: 10.1021/es100485e.
- [43] S Castiglioni, S Valsecchi, S Polesello, M Rusconi, M Melis, M Palmiotto, A Marnenti, E Davoli, and E Zuccato. “Sources and fate of perfluorinated compounds in the aqueous environment and in drinking water of a highly urbanized and industrialized area in Italy”. In: *J Hazard Mater* 282 (2015), pp. 51–60. DOI: 10.1016/j.jhazmat.2014.06.007.
- [44] P Rostkowski, S Taniyasu, N Yamashita, JJ Falandysz, Ł Zegarowski, A Chojnacka, K Pazdro, and J Falandysz. “Survey of perfluorinated compounds (PFCs) in surface waters of Poland”. In: *J Environ Sci Health A* 44.14 (2009), pp. 1518–1527. DOI: 10.1080/10934520903263330.
- [45] JL Domingo, I Ericson-Jogsten, G Perelló, M Nadal, B Van Bavel, and A Kärrman. “Human Exposure to Perfluorinated Compounds in Catalonia, Spain: Contribution of Drinking Water and Fish and Shellfish”. In: *J Agric Food Chem* 60.17 (2012), pp. 4408–4415. DOI: 10.1021/jf300355c.
- [46] M Llorca, M Farré, Y Picó, J Müller, TP Knepper, and D Barceló. “Analysis of perfluoroalkyl substances in waters from Germany and Spain”. In: *Sci Total Environ* 431 (2012), pp. 139–150. DOI: 10.1016/j.scitotenv.2012.05.011.
- [47] MS McLachlan, KE Holmström, M Reth, and U Berger. “Riverine Discharge of Perfluorinated Carboxylates from the European Continent”. In: *Environ Sci Technol* 41.21 (2007), pp. 7260–7265. DOI: 10.1021/es071471p.
- [48] J Hölzer, T Göen, P Just, R Reupert, K Rauchfuss, M Kraft, J Müller, and M Wilhelm. “Perfluorinated compounds in fish and blood of anglers at Lake Möhne, Sauerland area, Germany”. In: *Environ Sci Technol* 45.19 (2011), pp. 8046–8052. DOI: 10.1021/es104391z.
- [49] Y Pan, Y Shi, J Wang, Y Cai, and Y Wu. “Concentrations of perfluorinated compounds in human blood from twelve cities in China”. In: *Environ Toxicol Chem* 29.12 (2010), pp. 2695–2701. DOI: 10.1002/etc.342.
- [50] C Kubwabo, N Vais, and FM Benoit. “A pilot study on the determination of perfluorooctanesulfonate and other perfluorinated compounds in blood of Canadians”. In: *J Environ Monit* 6 (2004), pp. 540–545. DOI: 10.1039/b314085g.
- [51] L Tao, K Kannan, CM Wong, KF Arcaro, and JL Butenhoff. “Perfluorinated compounds in human milk from Massachusetts, U.S.A”. In: *Environ Sci Technol* 42.8 (2008), pp. 3096–3101. DOI: 10.1021/es702789k.

- [52] P Grandjean and R Clapp. “Changing interpretation of human health risks from perfluorinated compounds”. In: *Public Health Rep* 129.6 (2014), pp. 482–485. DOI: 10.1177/003335491412900605.
- [53] K Steenland, T Fletcher, and DA Savitz. “Epidemiologic evidence on the health effects of perfluorooctanoic acid (PFOA)”. In: *Environ Health Perspect* 118.8 (2010), pp. 1100–1108. DOI: 10.1289/ehp.0901827.
- [54] S Liu, R Yang, N Yin, and F Faiola. “The short-chain perfluorinated compounds PFBS, PFHxS, PFBA and PFHxA, disrupt human mesenchymal stem cell self-renewal and adipogenic differentiation”. In: *J Environ Sci* 88 (2020), pp. 187–199. DOI: 10.1016/j.jes.2019.08.016.
- [55] T Stahl, D Mattern, and H Brunn. “Toxicology of perfluorinated compounds”. In: *Environ Sci Eur* 23.38 (2011). DOI: 10.1186/2190-4715-23-38.
- [56] *Regulation (EU) 2019/1021 of the European Parliament and of the Council of 20 June 2019 on Persistent Organic Pollutants*. 2019. URL: <https://eur-lex.europa.eu/legal-content/en/TXT/?uri=CELEX:32019R1021>.
- [57] *Directive 2013/39/EU of the European Parliament and of the Council of 12 August 2013 amending Directives 2000/60/EC and 2008/105/EC as regards priority substances in the field of water policy Text with EEA relevance*. 2013. URL: <https://eur-lex.europa.eu/legal-content/EN/ALL/?uri=CELEX%3A32013L0039>.
- [58] MF Rahman, S Peldszus, and WB Anderson. “Behaviour and fate of perfluoroalkyl and polyfluoroalkyl substances (PFASs) in drinking water treatment: a review”. In: *Water Res* 50 (2014), pp. 318–340. DOI: 10.1016/j.watres.2013.10.045.
- [59] J Chen, PY Zhang, and J Liu. “Photodegradation of perfluorooctanoic acid by 185 nm vacuum ultraviolet light”. In: *J Environ Sci* 19.4 (2007), pp. 387–390. DOI: 10.1016/s1001-0742(07)60064-3.
- [60] H Hori, E Hayakawa, H Einaga, S Kutsuna, K Koike, T Ibusuki, H Kiatagawa, and R Arakawa. “Decomposition of environmentally persistent perfluorooctanoic acid in water by photochemical approaches”. In: *Environ Sci Technol* 38.22 (2004), pp. 6118–6124. DOI: 10.1021/es049719n.
- [61] H Tang, Q Xiang, M Lei, J Yan, L Zhu, and J Zou. “Efficient degradation of perfluorooctanoic acid by UV–Fenton process”. In: *Chem Eng J* 184 (2012), pp. 156–162. DOI: 10.1016/j.cej.2012.01.020.
- [62] SD Richardson and TA Ternes. “Water Analysis: Emerging Contaminants and Current Issues”. In: *Anal Chem* 86.6 (2014), pp. 2813–2848. DOI: 10.1021/ac500508t.

- [63] A Cassini, LD Högberg, D Plachouras, A Quattrocchi, A Hoxha, GS Simonsen, M Colomb-Cotinat, ME Kretzschmar, B Devleeschauwer, M Cecchini, DA Ouakrim, TC Oliveira, MJ Struelens, C Suetens, and DL Monnet. “Attributable deaths and disability-adjusted life-years caused by infections with antibiotic-resistant bacteria in the EU and the European Economic Area in 2015: a population-level modelling analysis”. In: *Lancet Infect Dis* 19.1 (2019), pp. 56–66. DOI: 10.1016/S1473-3099(18)30605-4.
- [64] T Troughon and S Lefebvre. “A Review of Enrofloxacin for Veterinary Use”. In: *Open J Vet Med* 6.2 (2016), pp. 40–58. DOI: 10.4236/ojvm.2016.62006.
- [65] H Nakata, K Kannan, PD Jones, and JP Giesy. “Determination of fluoroquinolone antibiotics in wastewater effluents by liquid chromatography-mass spectrometry and fluorescence detection”. In: *Chemosphere* 58.6 (2005), pp. 759–766. DOI: 10.1016/j.chemosphere.2004.08.097.
- [66] EM Golet, AC Alder, and W Giger. “Environmental exposure and risk assessment of fluoroquinolone antibacterial agents in wastewater and river water of the Glatt Valley Watershed, Switzerland”. In: *Environ Sci Technol* 36.17 (2002), pp. 3645–3651. DOI: 10.1021/es0256212.
- [67] R Andreozzi, M Raffaele, and P Nicklas. “Pharmaceuticals in STP effluents and their solar photodegradation in aquatic environment”. In: *Chemosphere* 50.10 (2003), pp. 1319–1330. DOI: 10.1016/s0045-6535(02)00769-5.
- [68] R Wei, F Ge, M Chen, and R Wang. “Occurrence of ciprofloxacin, enrofloxacin, and florfenicol in animal wastewater and water resources”. In: *J Environ Qual* 41.5 (2012), pp. 1481–1486. DOI: 10.2134/jeq2012.0014.
- [69] Z Ye, HS Weinberg, and MT Meyer. “Trace analysis of trimethoprim and sulfonamide, macrolide, quinolone, and tetracycline antibiotics in chlorinated drinking water using liquid chromatography electrospray tandem mass spectrometry”. In: *Anal Chem* 79.3 (2007), pp. 1135–1144. DOI: 10.1021/ac060972a.
- [70] F Adachi, A Yamamoto, K Takakura, and R Kawahara. “Occurrence of fluoroquinolones and fluoroquinolone-resistance genes in the aquatic environment”. In: *Sci Total Environ* 444 (2013), pp. 508–514. DOI: 10.1016/j.scitotenv.2012.11.077.
- [71] DW Graham, S Olivares-Rieumont, CW Knapp, L Lima, D Werner, and E Bowen. “Antibiotic resistance gene abundances associated with waste discharges to the Almendares River near Havana, Cuba”. In: *Environ Sci Technol* 45.2 (2011), pp. 418–424. DOI: 10.1021/es102473z.

- [72] I Ebert, J Bachmann, U Kühnen, A Küster, C Kussatz, D Maletzki, and C Schlüter. “Toxicity of the fluoroquinolone antibiotics enrofloxacin and ciprofloxacin to photoautotrophic aquatic organisms”. In: *Environ Toxicol Chem* 30.12 (2011), pp. 2786–2792. DOI: 10.1002/etc.678.
- [73] L Migliore, S Cozzolino, and M Fiori. “Phytotoxicity to and uptake of enrofloxacin in crop plants”. In: *Chemosphere* 52.7 (2003), pp. 1233–1244. DOI: 10.1016/S0045-6535(03)00272-8.
- [74] M Sturini, A Speltini, F Maraschi, A Profumo, L Pretali, E Fasani, and A Albini. “Photochemical degradation of marbofloxacin and enrofloxacin in natural waters”. In: *Environ Sci Technol* 44.12 (2010), pp. 4564–4569. DOI: 10.1021/es100278n.
- [75] S Babić, M Periša, and I Škorić. “Photolytic degradation of norfloxacin, enrofloxacin and ciprofloxacin in various aqueous media.” In: *Chemosphere* 91.11 (2013), pp. 1635–1642. DOI: 10.1016/j.chemosphere.2012.12.072.
- [76] Y Li, J Niu, and W Wang. “Photolysis of Enrofloxacin in aqueous systems under simulated sunlight irradiation: Kinetics, mechanism and toxicity of photolysis products”. In: *Chemosphere* 85.5 (2011), pp. 892–897. DOI: 10.1016/j.chemosphere.2011.07.008.
- [77] H Guo, T Ke, N Gao, Y Liu, and X Cheng. “Enhanced degradation of aqueous norfloxacin and enrofloxacin by UV-activated persulfate: Kinetics, pathways and deactivation”. In: *Chem Eng J* 316 (2017), pp. 471–480. DOI: 10.1016/j.cej.2017.01.123.
- [78] JD Coyle. *Introduction to Organic Photochemistry*. Wiley, 1991. URL: <https://www.wiley.com/en-us/Introduction+to+Organic+Photochemistry-p-9780471909750>.
- [79] K Kahn and B Kirtman. *Description of Electronically Excited States*. 2012. URL: https://people.chem.ucsb.edu/kahn/kalju/chem126/public/elspect_theory.html.
- [80] DR Arnold, NC Baird, JR Bolton, JCD Brand, PWM Jacob, P de Mayo, and WR Ware. *Photochemistry: An Introduction*. New York - London: Academic Press, Inc, 1975. DOI: 10.1021/ed052pA218.1.
- [81] P Boule, DW Bahnemann, and P Robertson. *Environmental Photochemistry Part II*. Berlin Heidelberg: Springer-Verlag, 2005. DOI: 10.1007/b89482.
- [82] D Frackowiak. “The Jablonski diagram”. In: *J Photochem and Photobiol B Biol* 2.3 (1988), p. 399. DOI: 10.1016/1011-1344(88)85060-7.
- [83] L Critchley. *What is the Difference Between Fluorescence and Phosphorescence?* 2018. URL: <https://www.azooptics.com/Article.aspx?ArticleID=132>.

- [84] O Legrini, E Oliveros, and AM Braun. “Photochemical processes for water treatment”. In: *Chem Rev* 93.2 (1993), pp. 671–698. DOI: 10.1021/cr00018a003.
- [85] R Norrish and C Bamford. “Photo-decomposition of Aldehydes and Ketones”. In: *Nature* 140 (1937), pp. 195–196. DOI: 10.1038/140195b0.
- [86] T Laue and A Plagens. *Named Organic Reactions, 2nd Edition*. Wiley, 2005. DOI: 10.1002/0470010428.
- [87] E Koumaki, D Mamais, C Noutsopoulos, MC Nika, AA Bletsou, NS Thomaidis, A Eftaxias, and G Stratogianni. “Degradation of emerging contaminants from water under natural sunlight: The effect of season, pH, humic acids and nitrate and identification of photodegradation by-products”. In: *Chemosphere* 138 (2015), pp. 675–681. DOI: 10.1016/j.chemosphere.2015.07.033.
- [88] M Sturini, A Speltini, F Maraschi, A Profumo, L Pretali, EA Irastorza, E Fasani, and A Albini. “Photolytic and photocatalytic degradation of fluoroquinolones in untreated river water under natural sunlight”. In: *Appl Catal B Environ* 119–120 (2012), pp. 32–39. DOI: 10.1016/j.apcatb.2012.02.008.
- [89] I Abusallout and G Hua. “Photolytic dehalogenation of disinfection byproducts in water by natural sunlight irradiation”. In: *Chemosphere* 159 (2016), pp. 184–192. DOI: 10.1016/j.chemosphere.2016.05.090.
- [90] VJ Pereira, HS Weinberg, KG Linden, and PC Singer. “UV degradation kinetics and modeling of pharmaceutical compounds in laboratory grade and surface water via direct and indirect photolysis at 254 nm”. In: *Environ Sci Technol* 41.5 (2007), pp. 1682–1688. DOI: 10.1021/es061491b.
- [91] N De la Cruz, J Giménez, S Esplugas, D Grandjean, LF Alencastro, and C Pulgarín. “Degradation of 32 emergent contaminants by UV and neutral photo-fenton in domestic wastewater effluent previously treated by activated sludge”. In: *Water Res* 46.6 (2012), pp. 1947–1957. DOI: 10.1016/j.watres.2012.01.014.
- [92] Z Varga, E Nicol, and S Bouchonnet. “Photodegradation of benzisothiazolinone: Identification and biological activity of degradation products”. In: *Chemosphere* 240 (2020), p. 124862. DOI: 10.1016/j.chemosphere.2019.124862.
- [93] N Cazzaniga, Z Varga, E Nicol, and S Bouchonnet. “UV-visible photodegradation of naproxen in water - Structural elucidation of photoproducts and potential toxicity”. In: *Eur J Mass Spectrom* 26.6 (2020), pp. 400–408. DOI: 10.1177/1469066720973412.
- [94] N De la Cruz, L Esquius, D Grandjean, A Magnet, A Tungler, LF Alencastro, and C Pulgarín. “Degradation of emergent contaminants by UV, UV/H₂O₂ and neutral photo-Fenton at pilot scale in a domestic wastewater treatment plant”. In: *Water Res* 47.15 (2013), pp. 5836–5845. DOI: 10.1016/j.watres.2013.07.005.

- [95] M Zupanc, T Kosjek, M Petkovšek, M Dular, B Kompare, B Širok, Ž Blažeka, and E Heath. “Removal of pharmaceuticals from wastewater by biological processes, hydrodynamic cavitation and UV treatment”. In: *Ultrason Sonochem* 20.4 (2013), pp. 1104–1112. DOI: 10.1016/j.ultsonch.2012.12.003.
- [96] J Chen, P-Y Zhang, and J Liu. “Photodegradation of perfluorooctanoic acid by 185 nm vacuum ultraviolet light”. In: *J Environ Sci* 19.4 (2007), pp. 387–390. DOI: 10.1016/S1001-0742(07)60064-3.
- [97] K Zoschke, H Börnick, and E Worch. “Vacuum-UV radiation at 185 nm in water treatment – A review”. In: *Water Res* 52 (2014), pp. 131–145. DOI: 10.1016/j.watres.2013.12.034.
- [98] AM Braun, MT Maurette, and E Oliveros. *Photochemical technology*. Chichester: Wiley, 1991. DOI: 10.1002/ange.19921041147.
- [99] D Avisar, Y Lester, and H Mamane. “pH induced polychromatic UV treatment for the removal of a mixture of SMX, OTC and CIP from water”. In: *J Hazard Mater* 175.1-3 (2010), pp. 1068–1074. DOI: 10.1016/j.jhazmat.2009.10.122.
- [100] EJ Rosenfeldt and KG Linden. “Degradation of endocrine disrupting chemicals bisphenol A, ethinyl estradiol, and estradiol during UV photolysis and advanced oxidation processes”. In: *Environ Sci Technol* 38.20 (2004), pp. 5476–5483. DOI: 10.1021/es035413p.
- [101] C Zamy, P Mazellier, and B Legube. “Phototransformation of selected organophosphorus pesticides in dilute aqueous solutions”. In: *Water Res* 38.9 (2004), pp. 2305–2314. DOI: 10.1016/j.watres.2004.02.019.
- [102] S De Vaugelade, E Nicol, S Vujovic, S Bourcier, S Pirnay, and S Bouchonnet. “Ultraviolet–visible phototransformation of dehydroacetic acid – Structural characterization of photoproducts and global ecotoxicity”. In: *Rapid Commun Mass Spectrom* 32.11 (2018), pp. 862–870. DOI: 10.1002/rcm.8104.
- [103] S Guittonneau, J de Laat, M Dore, JP Duguet, and C Bonnel. “Etude comparative de la dégradation de quelques molécules aromatiques simples en solution aqueuse par photolyse UV et par photolyse du peroxyde d’hydrogene”. In: *Environ Technol Lett* 9.10 (1988), pp. 1115–1128. DOI: 10.1080/09593338809384673.
- [104] E Nicol, Z Varga, S Vujovic, and S Bouchonnet. “Laboratory scale UV-visible degradation of acetamiprid in aqueous marketed mixtures - Structural elucidation of photoproducts and toxicological consequences”. In: *Chemosphere* 248 (2020), p. 126040. DOI: 10.1016/j.chemosphere.2020.126040.

- [105] Y Lassalle, A Kinani, A Rifai, Y Souissi, C Clavaguera, S Bourcier, F Jaber, and S Bouchonnet. “UV-visible degradation of boscalid – structural characterization of photoproducts and potential toxicity using in silico tests”. In: *Rapid Commun Mass Spectrom* 28.10 (2014), pp. 1153–1163. DOI: 10.1002/rcm.6880.
- [106] AP Roberts, MM Alloy, and JT Oris. “Review of the photo-induced toxicity of environmental contaminants”. In: *Comp Biochem Physiol C Toxicol Pharmacol* 191 (2017), pp. 160–167. DOI: 10.1016/j.cbpc.2016.10.005.
- [107] DP Arfsten, DJ Schaeffer, and DC Mulveny. “The effects of near ultraviolet radiation on the toxic effects of polycyclic aromatic hydrocarbons in animals and plants: a review”. In: *Ecotoxicol Environ Saf* 33.1 (1996), pp. 1–24. DOI: 10.1006/eesa.1996.0001.
- [108] TP Wang, J Kagan, RW Tuveson, and GR Wang. “alpha-Terthienyl photosensitizes damage to pBR322 DNA”. In: *Photochem Photobiol* 53.4 (1991), pp. 463–467. DOI: 10.1111/j.1751-1097.1991.tb03657.x.
- [109] MA Lampi, J Gurska, KI McDonald, F Xie, XD Huang, DG Dixon, and BM Greenberg. “Photoinduced toxicity of polycyclic aromatic hydrocarbons to *Daphnia magna*: ultraviolet-mediated effects and the toxicity of polycyclic aromatic hydrocarbon photoproducts”. In: *Environ Toxicol Chem* 25.4 (2006), pp. 1079–1087. DOI: 10.1897/05-276r.1.
- [110] OS Keen and KG Linden. “Degradation of antibiotic activity during UV/H₂O₂ advanced oxidation and photolysis in wastewater effluent”. In: *Environ Sci Technol* 47.22 (2013), pp. 13020–13030. DOI: 10.1021/es402472x.
- [111] AD Dotson, OS Keen, D Metz, and KG Linden. “UV/H₂O₂ treatment of drinking water increases post-chlorination DBP formation”. In: *Water Res* 44.12 (2010), pp. 3703–3713. DOI: 10.1016/j.watres.2010.04.006.
- [112] D Vione and L Carena. “The Possible Production of Harmful Intermediates Is the ”Dark Side” Of the Environmental Photochemistry of Contaminants (Potentially Adverse Effects, And Many Knowledge Gaps)”. In: *Environ Sci Technol* 54.9 (2020), pp. 5328–5330. DOI: 10.1021/acs.est.0c01049.
- [113] EL Schymanski, J Jeon, R Gulde, K Fenner, M Ruff, HP Singer, and J Hollender. “Identifying small molecules via high resolution mass spectrometry: communicating confidence”. In: *Environ Sci Technol* 48.4 (2014), pp. 2097–2098. DOI: 10.1021/es5002105.
- [114] EM Thurman. *Organic geochemistry of natural waters*. Netherlands: Springer, 1985. DOI: 10.1007/978-94-009-5095-5.

- [115] J Swietlik, A Dabrowska, U Raczyk-Stanisławiak, and J Nawrocki. “Reactivity of natural organic matter fractions with chlorine dioxide and ozone”. In: *Water Res* 38.3 (2004), pp. 547–558. DOI: 10.1016/j.watres.2003.10.034.
- [116] IA Katsoyiannis, S Canonica, and U Gunten. “Efficiency and energy requirements for the transformation of organic micropollutants by ozone, O₃/H₂O₂ and UV/H₂O₂”. In: *Water Res* 45.13 (2011), pp. 3811–3822. DOI: 10.1016/j.watres.2011.04.038.
- [117] C Lee, J Yoon, and U Von Gunten. “Oxidative degradation of N-nitrosodimethylamine by conventional ozonation and the advanced oxidation process ozone/hydrogen peroxide”. In: *Water Res* 41.3 (2007), pp. 581–590. DOI: 10.1016/j.watres.2006.10.033.
- [118] JG Jacangelo, J DeMarco, DM Owen, and SJ Randtke. “Selected processes for removing NOM: an overview”. In: *J Am Water Work Assoc* 87.1 (1995), pp. 64–77. DOI: 10.1002/j.1551-8833.1995.tb06302.x.
- [119] WH Glaze, J-W Kang, and DH Chapin. “The Chemistry of Water Treatment Processes Involving Ozone, Hydrogen Peroxide and Ultraviolet Radiation”. In: *Ozone Sci Eng* 9.4 (1987), pp. 335–352. DOI: 10.1080/01919518708552148.
- [120] A Gomes, E Fernandes, and JL Lima. “Fluorescence probes used for detection of reactive oxygen species”. In: *J Biochem Biophys Methods* 65.2-3 (2005), pp. 45–80. DOI: 10.1016/j.jbbm.2005.10.003.
- [121] S Gligorovski, R Strekowski, S Barbati, and D Vione. “Environmental Implications of Hydroxyl Radicals (•)OH”. In: *Chem Rev* 115.24 (2015), pp. 13051–13092. DOI: 10.1021/cr500310b.
- [122] J Lee, U Gunten, and JH Kim. “Persulfate-Based Advanced Oxidation: Critical Assessment of Opportunities and Roadblocks”. In: *Environ Sci Technol* 54.6 (2020), pp. 3064–3081. DOI: 10.1021/acs.est.9b07082.
- [123] R Dewil, D Mantzavinos, I Poulios, and MA Rodrigo. “New perspectives for Advanced Oxidation Processes”. In: *J Environ Manage* 195.2 (2 2017), pp. 93–99. DOI: 10.1016/j.jenvman.2017.04.010.
- [124] PBL Chang and TM Young. “Kinetics of methyl tert-butyl ether degradation and by-product formation during UV/hydrogen peroxide water treatment”. In: *Water Res* 34.8 (2000), pp. 2233–2240. DOI: 10.1016/S0043-1354(99)00392-9.
- [125] N Clarke and G Knowles. “High purity water using H₂O₂ and UV radiation”. In: *Effluent Water Treat J* 23 (1982), pp. 335–341.

- [126] MY Ghaly, TS Jamil, IE El-Seesy, ER Souaya, and RA Nasr. “Treatment of highly polluted paper mill wastewater by solar photocatalytic oxidation with synthesized nano TiO₂”. In: *Chem Eng J* 168.1 (2011), pp. 446–454. DOI: 10.1016/j.cej.2011.01.028.
- [127] J Zhang, B Tian, L Wang, M Xing, and J Lei. “Mechanism of Photocatalysis”. In: *Photocatalysis*. Vol. 100. Singapore: Springer, 2018. DOI: 10.1007/978-981-13-2113-9_1.
- [128] HJH Fenton. “Oxidation of tartaric acid in presence of iron”. In: *J Chem Soc, Trans* 65 (1894), pp. 899–910. DOI: 10.1039/CT8946500899.
- [129] J De Laat and H Gallard. “Catalytic Decomposition of Hydrogen Peroxide by Fe(III) in Homogeneous Aqueous Solution: Mechanism and Kinetic Modeling”. In: *Environ Sci Technol* 33.16 (1999), pp. 2726–2732. DOI: 10.1021/es981171v.
- [130] G Ruppert, R Bauer, and G Heisler. “The photo-Fenton reaction — an effective photochemical wastewater treatment process”. In: *J Photochem Photobiol A Chem* 73.1 (1993), pp. 75–78. DOI: 10.1016/1010-6030(93)80035-8.
- [131] JH Baxendale and JA Wilson. “The photolysis of hydrogen peroxide at high light intensities”. In: *Trans Faraday Soc* 53 (1957), pp. 344–356. DOI: 10.1039/TF9575300344.
- [132] GV Buxton. “Critical Review of rate constants for reactions of hydrated electrons, hydrogen atoms and hydroxyl radicals (OH/O in Aqueous Solution)”. In: *J Phys Chem Ref Data* 17.2 (1988), pp. 513–886. DOI: 10.1063/1.555805.
- [133] AA Jr Krasnovsky. “Primary mechanisms of photoactivation of molecular oxygen. History of development and the modern status of research”. In: *Biochem (Moscow)* 72.10 (2007), pp. 1065–1080. DOI: 10.1134/s0006297907100057.
- [134] D Dvoranová, Z Barbieriková, and V Brezová. “Radical intermediates in photoinduced reactions on TiO₂ (an EPR spin trapping study)”. In: *Molecules* 19.11 (2014), pp. 17279–17304. DOI: 10.3390/molecules191117279.
- [135] A Hatipoglu, D Vione, Y Yalçın, C Minero, and Z Çınar. “Photo-oxidative degradation of toluene in aqueous media by hydroxyl radicals”. In: *J Photochem Photobiol A Chem* 215.1 (2010), pp. 59–68. DOI: 10.1016/j.jphotochem.2010.07.021.
- [136] G Liu, J Ji, H Huang, R Xie, Q Feng, Y Shu, Y Zhan, R Fang, M He, S Liu, X Ye, and DYC Leung. “UV/H₂O₂: An efficient aqueous advanced oxidation process for VOCs removal”. In: *Chem Eng J* 324 (2017), pp. 44–50. DOI: 10.1016/j.cej.2017.04.105.

- [137] Z Shu, M Bolton JR Belosevic, and MG El Din. “Photodegradation of emerging micropollutants using the medium-pressure UV/H₂O₂ Advanced Oxidation Process”. In: *Water Res* 47.8 (2013), pp. 2881–9. DOI: 10.1016/j.watres.2013.02.045.
- [138] OM Alfano, RJ Brandi, and AE Cassano. “Degradation kinetics of 2,4-D in water employing hydrogen peroxide and UV radiation”. In: *Chem Eng J* 82.1-3 (2001), pp. 209–218. DOI: 10.1016/S1385-8947(00)00358-2.
- [139] DW Sundstrom, B Weir, and H Klei. “Destruction of aromatic pollutants by UV light catalyzed oxidation with hydrogen peroxide”. In: *Environ Prog* 8.1 (1989), pp. 6–11. DOI: 10.1002/EP.3300080107.
- [140] Y Penru, AR Guastalli, S Esplugas, and S Baig. “Application of UV and UV/H₂O₂ to seawater: Disinfection and natural organic matter removal”. In: *J Photochem Photobiol A Chem* 233 (2012), pp. 40–45. DOI: 10.1016/j.jphotochem.2012.02.017.
- [141] M Pera-Titus, V Garcia-Molina, MA Baños, J Giménez, and S Esplugas. “Degradation of chlorophenols by means of advanced oxidation processes: a general review”. In: *Appl Catal B Environ* 47.4 (2004), pp. 219–256. DOI: 10.1016/j.apcatb.2003.09.010.
- [142] Y Lester, D Avisar, and H Mamane. “Photodegradation of the antibiotic sulphamethoxazole in water with UV/H₂O₂ advanced oxidation process”. In: *Environ Technol* 31.2 (2010), pp. 175–183. DOI: 10.1080/09593330903414238.
- [143] RA Al-Rasheed. “Water treatment by heterogeneous photocatalysis an overview”. In: *SWCC Acquired Experience Symposium*. Jeddah, 2005. URL: <https://www.semanticscholar.org/paper/WATER-TREATMENT-BY-HETEROGENEOUS-PHOTOCATALYSIS-AN-Al-Rasheed-Arabia/cf1d31a956c542769d46e886c79255fa4701e654>.
- [144] J Tang, Z Zou, and J Ye. “Efficient photocatalytic decomposition of organic contaminants over CaBi₂O₄ under visible-light irradiation”. In: *Angew Chem Int Ed* 43.34 (2004), pp. 4463–4466. DOI: 10.1002/anie.200353594.
- [145] N Miranda-García, S Suárez, B Sánchez, JM Coronado, S Malato, and M Ignacio Maldonado. “Photocatalytic degradation of emerging contaminants in municipal wastewater treatment plant effluents using immobilized TiO₂ in a solar pilot plant”. In: *Appl Catal B Environ* 103.3-4 (2011), pp. 294–301. DOI: 10.1016/j.apcatb.2011.01.030.
- [146] S Ahmed, MG Rasul, R Brown, and MA Hashib. “Influence of parameters on the heterogeneous photocatalytic degradation of pesticides and phenolic contaminants in wastewater: a short review”. In: *J Environ Manage* 92.3 (2011), pp. 311–330. DOI: 10.1016/j.jenvman.2010.08.028.

- [147] CM Teh and AR Mohamed. “Roles of titanium dioxide and ion-doped titanium dioxide on photocatalytic degradation of organic pollutants (phenolic compounds and dyes) in aqueous solutions: A review”. In: *J Alloys Compd* 509.5 (2011), pp. 1648–1660. DOI: 10.1016/j.jallcom.2010.10.181.
- [148] MP Blanco-Vega, JL Guzmán-Mar, M Villanueva-Rodríguez, L Maya-Treviño, LL Garza-Tovar, A Hernández-Ramírez, and L Hinojosa-Reyes. “Photocatalytic elimination of bisphenol A under visible light using Ni-doped TiO₂ synthesized by microwave assisted sol-gel method”. In: *Mater Sci Semicond Process* 71 (2017), pp. 275–282. DOI: 10.1016/j.mssp.2017.08.013.
- [149] F Méndez-Arriaga, S Esplugas, and J Giménez. “Photocatalytic degradation of non-steroidal anti-inflammatory drugs with TiO₂ and simulated solar irradiation”. In: *Water Res* 42.3 (2008), pp. 585–594. DOI: 10.1016/j.watres.2007.08.002.
- [150] L Hu, PM Flanders, PL Miller, and TJ Strathmann. “Oxidation of sulfamethoxazole and related antimicrobial agents by TiO₂ photocatalysis”. In: *Water Res* 41.12 (2007), pp. 2612–2626. DOI: 10.1016/j.watres.2007.02.026.
- [151] S Malato, MI Maldonado, P Fernández-Ibáñez, I Oller, I Polo, and R Sánchez-Moreno. “Decontamination and disinfection of water by solar photocatalysis: The pilot plants of the Plataforma Solar de Almeria”. In: *Mater Sci Semicond Process* 42 (2016), pp. 15–23. DOI: 10.1016/j.mssp.2015.07.017.
- [152] ER Bandala, S Gelover, MT Leal, C Arancibia-Bulnes, A Jimenez, and CA Estrada. “Solar photocatalytic degradation of Aldrin”. In: *Catal Today* 76.2-4 (2002), pp. 189–199. DOI: 10.1016/S0920-5861(02)00218-3.
- [153] G Iervolino, I Zammit, V Vaiano, and L Rizzo. “Limitations and Prospects for Wastewater Treatment by UV and Visible-Light-Active Heterogeneous Photocatalysis: A Critical Review”. In: *Top Curr Chem* 378.7 (2019). DOI: 10.1007/s41061-019-0272-1.
- [154] MN Chong, B Jin, CW Chow, and C Saint. “Recent developments in photocatalytic water treatment technology: a review”. In: *Water Res* 44.10 (2010), pp. 2997–3027. DOI: 10.1016/j.watres.2010.02.039.
- [155] H Fallmann, T Krutzler, R Bauer, S Malato, and J Blanco. “Applicability of the Photo-Fenton method for treating water containing pesticides”. In: *Catal Today* 54.2-3 (1999), pp. 309–319. DOI: 10.1016/S0920-5861(99)00192-3.
- [156] MM Ballesteros Martín, JA Sánchez Pérez, JL Casas López, I Oller, and Malato Rodríguez S. “Degradation of a four-pesticide mixture by combined photo-Fenton and biological oxidation”. In: *Water Res* 43.3 (2009), pp. 653–660. DOI: 10.1016/j.watres.2008.11.020.

- [157] M Lapertot, S Ebrahimi, S Dazio, A Rubinelli, and C Pulgarin. “Photo-Fenton and biological integrated process for degradation of a mixture of pesticides”. In: *J Photochem Photobiol A Chem* 186.1 (2007), pp. 34–40. DOI: 10.1016/j.jphotochem.2006.07.009.
- [158] F Méndez-Arriaga, S Esplugas, and J Giménez. “Degradation of the emerging contaminant ibuprofen in water by photo-Fenton”. In: *Water Res* 44.2 (2010), pp. 589–595. DOI: 10.1016/j.watres.2009.07.009.
- [159] H Shemer, YK Kunukcu, and KG Linden. “Degradation of the pharmaceutical metronidazole via UV, Fenton and photo-Fenton processes”. In: *Chemosphere* 63.2 (2006), pp. 269–276. DOI: 10.1016/j.chemosphere.2005.07.029.
- [160] MG Alalm, A Tawfik, and S Ookawara. “Degradation of four pharmaceuticals by solar photo-Fenton process: Kinetics and costs estimation”. In: *J Environ Chem Eng* 3.1 (2015), pp. 46–51. DOI: 10.1016/j.jece.2014.12.009.
- [161] S Arzate, MC Campos-Mañas, S Miralles-Cuevas, A Agüera, JL García Sánchez, and JA Sánchez Pérez. “Removal of contaminants of emerging concern by continuous flow solar photo-Fenton process at neutral pH in open reactors”. In: *J Environ Manage* 261 (2020), p. 110265. DOI: 10.1016/j.jenvman.2020.110265.
- [162] H Katsumata, S Kawabe, S Kaneco, T Suzuki, and K Ohta. “Degradation of bisphenol A in water by the photo-Fenton reaction”. In: *J Photochem Photobiol A Chem* 162.2-3 (2004), pp. 297–305. DOI: 10.1016/S1010-6030(03)00374-5.
- [163] S Malato, J Caceres, A Agüera, M Mezcua, D Hernando, J Vial, and AR Fernández-Alba. “Degradation of Imidacloprid in Water by Photo-Fenton and TiO₂ Photocatalysis at a Solar Pilot Plant: A Comparative Study”. In: *Environ Sci Technol* 35.21 (2001), pp. 4359–4366. DOI: 10.1021/es000289k.
- [164] N Klammerth, N Miranda, S Malato, A Agüera, AR Fernández-Alba, MI Maldonado, and JM Coronado. “Degradation of emerging contaminants at low concentrations in MWTPs effluents with mild solar photo-Fenton and TiO₂”. In: *Catal Today* 144.1-2 (2009), pp. 124–130. DOI: 10.1016/j.cattod.2009.01.024.
- [165] L Clarizia, D Russo, I Di Somma, R Marotta, and R Andreatti. “Homogeneous photo-Fenton processes at near neutral pH: A review”. In: *Appl Catal B Environ* 209 (2017), pp. 358–371. DOI: 10.1016/j.apcatb.2017.03.011.
- [166] I Sciscenko, S Mestre, J Climent, F Valero, C Escudero-Oñate, I Oller, and A Arques. “Magnetic Photocatalyst for Wastewater Tertiary Treatment at Pilot Plant Scale: Disinfection and Enrofloxacin Abatement”. In: *Water* 13.3 (2021), p. 329. DOI: 10.3390/w13030329.



Chapter 2

Materials and methods



2.1 Photodegradation set-ups and parameters

The photodegradation set-ups and their specifications are detailed in the results chapters, in the framework of the articles. In the laboratory modeling approach, the irradiation set-up usually consists of light sources emitting at a suitable wavelength to achieve the desired photochemical process. The molecules are solubilized and placed in a cell or reactor. The material of the cell (usually quartz) must not absorb in the wavelengths of irradiation. Usually, ultrapure solvents, mainly water or acetonitrile, are used as reaction medium. This choice is to simplify the model, thus allowing the detection of multiple photoproducts that can often be in very low concentrations. By increasing the samples' complexity from solvent mixtures to real environmental sample conditions, the exhaustive detection of photoproducts becomes a real analytical challenge.

The goal of applying AOPs is to enhance the photodegradation rate as much as possible while limiting byproducts formation. This can be realized through various methods, such as the addition of photocatalysts, photosensitizers, or hydrogen-peroxide in photolysis experiments. Their concentrations have to be correctly estimated, as the amount of the generated reactive species has to be comparable with the concentration of the parent compound. The wavelength of irradiation and pH of the medium must be adequately selected to activate the applied process. If necessary, pre-treatment should be applied to minimize the number of molecules that have a filtering effect or act as photochemical quenchers in the water matrix.

Sampling is carried out at appropriate irradiation times to provide a relevant kinetic model for the degradation of the parent compound and to detect the potential intermediate species. As many molecules show exponential decay, the sampling frequency is usually higher at the beginning of the reaction.

2.2 *In vitro* and *in silico* toxicity estimations

There is still a substantial lack of toxicological data; in 2009, this was true for 86% of the registered chemicals [1]. In 2007, the most extensive assessment started, thanks to the newly introduced EU regulation Registration, Evaluation, Authorization and Restriction of Chemicals (REACH) [2]. Since the scarcity of information is high, *in vivo* tests proved not to be enough, being expensive, time-consuming, and restricted by the moral questions on animal testing [3]. Standardized *in vivo* toxicity testing exists for approximately 1000 compounds, but it would be highly challenging to extend it to the dynamically changing list of CECs, even more to their transformation products [4]. *In vitro* tests are good complementary methods to assess toxicity. High throughput *in vitro* bioassays, for which automated equipment is used to test the samples, resulted in the rapid analysis of a large

number of samples. *In vitro* tests screen biological activity and work on the level of model organisms, cells, or molecules, usually based on receptor-binding mechanisms resulting in inhibition [5]. Despite their everyday use in biotechnology and the pharmaceutical industry, they became popular only in the recent years in the field of environmental analysis. *In vitro* bioassays have been developed for the screening of endocrine-disrupting activities in wastewater [6], surface water, and river water [7].

When carrying out photodegradation reactions, performing *in vitro* analysis on samples helps to identify whether toxicity levels increase after irradiation, which indicate the formation of harmful photoproducts. In this project, *Vibrio Fischeri* was used as a test organism to study the potential toxicity of the photoproducts of naproxen. This test is based on quantifying the inhibition of bioluminescence of this marine bacterium; it uses a simple protocol described in the article on the photodegradation of naproxen in the chapter 3. The test is versatile, fast, and correlates well with other toxicity testing methods [8].

However, *in vitro* testing can be constrained by the mechanism of various types of toxicity that can differ in the studied organisms. The use of multiple types of bioassays is thus recommended, which is not available in every laboratory. Furthermore, it is interesting to study the individual photoproduct contribution to toxicity to draw conclusions about potential toxicity-inducing structures and functional groups. One way to achieve this is through *in silico* approaches based on computational methods, which allow assessing and prioritizing compounds. It is to be noted that contrarily to *in vivo* and *in vitro* bioassays, *in silico* estimations do not take into consideration potential synergistic or antagonist effects; that is the reason why some biologists still consider such tests are poorly relevant. Despite this, it can be considered an ideal tool for preliminary assessment.

There are many types of computational toxicology approaches. The individual toxicity estimations were performed using the Toxicity Estimation Software Tool (TEST) by United States Environmental Protection Agency (EPA) [9] and VEGA [10, 11]. These are based on different computational approaches, the most widespread relying on quantitative structure-activity relationship (QSAR), which use molecular descriptors for toxicity prediction. When a given QSAR model is applied to a set of chemicals, the mechanism of toxic behavior is considered to be comparable along these chemicals.

Another approach is referred to as “read-across,” where toxicity is predicted by using the toxicity of analogous chemicals, thus filling the literature gaps by using chemical similarities [3]. This approach can be used to predict the toxicity of ill-defined compounds and thus constitutes an ideal tool to estimate the toxicity of photoproducts, as these might not be molecules previously described in the literature or databases. Therefore, *in silico* methods can be fast and efficient, and considerations behind their implementation are ethical and economical. When using such tools, one needs to be careful since there are some limitations, such as the transparency and quality of the experimental data.

The descriptors and models may not always be explicit, and it is crucial to choose the applicability domain correctly [12, 13].

When applying *in silico* methods, there are many existing endpoints, but their reliability can differ. The highest percentage of correct predictions are those with reasonably well-understood mechanisms on how the toxicant acts. These are toxicity tests with simple endpoints, such as aquatic toxicity testing (e.g., fathead minnow) and sensitization [14]. One also needs to have a critical view of the existing toxicity data since most of them use lethal concentrations, which can be much higher than those that actually get into contact with the ecosystem, animals, or humans. This work aims at using existing *in silico* tools reasonably, compare different approaches, choose the endpoints which are more straightforward and whose mechanism is better understood. When analyzing the data, it is essential to consider the toxicity results only from calculations with adequate reliability for an accurate prediction. The reliability can be quantified using external validation, considering parameters such as the applicability domain, predictive power, and prediction accuracy.

Where it is possible, the results are compared with experimental values, but sometimes the detected photoproduct is not CAS registered, and there is limited data about it. As there is no available free tool for the *in silico* testing of *Vibrio Fischeri*, no comparison could be made between *in silico* and *in vitro* toxicity estimations. However, the applied tools can be good indicators of potentially harmful effects; they point out the molecules worth investigating further. To understand in-depth the toxicity of a mixture and individual compounds, the smart combination of different approaches is necessary, together with the introduction of efficient guidelines and standardization [1].

2.3 HRMS and non-targeted analysis

Most of the parameters related to the analysis of the samples are presented in the results chapters. In this section, the capabilities offered by HRMS are described, which is a result of advances in mass spectrometry. It is also crucial to define the terminology to describe the mass spectrometry data with uniformity.

In mass spectrometry, resolving power and mass resolution are commonly used interchangeably, as they both are performance parameters. According to IUPAC recommendations, the resolving power can be defined using the valley between two peaks. If two peaks, m_1 and m_2 , of equal intensity are separated by a valley that corresponds to the minimum of the respective percentage (usually 10% and must be specified) of the height of the peak, then the resolving power is defined as $\frac{m_1}{(m_1 - m_2)}$. In the case of peak width definition, the most commonly used is the full width at half maximum (FWHM), where δm is the width of the peak at 50% height, the resolving power is $\frac{m}{\delta m}$. Mass resolution

is defined as the ability of the mass spectrometer to separate two peaks with small m/z differences and is represented by peak width in mass units [15, 16].

Another way to characterize the obtained m/z values is the precision in mass. This is indicated in ppm or Dalton (see equation 2.1) and considers the measured mass and the theoretical mass. This approach was used throughout the thesis to characterize the accuracy of measurement. Error below 3 ppm was routinely achieved, and error values below 1 ppm were obtained with good calibration for m/z values below 500 Da. This is enough to achieve unique elemental compositions when considering C, H, N, O, and S atoms [17].

$$error(ppm) = \frac{|M_{exp} - M_{th}| * 10^6}{M_{th}} \quad (2.1)$$

The aim is to have only one elemental composition corresponding to each peak, thus separating isobaric ions. Besides accurate m/z measurements, the isotopic pattern is an excellent asset in assessing chemical formulae at low masses. At higher masses, a list of potential molecular formulae will be available. Furthermore, every isotope has a different mass defect (Figure 2.3.1), which is the difference between the exact mass of an atom and the nearest integer value, facilitating the assessment of unique molecular formulae.

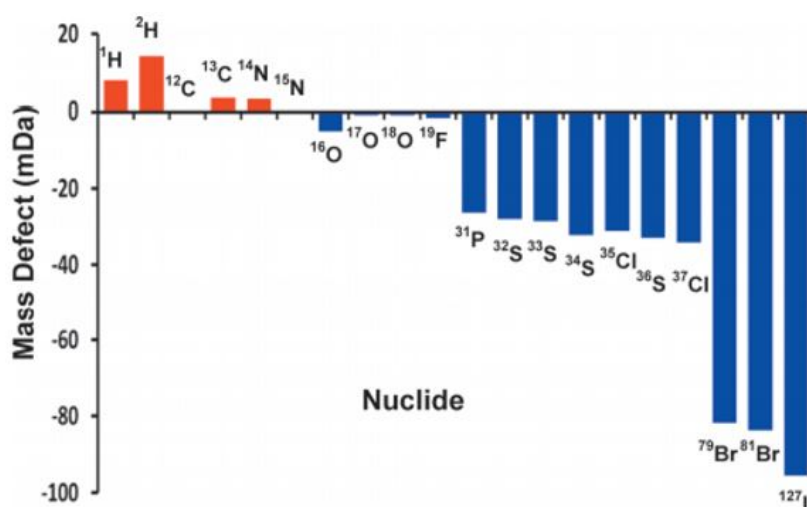


Figure 2.3.1: Mass defects of common elements and their isotopes [18]

HRMS represented the core of this work, as it is indispensable for the assessment of photoproducts and the direct-infusion analysis of highly complex samples. To separate and accurately assess the formulae of analytes of low concentrations in complex matrices, a high resolving power ($\geq 50,000$) is essential. As an example, Figure 2.3.2 shows that in HRMS measurements, multiple ions can be separated at a single nominal m/z value (m/z

191 in the present case), which is indispensable for analyzing complex mixtures [19].

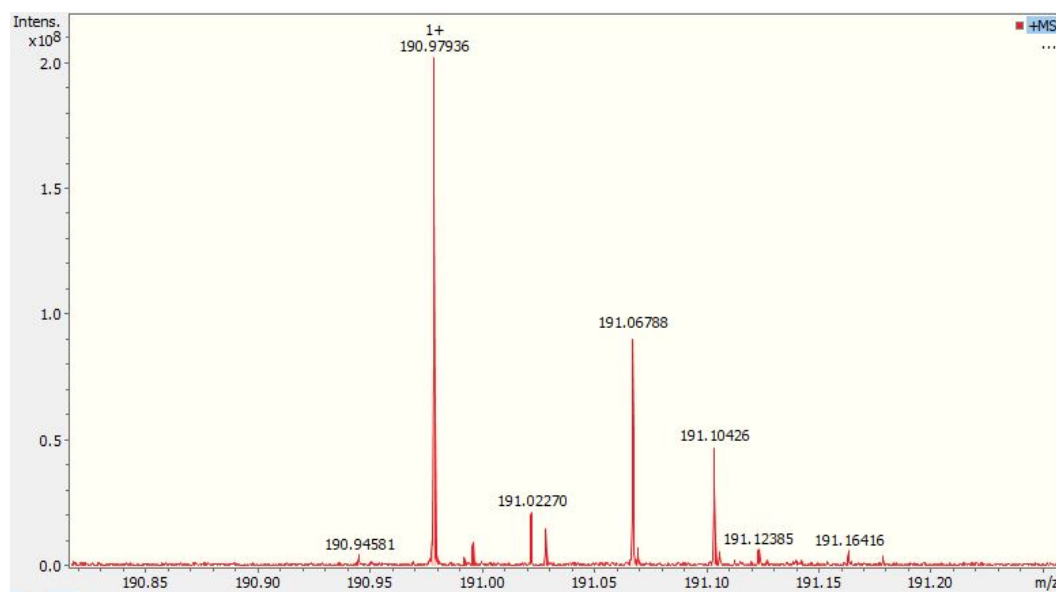


Figure 2.3.2: Number of ions that can be detected at the nominal m/z 191 using ultrahigh resolution MS

This kind of high resolving power and advanced separation of close m/z values made possible the development of non-targeted analysis, which is of high value in environmental chemistry. Target screening of known and commonly detected contaminants should be completed by non-targeted analysis to identify a broader range of chemicals. As presented in Figure 2.3.3, only a limited number of molecules will be detected from a complex sample by doing targeted analysis. If non-targeted analysis is applied, the number of detected molecules can be largely increased. However, many compounds will be lost, as they either go undetected by the mass spectrometer, unresolved by chromatography, or are non-extractable by the selected sample preparation process.

There are mainly two ways to reduce the loss of contaminants during extraction: (i) using a combination of sample extraction protocols to cover a wide range of molecular weights and polarities, (ii) minimizing sample preparation to a filtration or centrifugation step. Regarding chromatography, a combination of LC-MS and GC-MS - with various columns - and even direct infusion MS for some sample types can be used to avoid losing too many analytes. To achieve efficient ionization and detect a high number of compounds in LC-MS coupling, it is also recommended to use complementary ionization sources, as the ionization efficiency of each source correlates with the polarity of the analytes and their molecular weights.

Another challenge is presented by the data processing step. It is tedious work involving the use of a combination of software and databases, for which workflows are proposed in

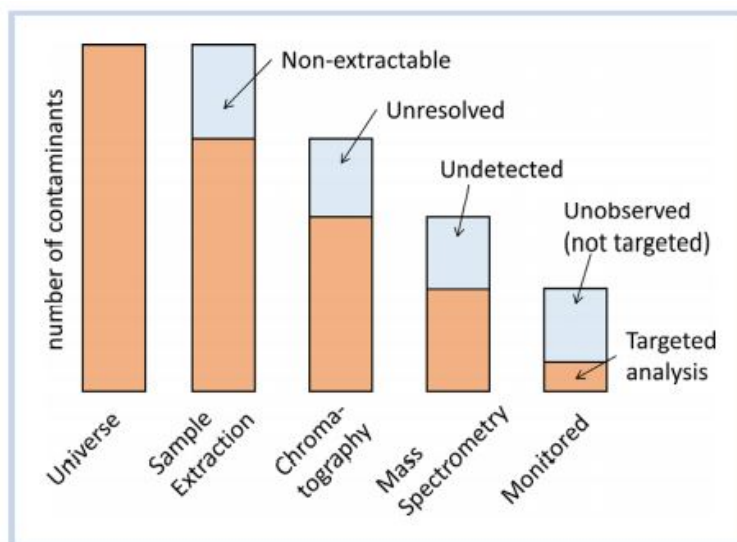


Figure 2.3.3: Number of contaminants lost at each sample preparation and analysis step [20]

the literature [21]. In our project, the aim of developing the SPIX software (see chapter 5) was to provide a new tool for data analysis, with a novel approach concerning the analysis of non-targeted datasets.

2.4 ESI and FT-ICR MS

To obtain the HRMS datasets, the majority of the mass spectrometry data presented were obtained from a Fourier Transform – Ion Cyclotron Resonance Mass Spectrometer (FT-ICR MS) instrument equipped with an electrospray ionization (ESI) source. This type of mass spectrometer provides the highest resolving power on the market, thus allowing the analysis of highly challenging, complex samples. The basic operating principle of this core instrument is presented in this section.

For this study, the ESI source was selected, due to its ability to ionize molecules on a wide range of molecular weight with medium to high polarity, which is suitable for a large number of CECs. A high number of contaminants and their transformation products were detected. In the case of naproxen, for which very few photoproducts were detected by LC-MS analysis, GC-MS was employed as an additional analytical tool.

The principle of ESI is shown in Figure 2.4.1. After the samples are injected, they are transferred through a fine capillary, where a high voltage is applied. The liquid will form a Taylor cone due to the high electric potential applied between the capillary and the metal counter-electrode. The resulting charged jet will easily break into small droplets and the solvent will evaporate, until the charge of a droplet becomes too high, thus it will release

ions in the gas phase.

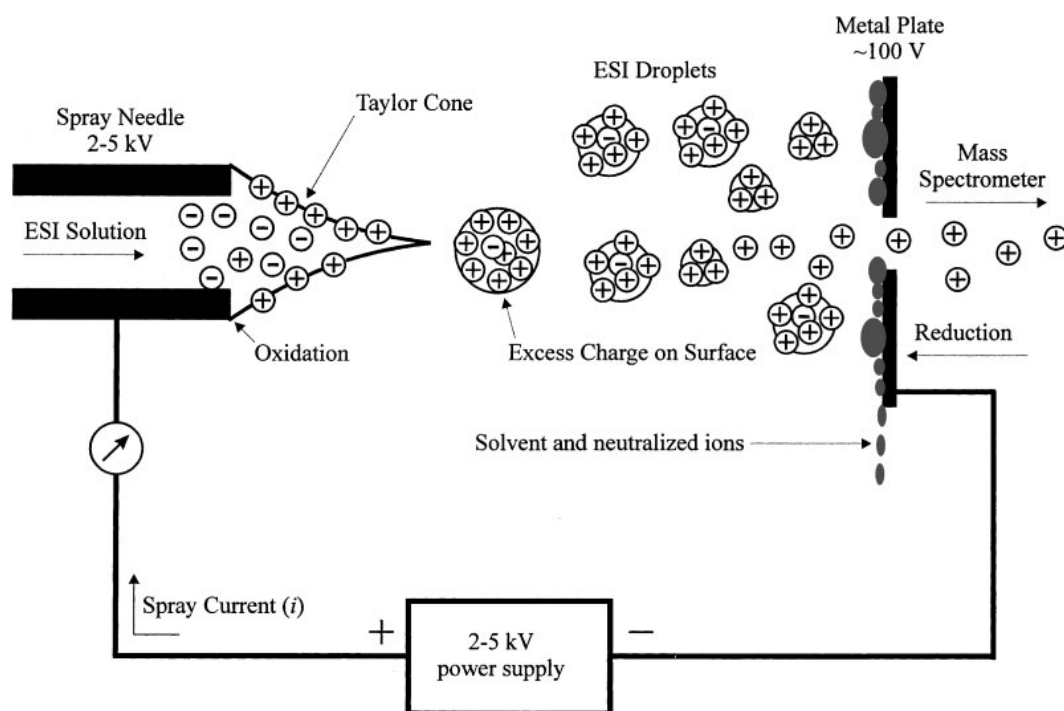


Figure 2.4.1: Principle of operation of an electrospray ionization source [22]

In our laboratory, the FT-ICR SolarixXR (Bruker Daltonics, Bremen, Germany)(Figure 2.4.2) is equipped with a 9.4 T superconducting magnet and an ICR cell, with a paracell configuration.

FT-ICR MS instruments reach ultrahigh mass accuracy (< 1 ppm) and mass resolving power ($> 100\,000$, even $10\,000\,000$), depending on the strength of the magnetic field and the geometry of the ICR cell, in which the ions are trapped for frequency measurement [23, 24].

After the ionization of the compounds, ions are transferred to a quadrupole, where the selection of particular m/z values can be carried out. At this step, fragmentation experiments can be performed, via collision-induced dissociation (CID). Product ions reach, through an octupole, the ICR cell, historically known as a Penning trap. The ions are confined in the trap under high vacuum. Here, the ions will follow a cyclotron rotation trajectory, induced by the static magnetic field (B). The angular frequency (ω_c) will differ based on mass and charge (m and z) according to equation 2.2 [25, 26].

$$\omega_c = \frac{zB}{m} \quad (2.2)$$

In the ICR cell, a radio frequency electric field is applied on the transmitter plates, to excite ions, resulting in a larger cyclotron, synchronous radius [27]. The force exerted on



Figure 2.4.2: Image of the FT-ICR SolarixXR at the Laboratoire de Chimie Moléculaire (LCM)

the ions by the electric and magnetic field can be described by the Lorentz force. The receiver plates detect the current induced by the rotation of the ions (Figure 2.4.3). A transient signal is obtained, from the sum of all detected currents, which is then processed by Fourier transform to assess the m/z – intensity pair values.

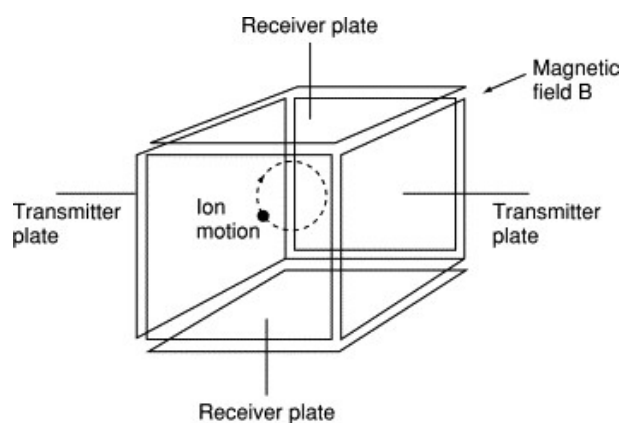


Figure 2.4.3: Schematic representation of an ICR cell [28]

Beyond performing a good calibration and optimizing the parameters of the instrument, it

is also necessary to tune the acquisition parameters. For the analysis of complex samples, it is essential to average a large number of spectra to obtain a good signal-to-noise ratio (SNR). It is recommended to sum many FT-ICR mass spectra (> 100) to improve SNR and dynamic range, but when too many ions reach the trap at once, the space-charge effect can shift the peak position, thus degrading mass accuracy. This can be a limiting factor when using MS instruments based on ion trapping.

2.5 Direct infusion mass spectrometry (DI-MS)

One of the options using FT-ICR MS is the infusion mode, where samples are directly introduced in the mass spectrometer without prior chromatographic separation. Using direct infusion MS for non-targeted analysis permits an extensive overview of all the detected m/z values. This is an ideal comprehensive approach, especially when there are not a lot of interferences caused by complex matrices. On the other hand, some elements of complex matrices can be analyzed only in direct infusion MS; great examples, widely studied in the field of environmental analysis, are humic-like substances [29, 30].

Another aspect is that the optimization and careful selection of chromatographic approaches is tedious and subjective work, resulting in the loss of some compounds, as different experimental conditions are required, based on their chemical characteristics, such as volatility, polarity, molecular weight, functional groups. Employing direct infusion mass spectrometry can minimize the loss of detectable compounds caused by hyphenated techniques. Moreover, the data management of DI-MS is facilitated as it is two-dimensional. Sample preparation can be simplified as well, and by removing the chromatographic part, optimizing the experiments is a faster process, thus reducing the operator-related subjectivity and errors. Last but not least, the measurements of samples require shorter analysis times with direct infusion methods (2-5 minutes) compared to longer LC-MS runs (typically 20-30 minutes).

However, there are some limitations when using DI-MS. Often, ion suppression can occur, which is a phenomenon at the early stages of the ionization process. Its mechanism is still not fully understood, however in multicomponent samples with high analyte concentrations, there is a competition for either space or charge in the ion source, resulting in the suppression of some of the signals [15]. When looking at operator-related subjectivity, some of its aspects will persist using DI-MS, such as choice of instrument, its parameters, experimental conditions (spray-solvent composition, pH, sample volume, flow, temperature, voltage, etc.), and sample preparation. The latter can be reduced to a filtration or centrifugation step, which is usually the minimum requirement for environmental water samples. A systematic approach such as experimental design can help in finding optimal experimental conditions and minimize operator-related subjectivity. The last point

to consider is that isomeric compounds cannot be separated using DI-MS solely, without a prior separation method. This can be an issue when studying degradation mechanisms, as it is common for photoproducts to take isomeric forms. DI-MS is suitable as a holistic approach to obtain a fast overview of the data, but when we look at in-depth structural elucidations, additional dimensions, such as chromatographic separations and MS fragmentation experiments, are essential.

Parameters for DI-MS analysis of irradiated benzisothiazolinone (BIT) samples

For the development of the SPIX software, additional samples were taken during the modeling approach, as described in chapter 3.2. The samples were taken in triplicate from three parallel reactors. They were analyzed using DI-MS, in a randomized order, with blank samples (containing only the solvent) and quality control samples analyzed every five samples. A tune mix (Agilent Technologies, Les Ulis, France) was used for mass calibration. Between each measurement the instrument was cleaned twelve times using four different solvents (water; mixture of 25% water, 25% acetonitrile, 25% methanol, 25% isopropanol; isopropanol; acetonitrile). The samples were diluted to a starting concentration of benzisothiazolinone at 2-5 ppm, using 90% water, 10% acetonitrile and 0,1% formic acid. The FT-ICR MS measurements were performed in both positive and negative ionization modes, using an electrospray ionization source. The flow rate was 120 $\mu\text{l/h}$. Nitrogen was the nebulizer (1 bar) and drying gas (4 L/min flow), the temperature of the latter being 180 °C. The capillary voltage and endplate offset potentials were set at -4500 and -500 V, respectively. The spectra were acquired with 4M data points on a m/z range from 57.7 to 1000 Th. Accumulation time was set to 0.02 s. A total of 100 scans were accumulated for each spectrum recording. Exact formulae were assigned with error < 1 ppm.

2.6 Data processing

As a high amount of information can be extracted from high-resolution datasets, data processing is a crucial step. In this part, aspects and considerations of the data analysis using Bruker Compass DataAnalysis will be briefly presented. The software was used to visualize chromatograms and mass spectra. Chromatographic peak areas were integrated to quantify the degradation of parent compounds.

From mass spectrometry data, the most critical aspect was the assessment of unique molecular formulae to photodegradation products. An established approach in mass spectrometry data analysis, when having a large number of molecules, is following the seven golden rules [31]. This helps in assessing the molecular formulae with the highest accuracy and allows the refining of the parameters, to decrease computational power. Some of these parameters were incorporated in the DataAnalysis software, others can be selected

by the user. The most commonly used ones in this project were restricting the number of elements, filtering the isotopic pattern, H/C element ratio restriction, and setting the type of heteroatoms possibly present in the molecule. When processing the mass spectra of the irradiated samples, constraints were set in the software, based on the mass accuracy of the parent compound as well, that is an indicator of the overall goodness of the calibration. In positive mode, the formation of adduct ions was considered, especially the highly common sodium adduct. Dimerization of the molecules was also taken into account, although it is difficult to assess whether this occurs during the photochemical reaction or in the ion source.

The interface for manual assessment of molecular formulae is shown in Figure 2.6.1. m/z 152.01649 corresponds to protonated benzisothiazolinone in positive mode. The software implicitly takes C, H, N, and O in the formula, S was added as it is in the composition of the parent compound. The type of adduct, mass error tolerance, and charge can be set.

Meas. m/z	#	Ion Formula	Score	m/z	err [ppm]	Mean err [ppm]	mSigma
152.01649	1	C ₇ H ₉ NOS	100.00	152.01646	-0.17	-0.14	3.7

Figure 2.6.1: Interface of the Bruker Compass DataAnalysis software, showing the parameters for manual formula assessment

It can be observed that the error of measurement is very low; the measured m/z value is 152.01649, whereas the theoretical value is 152.01646, resulting in a mass error of -

0.17 ppm. The mean error includes the errors between the measured mass of the isotopes versus the theoretical value. Furthermore, the carbon number can be estimated based on the molecular mass, and the electron configuration can be set to even or odd. The mass list was generated, either manually or automatically, based on the aforementioned criteria. The masses were also assessed for the MS² spectra of CID experiments, thus providing the basis for structural elucidation. With this software, the necessary data for the modeling approach was processed and extracted, and the assessment of photodegradation pathways could be achieved.

References

- [1] T Hartung. “Toxicology for the twenty-first century”. In: *Nature* 460 (2009), pp. 208–212. DOI: 10.1038/460208a.
- [2] *Registration, Evaluation, Authorisation and Restriction of Chemicals (REACH)*. 2007. URL: <https://echa.europa.eu/regulations/reach/understanding-reach>.
- [3] AB Raies and VB Bajic. “In silico toxicology: computational methods for the prediction of chemical toxicity”. In: *WIREs Comput Mol Sci* 6.2 (2016), pp. 147–172. DOI: 10.1002/wcms.1240.
- [4] KA Maruya, NG Dodder, AC Mehinto, ND Denslow, D Schlenk, SA Snyder, and SB Weisberg. “A tiered, integrated biological and chemical monitoring framework for contaminants of emerging concern in aquatic ecosystems”. In: *Integr Environ Assess* 12.3 (2016), pp. 540–547. DOI: 10.1002/ieam.1702.
- [5] MS Attene-Ramos, R Huang, S Sakamuru, KL Witt, GC Beeson, L Shou, RG Schnellmann, CC Beeson, RR Tice, CP Austin, and M Xia. “Systematic study of mitochondrial toxicity of environmental chemicals using quantitative high throughput screening”. In: *Chem Res Toxicol* 26.9 (2013), pp. 1323–1332. DOI: 10.1021/tx4001754.
- [6] SC van der Linder, MB Heringa, HY Man, E Sonneveld, LM Puijker, A Brouwer, and B Van der Burg. “Detection of multiple hormonal activities in wastewater effluents and surface water, using a panel of steroid receptor CALUX bioassays”. In: *Environ Sci Technol* 42.15 (2008), pp. 5814–5820. DOI: 10.1021/es702897y.
- [7] B Jarosova, L Blaha, B Vrana, T Randak, R Grabic, JP Giesy, and K Hilscherova. “Changes in concentrations of hydrophilic organic contaminants and of endocrine-disrupting potential downstream of small communities located adjacent to headwaters”. In: *Environ Int* 45 (2012), pp. 22–31. DOI: 10.1016/j.envint.2012.04.001.
- [8] S Parvez, C Venkataraman, and S Mukherji. “A review on advantages of implementing luminescence inhibition test (*Vibrio fischeri*) for acute toxicity prediction of chemicals”. In: *Environ Int* 32.2 (2006), pp. 265–268. DOI: 10.1016/j.envint.2005.08.022.
- [9] *Toxicity Estimation Software Tool (TEST)*. URL: <https://www.epa.gov/chemical-research/toxicity-estimation-software-tool-test>.
- [10] E Benfenati, A Manganaro, and G Gini. “VEGA-QSAR: AI inside a platform for predictive toxicology”. In: *CEUR Workshop Proceedings*. Vol. 1107. CEUR-WS, 2013, pp. 21–28. URL: <https://moh-it.pure.elsevier.com/en/publications/vega-qsar-ai-inside-a-platform-for-predictive-toxicology>.


- [11] VEGA. URL: <https://www.vegahub.eu/>.
- [12] LG Valerio Jr. “In silico toxicology for the pharmaceutical sciences”. In: *Toxicol Appl Pharmacol* 241.3 (2009), pp. 356–370. DOI: 10.1016/j.taap.2009.08.022.
- [13] S Weaver and MP Gleeson. “The importance of the domain of applicability in QSAR modeling”. In: *J Mol Graph Model* 26.8 (2008), pp. 1315–1326. DOI: 10.1016/j.jmgm.2008.01.002.
- [14] C Merlot. “Computational toxicology—a tool for early safety evaluation”. In: *Drug Discov Today* 15.1-2 (2010), pp. 16–22. DOI: 10.1016/j.drudis.2009.09.010.
- [15] KK Murray, RK Boyd, MN Eberlin, GJ Langley, L Li, and Y Naito. “Definitions of terms relating to mass spectrometry (IUPAC Recommendations 2013)”. In: *Pure Appl Chem* 85.7 (2013), pp. 1515–1609. DOI: 10.1351/PAC-REC-06-04-06.
- [16] F Xian, CL Hendrickson, and AG Marshall. “High resolution mass spectrometry”. In: *Anal Chem* 84.2 (2012), pp. 708–719. DOI: 10.1021/ac203191t.
- [17] S Kim, RP Rodgers, and AG Marshall. “Truly “exact” mass: Elemental composition can be determined uniquely from molecular mass measurement at 0.1 mDa accuracy for molecules up to 500 Da”. In: *Int J Mass Spectrom* 251.2-3 (2006), pp. 260–265. DOI: 10.1016/j.ijms.2006.02.001.
- [18] AG Marshall, GT Blakney, T Chen, NK Kaiser, AM McKenna, RP Rodgers, BM Ruddy, and F Xian. “Mass resolution and mass accuracy: how much is enough?” In: *Mass Spectrom (Tokyo)* 2 (2013), S0009. DOI: 10.5702/massspectrometry.S0009.
- [19] M Kellmann, H Muenster, P Zomer, and H Mol. “Full scan MS in comprehensive qualitative and quantitative residue analysis in food and feed matrices: How much resolving power is required?” In: *J Am Soc Mass Spectrom* 20.8 (2009), pp. 1464–1476. DOI: 10.1016/j.jasms.2009.05.010.
- [20] KA Maruya, NG Dodder, A Sengupta, DJ Smith, JM Lyons, AT Heil, and JE Drewes. “Multimedia screening of contaminants of emerging concern (CECS) in coastal urban watersheds in southern California (USA)”. In: *Environ Toxicol Chem* 35.8 (2016), pp. 1986–1994. DOI: 10.1002/etc.3348.
- [21] AA Bletsou, J Jeon, J Hollender, E Archontaki, and NS Thomaidis. “Targeted and non-targeted liquid chromatography-mass spectrometric workflows for identification of transformation products of emerging pollutants in the aquatic environment”. In: *Trends Anal Chem* 66 (2015), pp. 32–44. DOI: 10.1016/j.trac.2014.11.009.
- [22] E Tobolkina. “New analytical tools combining gel electrophoresis and mass spectrometry”. PhD thesis. EPFL, 2014. DOI: 10.13140/RG.2.1.4866.5125.

- [23] AG Marshall, CL Hendrickson, and GS Jackson. “Fourier transform ion cyclotron resonance mass spectrometry: A primer”. In: *Mass Spec Reviews* 17.1 (1998), pp. 1–35. DOI: 10.1002/(SICI)1098-2787(1998)17:1<1::AID-MAS1>3.0.CO;2-K.
- [24] AG Marshall and S Guan. “Advantages of High Magnetic Field for Fourier Transform Ion Cyclotron Resonance Mass Spectrometry”. In: *Rapid Comm Mass Spec* 10.14 (1996), pp. 1819–1823. DOI: 10.1002/(SICI)1097-0231(199611)10:14<1819::AID-RCM686>3.0.CO;2-Z.
- [25] EB Kujawinski. “Electrospray Ionization Fourier Transform Ion Cyclotron Resonance Mass Spectrometry (ESI FT-ICR MS): Characterization of Complex Environmental Mixtures”. In: *Environ Forensics* 3.3-4 (2002), pp. 207–216. DOI: 10.1080/713848382.
- [26] Y Cho, A Ahmed, A Islam, and S Kim. “Developments in FT-ICR MS instrumentation, ionization techniques, and data interpretation methods for petroleomics”. In: *Mass Spectrom Rev* 34.2 (2015), pp. 248–263. DOI: 10.1002/mas.21438.
- [27] AG Marshall and FR Verdun. In: *Fourier Transforms in NMR, Optical, and Mass Spectrometry*. New York: Elsevier Science, 1990. URL: <https://www.elsevier.com/books/fourier-transforms-in-nmr-optical-and-mass-spectrometry/marshall/978-0-444-87360-6>.
- [28] DL Andrews. In: *Perspectives in Modern Chemical Spectroscopy*. Berlin Heidelberg: Springer-Verlag, 1990. URL: <https://www.springer.com/gp/book/9783540522188>.
- [29] A Piccolo and M Spiteller. “Electrospray ionization mass spectrometry of terrestrial humic substances and their size fractions”. In: *Anal Bioanal Chem* 377 (2003), pp. 1047–1059. DOI: 10.1007/s00216-003-2186-5.
- [30] J D’Andrilli, CM Foreman, AG Marshall, and DM McKnight. “Characterization of IHSS Pony Lake fulvic acid dissolved organic matter by electrospray ionization Fourier transform ion cyclotron resonance mass spectrometry and fluorescence spectroscopy”. In: *Org Geochem* 65 (2013), pp. 19–28. DOI: 10.1016/j.orggeochem.2013.09.013.
- [31] T Kind and O Fiehn. “Seven Golden Rules for heuristic filtering of molecular formulas obtained by accurate mass spectrometry”. In: *BMC Bioinformatics* 8 (2007), p. 105. DOI: 10.1186/1471-2105-8-105.



Chapter 3

Modeling approach - Results on direct photochemical reactions



3.1 General approach

In this section, the direct photolysis of benzisothiazolinone and naproxen is presented. The experiments were performed under laboratory conditions. The light-induced degradation of pollutants is efficient and can be a sustainable approach, but some essential parameters have to be considered to achieve satisfactory degradation efficiency and avoid the formation of harmful byproducts. Ideally, the mineralization of the parent compound should be achieved.

When performing photodegradation experiments, one of the key parameters is the selected wavelength of irradiation. In the case of direct photolysis, this has to be relevant in terms of the absorption characteristics of the molecules of interest, as the energy of the radiation should induce electronic transitions in the molecules. UV-Vis spectroscopy is one of the analytical techniques widely used to obtain the absorption spectra of the molecules. There has to be an overlap between the wavelength of emission and wavelength of absorption; otherwise, no interaction will occur. For example, the absorption spectrum of benzisothiazolinone is shown in Figure S3.2.1, and it can be deduced from it that if irradiation occurs with a maximum wavelength around 254 nm (which is the case of many commercial UV lamps), the molecule will absorb and interaction will occur. Moreover, high-pressure mercury lamps emit polychromatic light on a wavelength range between 200 and 600 nm, potentially inducing different electronic transitions. The characteristic absorption spectrum with its various local maxima are indicators of the molecular structure and its functional groups.

In terms of the reaction medium, the process can be carried out in different types of solvents. The solvents should be pure, otherwise, indirect photochemical processes might be induced, and in these studies, we were interested in the direct photochemical processes. Aqueous medium is the most studied one, as it is the most relevant in terms of applicability.

The pH of the mixture is also an important factor. It can affect the molecules' solubility and change the absorption characteristics, for example, for zwitterionic molecules. The pH can also influence the outcome of some analytical measurements, such as the ionization efficiency in the ion source of the mass spectrometer (especially regarding electrospray ionization).

In these studies, either liquid or gas chromatography was employed depending on the properties of the molecules; chromatography was coupled with mass spectrometry which is the most suitable technique for the determination of molecular formulae. For most of the experiments, high-resolution mass spectrometry was used due to its capability to provide accurate mass measurements allowing differentiation of isobaric ions. MS^2 spectra were recorded to collect structural information on the photoproducts. By studying each

product's fragmentation pattern, their structures can be tentatively assessed, which may permit to (i) elucidate the photodegradation pathways and (ii) perform *in silico* toxicity estimations.

Preliminary toxicity measurements were performed by means of *in vitro* measurements and *in silico* calculations. By using bioassays conducted on *Vibrio fischeri* bacteria, it can be assessed whether the overall toxicity of the mixture increases or decreases during the irradiation; this non-specific approach takes into account potential agonist and antagonist effects. After structural elucidation, it is possible to use *in silico* toxicity calculations to estimate potential harmful effects of the transformation product individually. These are not highly accurate measurements but preliminary indicators of potential toxicities, which, contrarily to *in vitro* bioassays, do not take into account potential synergistic effects.

3.2 Photolysis of benzisothiazolinone

At the start of this project, benzisothiazolinone was selected as the first model molecule. This biocide molecule with potentially harmful effects on human health and the environment is still used in commercial mixtures with pesticides. Irradiation experiments and analytical measurements were performed and their parameters optimized. Structural elucidation based on mass spectrometry data (HRMS, MS²) combined with knowledge on classical photochemical reaction pathways yielded the assessment of photoproduct structures. It is important to acknowledge the confidence level of the identification as presented in chapter 1 (Figure 1.2.7); in this case, probable/tentative (levels 2-3) structures were proposed. In some instances, standards were used to confirm the structures by matching chromatographic retention times and fragmentation patterns, thus achieving level 1 of identification confidence. Preliminary *in vitro* and *in silico* toxicity tests were performed as well. More details about the generalities, materials, methods, and results are presented in the article below, published in Chemosphere.

Photodegradation of benzisothiazolinone: Identification and biological activity of degradation products

Zsuzsanna Varga, Edith Nicol, Stéphane Bouchonnet

Laboratoire de Chimie Moléculaire – CNRS / Ecole Polytechnique, Institut Polytechnique de Paris, 91128, Palaiseau, France

Abstract

The photodegradation of benzisothiazolinone was studied in water under UV-Vis irradiation and led to fourteen photoproducts. Chemical structures of these compounds were elucidated using GC-MS, LC-MS/MS, and FT-ICR-MS experiments. Based on the chemical structures determined and their appearance order, a photo induced-degradation mechanism of benzisothiazolinone has been proposed, which combines isomerization, oxidation, hydroxylation, hydrolysis, and elimination processes. *In silico* tests on mutagenicity, Fathead minnow LC50 and oral rat LD50 were carried out to estimate the toxicity of the photoproducts. Compared with experimental data, the calculated oral rat LD50 values were found to be the most relevant and thus used for toxicity estimation. The photoproducts including a phenolic or a sulfino group or both functions were found potentially more toxic than benzisothiazolinone.

Introduction

1,2-benzisothiazol-3(2H)-one (referred to as benzisothiazolinone or BIT, is an antimicrobial agent used as a preservative in mainly aqueous-based chemical chemicals. Banned

from cosmetic products, BIT can be found in paints, lacquers, polishes, printing inks, emulsions, cleaning agents, disposable gloves; it is also widely used as a preservative for pesticides [1–4]. Due to environmental considerations, water-based paints recently replaced solvent-based paints, which require the addition of biocides; isothiazolinones are widely used for this purpose [5]. BIT is also used in paper-based jointing but it degrades during sunlight exposure losing its biocidal efficiency [6].

Isothiazolinone-type biocides act against various fungi and bacteria by the active sulfur moiety able to oxidize thiol functional groups to form disulfides (e.g. with cysteine) [7]. Besides the biocidal effects on unwanted compounds by reacting with intracellular sulfur-containing proteins [8, 9], isothiazolinones have also lethal effects on living organisms, the median lethal concentration (LC50) of BIT for zebrafish embryos being 1.03 mg/L [10]. Growth inhibition effect on *Escherichia coli* and *Schizosaccharomyces pombe* was measured; this inhibitory activity was quenched by thiolcontaining materials (glutathione, cysteine), confirming the mechanism of interaction [8]. According to the European Chemicals Agency, BIT is very toxic to aquatic life, causes eye damage and skin irritation [11]. Toxicity tests on zebrafish embryos were performed during ozonation processes and a decrease was found in the overall toxicity of the mixture, due to oxidation of the reductive sulfur in the parent compound [10] BIT is a developmental toxicant in rats but shows negative mutagenicity [12]. Isothiazolinones were shown to cause severe contact dermatitis and allergy in humans mainly with a high level of occupational exposure [13, 14].

It has been shown that isothiazolinones degrade rapidly in soil [15]. Indeed, BIT is easily degraded in the environment but there is no extensive study on the structure of its transformation products, their persistence, and their toxicity. Conventional wastewater treatment plant efficiently removes isothiazolinones at low concentrations [2]. In reverse osmosis (RO) wastewater treatment plants, BIT is used thanks to its compatibility and non-oxidizing nature and it prevents biofilm growth on membranes [16]. Nevertheless, studies demonstrated that some isothiazolinones increase the genotoxicity of the RO concentrates [17]. BIT is added at high concentrations (around 160 mg/l) for which the removal efficiencies of existing approaches are low; ozonation was proposed as an efficient way to degrade BIT [10]. Considering the photochemical degradation, the kinetics was studied under irradiation with a low-pressure UV-C lamp. The process was described to follow pseudo-first order kinetics. Radical species quenching studies were carried out, where the photodegradation of BIT was concluded to be both direct, due to UV absorbance of BIT and indirect, induced by radical oxygen species formation, a widespread mechanism of micropollutant photodegradation [18].

Different analytical methods were developed for the quantitation of BIT in various matrices. Ultrasonic assisted extraction combined with LC-MS was used to determine BIT at 9.9 mg/kg in hygienic consumer products, specifically in liquid detergents [19]. BIT

was analyzed by matrix solid-phase dispersion followed by LC-MS/MS in household products where it is used as a substitute to chlorinated isothiazolinone; it was found at quite high concentrations in laundry detergent (0.0255% w/w), surface cleaner cream (0.0116 %w/w) and liquid surface cleaner (0.00377% w/w) [20]. BIT was found in 94% of 47 paints analyzed by LC-MS at concentrations ranging from 28.6 to 1110.74 ppm. These analyses also showed that these products were sometimes labeled incorrectly, e.g. one paint labeled “preservative free” contained BIT at 71.5 ppm [21]. Isothiazolinones were monitored and not detected in environmental waters using derivatization of BIT followed by pre-concentration and GC-MS analysis, with limits of detection ranging from 0.01 to 0.1 µg/L [2].

This work aimed at performing accurate structural elucidation of the photodegradation products of BIT using chromatography and tandem mass spectrometry approaches. Benzisothiazolinone was degraded using two different types of photoreactors in water. Structural elucidation of BIT photoproducts allowed to suggest a coherent degradation pathway on one hand, and to carry out *in silico* toxicity tests to estimate the toxicity of the photoproducts on another hand.

Materials and methods

Chemicals, reagents and sample preparation

1,2-benzisothiazol-3(2H)-one (CAS: 2634-33-5), benzamide, salicylamide, 4-hydroxybenzamide and chromatography grade solvents: acetonitrile (ACN), methanol, dichloromethane and formic acid (FA) were purchased from Sigma Aldrich (Saint-Quentin-Fallavier, France). A Purelab Chorus 1 water purification system (Veolia, Wissous, France) was used to produce ultrapure water with a conductance of 18.2 S/cm. BIT solutions were prepared at different concentrations: 5, 10, 25, 50 and 100 ppm in water (solubility 1.1 g/l at 20°C [22]) and in acetonitrile. Some experiments were carried out with degassing of the initial solution using nitrogen bubbling for 30 min. Different irradiation times were tested to determine the appearance order of photoproducts. Solutions were irradiated for 6 h. Sampling was carried out every 10 min during the first hour and then every hour until the end. For GC-MS analysis, all samples (ACN solutions and aqueous samples) were dried using an Xcelvap automated evaporation/concentration system (Horizon Technologies, Bullion, France) and 1ml of dichloromethane was added. For LC-MS measurements, the samples of different BIT starting concentrations were diluted, in a mixture made of 50% ACN, 50% H₂O and 0.1% formic acid to reach a final concentration of 5 ppm. For HRMS analysis in the infusion mode, samples were diluted in a 90% water/10% ACN/0.1% FA mixture, for a starting concentration of BIT of 5 ppm. All the samples were stored away from light at 4°C; HPLC-MS data showed that degradation was negligible under these conditions, in agreement with literature data where the hydrolytic stability of the compound

is mentioned [12].

Irradiation experiments

The UV-Vis absorption spectrum of BIT was recorded in the range of 190-500 nm, using a 6800 UV-Vis Jenway spectrophotometer (Cole-Parmer, Villepinte, France), with a 1 cm length quartz cell. Based on this spectrum, two irradiation setups were used for photodegradation experiments. The photodegradation of BIT was mainly studied by a Philips HPL-N 125W/542 E27 SC high-pressure mercury lamp (France-Lampes, Saint-Cirq, France) with a wavelength range of 200-650 nm, a maximum irradiation wavelength at 254 nm, and a radiation flux of 6200 lm. The setup consisted of one lamp, circularly surrounded by 6 quartz tubes of 120 ml, all of the elements being in a water bath with water circulation so that the reaction temperature was kept below 28°C. The samples were also irradiated using a Q-sun test chamber Xe-1-B/S (Q-Lab Saarbücken, Germany) equipped with a xenon arc lamp; a natural light filter X-7640 from the same manufacturer has been used for the reproduction of full sunlight spectrum. The lamp power was 1800 W and the irradiation $0.68 \text{ Wm}^{-2} \text{ nm}^{-1}$ at a black-standard temperature of 55°C.

GC-MS analysis

Gas chromatographic separations were carried out on an Agilent 450-GC instrument equipped with a 60m "FactorFour VF-Xms" (10% phenyl, 90% methylpolysiloxane) capillary column, with an internal diameter of 0.25 mm and film thickness of 0.25 μm (Agilent Technologies, Les Ulis, France), coupled with an Agilent 240-MS ion trap mass spectrometer. Samples were injected in splitless mode using an Agilent CP-8400 autosampler, the injection volume was 1 μl and injector temperature was 280°C. A gradient temperature program was used with an initial temperature of 50°C, held for 0.5 min then increased to 280°C with a ramp of 10°C/min. The carrier gas was high purity helium, with a flow of 1.4 ml/min. Measurements were carried out in electron ionization and positive chemical ionization using methanol as the reagent gas. The filament emission current was set to 10 μA and automatic gain control was used for all experiments. The electron multiplier voltage was automatically optimized at 2200 V for a gain value of 10^5 . In the full scan mode, ions were scanned on the range of m/z 50 to m/z 500. Tandem experiment measurements were performed with an ionization storage level of m/z 35 and an isolation window of 3 m/z , using a resonant waveform type with an excitation storage level of m/z 50 and an excitation amplitude of 0.8 V.

LC-MS analysis

LC separations were carried out on an Acquity HPLC system (Waters Technologies, Guyancourt, France) coupled with a SolarixXR FT-ICR mass spectrometer equipped with a 9.4 T super conducting magnet (Bruker Daltonics, Bremen, Germany). A Pursuit XRs^{Ultra} C18 column (2.8 μm x 50 mm x 2 mm) (Agilent Technologies, Les Ulis France) was used in gradient mode. Water 0.1% FA(solvent A) and acetonitrile 0.1% FA (solvent

B) were used as solvents with a flow rate of 0.2 ml/min. The gradient started at 95% of solvent A for 3 min, then changed linearly to 50% of solvent A in 9 min and then to 5% of solvent A after 12 min of LC run. It was kept at 5% of solvent A for 5 min and then set back to the initial percentage of solvent A (95%) for 5 min of equilibrium. An electrospray ionization source was used in both positive and negative modes with a sample flow of 200 μ L/min for both positive and negative mode the nebulizer and drying gas was nitrogen with a flow of 8 L/min at 250°C for drying gas and 1 bar for nebulizer gas. The capillary voltage was set at - 4500 V and 4000 V in both positive and negative modes, respectively; the spray shield was set at -500 V. The detection mode was broadband with a 4 Mpt resolution in the range of 57.5–700 m/z with a data reduction of noise of 95%. For tandem MS experiments, precursor ions were isolated with an isolation window of 1 m/z and dissociated with collision energies of 10, 15, 20 and 25 V to study the fragmentation mechanisms. Indirect infusion mode, the flow rate was 120 μ L/h. The spectra were acquired with 4M data points on a range of 57.7–1000 m/z. Accumulation time was set to 0.02 s. 100 scans were recorded for each spectrum. The Bruker DataAnalysis software was used to process the chromatograms and spectra.

In silico bioassays

Preliminary toxicity assessments were performed using the T.E.S.T. software developed by the US Environmental Protection Agency (EPA). This software incorporates different endpoints and approaches, with various individual predictions. The different individual approaches include hierarchical clustering, the Food and Drug Administration (FDA) method, single model, group contribution and nearest neighbor [23]. The reliability of the results in the T.E.S.T. software should be assessed based on the capability of each individual prediction to calculate the toxicity values and then study concordance of the results. A complete description of T.E.S.T. and the included methods can be found on the EPA website [23]. Different QSAR methodologies are available to model mutagenicity. The biological testing background of most of them, including T.E.S.T., is the Ames test, which is based on a bacterial mutation of *Salmonella typhimurium*, reverting the bacteria from histidine dependence to histidine independence [24]. The correlation between carcinogenicity in animals and positive mutagenicity in the Ames test was found to be high [25]. The QSAR models for mutagenicity of the compounds of interest were found to be generally of high reliability.

Results and discussion

Physicochemical analysis and photoproducts structural elucidation

The UV/Vis absorption spectrum of BIT shows a high absorbance in the UV region and an additional absorption band with a maximum at 319 nm (Supplementary figure S3.2.1). The photodegradation was evidenced by the decrease of the molecule's absorption bands

with time (Figure 3.2.1). A strong decrease in concentration can be observed during the first 15 min of irradiation, whereas the degradation slows down later on. This is in good agreement with the exponential decrease evidenced by LC-MS experiments (see below). Whatever the chromatograph, using chromatography introduces some subjectivity in the detection process. Actually, the choice of stationary and mobile phases induces some selectivity regarding elution and thus detection of molecules. Therefore, direct infusion MS was used prior to LC-MS coupling, to carry out nontargeted investigation of transformation products in ESI-HRMS. The irradiated solutions were analyzed in both positive and negative modes for the same reasons. The ions detected in direct ESI-HRMS were the same as those detected in LC-MS. Retention times in LC-MS and GC-MS couplings, appearance times of photoproducts during the irradiation process, exact m/z values of $[M+H]^+$ and $[M - H]^-$ ions and corresponding formulae are listed in Table 3.2.1. Exact m/z values and corresponding formulae of collision-induced product ions from $[M+H]^+$ or $[M - H]^-$ ions are given in Supplementary information, Table S3.2.1.

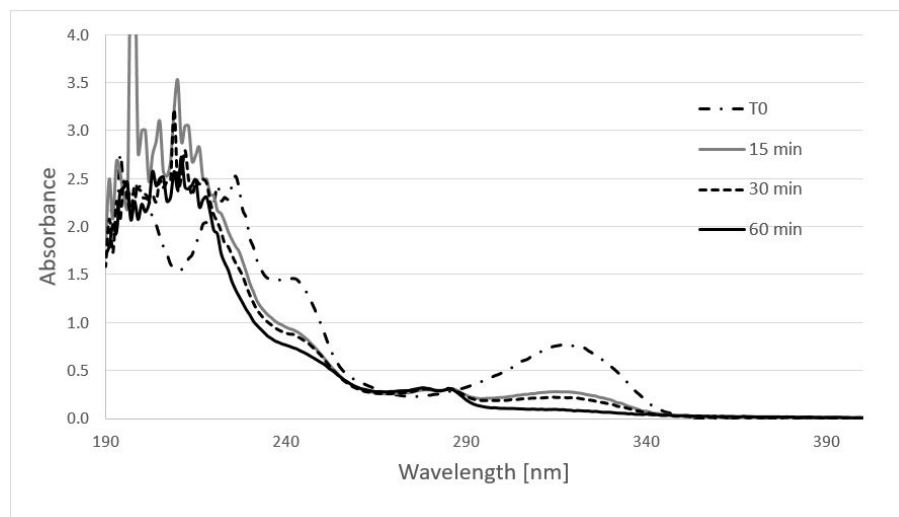
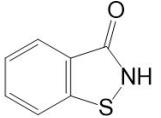
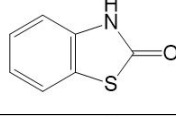
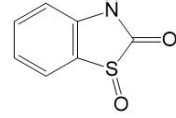
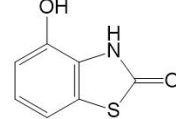
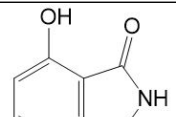
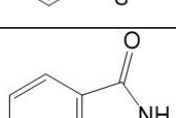
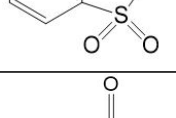
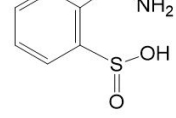
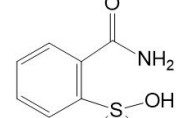
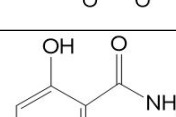
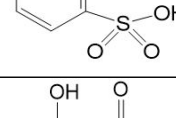
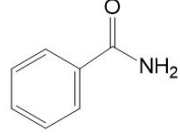
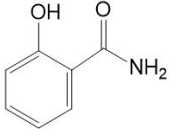
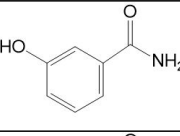
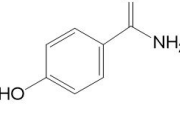


Figure 3.2.1: UV-Vis absorption spectrum of BIT (1.2 mM) in ultrapure water at different irradiation times ranging from 0 to 60 minutes

Table 3.2.1: Photoproducts of BIT detected in LC-MS and GC-MS couplings

Compound	Time of first detection (min)	Time where it not present any-more (min)	RT in LC-MS (min)	RT in GC-MS (min)	m/z measured for $[M+H]^+$ in ESI+	m/z measured for $[M-H]^-$ in ESI-	Theoretical mass of the neutral	Empirical formula of the neutral	Chemical structure

BIT	0	120	7.2	17.8	152.01642	150.00203	151.00918	C ₇ H ₅ NOS	
PP1	10	480	9.3	19.3	152.01636	150.00206	151.00918	C ₇ H ₅ NOS	
PP2a	10	120	5.4	20.3	168.01123	165.99698	167.00410	C ₇ H ₅ NO ₂ S	
PP2b	50	420	7.0	-	168.01120	165.99700	167.00410	C ₇ H ₅ NO ₂ S	
PP2c	50	420	8.3	-	168.01122	165.99699	167.00410	C ₇ H ₅ NO ₂ S	
PP3	10	120	3.8	-	-	181.99191	182.99901	C ₇ H ₅ NO ₃ S	
PP4	10	120	1.2	-	168.01123	184.00756	185.01466	C ₇ H ₇ NO ₃ S	
PP5	10	480	1.8	-	202.01665	200.00250	201.00957	C ₇ H ₇ NO ₄ S	
PP6a	30	480	0.9	-	-	215.99742	217.00449	C ₇ H ₇ NO ₅ S	
PP6b	30	480	1.5	-	-	215.99741	217.00449	C ₇ H ₇ NO ₅ S	
PP6c	30	480	2.3	-	-	215.99742	217.00449	C ₇ H ₇ NO ₅ S	

PP7	50	480	5.6	14.9	122.05992	-	121.05276	C ₇ H ₇ NO	
PP8a	50	480	7.3	16.5	138.05482	-	137.04768	C ₇ H ₇ NO ₂	
PP8b	50	480	2.5	-	138.05480	-	137.04768	C ₇ H ₇ NO ₂	
PP8c	50	360	7.1	-	138.05483	-	137.04768	C ₇ H ₇ NO ₂	

PP1 is among the first appearing photoproducts. It is eluted at 19.3 min in GC-MS; it has the same mass as the parent compound (eluted at 17.8 min) and its EI mass spectrum shows a very similar fragmentation pattern. Its exact formula (C₇H₅NOS) has been determined by HRMS and confirmed that PP1 corresponds to an isomer of BIT. 1,3-benzothiazol-2(3H)-one was postulated on the basis of PP1 mass spectrum. It was synthesized and analyzed using GC-MS; both its retention time and EI mass spectrum confirmed that PP1 corresponds to 1,3-benzothiazol-2(3H)-one (Table 3.2.1). Light-induced isomerization of BIT has been reported in an old study in which three possible isomerization mechanisms were postulated but none was demonstrated [26]. Considering the rapid isomerization of BIT into PP1, consequent oxidation processes will have to be considered from both isomers.

Three photoproducts (referred as PP2a, PP2b, and PP2c) were detected with retention times of 5.4, 6.9 and 8.3 min in LC-MS coupling. They all have a molecular weight of 167 (confirmed by both EI and CI mass spectra in GC-MS) and have been assumed to result from oxygen addition onto the parent compound. For the first one, the concerted losses of CO and SO (m/z 168.01196 \rightarrow m/z 96.04471 in CID measurements, Table S3.2.1) from the protonated molecule allowed to conclude that the oxygen atom was added onto the sulfur one. The fact that the nitrogen atom was retained in the m/z 96.04471 product ion permitted to conclude in favor of the structure depicted in Table 3.2.1, which results from oxidation of PP1 (and not from BIT). Both other PP2 isomers appear after 3 h of irradiation; they display exactly the same CID dissociation pathways. Eliminations of HNCO and HS. from protonated molecules show that the oxygen atom has been added on the aromatic ring. Hydroxylation of aromatic rings under UV-Vis irradiation has been widely reported in the literature [27, 28]. Because it can play an important role regarding toxicity, the exact position of the hydroxyl group has been determined based

on CID experiments as depicted in Supplementary figures S3.2.2 and S3.2.3. All the possible structures resulting from hydroxyl addition on the aromatic ring either from BIT or PP1 have been considered in a systematic way: only two of them can undergo two consecutive eliminations of carbon monoxide from the protonated species in positive ESI; their formulae are presented in Table 3.2.1.

The photoproduct referred as PP3 appears after only 10 min of irradiation. Its exact formula corresponds to the addition of two oxygen atoms on BIT or PP1. In CID experiments, the elimination of SO₂ from the deprotonated species (m/z 181.99191 \rightarrow m/z 118.02998, Table S3.2.1) leaves no doubt that both oxygen atoms have been added to the sulfur atom. Three mechanisms could be responsible for the formation of PP3: straight addition of a dioxygen molecule onto the sulfur atom from either BIT or PP1, or oxidation of PP2a. As this photoproduct is no more observed when irradiating a degassed solution, it can be concluded in favor of direct dioxygen addition on the sulfur atom. CID results do not permit to discriminate between oxidation of either BIT or PP1 but the structures elucidated for PP4 to PP8 photoproducts are strongly in favor of BIT oxidation, as discussed in the next section. It is to be noted that the structure suggested for PP3 corresponds to saccharin, which has been proved to be an oxidation product of BIT in a study dedicated to BIT ozonation [10].

PP4 has been detected in negative ESI, at a very short retention time (1.2 min) in reverse-phase chromatography suggesting a highly polar structure. Its mass spectrum exhibits a major ion resulting from deprotonation of the molecule. For these reasons, the structure suggested for PP4 in Table 3.2.1 includes a SOOH group, which allows easy removal of a proton in negative ESI. The SO₂ elimination in CID experiments is in good agreement with the proposed structure.

PP5 has been detected in both positive and negative ESI. Its elemental composition corresponds to that of PP4 plus a hydroxyl group. In the negative mode, observation of the deprotonated molecule indicates an acidic function (in agreement with the short eluting time in LC-MS). In the positive mode, the consecutive losses of ammonia and SO₂ imply that the amido function has been kept and that the sulfur atom carries two oxygen atoms. This implies that the additional hydroxyl group is bound to the aromatic ring. It has been located in ortho position with regard to the amido function since the formation of both PP2b and PP2c photoproducts shows that hydroxylation in this position is favored over additions onto other positions of the ring. The consecutive losses of SO₂ and H₂O from [PP5 - H]⁻ in CID experiments (m/z 200.00250 \rightarrow m/z 118.02997) confirm this hypothesis (see the dissociation pathways of [PP5 - H]⁻ in Supplementary figure S3.2.4).

Three photoproducts referred as PP6a to PP6c were detected at short retention times (between 0.9 and 2.3 min) in negative ESI. Their exact formulae correspond to the addition of an oxygen atom onto PP5. In CID experiments, the isomer eluting at 0.9 min undergoes

losses of NH_3 and $\text{O}=\text{C}=\text{NH}$ indicating that it still has the amido function; it demonstrates that the aromatic ring has been hydroxylated. The ammonia elimination, barely observed in negative ESI, has to be charge-induced. By analogy with other photoproducts and to rationalize the NH_3 loss (see Supplementary figure S3.2.5), the hydroxyl group was assumed to be in ortho position relative to the amido group. In the negative mode, the losses of HCNO and SO_2 from $[\text{PP6b} - \text{H}]^-$ indicate that two hydroxyl groups are carried by the aromatic ring in the PP6b structure. Unfortunately, CID experiments provided two few ions to allow the location of these hydroxyl groups. Both losses of HCNO_2 and SO_3 from $[\text{PP6c} - \text{H}]^-$ allowed the easy determination of the PP6c structure, as depicted in Supplementary figure S3.2.5.

PP7 has been easily identified as benzamide based on GC-MS and LC-MS analysis of the corresponding standard. As for PP7, PP8 isomers (PP8a to PP8c, see Table 3.2.1) were easily identified since salicylamide and 4-hydroxybenzamide were commercially available and were used to check mass spectra and retention times in GC-MS.

Mechanistic approach of BIT photodegradation

The photodegradation of BIT and the appearance of photoproducts were monitored using LC-MS in both positive and negative modes, at various concentrations ranging from 5 to 100 ppm. The detected photoproducts were the same regardless the initial BIT concentration, although the reaction kinetics slightly differed, the photodegradation being slower at higher concentrations, as displayed in Supplementary figure S3.2.6. At 5 ppm, BIT is undetectable after 30 min of irradiation while the initial amount of BIT has been reduced by 60% at 100 ppm for the same irradiation time. For each photoproduct, Table 3.2.1 gives the time at which it is first detected and the time at which it is no longer detected. Based on the kinetics of the appearance and disappearance of photoproducts, stepwise photodegradation mechanisms were proposed (Figure 3.2.2). Structures between brackets were not observed, likely because of too short lifetimes. It is to be noted that the formation of sulfite ions, reported by a previous study, was not evidenced in the present work but is in good agreement with the observed decrease of the mixture pH [10].

Isomerization of BIT into PP1 is very fast; it is not possible to state if this isomerization is partially reversible. Isomerization of other compounds including five-membered ring structures (PP2 isomers) could also not be established but could explain the formation of PP4 from PP2a (see Figure 3.2.2). From BIT or PP1, the formation of all the photoproducts can be rationalized by successive or competitive mechanisms including direct oxygen addition onto the sulfur atom (so that it reaches its highest oxidation state), hydroxyl addition, hydrolysis, and SO_3 elimination. The comparison of results between degassed and non-degassed solutions showed that the same photoproducts are produced in both cases. They are less abundant in degassed solutions, for which BIT dimers are also observed. This is likely because a reduced concentration in oxygen disfavors mechanisms involving

dissolved oxygen and thus favors intermolecular reactions between BIT excited species.

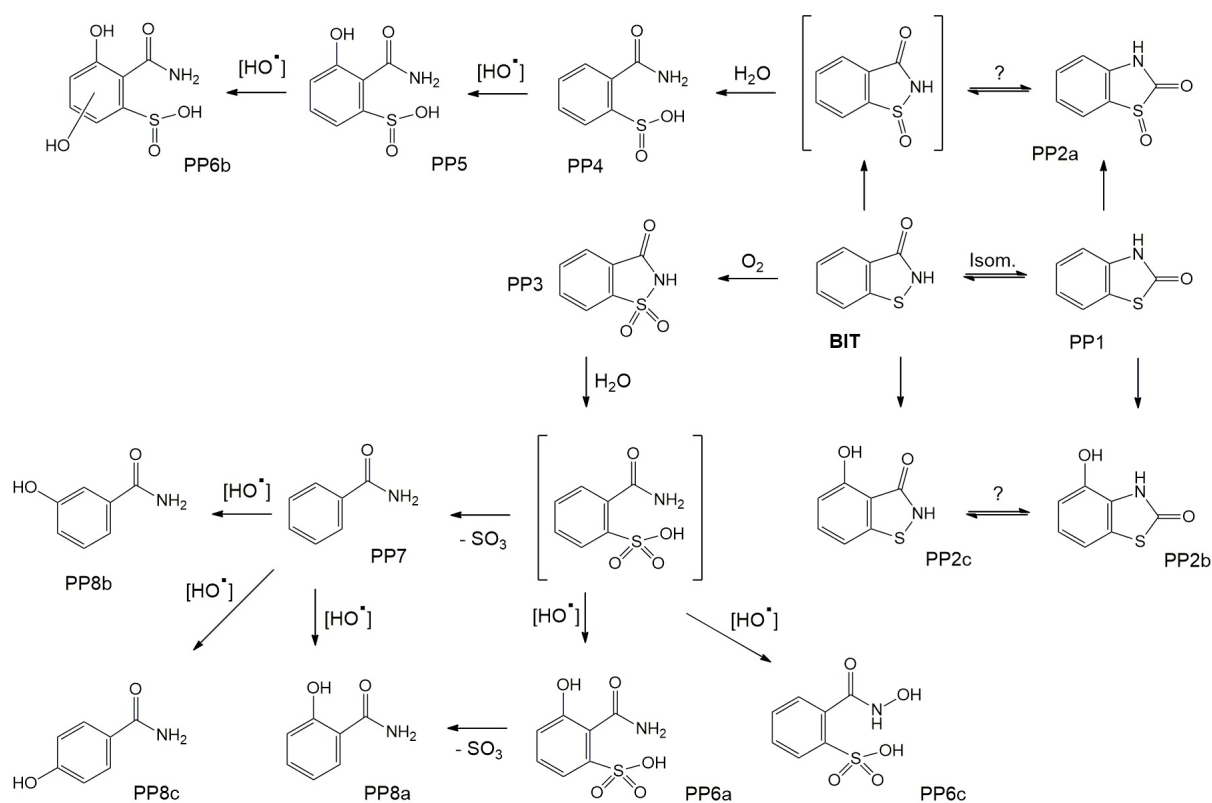


Figure 3.2.2: Suggested pathways for the photodegradation of BIT

In silico toxicity estimations

For each photoproduct, QSAR results on mutagenicity, oral rat and Fathead minnow toxicity were considered to be compared to that of the parent compound. The results of *in silico* toxicity estimations are summarized in Table 3.2.2. Since the structure of PP6b was not accurately determined (the position of the second hydroxyl group on the aromatic ring could not be stated, see Table 3.2.1), toxicity estimation could not be performed on this compound.

Regarding mutagenicity, T.E.S.T. works with a dataset of 5743 chemicals and provides a binary result (positive/negative). Experimental values were provided by the software for BIT, PP3, PP7, and PP8a; they were all in accordance with the calculated results. *In silico* estimations showed non-mutagenicity for all the photoproducts except PP4. For this compound, only 2 out of 3 individual predictions provided any result and both results were contradictory, therefore the mutagenicity positive result for PP4 is of low reliability; it might be a false positive result and should be treated accordingly. Fathead minnow LC_{50} (96 h), represents the concentration that kills half of the fish population (*Pimephales promelas*) in 4 days. The training set was obtained from the ECOTOX database, with a dataset containing 823 chemicals.

Table 3.2.2: Toxicity values estimated by the T.E.S.T. software for BIT and its photoproducts except PP6b

Compounds	Mutagenicity (Ames test)	Fathead minnow LC50 (96h) [mg/L]	Oral rat LD50 [mg/kg]
BIT	Negative	25	894
PP1	Negative	NA	1169
PP2a	Negative	148	527
PP2b	Negative	NA	3235
PP2c	Negative	36	941
PP3	Negative	NA	1685
PP4	Positive	140	649
PP5	Negative	79	412
PP6a	Negative	55	NA
PP6c	Negative	NA	3385
PP7	Negative	186	1123
PP8a	Negative	166	1619
PP8b	Negative	144	897
PP8c	Negative	126	608

The parent compound showed to be the most toxic but LC_{50} values could not be estimated for PP1, PP2b, PP3, and PP6c: none of the individual models provided a result since the requirements for reliable toxicity assessment were not fulfilled for these compounds. For PP8a (salicylamide) the proposed experimental toxicity value was in good agreement with the calculated one but for PP7, for which an experimental result was also available, the experimental value was 3.5 times higher than the calculated one. The oral rat LD_{50} endpoint gives the amount of chemical, in terms of the mass of the chemical over weight of the rat, which kills half of the rats when orally ingested. In this case, the ChemIDplus database was used to calculate toxicity data of interest with a final dataset of 7413 chemicals. For this endpoint, there was no prediction for photoproduct PP6a but the others proved to be of high reliability. Experimental values showed good accordance with the calculated ones for the parent compound. Photoproducts PP2a, PP2c, PP4, PP5, PP8b, and PP8c exhibited slightly higher or similar toxicity as the parent compound. Compound PP5 fell into the moderately toxic category (50–500 mg/kg) on the Hodge and Sterner scale [29]. All the other compounds were categorized as slightly toxic. For PP8a different oral rat toxicity values were reported in the literature but generally, the experimental values were approximately 2 times lower, closer to the toxicity values determined for PP8b and PP8c (Table 3.2.2) [30, 31]. It could explain the discrepancy among the PP8 compound family, in which photoproducts display isomeric structures. Given that oral rat toxicity calculations proved to be of adequate reliability, toxicophores of the critical compounds are further discussed. The potential toxicity of PP2a cannot be compared to those of other compounds since its structure includes a very specific and uncommon $-SO-CO-NH-$

structure (Table 3.2.1). It is interesting to note that, at the exception of PP2a, all the photoproducts exhibiting potential toxicity include either a phenolic (PP2c, PP8b and PP8c) or sulfinic (-SO₂H) group (PP4). Furthermore, the most toxic compound (PP5) is the one including both functions. The toxicity of phenolic compounds has been widely reported but that of the sulfinic group is not discussed in the literature, therefore no conclusion could be drawn but it might be interesting to investigate further this class of compounds.

Conclusion

The UV-VIS irradiation of an aqueous solution of benzisothiazolinone led to the formation of fourteen photoproducts, their chemical structures were elucidated based on GC-MS, LC-MS/MS, and FT-ICR-MS experiments. Based on the chemical structures determined and their appearance order, a photo induced degradation mechanism of benzisothiazolinone was proposed, which combines isomerization, oxidation, hydroxylation, hydrolysis, and elimination processes. Regarding to toxicity estimations, the absence of mutagenicity of photoproducts and the moderate oral rat LD50 values determined for some of them (while most of them are less toxic than the parent compound) leads to consider direct photodegradation as a potential powerful tool to remove benzisothiazolinone, even when it is used in large amounts in some wastewater treatment plants. This is even more interesting considering that these photoproducts were not persistent after a few hours of UV-light irradiation.

Acknowledgments

We are very thankful to Dr Gregory Danoun, Researcher at the LCM, who performed the synthesis of BIT.

This work is part of a project that has received funding from the European Union's Horizon 2020 research and innovation program under the Marie Skłodowska-Curie Grant Agreement No 765860 (AQUALity). Financial support from the National FT-ICR network (FR3624CNRS) and from the Ile de France Region are also gratefully acknowledged.

Supplementary data

Table S3.2.1: Exact m/z values and corresponding formulae of collision-induced product ions from $[M+H]^+$ and $[M-H]^-$ ions in LC-MS/MS

Compound	Retention time in LC-MS (min)	$[M+H]^+$ in ESI+ (m/z)	Daughter ions of $[M+H]^+$ (m/z)	Raw formula of the daughter ion	$[M-H]^-$ in ESI- (m/z)	Daughter ions of $[M-H]^-$ (m/z)	Raw formula of the daughter ion
BIT	7.2	152.01642	-	-	-	-	-
PP1	9.3	152.01636	-	-	-	-	-
PP2a	5.4	168.01196	151.00915 150.00133 122.00631 96.04471	C_7H_5NOS (-OH [•]) C_7H_4NOS (-H ₂ O) C_6H_4NS (-H ₂ O, -CO) C_5H_6NO (-CO, -SO)	-	-	-
PP2b	7.0	168.01196	140.01695 135.03148 125.00600 112.02193 108.04477	C_6H_6NOS (-CO) $C_7H_5NO_2$ (-HS [•]) C_6H_5OS (-CHNO) C_5H_6NS (-CO, -CO) C_6H_6NO (-COS)	-	-	-
PP2c	8.3	168.01196	140.01695 135.03148 125.00600 122.00632 112.02193	C_6H_6NOS (-CO) $C_7H_5NO_2$ (-HS [•]) C_6H_5OS (-CHNO) C_6H_4NS (-H ₂ O, -CO) C_5H_6NS (-CO, -CO)	-	-	-
PP3	3.8	-	-	-	181.99191	118.02998	C_7H_4NO (-SO ₂)
PP4	1.2	-	-	-	184.00756	120.04494	C_7H_6NO (-SO ₂)
PP5	1.8	202.01665	184.99094 121.02882	$C_7H_5O_4S$ (-NH ₃) $C_7H_5O_2$ (-NH ₃ , -SO ₂)	200.00250	156.99666 136.04055 118.02997 93.03468	$C_6H_5O_3S$ (-CHNO) $C_7H_6NO_2$ (-SO ₂) C_7H_4NO (-SO ₂ , -H ₂ O) C_6H_5O (-CHNO, -SO ₂)
PP6a	0.9	-	-	-	215.99742	198.07082 172.99153	$C_7H_3O_5S$ (-NH ₃) $C_6H_5O_4S$ (-CHNO)
PP6b	1.5	-	-	-	215.99741	172.99153 152.03542	$C_6H_5O_4S$ (-CHNO) $C_7H_6NO_3$ (-SO ₂)
PP6c	2.3	-	-	-	215.99742	156.99660 136.04048	$C_6H_5O_3S$ (-CHNO ₂) $C_7H_6NO_2$ (-SO ₃)
PP7	5.6	122.05992	105.03384 79.05447	C_7H_5O (-NH ₃) C_6H_7 (-CHNO)	-	-	-
PP8a	7.3	138.05482	121.02882 111.04443 95.04946	$C_7H_5O_2$ (-NH ₃) $C_6H_7O_2$ (-CHN) C_6H_7O (-CHNO)	-	-	-
PP8b	2.5	138.05480	121.02882 111.04443 95.04946	$C_7H_5O_2$ (-NH ₃) $C_6H_7O_2$ (-CHN) C_6H_7O (-CHNO)	-	-	-

PP8c	7.1	138.05483	120.04480 92.04979	C ₇ H ₆ NO (-H ₂ O) C ₆ H ₆ N (-H ₂ O, -CO)	-	-	-
------	-----	-----------	-----------------------	--	---	---	---

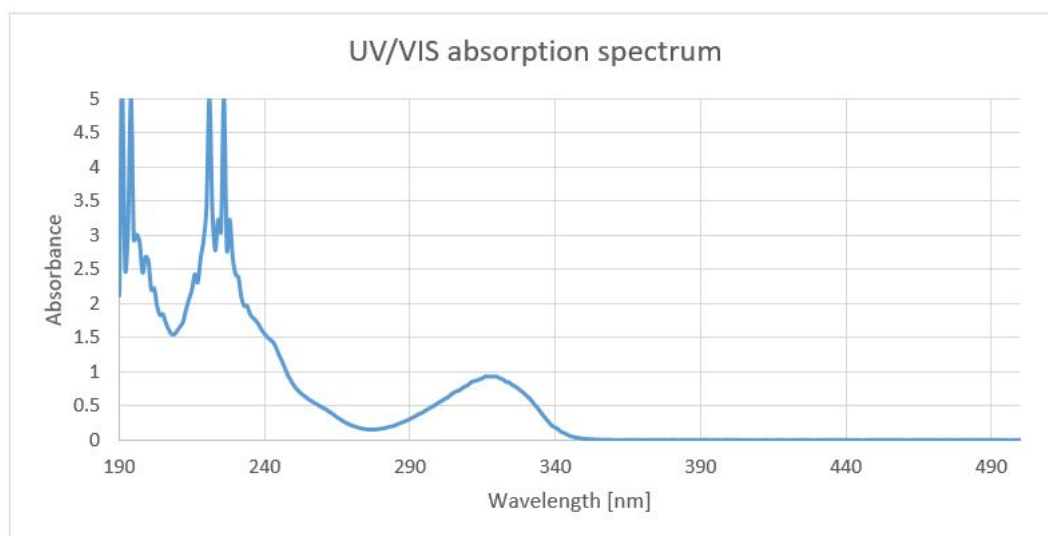


Figure S3.2.1: UV-Vis absorption spectrum of BIT (1.2 mM) in ultrapure water

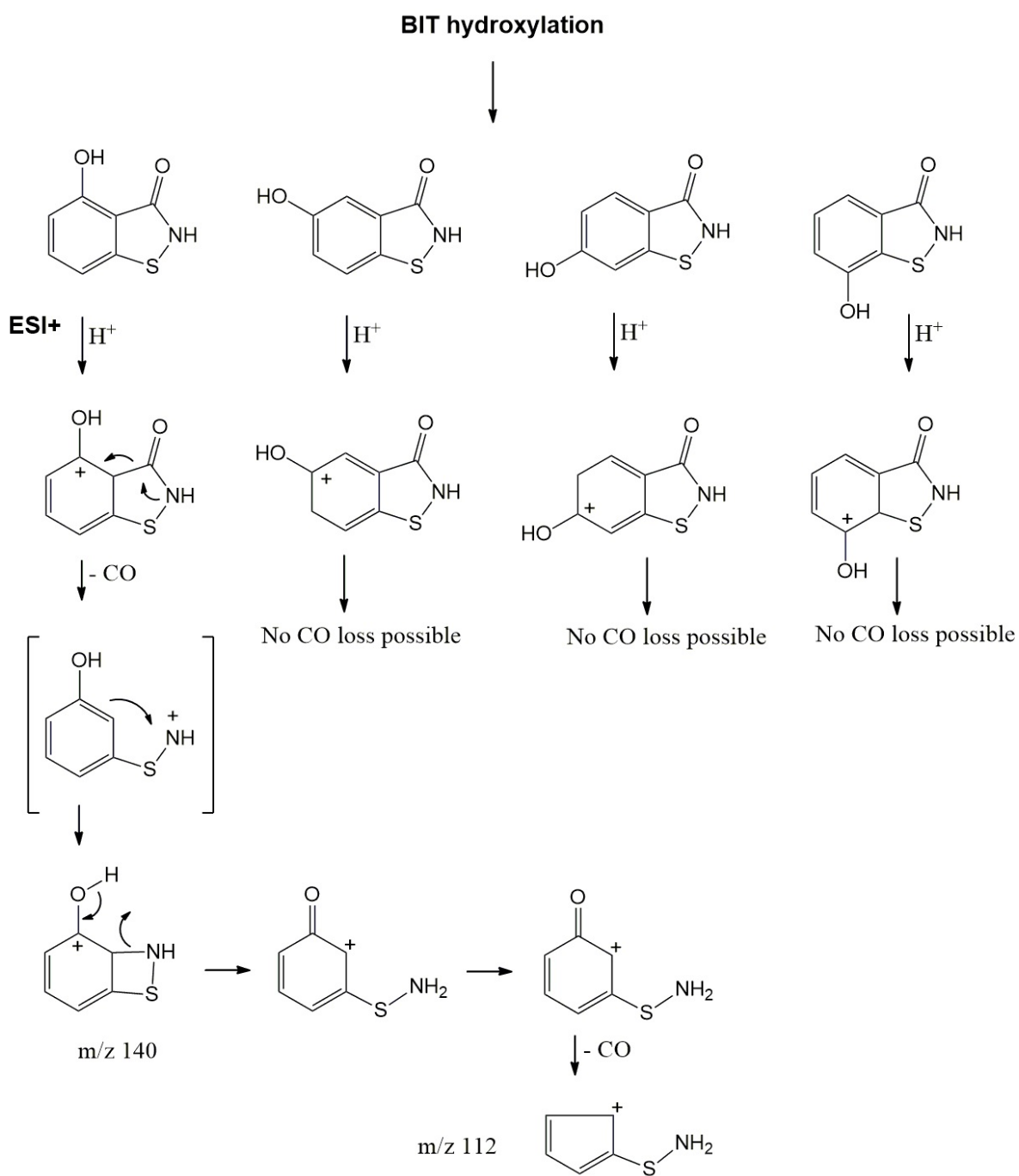


Figure S3.2.2: Consecutive CO eliminations from hydroxylated isomers of BIT and PP1 (a)

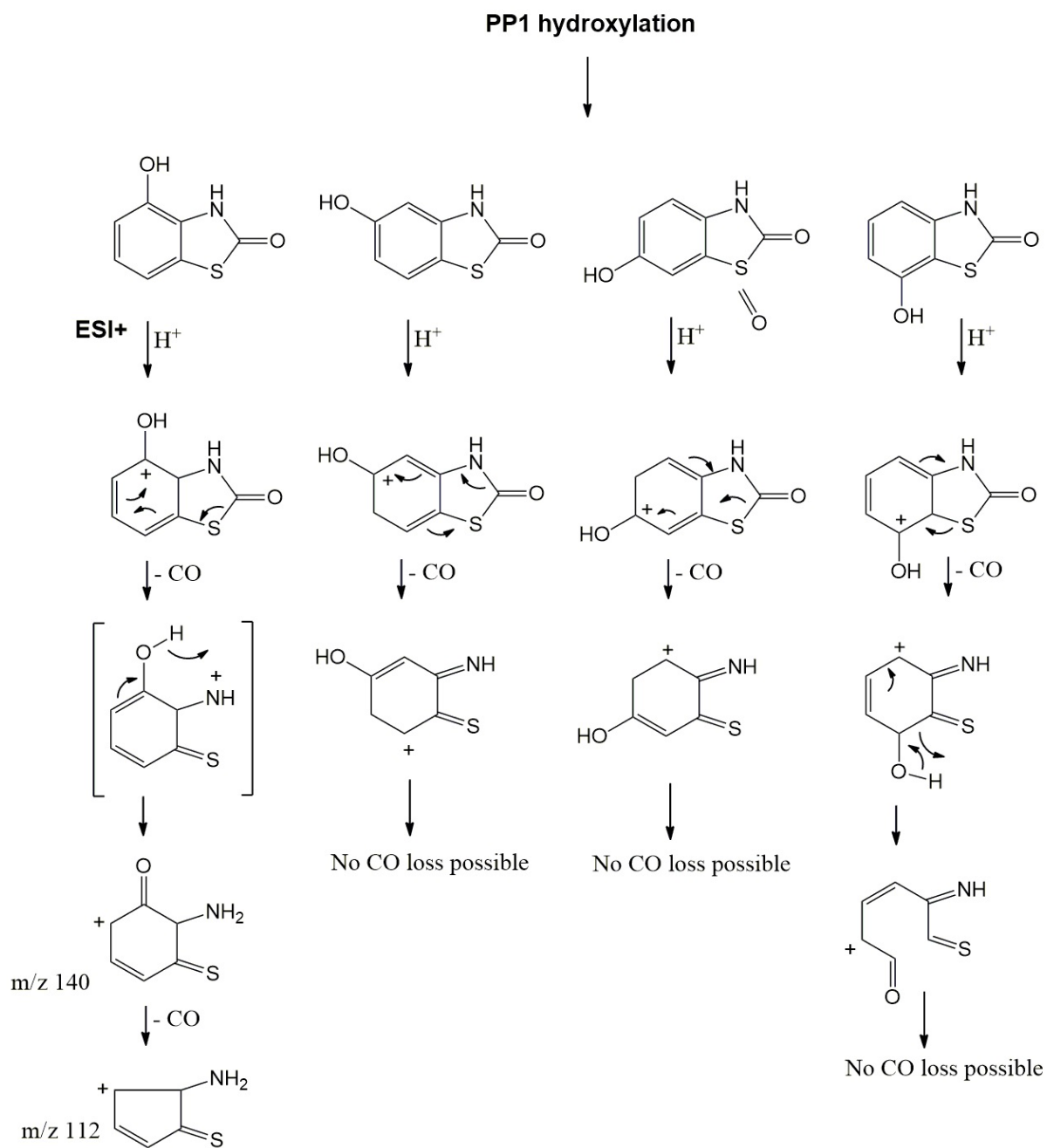


Figure S3.2.3: Consecutive CO eliminations from hydroxylated isomers of BIT and PP1 (b)

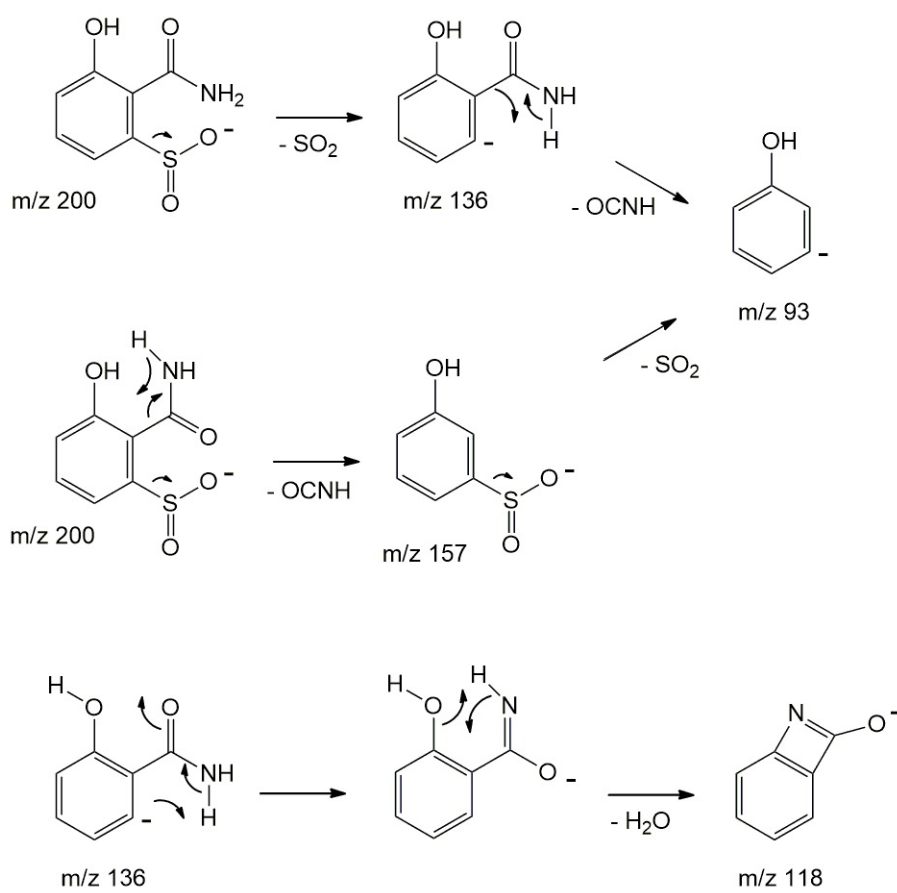
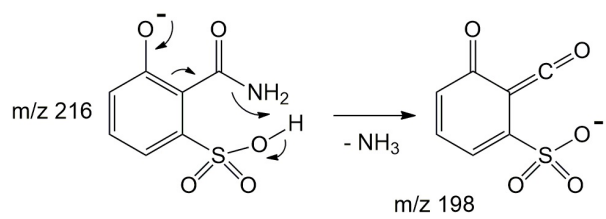
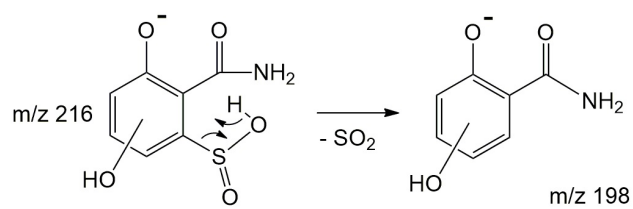
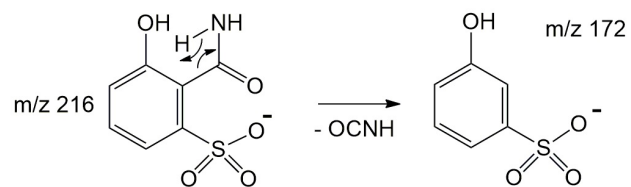


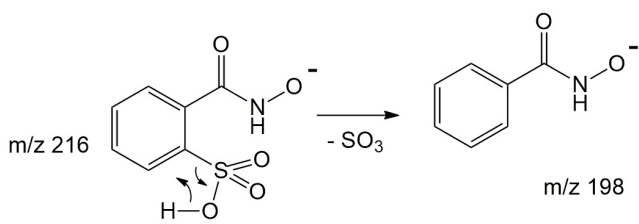
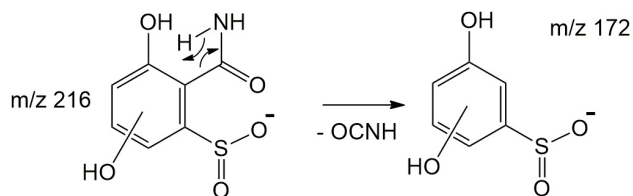
Figure S3.2.4: Dissociation pathways of $[PP5 - H]^-$ under collisional activation



[PP6a - H]⁻



[PP6b - H]⁻



[PP6c - H]⁻

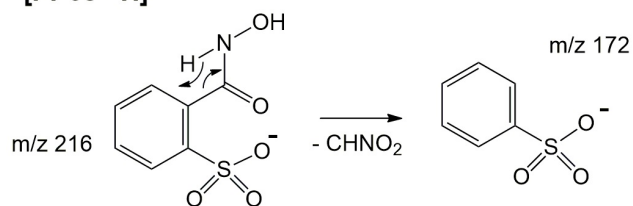


Figure S3.2.5: Dissociation pathways of PP6 isomers

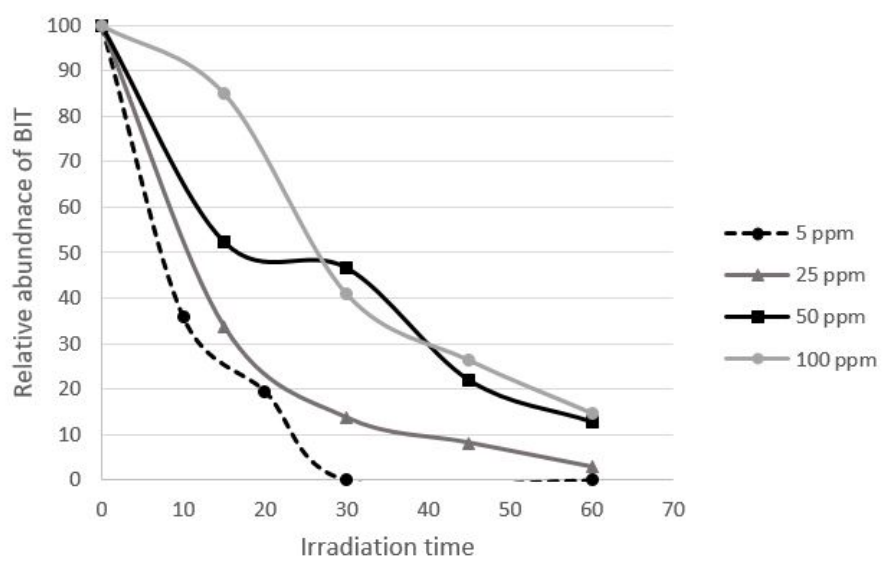


Figure S3.2.6: Relative amount of BIT as a function of irradiation time for concentrations of BIT ranging from 5 to 100 ppm

References

- [1] JF Schwensen, MD Lundov, R Bossi, P Banerjee, E Gimenez-Arnau, JP Lepoittevin, C Lidén, w Uter, K Yazar, IR White, and JD Johansen. “Methylisothiazolinone and benzisothiazolinone are widely used in paint: A multicentre study of paints from five European countries”. In: *Contact Derm* 72.3 (2014), pp. 127–138. DOI: 10.1111/cod.12322.
- [2] A Rafoth, S Gabriel, F Sacher, and HJ Brauch. “Analysis of isothiazolinones in environmental waters by gas chromatography-mass spectrometry”. In: *J Chromatogr A* 1164.1-2 (2007), pp. 74–81. DOI: 10.1016/j.chroma.2007.07.040.
- [3] MA Flyvholm. “Preservatives in registered chemical products”. In: *Contact Derm* 53.1 (2005), pp. 27–32. DOI: 10.1111/j.0105-1873.2005.00629.x.
- [4] K Aalto-Korte, L Ackermann, ML Henriks-Eckerman, J Valimaa, H Reinikka-Railo, E Leppanen, and R Jolanki. “1,2-Benzisothiazolin-3-one in disposable polyvinyl chloride gloves for medical use”. In: *Contact Derm* 57.6 (2007), pp. 365–370. DOI: 10.1111/j.1600-0536.2007.01278.x.
- [5] E Amsler, O Aerts, N Raison-Peyron, M Debons, B Milpied, F Giordano-labadie, J Waton, MC Ferrier-Le Bouëdec, I Lartigau, C Pecquet, H Assier, M Avenel-Audran, C Bernier, F Castelain, E Collet, MN Crépy, N Genillier, P Girardin, P Pralong, F Tetart, D Vital-Durand, A Soria, and A Barbaud. “Airborne allergic contact dermatitis caused by isothiazolinones in water-based paints: a retrospective study of 44 cases”. In: *Contact Derm* 77.3 (2017), pp. 163–170. DOI: 10.1111/cod.12795.
- [6] MJ Lugg. “Photodegradation of the biocide 1, 2-benziothiazolin-3-one used in a paper-based jointing material”. In: *Int Biodeter Biodegradation* 48.1-4 (2001), pp. 252–254. DOI: 10.1016/S0964-8305(01)00091-9.
- [7] PJ Collier, A Ramsey, RD Waigh, KT Douglas, P Austin, and P Gilbert. “Chemical reactivity of some isothiazolone biocides”. In: *J Appl Bacter* 69.4 (1990), pp. 578–584. DOI: 10.1111/j.1365-2672.1990.tb01551.x.
- [8] PJ Collier, AJ Ramsey, P Austin, and P Gilbert. “Growth inhibitory and biocidal activity of some isothiazolone biocides”. In: *J Appl Bacteriol* 69.4 (1990), pp. 569–577. DOI: 10.1111/j.1365-2672.1990.tb01550.x.
- [9] SL Morris, RC Walsh, and JN Hansen. “Identification and characterization of some bacterial membrane sulfhydryl groups which are targets of bacteriostatic and antibiotic action”. In: *J Biol Chem* 259.21 (1984), pp. 13590–13594. DOI: 10.1016/S0021-9258(18)90734-9.

- [10] A Li, Z Chen, QY Wu, MH Huang, ZY Liu, P Chen, LC Mei, and HY Hu. “Study on the removal of benzisothiazolinone biocide and its toxicity: The effectiveness of ozonation”. In: *Chem Eng J* 300 (2016), pp. 376–383. DOI: 10.1016/j.cej.2016.04.021.
- [11] European Chemicals Agency. *1,2-benzisothiazol-3(2H)-one*. 2019. URL: <https://echa.europa.eu/substance-information/-/substanceinfo/100.018.292>.
- [12] U.S. Environmental Protection Agency. *Reregistration Eligibility Decision (RED) for Benzisothiazolin-3-one*. 2005. URL: https://archive.epa.gov/pesticides/reregistration/web/pdf/benzisothiazolin_red.pdf.
- [13] D Bregnbak, MD Lundov, C Zachariae, T Menné, and JD Johansen. “Five cases of severe chronic dermatitis caused by isothiazolinones”. In: *Contact Derm* 69.1 (2013), pp. 57–59. DOI: 10.1111/cod.12081.
- [14] N Bang Pedersen. “Occupational allergy from 1,2-benzisothiazolin-3-one and other preservatives in plastic emulsions”. In: *Contact Derm* 2.6 (1976), pp. 340–342. DOI: 10.1111/j.1600-0536.1976.tb03072.x.
- [15] UE Bollmann, D Fernández-Calviño, K Koefoed, MS Storgaard, H Sanderson, and K Bester. “Biocide runoff from building facades: Degradation kinetics in soils”. In: *Environ Sci Technol* 51.7 (2017), pp. 3694–3702. DOI: 10.1021/acs.est.6b05512.
- [16] F Tang, YX Sun, Y Shi, X Li, and HY Hu. “Chemicals consumption and cost analysis of a microfiltration-reverse osmosis process for wastewater reclamation”. In: *Environ Sci (China)* 32.9 (2012), pp. 1613–1619.
- [17] F Tang, HY Hu, QY Wu, X Tang, YX Sun, XL Shi, and JJ Huang. “Effects of chemical agent injections on genotoxicity of wastewater in a microfiltration-reverse osmosis membrane process for wastewater reuse”. In: *J Hazard Mater* 260 (2013), pp. 231–237. DOI: 10.1016/j.jhazmat.2013.05.035.
- [18] T Wang, QY Wu, WL Wang, Z Chen, BT Li, A Li, ZY Liu, and HY Hu. “Self-sensitized photodegradation of benzisothiazolinone by low-pressure UV-C irradiation: Kinetics, mechanisms, and the effect of media”. In: *Sep Purif Technol* 189 (2017), pp. 419–424. DOI: 10.1016/j.seppur.2017.08.031.
- [19] JJ Heo, UJ Kim, and JE Oh. “Simultaneous quantitative analysis of four isothiazolinones and 3-iodo-2-propynyl butyl carbamate present in hygienic consumer products”. In: *Environ Eng Res* 24.1 (2019), pp. 137–143. DOI: 10.4491/eer.2018.144.

- [20] G Alvarez-Rivera, T Dagnac, M Lores, C Garcia-Jares, L Sanchez-Prado, JP Lamas, and M Llompарт. “Determination of isothiazolinone preservatives in cosmetics and household products by matrix solid-phase dispersion followed by high-performance liquid chromatography-tandem mass spectrometry”. In: *J Chromatogr A* 1270 (2012), pp. 41–50. DOI: 10.1016/j.chroma.2012.10.063.
- [21] MC Goodier, PD Siegel, LY Zang, and EM Warshaw. “Isothiazolinone in Residential Interior Wall Paint : A High-Performance Liquid Chromatographic – Mass Spectrometry Analysis”. In: *Am Contact Derm Soc* 29.6 (2018), pp. 332–338. DOI: 10.1097/DER.0000000000000410.
- [22] Scientific Committee on Consumer Safety. “Opinion on Benzisothiazolinone”. In: (2012), pp. 1–32. DOI: 10.2772/83092.
- [23] T Martin. “User’s Guide for T.E.S.T. (version 5.1) (Toxicity Estimation Software Tool) A Program to Estimate Toxicity from Molecular Structure”. In: (2016), p. 63. URL: https://cfpub.epa.gov/si/si_public_record_report.cfm?dirEntryId=326210&Lab=NRML.
- [24] K Mortelmans and E Zeiger. “The Ames Salmonella/microsome mutagenicity assay”. In: *Mutation Research* 455 (2000), pp. 29–60. DOI: 10.1016/S0027-5107(00)00064-6.
- [25] JG Hengstler and F Oesch. “Ames Test”. In: *Encyclopedia of Genetics*. 2001, pp. 51–54. DOI: 10.1006/rwgn.2001.1543.
- [26] LJ Darlage. “Thermal, photochemical, and electron impact induced transformations of 1,2-benzisoxazolin-3-ones and related heterocyclic compounds”. PhD thesis. Iowa State University, 1971. URL: <https://lib.dr.iastate.edu/rtd/4442/>.
- [27] T Matsuura and K Omura. “Photochemical hydroxylation of aromatic compounds”. In: *Synthesis* 3 (1974), pp. 173–184. DOI: 10.1055/s-1974-23269.
- [28] S Kinani, Y Souissi, A Kinani, S Vujovic, S Ait-Aissa, and S Bouchonnet. “Photodegradation of fluorene in aqueous solution : Identification and biological activity testing of degradation products”. In: *J Chromatogr A* 1442 (2016), pp. 118–128. DOI: 10.1016/j.chroma.2016.03.012.
- [29] HC Hodge and JH Sterner. “Tabulation of Toxicity Classes”. In: *Am Ind Hyg Assoc J* 10.4 (1949), pp. 93–96. DOI: 10.1080/00968204909344159.
- [30] EI Goldenthal. “A Compilation of LD50 Values in Newborn and Adult Animals”. In: *Toxicol App. Pharmacol* 18 (1971), pp. 185–207. DOI: 10.1016/0041-008X(71)90328-0.

- [31] GC Boxill, CB Nash, and AG Wheeler. “Comparative Pharmacological and Toxicological Evaluation of N-Acetyl-p-Aminophenol , Salicylamide , and Acetylsalicylic Acid”. In: *J Am Pharm Assoc* 47 (1958), pp. 479–487. DOI: 10.1002/jps.3030470706.

3.3 Photolysis of naproxen

Another molecule selected to apply the in-lab approach on, was the widely used anti-inflammatory drug naproxen. In this case, the approach was highly similar to the one used for the degradation of benzisothiazolinone. The same instrumentation was used, except that in the case of naproxen, GC-MS was employed as well, in combination with the derivatization of the molecules, as some compounds were suitable to be GC analyzed due to their low molecular weight and low polarity.

UV-visible photodegradation of naproxen in water – Structural elucidation of photoproducts and potential toxicity

Noemi Cazzaniga, Zsuzsanna Varga, Edith Nicol and Stéphane Bouchonnet

Laboratoire de Chimie Moléculaire – CNRS / Ecole Polytechnique, Institut Polytechnique de Paris, 91128, Palaiseau, France

Abstract

The UV-visible photodegradation of naproxen (6-methoxy- α -methyl-2-naphthaleneacetic acid, CAS: 22204-53-1), one of the most used and detected non-steroidal anti-inflammatory drugs (NSAIDs) in the world, and its ecotoxicological consequences were investigated in an aqueous medium. The photo-transformation products were analyzed and the structures of photoproducts were elucidated using gas chromatography coupled with tandem mass spectrometry (GC-MS/MS) and high-performance liquid chromatography coupled with ultrahigh-resolution Fourier transform ion cyclotron resonance mass spectrometry (LC-FTICR-MS). Seven photoproducts were detected and characterized, photo-transformation mechanisms have been postulated to rationalize their formation under irradiation. *In silico* QSAR (Quantitative Structure-Activity Relationship) toxicity predictions were performed with the Toxicity Estimation Software Tool (T.E.S.T.) and *in vitro* assays were carried out on *Vibrio fischeri* bacteria. Some of the obtained photoproducts exhibit higher potential toxicity than naproxen itself but the whole toxicity of the irradiated solution is not of major concern.

Introduction

As the human body does not break them down entirely, pharmaceuticals and their metabolites represent a significant source of environmental contamination and their ever-increasing consumption is a major issue for the environment and human safety. The volume of medicines used globally will reach 4.5 trillion doses by the end of 2020 on a 1.4 trillion dollar market [1]. Frequent use and active consumption of pharmaceuticals led to increased levels of drug-related residues in the environment. More than 600 active

pharmaceutical ingredients (APIs) or their metabolites and photo-degradation products have been identified, mainly in surface water and wastewater, but also in groundwater, soil, and other environmental matrices [2]. High concentrations of pharmaceutical products reach wastewater treatment plants (WWTP), mainly through human urinary, fecal excretion, and industrial discharges, and a considerable variety of drugs is not mineralized by conventional treatment processes. It is now turned out that hospital effluents are also significant sources of aquatic environmental pollution [3]. Consequently, more and more research is devoted to design specific pilot plants suitable for the degradation of biocides and drugs in hospital effluents, aiming at reducing the pharmaceutical burden of wastewater treatment plants and the associated risk.

In the past years, different prioritization approaches, based on consumption data, experimental toxicological and physicochemical data, and *in silico* predictions, were carried out to screen and identify the most environmentally hazardous pharmaceuticals. A recent study using a QSAR (Quantitative Structure-Activity Relationship) approach has shown that pharmaceutical products constitute a new generation of contaminants of emerging concern that can affect wildlife and the ecosystem even at low concentrations [4]. The majority (83%) of the drugs screened were predicted to be non-PBT (Persistent, Bioaccumulative, Toxic) and therefore, may not be considered dangerous for the ecosystem. 35 drugs have been identified as potential PBTs, for which an experimental evaluation will have to be made to confirm the expected PBT behavior [5, 6].

Contrary to chronic toxicity, the acute toxicity of nonsteroidal anti-inflammatory drugs (NSAIDs) has not been widely studied, except in the case of propranolol, which shows high acute toxicity. 17% of the medicines exhibited human LC50 values lower than 100 mg/L, which according to EU Directive 93/ 67/EEC [7] correspond to acute toxicity, 38% exhibited LC50 values above 100 mg/L and were thus classified as not harmful to aquatic organisms. The remaining 45% showed a considerable variability of acute toxicity values depending on the way they were evaluated. In the case of naproxen, the provided EC50 values fall in a range as wide as 10-1000 mg/L [8, 9].

According to statistics conducted in 2017 on clinical drugs, naproxen was the 71st most prescribed medication in the United States, with more than eleven million prescriptions. It belongs to the priority list of substances defined by the Global Water Research Coalition [10]; it is also on the list of contaminants of emerging concern compiled by the NORMAN network, specialized in monitoring and biomonitoring of emerging environmental substances [11]. Naproxen is one of the most commonly detected pharmaceutical compounds in the environment, with concentrations in surface waters up to 32 µg/L [9]. It is mainly excreted in urine (95% of the quantity ingested) and is not effectively removed by current wastewater treatments. A naproxen concentration of 6 µg/L has been reported in raw urban wastewater and effluent from a system of activated sludge, a common treat-

ment adopted for urban wastewaters prior to final discharge into surface water bodies [12]. In another study conducted on raw urban wastewater and effluent from an activated sludge system, Ibuprofen was detected at the highest concentration (373 $\mu\text{g/L}$), followed by naproxen (53 $\mu\text{g/L}$). No significant reduction was found for ibuprofen and naproxen in the pre-treatment and sedimentation step; because of their acidic structures and their very low solid-liquid partition K_d coefficients, both molecules undergo very poor sorption onto sludge and mainly remain in the aqueous phase [13].

It has been demonstrated that naproxen, by itself or through its metabolites, can affect organisms that inhabit ecosystems and one of the most important aspects of studies on the degradation of pollutants is the toxicity of degradation products, which in some cases can be higher than that of the parent molecule [14]. The main objective of the present work was to characterize the photoproducts generated from direct photolysis of naproxen, based on GC-MS and LC-MS investigations. Ultrahigh-resolution measurements permitted direct assignment of exact formulae while tandem experiments allowed structural elucidation for the major part of photoproducts. The second aim of this work was to estimate the potential toxicity of the photoproducts using both *in silico* (QSAR calculations) and *in vitro* (luminescence inhibition tests on *Vibrio fischeri* marine bacteria) approaches, to determine whether UV-visible photodegradation could be an efficient solution for the safe removal of naproxen, for instance from hospital effluents.

Experimental

Chemicals and reagents

Naproxen (6-methoxy- α -methyl-2-naphthaleneacetic acid, CAS: 22204-53-1) was provided by Sigma Aldrich (Madrid, Spain). Acetonitrile (ACN), methanol and dichloromethane (Sigma Aldrich, Saint Quentin Fallavier, France) were of chromatographic grade, i.e. with purity > 99.99%. BSFTA (N,O-Bis (trimethylsilyl)trifluoroacetamide) and formic acid were also from Sigma Aldrich (Saint Quentin Fallavier, France). Ultrapure water (conductance of 18.2 S/cm) was obtained purifying tap water with a Purelab Chorus 1 system (Veolia, Wissous, France).

Sample preparation

Naproxen solutions were prepared at four concentrations: 2, 10, 100, and 500 ppm in water to which 0.1% acetonitrile was added regarding the poor solubility of naproxen in pure water close to neutral pH (around 4 mg/L at 25°C according to the Henderson-Hasselbach equation). Different irradiation times were tested, to determine the appearance order of photoproducts. The solutions were irradiated up to a maximum of 6 hours with sampling at t 0-2-5-10-15-30-45-60-80-100-120 minutes, then every thirty minutes up to the fourth hour, and every hour until the end of the analysis. For GC-MS analysis, all samples were dried using an Xcelvap automated evaporation/concentration system (Biotage, Uppsala,

Sweden) for an hour, then put in an oven (WTC Binder 7200, Tuttlingen, Germany) for 10 minutes at 80°C to remove any trace of water. Silylation was achieved by adding 100 µL of BSTFA (N,O-Bis (trimethylsilyl) trifluoroacetamide) and placing the sample in the oven for 30 minutes. 100 µL of dichloromethane (DCM) was added prior to GC-MS analysis to reconstitute the sample. For LC-MS coupling measurements, samples were dissolved in ultrapure water to reach a final concentration of 2 ppm for nondegraded naproxen at t_0 . For HRMS analysis in direct infusion mode, samples were diluted in a mixture of H₂O/ACN/FA 90/10/0.1%, to reach a 2 ppm concentration for naproxen at t_0 . All samples were stored sheltered from light at 4°C.

Photolysis experiments

Photodegradation experiments were conducted using a home-made photoreactor equipped with a highpressure mercury lamp HPL-N 125 W/542 E27 SC (Phillips, Ivry-sur-Seine, France) that emits light on wavelengths between 200 nm and 650 nm, with maximum irradiation at 254 nm and a radiation flow of 6200 lm. The lamp is located in a quartz tube at the center of an AL04-12 sonicator (Advantage-Lab GmbH, Darmstadt, Germany) and samples are placed in quartz tubes around, at equal distance to the lamp. The sonicator is used to achieve the solubilization of compounds before irradiation. To avoid thermal degradation, the temperature was manually adjusted to 30±5°C flowing cold-water through the sonicator manifold.

GC-MS operating conditions

Gas chromatographic separations were carried out on an Agilent 7890B GC instrument equipped with a 30 m HP-5MS column (5% Phenylmethylpolysiloxane) with an internal diameter of 0.25 mm and film thickness of 0.25 µm, coupled with an Agilent 7000 D GC/TQ triple quadrupole mass spectrometer (Agilent Technologies, Les Ulis, France). Samples were injected in splitless mode using an Agilent 7693 A autosampler, the injection volume was 1 µL and the injector temperature was 280°C. A gradient temperature program was used with an initial temperature of 50°C, held for 0.5 min then increased to 320°C with a ramp of 20°C/min. The carrier gas was high purity helium, with an autoregulated flow of 1.2 ml/min. Measurements were carried out in electron ionization (70 eV) with a filament emission current of 35 µA. The electron multiplier voltage was automatically optimized at 1090 V, for a gain value of 10⁵. In the full scan mode, ions were scanned from m/z 50 to m/z 600. Tandem experiment measurements were performed, using argon as the collision gas, with collision energies of 15, 30, and 45 eV. The source temperature was set to 230°C.

LC-MS operating conditions

Chromatographic separations were carried out using an Acquity HPLC system (Waters Technologies, Guyancourt, France) equipped with a C₁₈ Pursuit XRs Ultra 2.8 µm, 50 x 2.0 mm column (Agilent Technologies, Les Ulis, France) and coupled with an FT-ICR

SolarixXR 9.4 T (Bruker Daltonics, Bremen, Germany). The injection volume was 10 μ L, elution was performed using a 0.1 mL/min flow with a mixture of solvents A (water, formic acid 0.1%) and B (acetonitrile, formic acid 0.1%). After 10 minutes, the percentage of solvent B was increased from an initial value of 5% to 40% in 15 min, then to 90% in 5 min. The gradient was then set back to initial conditions (5% of B) during the last 20 min, for a total method duration of 50 min. An electrospray ionization source was used both in positive and negative mode, the nebulizer and drying gas was nitrogen with a flow of 8 L/min at 250°C for drying gas and 1 bar for nebulizer gas. The capillary voltage and end plate offset values were set to - 4500 V and - 4000 V, respectively for positive mode, and 3000 V and 2500 V, respectively for negative mode. Argon was used as the collision gas for tandem experiments. Ions were accumulated in the collision cell for 0.2 s in MS experiments and 2 s in MS/MS experiments. The ion detection mode was set to 4 Mpt with a 0.8389 s transient duration in broadband mode from m/z 57.7 to m/z 1000 to obtain a resolution higher than 350 000 at m/z 200. To reduce the size of the data file, 97% of the data (contributing to noise) were not recorded to get a data file size below 2 GB per analysis. Phosphoric acid was used for external mass calibration and exact chemical formulae were attributed with tolerance below 3 ppm. For tandem MS experiments, precursor ions were isolated with an isolation window of 1 m/z and dissociated, using argon as the collision gas, with collision energies of 10, 15, 20, and 25 V to study the fragmentation mechanisms.

In silico toxicity estimations

The toxicities of naproxen and its photoproducts were *in silico* evaluated regarding developmental toxicity, oral rat LD50 (mg/kg), and fathead minnow LC50 (96 h) (mg/L). The Toxicity Estimation Software Tool (T.E.S.T.) - based on Quantitative Structure-Activity Relationship (QSAR) mathematical models - was used for this purpose [15]. T.E.S.T. has been developed by the U.S. Environmental Protection Agency, its main features are briefly described in Supplementary information SI-1.

In vitro bioassays

Vibrio fischeri commercial *in vitro* test kit was used to evaluate the global ecotoxicity of solutions before (initial concentration of 50 μ g/L in naproxen) and after two times of irradiation: 30 and 80 min. The freeze-dried luminescent bacteria and the luminometer were purchased from Hach Lange (GmbH, Dusseldorf, Germany). The experimental method used in this study is based on the ISO 11348-3 protocol [16]. Luminescence was measured in duplicate before the addition of the test solution and after contact times of 5, 15, and 30 min; results were corrected using the values measured with control samples. The effective nominal concentration leading to 20% inhibition of bioluminescence is designated as the EC20.

Results and discussion

Kinetics of photoproducts and degradation efficiency

The relative concentration of naproxen in ultrapure water was followed by LC-MS over the irradiation time (6 hours), integrating the area of the corresponding chromatographic peak on the $[M+H]^+$ ion. The initial amount of naproxen (initial concentration of 2 ppm) was halved after about 30 minutes and the compound was no longer detected after 45 minutes. In order to correlate the appearance of some photoproducts with the disappearance of some others, their relative abundances (normalized data from GC-MS and LC-MS signals) were plotted as a function of irradiation time (Figure 3.3.1).

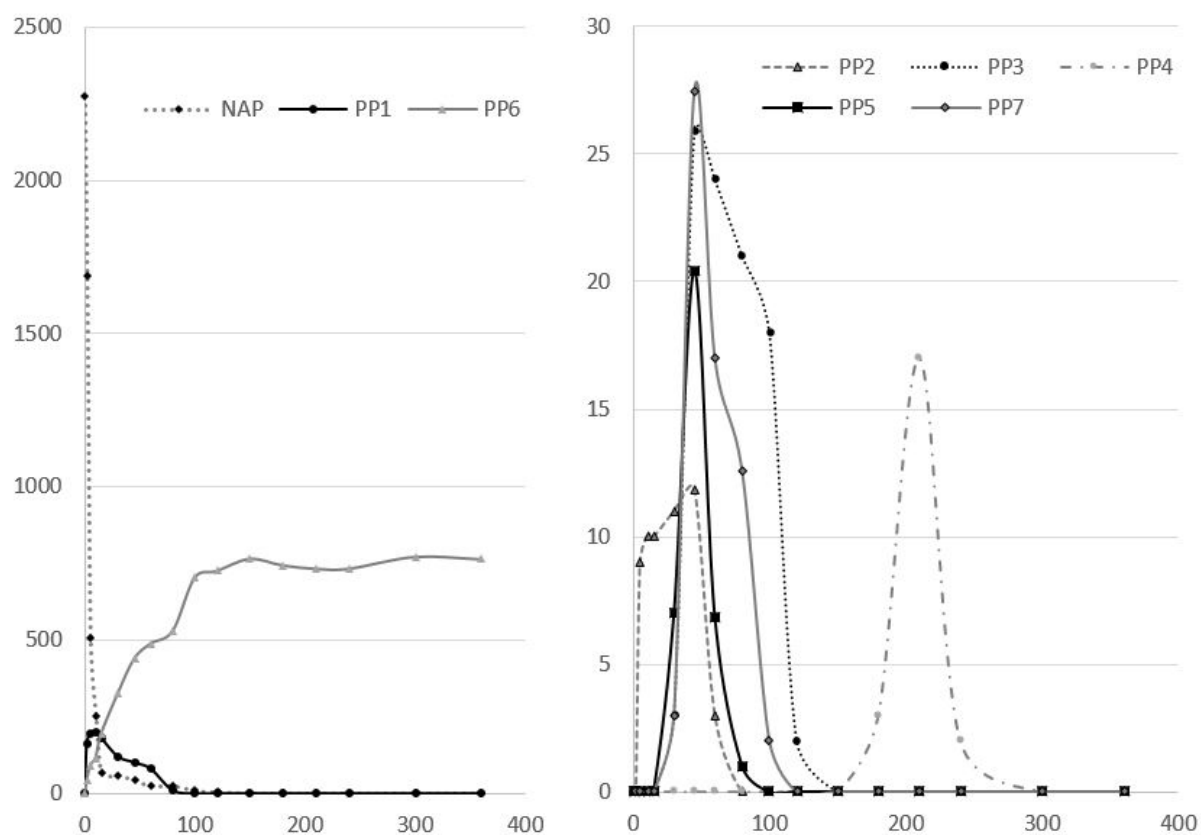


Figure 3.3.1: Relative abundances of naproxen and its photoproducts over time: compounds of major abundances (NAP, PP1 and PP6) on left side (relative abundances normalized to 2500) and compounds of minor abundances (PP2, PP3, PP4, PP5 and PP7) on right side (relative abundances normalized to 30).

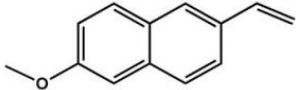
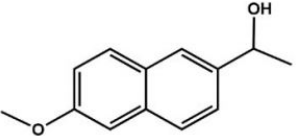
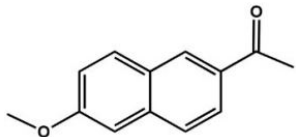
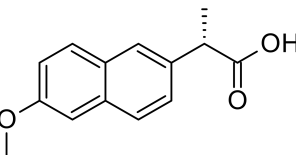
Photoproducts are referred to as PP1 to PP7; their structures are given in Table 3.3.2 and 3.3.1. To compare the relative amounts estimated by GC-MS and LC-MS couplings, LC-MS peak areas were corrected by a factor determined on the basis of the peak areas of naproxen detected by both techniques at t_0 . This empirical approach aimed at making possible a rough comparison between ion abundances from both techniques; it did not serve a quantification purpose, but allowed to discriminate reaction intermediates from

photoproducts likely to be found under real sunlight degradation. Seven photoproducts were determined. After a few minutes of irradiation, PP6 is by far the most abundant before PP1. Furthermore, PP6 appears as the only persistent compound at the end of the experiment while all the other photoproducts appear as reaction intermediates. Correlating their relative appearance and disappearance order helped to assign their chemical structures.

Table 3.3.1: Retention times, main ions, and elucidated structures of the photoproducts PP4 to PP7 detected by LC-ESI-MS

Ret. time (min)	Compound	Detection in ESI+ MH ⁺ ion (m/z)	MH ⁺ formula	Detection in ESI- MH ⁻ ion (m/z)	MH ⁻ formula	Structure of the compound
7.51	PP4	209.04502	C ₁₀ H ₉ O ₅ ⁺	207.02990	C ₁₀ H ₇ O ₅ ⁻	
8.26	PP5	197.04475	C ₉ H ₉ O ₅ ⁺	195.03025	C ₉ H ₇ O ₅ ⁻	
8.72	PP6	253.10742	C ₁₃ H ₁₇ O ₅ ⁺	251.09250	C ₁₃ H ₁₅ O ₅ ⁻	
13.00	Naproxen	231.10198	C ₁₄ H ₁₅ O ₃ ⁺	-	-	
13.14	PP7	201.09152	C ₁₃ H ₁₃ O ₂ ⁺	-	-	

Table 3.3.2: Retention times, main ions, and elucidated structures of the photoproducts PP1 to PP3 detected in GC-MS/MS (electron ionization)

Ret. time (min)	Compound	Silylated	Main ions in MS/MS (m/x) - precursor in bold ^a	Photoproducts
9.08	PP1	No	184 , 169, 141, 115	
10.12	PP3	Yes	274 , 259, 185, 141, 73	
10.18	PP2	No	200 , 185, 158, 157, 128	
11.00	Naproxen	Yes	302 , 287, 243, 185, 73	

^aNote that the provided m/z values correspond to ions from the silylated structure in the case of derivatized compounds, i.e. PP2 and naproxen. For both compounds, the molecular mass of the photoproduct and thus that of the molecular ion are shifted by 72 amu since the OH function has been replaced by OSi(CH₃)₃.

Structural elucidation of photoproducts

GC-MS experiments allowed the structural elucidation of photoproducts PP1 to PP3; retention times, ions, and chemical structures are given in Table 3.3.2. Dissociations of molecular ions were interpreted; the silylated compounds were easily identified due to the presence of a fairly intense ion at m/z 73 (Si(CH₃)₃)⁺ in their mass spectrum. Dissociation mechanisms of molecular ions are provided in Figure S3.3.1.

The retention times and m/z measured for protonated and deprotonated species in LC-ESI-MS are given in Table 3.3.1. Collision induced experiments permitted the structural elucidation of the photoproducts. Transitions and associated mechanisms are provided in Table S3.3.1 and Figure S3.3.2.

Based on the chemical structures of photoproducts, a photodegradation mechanism of naproxen has been proposed, which involves classical photochemistry pathways such as Norrish-type cleavage, hydrogen abstraction, oxygen addition (from water dissolved oxygen), hydrolysis, and concerted eliminations (see Figure 3.3.2). As is often the case with ketones, the photodegradation process begins by the Norrish-type cleavage of the C-CO bond of naproxen, leading to a radical which, in contact with a water molecule, can

abstract a hydrogen atom or a hydroxyl group to lead to PP1 and PP2, respectively. Photo-induced cleavages of C-H bonds have been recently demonstrated in a study by De Vaugelade et al. reporting the UV-Vis photodegradation of alpha-tocopherol [17]. Cleavage of such bonds is only observed if the resulting radical is strongly stabilized by mesomeric and/or inductive effects, which is the case when removing the hydrogen atom carried by the same carbon atom than the hydroxyl group in PP2. The resulting radical can lose a second hydrogen atom to lead to the ketone PP3. Successive oxygen additions on PP3, combined with hydrolysis reactions lead to PP6, then to PP5. By analogous mechanisms, the consecutive oxidation and hydrolysis of PP3 leads to PP4. Quite surprisingly, PP7 results from methanol elimination from naproxen, followed by hydrogen addition, the hydrogen atom is abstracted from a water molecule. This type of mechanism is not “classical” in photochemistry but both the structure of naproxen and the MS dissociation pathways of $PP7H^+$ allow unambiguous identification of the latter.

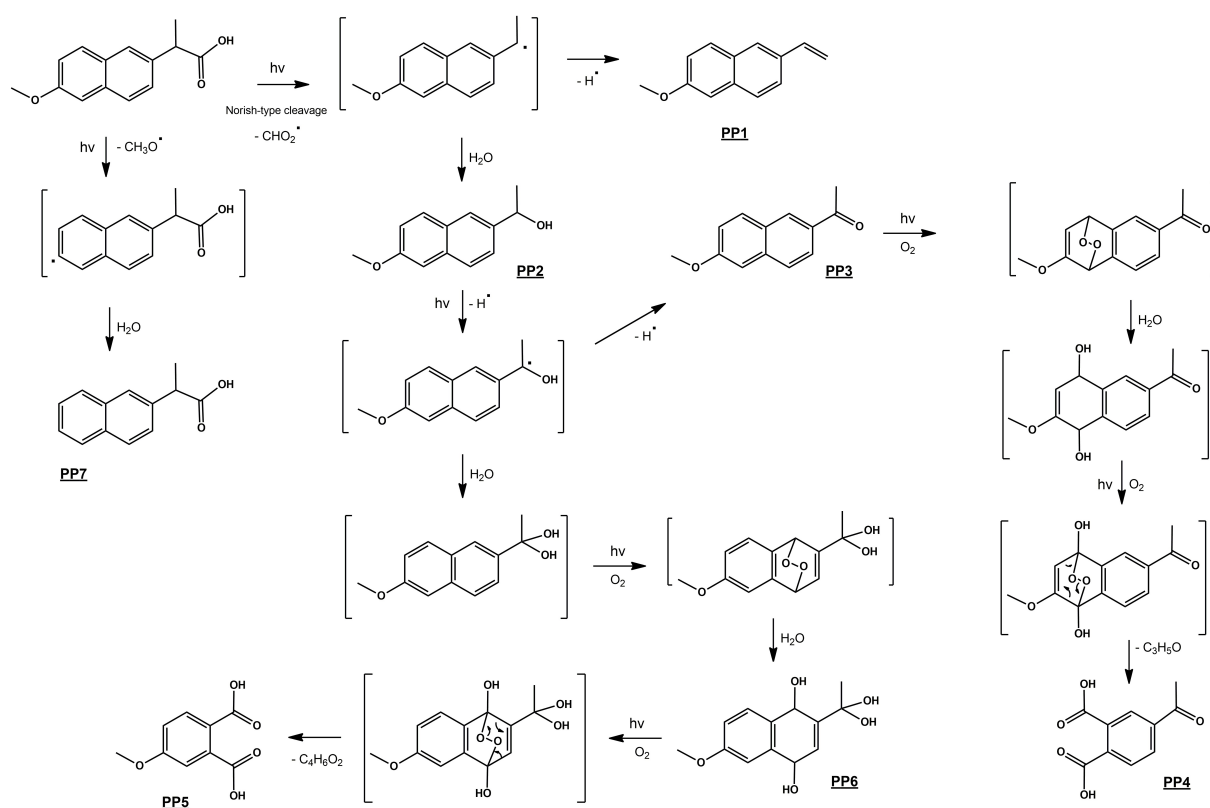


Figure 3.3.2: Mechanisms proposed for the photodegradation of naproxen in water

In silico and in vitro toxicity estimations

QSAR *in silico* tests were carried out with the T.E.S.T. software (see Supplementary information SI-1) regarding development toxicity, oral rat LD50 (mg/kg), and Fathead minnow LC50 (96 hours) (mg/L); results are presented in Table 3.3.3.

Considering developmental toxicity, all compounds except PP4 are potentially toxic, the

latter having a toxicity value coefficient of 0.37, which is below the threshold of toxicity value (0.50); they are expected to be at least as toxic as naproxen. Regarding oral rat toxicity, the values reported in Table 3.3.3 show that all photoproducts are in category III (slightly toxic) at the exception of except PP7 which belongs to category II corresponding to moderate toxicity. The higher toxicity of PP7 compared to other photoproducts is quite close to that of naproxen; this is consistent with the fact that the chemical structure of PP7 is the closest to that of the parent molecule. The lowest LC50 values were determined for PP5 and PP6, which exhibit the most hydrophilic structures and thus the lowest potentials for bioaccumulation. An oral rat LD50 experimental value of 248 mg/kg was provided for naproxen, which is comparable but below the estimated one (516 mg/kg) [18]. Nevertheless, it suggests that the *in-silico* approach used could underestimate the toxicity of naproxen and its photoproducts due to the lack of experimental data on similar structures. Regarding the toxic effect on Fathead minnow, PP1 exhibits by far the highest potential toxicity, in agreement with previous results [19]. PP2, PP3, and PP7 provide LC50 values close to that of the parent compound. The specificity of PP1 is that it does not include any CO nor OH group, which makes it much less polar than other compounds. Here again, the most hydrophilic compounds exhibit the lowest potential toxicity. In a previous study on UV photodegradation of naproxen by Cory et al., only PP2 and PP3 were detected though the experimental conditions were quite similar to those used in the present work [20]. Like in the present study, both phototransformation products of naproxen were found to be more stable than naproxen itself when exposed to simulated sunlight; their toxicity was investigated towards toad tadpoles and they have been shown to be much more toxic than the parent molecule.

Table 3.3.3: Toxicity values estimated by the T.E.S.T. software for BIT and its photoproducts except PP6b

Compound	Fathead Minnow LC50 (96 h) (mg/L)	Oral rat LD50 [mg/kg]	Developmental toxicity value ^a	Developmental toxicity
NAP	5.3	515.5	0.89	Toxicant
PP1	0.2	667.8	0.53	Toxicant
PP2	5.5	1817.9	0.85	Toxicant
PP3	6.6	1594.0	0.51	Toxicant
PP4	22.8	4230.5	0.37	Non-Toxicant
PP5	69.9	3913.9	0.69	Toxicant
PP6	19.4	1661.8	0.52	Toxicant
PP7	6.8	311.7	0.96	Toxicant

^aArbitrary unit.

In vitro bioassays based on the bioluminescence extinction of *Vibrio fischeri* were carried out on the solution of naproxen at different irradiation times according to the protocol described in the experimental section. Unlike *in silico* testing, this approach takes into account potential mixture effects. In the above-mentioned protocol, estimation of an EC50 value requires a minimum of three measurements for which the inhibition is between 10% and 90%, with a value above 50% for at least one of the three measurements. A naproxen solution at 50 ppm was submitted to photodegradation; sampling was performed at t_0 , t_{30} , and t_{80} (minutes). For each sample, the conditions were not met for EC50 determination, indicating a low ecotoxicity; an EC20 was thus evaluated, based on linear regression analysis of the dose-effect relationship. For a duration exposure of 15 minutes, the EC20 value decreases when increasing the irradiation time, from 11.7 at t_0 to 7.2 at 80 minutes, which traduces a slight increase in toxicity of the mixture. As shown in Figure 3.3.1, PP6 is by far the most abundant photoproduct in the mixture at 80 minutes. Regarding *in silico* estimations, PP6 exhibits Fathead Minnow LC50 and oral rat LD50 values higher than those estimated for naproxen so this photoproduct is not *a priori* expected to contribute to the increase in toxicity of the mixture. Different conclusions can be drawn from these estimations: (i) insufficient parametrization of the T.E.S.T. software regarding the molecules of interest makes the *in silico* estimations inaccurate in the present case, especially in the case of PP6, which displays a quite complex and unusual structure; (ii) with a Fathead Minnow LC50 estimated to be 25 times lower than that of naproxen (see Table 3.3.3), PP1, which is the second photoproduct in terms of abundance, could be responsible for the slight increase in toxicity of the mixture; (iii) a limited “cocktail effect” due to the concomitant presence of several photoproducts could also be suspected. Whatever the right explanation, both *in silico* and *in vitro* evaluations lead to the outcome that the ecotoxicity induced by naproxen photoproducts is not a major issue compared to that of naproxen itself. However, the long-term environmental effects of naproxen exposure at concentration levels close to those found in the environment remain poorly studied although detection of the drug in wastewater and river samples in the ng/L - µg/L range demonstrated the need for such knowledge [21–23].

Conclusion

The in-lab photodegradation of naproxen under UV-Visible irradiation led to the formation of seven photoproducts, which were characterized using LC-HRMS/MS and GC-MS techniques. A photodegradation pathway of naproxen has been suggested based on the elucidated structures and kinetics considerations. *In silico* and *in vitro* tests were conducted, on isolated molecules in the first case, on an irradiated aqueous solution of naproxen in the second one. The general conclusion is that photoproducts do not increase the global toxicity in an alarming way. It is interesting to note that naproxen was 90% degraded after only a few minutes and that all the photoproducts are eliminated after 5 hours of ir-

radiation with the exception of PP6, which remains in the mixture in significant amounts and whose toxicity would deserve to be further investigated after synthesis. Aside from the consequences of sunlight-induced degradation of naproxen in the environment, these results suggest that direct UV light irradiation – a technique gradually replacing the more classical photocatalytic processes – could be an efficient tool for naproxen removal from contaminated waters.

Funding

The author(s) disclosed the receipt of the following financial support for the research, authorship, and/or publication of this article: Financial support from the National FT-ICR network (FR 3624 CNRS) for conducting the research is gratefully acknowledged. This work is part of a project that has received funding from the European Union’s Horizon 2020 research and innovation program under the Marie Skłodowska-Curie Grant Agreement No 765860 (AQUALity).

Supplementary information

Table S3.3.1: Collision-induced ESI⁺ mass spectra of naproxen and its photoproducts

Compound	MH ⁺ precursor ion		Fragment ions	
	m/z	Formula	m/z	Formula
PP4	209	C ₁₀ H ₉ O ₅ ⁺	191	C ₁₀ H ₇ O ₄ ⁺
			149	C ₈ H ₅ O ₃ ⁺
			121	C ₇ H ₅ O ₂ ⁺
PP5	197	C ₉ H ₉ O ₅ ⁺	179	C ₉ H ₇ O ₄ ⁺
			163	C ₉ H ₇ O ₃ ⁺
			151	C ₈ H ₇ O ₃ ⁺
PP6	253	C ₁₃ H ₁₇ O ₅ ⁺	217	C ₁₃ H ₁₃ O ₃ ⁺
			203	C ₁₂ H ₁₁ O ₃ ⁺
			175	C ₁₁ H ₁₁ O ₂ ⁺
			157	C ₁₁ H ₉ O ⁺
PP7	201	C ₁₃ H ₁₃ O ₂ ⁺	183	C ₁₃ H ₁₁ O ⁺
			155	C ₁₂ H ₁₁ ⁺

SI-1. *In silico* toxicity estimations using the T.E.S.T. software

The Toxicity Estimation Software Tool (T.E.S.T.) is an Environmental Protection Agency online available computerized predictive system with Quantitative Structure Activity Relationships (QSAR) mathematical model [15]. T.E.S.T. has a variety of toxicity endpoints used to predict chemical toxicity values from the physical properties of the molecular structure. T.E.S.T. model uses a simple linear function of molecular descriptors such as the

octanol-water partition coefficient, the molecular weight or the number of benzene rings. Models for assessing toxicity solely from molecular structure are based on information-rich structural descriptors that quantify transport, bulk, and electronic attributes of a chemical structure. Besides molecular weight, the QSAR model employs size-corrected E-values for quantification of molecular bulk. The size-corrected E-values are computed from a rescaled count of valence electrons. Electrotological state values (E-values) as numerical quantifiers of molecular structure encode information about the electron content (valence, sigma, pi and lone-pair), topology and environment of an atom or a group of atoms in a molecule [24]. The predicted toxicity is estimated by taking an average of the predicted toxicities from the above QSAR methods, provided the predictions are within the respective applicability domains.

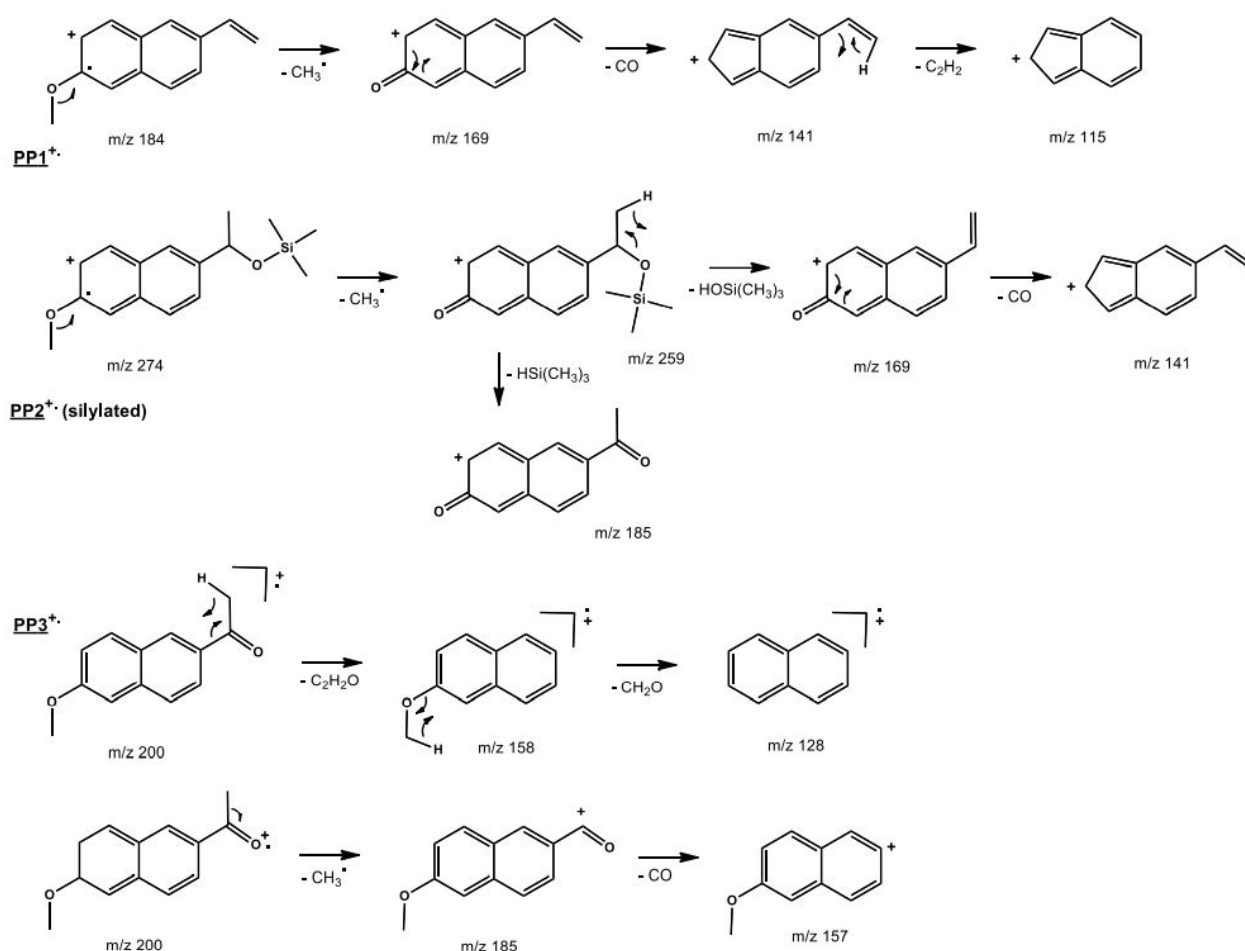


Figure S3.3.1: Dissociations of molecular ions of the photoproducts detected by GC-EI-MS

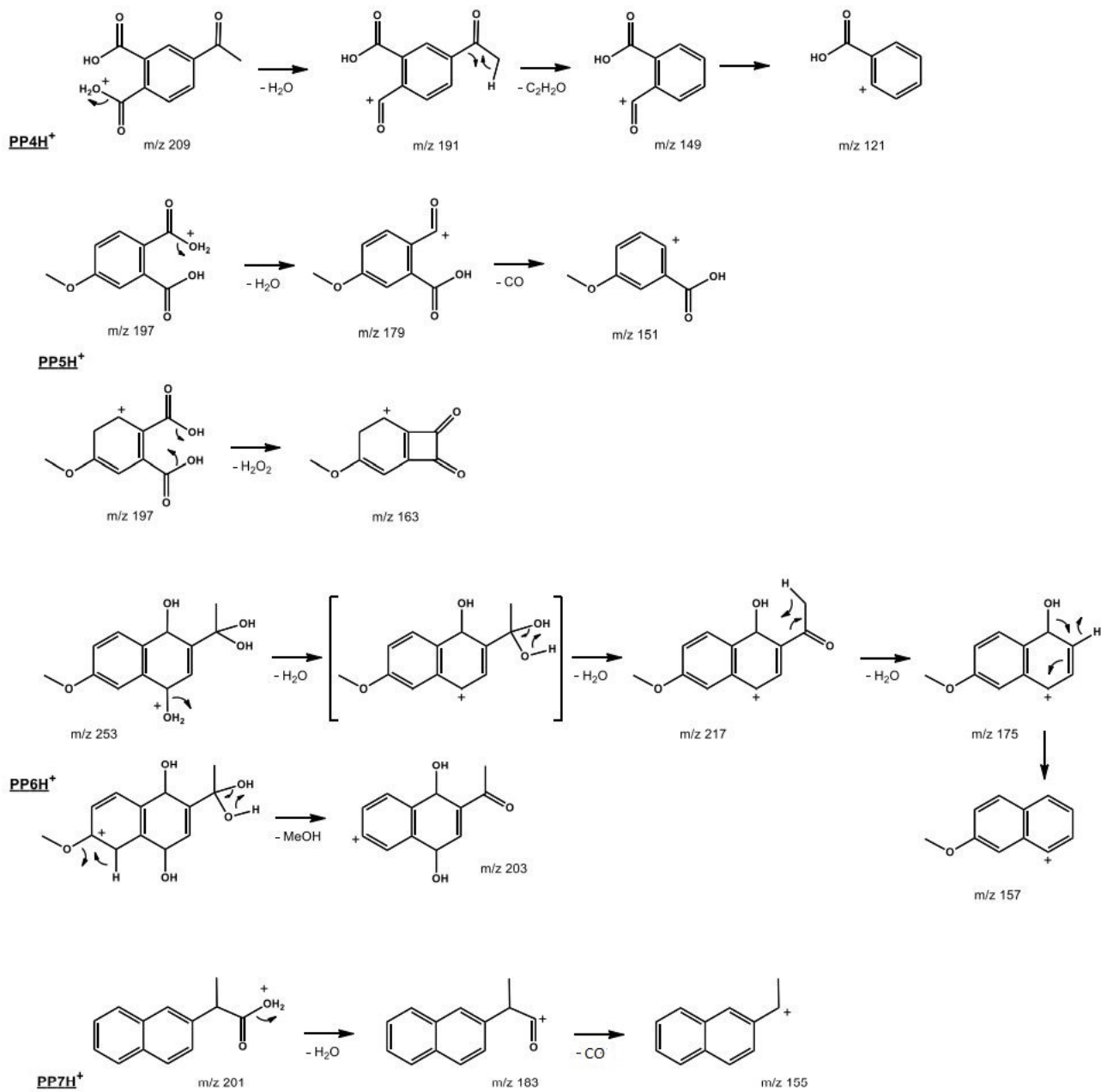


Figure S3.3.2: Dissociations of the pseudomolecular ions (MH^+) of the photoproducts detected by LC-ESI-MS

References

- [1] P Verlicchi, M Al Aukidy, and E Zambello. “Occurrence of pharmaceutical compounds in urban wastewater: Removal, mass load and environmental risk after a secondary treatment—A review”. In: *Sci Total Environ* 429 (2012), pp. 123–155. DOI: 10.1016/j.scitotenv.2012.04.028.
- [2] European Environmental Bureau. *The environmental and health impacts caused by emissions of APIs to the environment*. 2020. URL: <https://eeb.org/the-problem-of-pharmaceutical-pollution/>.
- [3] SML de Souza, EC de Vasconcelos, M Dziedzic, and CMR de Oliveira. “Environmental risk assessment of antibiotics: An intensive care unit analysis”. In: *Chemosphere* 77.7 (2009), pp. 962–967. DOI: 10.1016/j.chemosphere.2009.08.010.
- [4] European Commission. *Document on risk assessment. Technical Guidance Document on Risk Assessment Part II*. 2003. URL: <https://ec.europa.eu/jrc/en/publication/eur-scientific-and-technical-research-reports/technical-guidance-document-risk-assessment-part-1-part-2>.
- [5] A Sangion and P Gramatica. “PBT assessment and prioritization of contaminants of emerging concern: Pharmaceuticals”. In: *Environ Res* 147 (2016), pp. 297–306. DOI: 10.1016/j.envres.2016.02.021.
- [6] S Cassani and P Gramatica. “Identification of potential PBT behavior of personal care products by structural approaches”. In: *Sustain Chem and Pharm* 1 (2015), pp. 19–27. DOI: 10.1016/j.scp.2015.10.002.
- [7] “Commission directive 93/67/EEC of 20 July 1993 laying down the principles for assessment of risks to man and the environment of substances notified in accordance with council directive 67/548/EEC”. In: *Off J Eur Commun* L227 (1993), pp. 1–3. URL: <https://eur-lex.europa.eu/legal-content/en/ALL/?uri=CELEX:31993L0067>.
- [8] K Fent, AA Weston, and D Caminada. “Ecotoxicology of human pharmaceuticals”. In: *Aquat Toxicol* 76.2 (2006), pp. 122–159. DOI: 10.1016/j.aquatox.2005.09.009.
- [9] T aus der Beek, FA Weber, A Bergmann, S Hickmann, I Ebert, A Hein, and A Küster. *Pharmaceuticals in the environment: global occurrence and potential cooperative action under the strategic approach to international chemicals management (SAICM)*. 2016. URL: www.umweltbundesamt.de/sites/default/files/medien/1968/publikationen/iww_abschlussbericht_saicm_arzneimittel_final.pdf.


- [10] GWRC. *Pharmaceuticals and personal care products in the water cycle. An international review*. 2004. URL: <http://www.wrc.org.za/mdocs-posts/gwrc-phac-international-review/gwrc-phac-international-review-2/>.
- [11] Norman Network. 2005. URL: <https://www.norman-network.net/?q=Home>.
- [12] M Petrović, S Gonzalez, and D Barceló. “Analysis and removal of emerging contaminants in wastewater and drinking water”. In: *Trends Anal Chem* 22.10 (2003), pp. 685–696. DOI: 10.1016/S0165-9936(03)01105-1.
- [13] S Monteiro and A Boxall. “Occurrence and fate of human pharmaceuticals in the environment.” In: *Rev Environ Contam Toxicol* 202 (2010), pp. 53–154. DOI: 10.1007/978-1-4419-1157-5_2.
- [14] D Wojcieszynska and U Guzik. “Naproxen in the environment: its occurrence, toxicity to nontarget organisms and biodegradation.” In: *Appl Microbiol Biotechnol* 104 (2020), pp. 1849–1857. DOI: 10.1007/s00253-019-10343-x.
- [15] United States Environmental Protection Agency. *Toxicity Estimation Software Tool (TEST)*. 2016. URL: <https://www.epa.gov/chemical-research/toxicity-estimation-software-tool-test>.
- [16] ISO 11348-3:2007. In: *Water quality — determination of the inhibitory effect of water samples on the light emission of Vibrio Fisheri (Luminescent bacteria test) — part 3: method using freeze-dried bacteria*. 2007. URL: <https://www.iso.org/standard/40518.html>.
- [17] S De Vaugelade, E Nicol, S Vujovic, S Bourcier, S Pirnay, and S Bouchonnet. “UV–vis degradation of α -tocopherol in a model system and in a cosmetic emulsion—Structural elucidation of photoproducts and toxicological consequences”. In: *J Chrom A* 1517 (2017), pp. 126–133. DOI: 10.1016/j.chroma.2017.08.015.
- [18] *Naproxen Safety Data Sheet*. 2015. URL: <https://www.caymanchem.com/msdss/70290m.pdf>.
- [19] M Isidori, M Lavorgna, A Nardelli, A Parrella, L Previtera, and M Rubino. “Ecotoxicity of naproxen and its phototransformation products”. In: *Sci Total Environ* 348.1-3 (2005), pp. 93–101. DOI: 10.1016/j.scitotenv.2004.12.068.
- [20] WC Cory, AM Welch, JN Ramirez, and LC Rein. “Naproxen and its phototransformation products: persistence and ecotoxicity to toad tadpoles (*Anaxyrus terrestris*), individually and in mixtures.” In: *Environ Toxicol Chem* 38.9 (2019), pp. 2008–2019. DOI: 10.1002/etc.4514.

- [21] S Kern, K Fenner, HP Singer, RP Schwarzenbach, and J Hollender. “Identification of Transformation Products of Organic Contaminants in Natural Waters by Computer-Aided Prediction and High-Resolution Mass Spectrometry”. In: *Environ Sci Technol* 43.18 (2009), pp. 7039–7046. DOI: 10.1021/es901979h.
- [22] TA Ternes. “Occurrence of drugs in German sewage treatment plants and rivers”. In: *Water Res* 32.11 (1998), pp. 3245–3260. DOI: 10.1016/S0043-1354(98)00099-2.
- [23] M la Farré, I Ferrer, A Ginebreda, M Figueras, L Olivella, L Tirapu, M Vilanova, and D Barceló. “Determination of drugs in surface water and wastewater samples by liquid chromatography–mass spectrometry: methods and preliminary results including toxicity studies with *Vibrio fischeri*”. In: *J Chrom A* 938.1-2 (2001), pp. 187–197. DOI: 10.1016/S0021-9673(01)01154-2.
- [24] LH Hall, B Mohny, and LB. Kier. “The electrotopological state: structure information at the atomic level for molecular graphs”. In: *J Chem Inf Comput Sci* 31.1 (1991), pp. 76–82. DOI: 10.1021/ci00001a012.



Chapter 4

Modeling approach - Results on indirect photochemical experiments



4.1 General approach

Indirect photochemical reactions can be induced by reactive species present in the mixture, as described in chapter 1. In the following studies, the reactive species were generated through photocatalysis, Fenton-reactions, the presence of hydrogen peroxide, or the activation of photosensitizer molecules. When advanced oxidation processes are applied, the wavelength of the light should be adequate to activate the process in question.

The composition of the aqueous medium can range from ultrapure water to complex mixtures containing natural organic matter or wastewater. The addition of matrix components permits determining whether they could act as a photosensitizer or affect the nature of the photodegradation process. For this purpose, organic probes, which absorb light at higher wavelengths, could be added to study the effect of the transfer of the absorbed light energy from an intermediate to the parent molecule. Adjusting the pH is very important for the efficiency of some advanced oxidation processes, especially for the Fenton reaction.

Sampling frequency and total reaction time should be optimized, taking into consideration the reaction kinetics. Many photoreactions show exponential decay of the parent molecule. The analysis of the samples usually requires suitable sample preparation and analytical techniques such as GC-MS and LC-MS couplings. In the present studies, the aim was to minimize sample preparation steps to reduce the related variability and operator subjectivity. For the analysis of the samples, hyphenated chromatographic techniques with mass spectrometry, ionic chromatography, UV-Vis spectroscopy, total organic carbon, and pH measurements were used. HRMS and MS² experiments were applied to elucidate the photodegradation mechanisms. Regarding the determination of potential toxic effects of the photoproducts, the same approaches were used as for the direct photochemical experiments previously described.

The primary aim when applying advanced oxidation processes is to achieve high degradation efficiencies for the CECs. The ultimate goal is usually to design water treatment processes that can be applied on an industrial scale in terms of technical feasibility and cost. These systems should mineralize the compounds of interest, or at least reduce considerably the overall toxicity of the mixture. The study of the photodegradation of enrofloxacin in a pilot plant was an instructive work to understand AOPs on larger scales and study the effect of secondary treated wastewater on the process. These studies will help understand the photodegradation efficiencies of different AOPs, the formation of potentially harmful by-products, and their potential applications in water treatment on industrial levels.

4.2 Photodegradation experiments on perfluorooctanoic acid

In the framework of the AQUALity project, the first secondment of two months was carried out at the Institut de Chimie de Clermont-Ferrand under the supervision of Dr. Claire Richard. Classical photodegradation experiments were performed on perfluorooctanoic acid (PFOA). This was an instructive experience, as the main expertise of this laboratory is on photochemistry. Twelve irradiation experiments were carried out and are described in the materials and methods part.

The issue with perfluorinated substances such as perfluorooctanoic acid is twofold. Firstly, they are long-chain alkylic compounds; therefore, the characteristic absorption bands appear at very high energies (Figure 4.2.1). Secondly, due to the strength of the carbon-fluorine bond, it is incredibly challenging to achieve defluorination. Thus previous studies showed the shortening of the alkyl chain, but mineralization was achieved only under harsh reaction conditions. The general approach here was first to test the degradation of PFOA under irradiation with UV light and then add photosensitizers that absorb light at higher wavelengths and potentially transfer energy to the perfluorinated molecule. The photochemical experimental setups are described in the supplementary information SI-1.

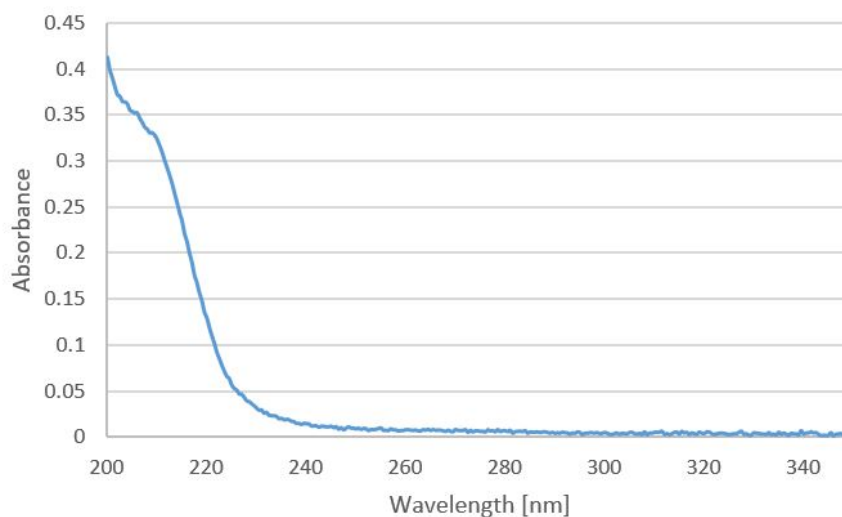
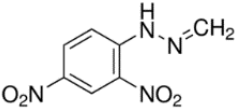
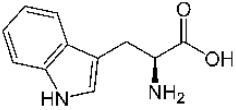
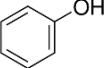
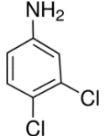


Figure 4.2.1: UV-Vis absorption spectrum of PFOA in ultrapure water.

Table 4.2.1 contains the selected organic probes used as photosensitizers, the wavelength of their absorption maximum, measured by UV-Vis spectroscopy, and the selected irradiation wavelength. Changes in UV-Vis absorption of the mixtures and pH values were frequently monitored during the experiments. The samples were analyzed using LC-MS to follow the eventual degradation of the parent compound and the potential formation of phototransformation products. Ionic chromatography was employed to measure possible

defluorination by fluoride ion quantification. The analytical parameters are presented in the supplementary information SI-2.

Table 4.2.1: Added photosensitizer molecules and local maximum absorbance

Molecule	Structure	Max absorbance [nm]	Max wavelength of irradiation [nm]
2,4-dinitro-phenylhydrazine		350	365
tryptophan		278	313
phenol		268	313
3,4-dichloroaniline		296	313

An aqueous PFOA solution at 10 μM was irradiated at 254 nm, and samples were taken at t_0 , 24 h, and 96 h. By LC-MS analysis, it was determined that the main degradation pathway was the stepwise dealkylation described in the literature [1]. When perfluorooctanoic acid ($\text{C}_8\text{HF}_{15}\text{O}_2$) is submitted to irradiation in water, the C-C bond is cleaved between the COOH and C_7F_{15} . The latter will form in water the thermally unstable alcohol $\text{C}_7\text{F}_{15}\text{OH}$, which in turn will undergo HF elimination, forming $\text{C}_6\text{F}_{13}\text{COF}$. This will hydrolyze and yield a perfluorocarboxylic acid with one less CF_2 unit.

Evidence of this elimination pathway was obtained by LC-MS (Table 4.2.2), where all the corresponding photoproducts of this mechanism were detected. A loss of CO_2 is also evidenced in the mass spectrum (m/z 413 \rightarrow m/z 369); this very common loss for carboxylic acids shows that the functional group was present in all compounds.

After 24 h, 40% of PFOA degraded into photoproducts and after 96 h, 94% of degradation was achieved. These seem to be promising results, despite the long irradiation times, but by analyzing the fluoride content using ionic chromatography, it was determined that 12.3% and 42.3% of defluorination were obtained in the samples at 24 and 96 h, respectively. This means that mineralization of the parent compound is not reached, and the obtained photoproducts are still perfluorocarboxylic acids, which can exert similar toxic effects as

the parent molecule.

Table 4.2.2: LC-MS measurement results

$[M-H]^-$	Retention time	m/z	Fragment	m/z
$C_8O_2F_{15}$	9,17	412,97	C_7H_{15}	368,98
$C_7O_2F_{13}$	7,86	362,97	C_6F_{13}	318,98
$C_6O_2F_{11}$	6,60	312,97	C_5F_{11}	268,98
$C_5O_2F_9$	5,40	262,97	C_4F_9	218,99
$C_4O_2F_7$	3,84	212,98	C_3F_7	168,99
$C_3O_2F_5$	2,17	162,98	C_2F_5	118,99
$C_2O_2F_3$	0,98	112,96	CF_3	68,99

The same type of measurements were performed on the irradiation of PFOA with organic probes. In this case, PFOA does not absorb at the wavelengths used for irradiation. Unfortunately, after 24 hours of irradiation, LC-MS and ionic chromatography measurements showed no evidence of PFOA degradation. This led to the conclusion that these compounds do not act as photosensitizers in an efficient way for this class of compounds. The experiments carried out did not have a satisfactory success in terms of degradation efficiency of the molecule due to its extreme persistence, but many lessons were learned in terms of good practices and correct parametrization when performing photochemical experiments.

Supplementary information

SI-1. Photodegradation experiments

The photodegradation experiments were carried out on 100 mL solution, with a concentration of 0.01 mM of the perfluorinated molecule, and the added photosensitizers concentration of 0.1 mM. The starting pH before irradiating the solution was adjusted to the value of 7.5 with NaOH, as PFOA is acidic. The samples were irradiated in a photoreactor with a circular setup. Six lamps were arranged around a sample holder equipped with a fan for cooling. The solutions were irradiated using three different set-ups, depending on the addition of photosensitizers and their absorbance spectrum. In the first case, when photolysis was performed in ultrapure water, the sample was irradiated at 254 nm in a device with six MAZDA TG 15W germicidal tubes placed around the quartz cylinder. When photosensitizers tryptophan, phenol and 3,2-dichloroaniline were added, the samples were irradiated in a Pyrex-cell placed photocircular reactor with six Duke sun lamp fluorescent tubes, emitting with a maximum emission at 313 nm. In the last experiment, when 2,4-dinitrophenylhydrazine was added as photosensitizers, the reaction was carried

out in a pyrex-glass reactor, irradiated with six Sylvania, F15 W/350BL polychromatic tubes, with a maximum emission at 365 nm. All of the cells were open to air.

SI-2. Analysis of the samples

The UV-Vis spectra of each sample was recorded by a Varian Cary 3 spectrophotometer in scan mode. The fluoride content was measured by ion chromatography on a Dionex DX320 instrument, equipped with an anion column IonPAC AS11 (Analytical column 5 x 250 mm). A KOH solution was used as eluent in gradient mode. For quantification the measurement were carried out in triplicates.

The LC-MS measurements were carried out on an Orbitrap Q-Exactive (ThermoScientific) mass spectrometry, combined with an UHPLC Ultimate 3000 RSLC (ThermoScientific). The chromatographic column was a Kinetex EVO C18 (Phenomenex, 100 x 2,1mm; 1,7 μ m). A flow of 0.45 mL/min was applied, at 30°C. H₂O+0.1% Formic acid (A) /ACN+0.1% Formic acid (B) gradient was used as following: the starting condition was 95% of solvent A; it was lowered until 1% in 7.5 min, kept at this value until 8.5 min and then increased back to 95% after 9 min and kept at this value until 11 min of elution. The injected sample volume was 5 μ L. Electrospray ionization was used in negative mode, with a scanning range from 80 to 1200 m/z. The achieved resolution was 35000. The capillary temperature was 320°C, the spray voltage was 3000 V. The sheath, auxiliary and sweep gas were N₂ with a flow of 50, 10 and 2 L/min, respectively. The auxiliary gas temperature was 400°C. The target gain was 10⁶ and the maximum injection time was 50 ms.

References

- [1] S Wang, Q Yang, F Chen, J Sun, K Luo, F Yao, X Wang, D Wang, X Li, and G Zeng. “Photocatalytic degradation of perfluorooctanoic acid and perfluorooctane sulfonate in water: A critical review”. In: *Chem Eng J* 328 (2017), pp. 927–942. DOI: 10.1016/j.cej.2017.07.076.

4.3 Photoinduced transformation of maprotiline

One of the aims of the AQUALity project was to establish collaborations between the partner institutions. This was realized through secondments or common projects. Nuno Gonçalves, one of the early stage researchers of AQUALity, carried out a 2 months project at the LCM laboratory, working on the degradation of maprotiline under photolysis and photocatalysis. This collaboration yielded a publication in the journal *Science of the Total Environment*; it is presented below.

Study of the photoinduced transformations of maprotiline in river water using liquid chromatography high-resolution mass spectrometry

Nuno P.F.Gonçalves^a, Zsuzsanna Varga^b, Stéphane Bouchonnet^b, Valeria Dulio^c, Nikiforos Alygizakis^{e,f}, Federica Dal Bello^d, Claudio Medana^d, Paola Calza^a

^a*Department of Chemistry, University of Turin, Torino, Italy*

^b*Laboratoire de Chimie Moléculaire, CNRS / Ecole Polytechnique, Institut Polytechnique de Paris, 91128, Palaiseau, France*

^c*INERIS, National Institute for Environment and Industrial Risks, Verneuil en Halatte, France*

^d*Department of Molecular Biotechnology and Health Sciences, University of Turin, Torino, Italy*

^e*Laboratory of Analytical Chemistry, Department of Chemistry, University of Athens, Panepistimiopolis Zografou, 15771 Athens, Greece*

^f*Environmental Institute, Okružná 784/42, 97241 Koš, Slovak Republic*

Abstract

Maprotiline was identified as a compound of potential interest further to a suspect screening test carried out for a list of more than 40,000 substances based on specific occurrence, hazard, and risk indicators. Despite the high frequency of appearance of this drug in wastewater treatment stations, his environmental fate is still unknown. Herein, we investigated for the first time the maprotiline degradation pathways in river water spiked with the drug at a concentration close to those detected in natural waters. Preliminary photocatalytic experiments in ultrapure water produced 32 transformation products (TPs) resulted mainly from the multiple hydroxylation/oxidation in different positions of the drug molecule. From the river water experiments, 12 TPs were formed by photolysis matching with those observed in ultrapure water experiments, and 2 were also formed resulted from biotic degradation. Employing HPLC-HRMS, we were able to elucidate the chemical structures of TPs and assess the overall degradation mechanism. Preliminary bioassays suggested lower toxicity of TPs relatively to the parent compound.

Introduction

The scientific progress observed in the last few decades had a remarkable impact on modern human lifestyle. The development of countless chemical substances part of our daily routine activities is now severely affecting the quality of water resources. The widespread presence of contaminants of emerging concern (CECs) is a major threat to aquatic ecosystems worldwide [1]. According to the NORMAN network [2], a CEC is defined as “a substance currently not included in routine environmental monitoring programs that may be a candidate for future legislation due to its adverse effects and/or persistency”. These substances are not necessarily new, most of them are “emerging” as result of the improvement in analytical techniques that recently allowed to detect and track trace concentrations in aquatic media [3, 4]. Their “concern” rises from the scarce information about their environmental fate, their hazards to human health and ecosystems, the degradation pathway and toxicity of their degradation products. The presence of a large number of contaminants coupled with the continuous improvement capability to detect new pollutants make CECs a complex challenge for regulatory agencies [5, 6].

Pharmaceuticals have emerged in the past few decades as the CECs epicenter [7–10]. The increasing number of new medicines together with their extensive use, persistence and high biological activity enlarged drastically their environmental impact [11]. Pharmaceuticals reach the environment mainly by excretions and erroneous disposal in the domestic sewer, hospital effluents and animal/fish farming. They include antibiotics, hormones, birth control pills, antidiabetics, beta-blockers, lipid regulators, impotence drugs, painkillers, tranquilizers, antidepressants and other medicines. Furthermore, the actual wastewater treatment facilities are not specifically designed to remove organic pollutants, thereby allowing their constant release into the environment [12–14].

Antidepressants are among the most prescribed pharmaceuticals in developed countries [15, 16], associated with psychiatric disorders also in the youngest generation. The consequent appearance of these complex mixtures in water stream impacts animals living in the aquatic environment [17]. Recent studies linked antidepressants exposure to different disorders in the aquatic biota [18, 19]. For example, oxazepam was reported to affect the activity, sociality and feeding rate of *Perca fluviatilis* even at the concentration level detected in wastewater treatment influents/effluents [20]. Such behavioral changes may have ecological and evolutionary consequences.

Maprotiline is a tetracyclic antidepressant drug approved in many countries, with a daily usual dosage of 150 to 225 mg used to treat depression associated with agitation or anxiety [21]. As a consequence of its wrong disposal and excretion in its unmetabolized form (3–4%) [22], like many other drugs, maprotiline drug has been reported in influent and effluent of wastewater treatment plants as well as in surface waters, usually at ng/L up

to few $\mu\text{g L}^{-1}$ concentration [14, 23, 24]. To the best of our knowledge, despite its frequent environmental occurrence, there is no information about the maprotiline environmental fate, its degradation pathway neither toxicity of its degradation products.

This study aims at investigating for the first time the maprotiline environmental fate in river water by initially performing a laboratory simulation to identify the degradation products by HPLC-HRMS and then search for them under natural conditions. For easier identification of the degradation products, maprotiline degradation experiments were firstly performed at high concentration in ultrapure water using TiO_2 as a benchmark photocatalyst. Subsequently, experiments were performed in spiked river water, at a concentration similar to those described in natural waters, for the elucidation of the drug environmental fate. Toxicity was estimated as well and preliminary bioassays were performed on the generated degradation species.

Materials and methods

Chemicals

Maprotiline hydrochloride (CAS: 10347-81-6), whose structure with the numbering of carbons atoms is shown in Figure 4.3.1, was purchased from Sigma-Aldrich (Milan, Italy). In order to avoid possible interference from ions adsorbed on the photocatalyst, TiO_2 (Evonik P25, Frankfurt, Germany) was irradiated and washed with distilled water, until there were no detectable signals due to chloride, sulfate and sodium ions. All the chemical reagents were used as received. Suspensions and standard solutions were prepared in ultrapure water.

The river water sample was collected from the River Po, Torino Italy, ($45^{\circ}02'40.4''\text{N}$ $7^{\circ}41'02.1''\text{E}$) on September 30th 2019. Samples were used after a rough pre-filtration step, carried out through a grade qualitative filter paper (Whatman) removing large suspended solids and filtered using a hydrophilic $0.45\ \mu\text{m}$ filter Sartolon Polyamide (Sartorius Biolab). River water samples had $1.83\ \text{mg L}^{-1}$ of total organic carbon (TOC), $44.81\ \text{mg L}^{-1}$ of inorganic carbon (IC), and $3.85\ \text{mg L}^{-1}$ of total nitrogen (TN) and $\text{pH} = 8.2$. The potential presence of maprotiline, identified TPs and the described metabolites in the explored river water sample were investigated by HPLC-HRMS before spiking and they were below the detection limit.

Methods

– Degradation experiments

The workflow for the maprotiline degradation pathway study is presented in Figure S4.3.1. Maprotiline photocatalytic degradation was carried out in ultrapure water in Pyrex glass cells ($2.3\ \text{cm}$ height \times $4.0\ \text{cm}$ diameter), filled with $5\ \text{mL}$ of maprotiline ($20\ \text{mg L}^{-1}$) and TiO_2 ($500\ \text{mg L}^{-1}$) suspension kept under magnetic stirring under irradiation for times ranging from $1\ \text{min}$ to $60\ \text{min}$. After irradiation, the photocatalyst was removed using

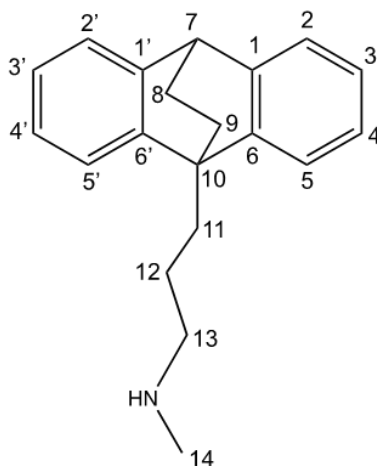


Figure 4.3.1: Numbering of maprotiline carbon atoms

a 0.45 μm Sartolon Polyamide (Sartorius Biolab) filter before analysis. The photolysis experiments were performed in the same conditions without the catalyst addition.

Photolysis experiments in river water sample were performed on a 200 mL water volume spiked with $10 \mu\text{g L}^{-1}$ of maprotiline divided into three Pyrex glass cells (7.5 cm height \times 9.5 cm diameter). Samples were irradiated for times ranging from 1 h to 72 h. The irradiation was carried out using a PHILIPS cleo 6 X 15 W TL-D Actinic BL with maximum emission wavelength at 365 nm. The UV integrated irradiance on the cells in the 290–400 nm wavelength range was $90 \pm 2 \text{ Wm}^{-2}$ (measured with a CO.FO.MEGRA (Milan, Italy) power-meter). To control the effect of water sample constituents on maprotiline fate, spiked water samples ($10 \mu\text{g L}^{-1}$) were kept in the dark collecting samples over time (0, 16, 24, 48 and 72 h). Samples were then freeze-dried (LABOGENE – CoolSafe 55-110). The obtained powder was dissolved into 10 mL of a 50:50 (v/v) methanol: acetonitrile mixture which was filtered with a 0.22 μm polypropylene filter (ThermoFisher Scientific). The sample was dried under a gentle nitrogen stream at room temperature, then reconstituted with 200 μL of acetonitrile (final preconcentration factor of 1000) for the LC-HRMS analysis.

–Analytical procedures

The identification of maprotiline TPs in ultrapure water and in river water samples was performed using an Ultimate 3000 High-Pressure Liquid Chromatography coupled with a LTQ-orbitrap MS (Thermo Scientific, Bremen, Germany) equipped with an ESI source. The chromatographic separation was achieved with a reverse phase C18 column (Gemini NX C18, $150 \times 2 \text{ mm}$, 3 μm , 110 \AA ; Phenomenex, Castel Maggiore, BO, Italy) using 20 mM aqueous formic acid (eluent A) and acetonitrile (eluent B). Gradient separation ramp started with 5% B, increased up to 40% B in 18 min and to 100% in 5 min; then the column was reconditioned. The flow was 0.2 mL/min and injection volume 20 μL .

For the ESI ion source used nitrogen as both sheath and auxiliary gas. Source parameters were set as followed: sheath gas 30 arbitrary unit (arb), auxiliary gas 25 arb, capillary voltage 4.0 kV and capillary temperature 275 °C. Full mass spectra were acquired in positive ion mode on m/z range between 50 and 500 Th, with a resolution of 30.000. MS^n spectra were acquired on the range between ion trap cut-off and precursor ion m/z values. Accuracy on recorded m/z (versus calculated) was ± 0.001 Th (without internal calibration).

For the structural elucidation of TPs, collision-induced dissociation (CID) experiments were performed on an Acquity HPLC system (Water Technologies, Guyancourt, France) coupled with a Bruker SolarixXR FT-ICR 9.4 T MS instrument (Bruker Daltonics, Bremen, Germany). For the chromatographic separation, an Agilent Pursuit XRsULTRA C18 (length 50 mm, diameter 2 mm, particle size 2.8 μm) column was used with an Agilent HPLC MetaGuard (Pursuit XRs C18, 3 μm , 2,0 mm) guard column (Agilent Technologies, Les Ulis, France). The flow was set to 0.2 mL/min, the total run time was 22 min with an acquisition time of 15 min. Gradient flow was used with solvent A being water with 0.1% formic acid and solvent B being acetonitrile with 0.1% formic acid. The LC method consisted of holding 95% of solvent A and 5% of solvent B for 3 min, after which a gradient of 9 min was applied, until the ratio of the two solvents reached 50–50%. The ratio of solvent A was promptly decreased to 5% and kept at this ratio until 17.1 min total run time, after it was reset to the initial 95%. After every measurement, 5 min were let for equilibration and washing using the latter solvent ratio. The injection volumes were 2 μL and 10 μL for LC-MS and LC- MS^n experiments, respectively. The autosampler (Water Technologies, Guyancourt, France) was kept at 4 °C for better preservation. Each sample was prepared before analysis by adding 10% volume of a mixture acetonitrile/formic acid (0.1%). Electrospray ionization was used as the ion source in positive mode with a sample flow of 0.2 mL/min. The capillary voltage was 4000 V and the spray shield was set at -500 V. Nitrogen was used as nebulizer gas (1 bar) and drying gas (8 L/min, 250 °C). The detection range was 57.7–1000 m/z , in broadband mode, with a data acquisition size of 4 Mpts and a data reduction of noise of 97%. For MS^2 experiments, isolation was carried out with a 1 m/z window and CID experiments were performed with collision energies of 5, 10, 15 and 20 V. Preliminary in-cell experiments were performed to assess the optimal parameters (isolation window, quadrupole voltage, and collision energy) for the MS^3 experiments. The Bruker Data Analysis software was used for data processing.

Total organic carbon (TOC) was measured using a Shimadzu TOC5000 analyzer (catalytic oxidation on Pt at 680 °C). The calibration was performed using standards of potassium phthalate.

Inorganic ions (NO_3^- , NO_2^- and NH_4^+) generated during maprotiline degradation were identified by ion chromatography analysis using a Dionex chromatograph equipped with

a Dionex 40 ED pump and a Dionex 40 ED conductimetric detector. For nitrate anions, a Dionex Ion Pac AS9-HC 4 × 250 mm column, and Ion Pac ASRS-ULTRA 4 mm conductivity suppressor were used while ammonium cations were analyzed using a Dionex Ion Pac CS12A 4 × 250 mm column, and an Ion Pac CSRS-ULTRA 4 mm conductivity suppressor, using 10 mM NaHCO₃ and 4 mM K₂CO₃ as eluent at 1 mL/min.

–Retrospective suspected screening

The retrospective suspected analysis was performed according to the workflow previously described [25]. The occurrence of maprotiline and the elucidated TPs were investigated in 130 digitally achieved chromatograms (58 wastewater and 72 river water samples). 34 wastewater samples from the river basins of Germany (Danube, Rhine, Ems, Weser, Elbe, Odra, Meuse, Eider, Trave, Peene) [26] and 24 additional wastewater samples from Danube River basin (12 countries) [27] and surface water samples from Danube, Dniester [28] and Donets were investigated, as described in Table S4.3.5.

–Toxicity

The acute toxicity of maprotiline and the degradation products issued from maprotiline (20 mgL⁻¹) degradation in ultrapure water in the presence of TiO₂ (500 mgL⁻¹) was evaluated for samples after different irradiation times using a Microtox Model 500 toxicity analyzer (Milan, Italy). The analyses were performed evaluating the bioluminescence inhibition assay in the marine bacterium *Vibrio fischeri* by monitoring changes in the natural emission of the luminescent bacteria. Freeze-dried bacteria, reconstitution solution, diluent (2% NaCl) and an adjustment solution (non-toxic 22% sodium chloride) were obtained from Azur (Milan, Italy). Samples were tested in a medium containing 2% sodium chloride, and the luminescence was recorded after 5, 15 and 30 min of incubation at 15 °C. The luminescence inhibition percentage was determined by comparing with a non-toxic control solution.

Results and discussion

Chemical selection approach

Maprotiline was selected as a compound of potential interest for further monitoring activities as a result of the application of the NORMAN prioritization scheme. This scheme was designed by NORMAN to deal with less-investigated substances for which knowledge gaps are identified (e.g. insufficient information on the exposure levels and/or adverse effects, or inadequate performance of the analytical methods for their measurement in the environment) [29]. The concept involves the application of a decision tree which allows the allocation of substances into six main action categories, based on the identified knowledge gaps and actions needed to address them. The priority within each category is then evaluated on the basis of specific occurrence, hazard (e.g. persistence, bioaccumulation, mobility, endocrine disruption potential) and risk indicators.

This workflow, originally designed to work with target monitoring data, is currently exploring the automatic query of non-target screening (NTS) mass spectral information archived in the Digital Sample Freezing Platform (DSFP).

As part of the NORMAN Database System (NDS) [30] and its interconnected databases (SusDat database [31] ECOTOX database,[32] the NORMAN Digital Sample Freezing Platform (DSFP) [33] is a virtual platform able to store an extensive number of raw HRMS data converted into a common (open) format, designed for retrospective screening. Thanks to a set of fully integrated tools NORMAN DSFP can provide reliable qualitative and semi-quantitative data on the occurrence of CECs, can represent the spatial distribution of contaminants and the degree of exceedance of threshold values and in this way support identification and prioritization of CECs frequently detected in environmental samples.

Maprotiline was identified as a compound of potential interest further to a suspect screening test carried out for a list of more than 40,000 substances (present at the time of the study in the SusDat database, 5th September 2019) on 46 composite effluent wastewater samples collected from Danube river basin (August 2017) [27] and from a national wastewater effluent campaign in Germany (May 2018) [26] archived in DSFP. Considering mass accuracy, plausibility of the chromatographic retention time (RT), isotopic pattern fit, number of experimental and predicted fragments, and % similarity of experimental and library spectra as criteria supporting the tentative identification of the suspects, maprotiline was elucidated at level 2A (probable structure by library spectrum match) as compared to other substances for which actions to improve the elucidation of the structure are needed before implementation of further monitoring effort.

In line with the purposes of the prioritization methodology (worstcase scenario approach), the lowest Provisional No Effect Concentration (PNEC) values were used – representing the most conservative ecotoxicological threshold values for the investigated suspect compounds. All PNEC values used in this study were extracted from the NORMAN Ecotoxicology database. In cases where no experimental data on the toxicity of detected substances were available, predicted PNECs (P-PNECs) were derived by QSTR models [34]. The substances were ranked based on three indicators: (i) Frequency of Appearance (FoA), calculated as percentage of sites where the substance was detected above the limit of detection (LOD); (ii) Frequency of PNEC exceedance (FoE), calculated as percentage of sites where the substance was detected above the PNEC, and (iii) extent of PNEC exceedance (EoE), calculated as the 95th percentile (MEC95) of the substance’s maximum observed concentration at each site divided by the PNEC. No PNEC value based on experimental data was available for maprotiline and therefore a predicted PNEC (P-PNEC) was used. Maprotiline was prioritized and allocated to the group of compounds with “Sufficient frequency of appearance (FoA)”, that is FoA (sites with positive detection) $\geq 20\%$, (67% of the investigated wastewater treatment stations) with 17% of the sites exceeding

the predicted PNEC value ($0.300 \mu\text{g L}^{-1}$).

Maprotiline degradation in ultrapure water

The direct photolysis of maprotiline in the considered time window (1 h) is negligible. The most likely reason is the fact that the molecule does not absorb radiations above 280 nm [35], while the sunlight irradiance below 300 nm is extremely limited [36]. To hasten the degradation process and generate degradation products, the drug degradation was firstly performed at high concentration (for easier identification) in ultrapure water using TiO_2 as photocatalyst. Figure 4.3.2 shows the maprotiline degradation in the presence of the heterogeneous photocatalyst activated under UVA irradiation. In the presence of the photocatalyst, the complete maprotiline removal was achieved after only 15 min, while the total organic carbon (TOC) measurements showed more than 85% of the pollutant mineralization in just 30 min under irradiation and > 95% after 1 h. This trend is in agreement with the ammonium and nitrate concentrations monitored during the degradation, as shown in Figure 4.3.2. The ammonium ion (73%) release was observed in a significantly higher amount than that of nitrate (15%) within 1 h of irradiation, as previously observed [37].

All samples were analyzed by HPLC-HRMS for the identification of maprotiline degradation products. The m/z ratios, proposed elemental compositions, as well as fragment ions and retention times are presented in Table S4.3.1 (see Supplementary information). In total, 32 degradation products were formed, many of them in the form of several isomeric species as summarized in Table S4.3.1. The formation of degradation products and their evolution over irradiation time are shown in Figure S4.3.2. For all degradation products, complete removal was observed after less than 30 min of irradiation, in agreement with the high percentage of mineralization (86%) obtained within the same experimental time.

Among the identified TPs, 18 resulted from the drug hydroxylation. Species with m/z 294.1858, 310.1806, 326.1755 and 342.1709 matches with formulae corresponding to mono-, di-, tri-, and tetrahydroxy derivative isomers. The main drug degradation products were those involving monohydroxylation (m/z 294, see Figure S4.3.3), and in particular the isomers 294-D and 294-E, which exhibited maximum intensity within 5 min, as shown in Figure S4.3.2. The species resulting from the addition of the second (m/z 310), third (m/z 326) and fourth (m/z 342) hydroxyl groups showed similar evolution profiles over time. Additionally, 9 degradation products resulting from the drug oxidation were identified.

Species with m/z 292.1709, 308.1648, 324.1609 match formulae corresponding to dehydrogenation of mono-, di-, and trihydroxy derivatives, respectively. It can be reasonably assumed that these TPs are a result of H_2 elimination from the corresponding species determined with m/z 294, 310 and 326. The TPs with m/z 308 showed a fast formation (maximum intensity at 5 min) but a longer persistence, nevertheless they were also completely removed within 30 min. A similar evolution over time was observed for the 3

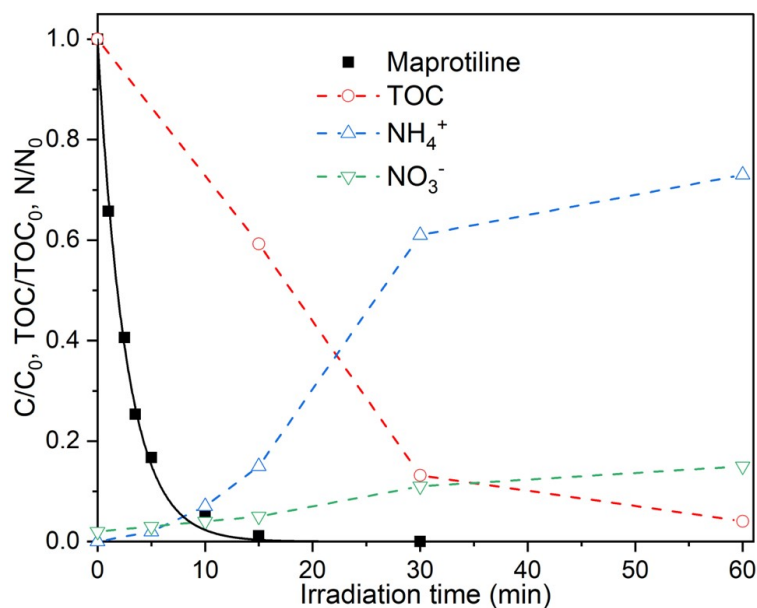


Figure 4.3.2: Maprotiline degradation (black line) and mineralization (colored lines) in the presence of TiO_2 (500 mgL^{-1}). (For interpretation of the references to color in this figure legend, the reader is referred to the web version of this article.).

isomeric species with m/z 284.1647 matching with the formula $\text{C}_{18}\text{H}_{22}\text{NO}_2^+$. Additionally, two species at m/z 258.1503 and 234.1505 ions were observed, matching respectively with the formulae $\text{C}_{16}\text{H}_{20}\text{NO}_2^+$ and $\text{C}_{14}\text{H}_{20}\text{NO}_2^+$, and both species presented the maximum intensity at 5 min and complete disappearance in 30 min. Furthermore, it could be noted a progressively lower abundance of TPs formed from the addition of multiple hydroxyl groups. Also, the species with m/z 284.1647, 258.1503 and 234.1505 were the lowest abundant TPs.

The potential acute toxicity of maprotiline and its TPs was assessed by using the *Vibrio fischeri* assay and the results are plotted in Figure 4.3.3. At time zero, the inhibition percentage related to maprotiline is low (12%) and, despite a slight increase in the first stage of degradation, then it decreases, so implying that the drug transformation proceeds through the formation of slightly toxic compounds. The sample at 30 min presents a percentage of inhibition close to zero in agreement with the complete removal of the identified TPs and the almost complete mineralization.

Structural elucidation of maprotiline main degradation products

Aiming at TPs structural elucidation, the maprotiline fragmentation pathway was firstly investigated by CID experiments, ascertaining the most likely losses from the protonated molecule. The maprotiline MH^+ (m/z 278.1910) MS^2 fragmentation pathways are presented in Figure 4.3.4 and was suggested based on the 5 observed product ions (see Table S4.3.1).

Five photoproducts with m/z 294 were detected with retention times between 9.0 and

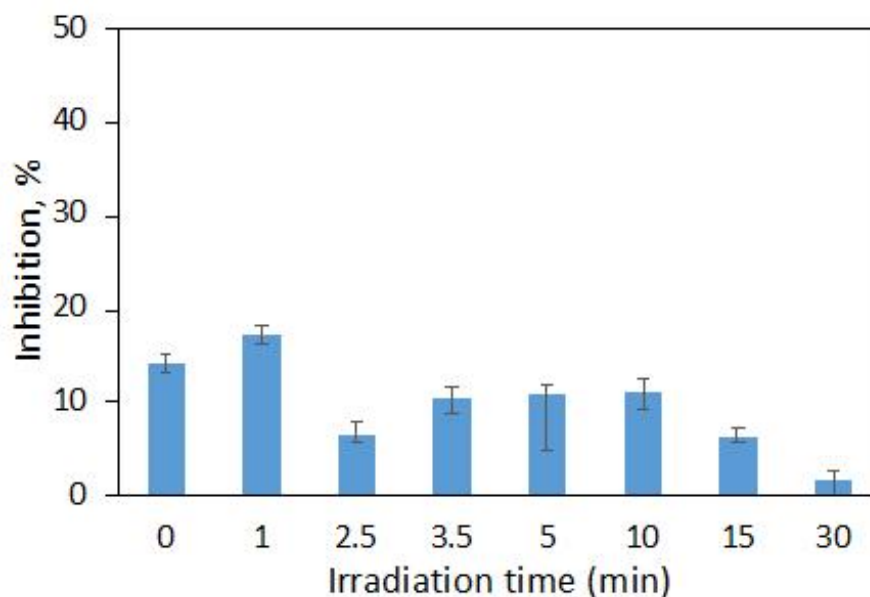


Figure 4.3.3: Inhibition effect on *Vibrio fischeri* bioluminescence in the presence of TPs resulting from maprotiline photocatalytic degradation as a function of irradiation time. Error bars correspond to standard deviations ($n = 3$).

11.3 min and, based on their empirical formula, were attributed to hydroxylated maprotiline. If one considers that these photoproducts result from hydroxyl addition onto an aromatic ring, as usually reported when photochemistry occurs in water matrix, the main dissociations of oxidized maprotiline are expected to be those displayed in Figure 4.3.5. It is to be noted that water loss from the protonated molecule is not informative considering that protonation of a hydroxyl group can lead to water elimination whatever its location on the ion [38].

The main ions observed in CID experiments on m/z 294 are those described in Figure 4.3.5, and are common for the photoproducts 294-A, 294-C, 294-D and 294-E (see Table 4.3.1) but not for 294-B, for which CID decomposition pathways are different. The protonated structure of the compound 294-D displays specific ions (m/z 263 and m/z 245), which allow to determine the position of the hydroxyl group according to the mechanism displayed in Figure S4.3.3. In the same way, the specific ion at m/z 157 allowed structural determination of the compound 294-E (see Figure S4.3.5). The CID mass spectra of the photoproducts 294-A and 294-C are the same and do not allow to discriminate between the compound resulting from hydroxyl addition on the carbon atom 3 or onto the carbon atom 4 (see Figure 4.3.1). The structures were suggested based on their relative retention times, in comparison with those of the elucidated structures. In the case of the photoproduct 294-B, CID experiments provided common ions with those resulting from CID of protonated maprotiline: m/z 276, m/z 250, m/z 219 and m/z 191, which show evidence that hydroxylation of this compound occurred on the bridge, i.e. on C8 or C9. The

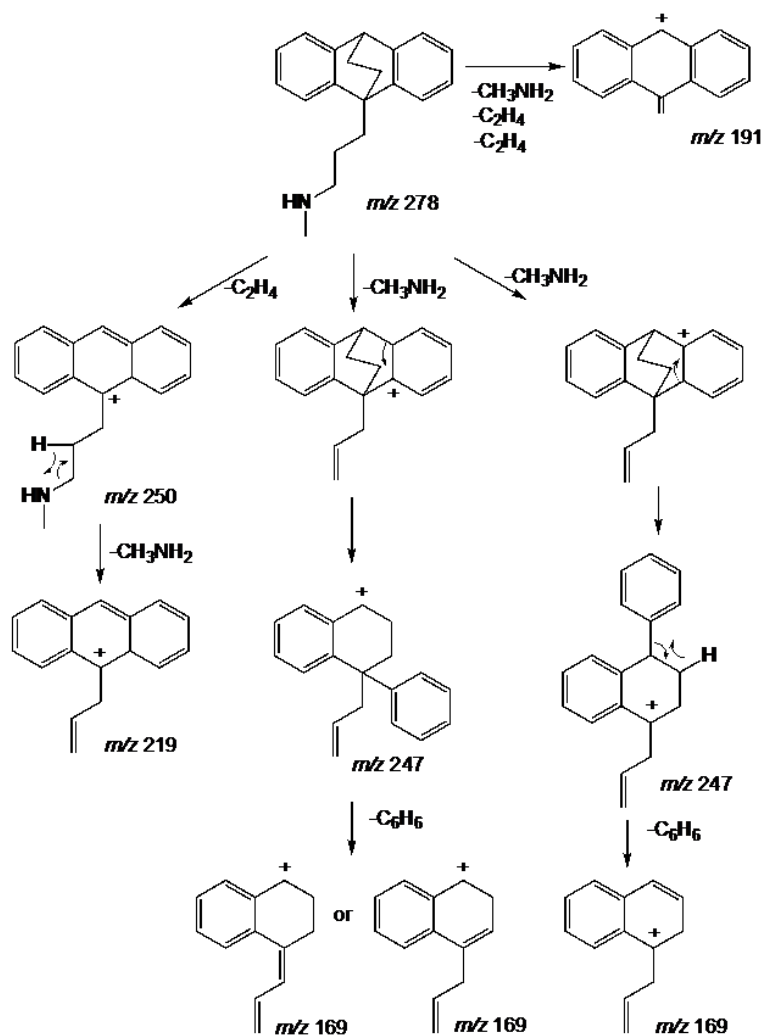


Figure 4.3.4: Suggested fragmentation pathways for protonated maprotiline in CID experiments

CID pathways depicted in Figure S4.3.6 demonstrate that it is not possible to establish whether the hydroxylation took place on carbon 8 or 9 since the CID mechanism begins by a water elimination that leads to the same ion in both cases. One should have expected hydroxylation to occur onto C7 because cleavage of the C7–H bond would have led to a very stable carbocation but the resulting compound would not have been able to undergo the subsequent losses of H_2O and C_2H_2 reported in Table 4.3.1 for the corresponding ion. Additional experiments (see below) allowed to establish that hydroxylation took place on C9.

Five photoproducts with a pseudo molecular ion at m/z 292 were detected with retention times between 9.4 and 11.6 min; in terms of molecular formulae, they result from the addition of one oxygen atom and the removal of two hydrogen atoms on maprotiline. It can be reasonably assumed that these five photoproducts result from H_2 elimination from the five photoproducts with a pseudo molecular ion at m/z 294.

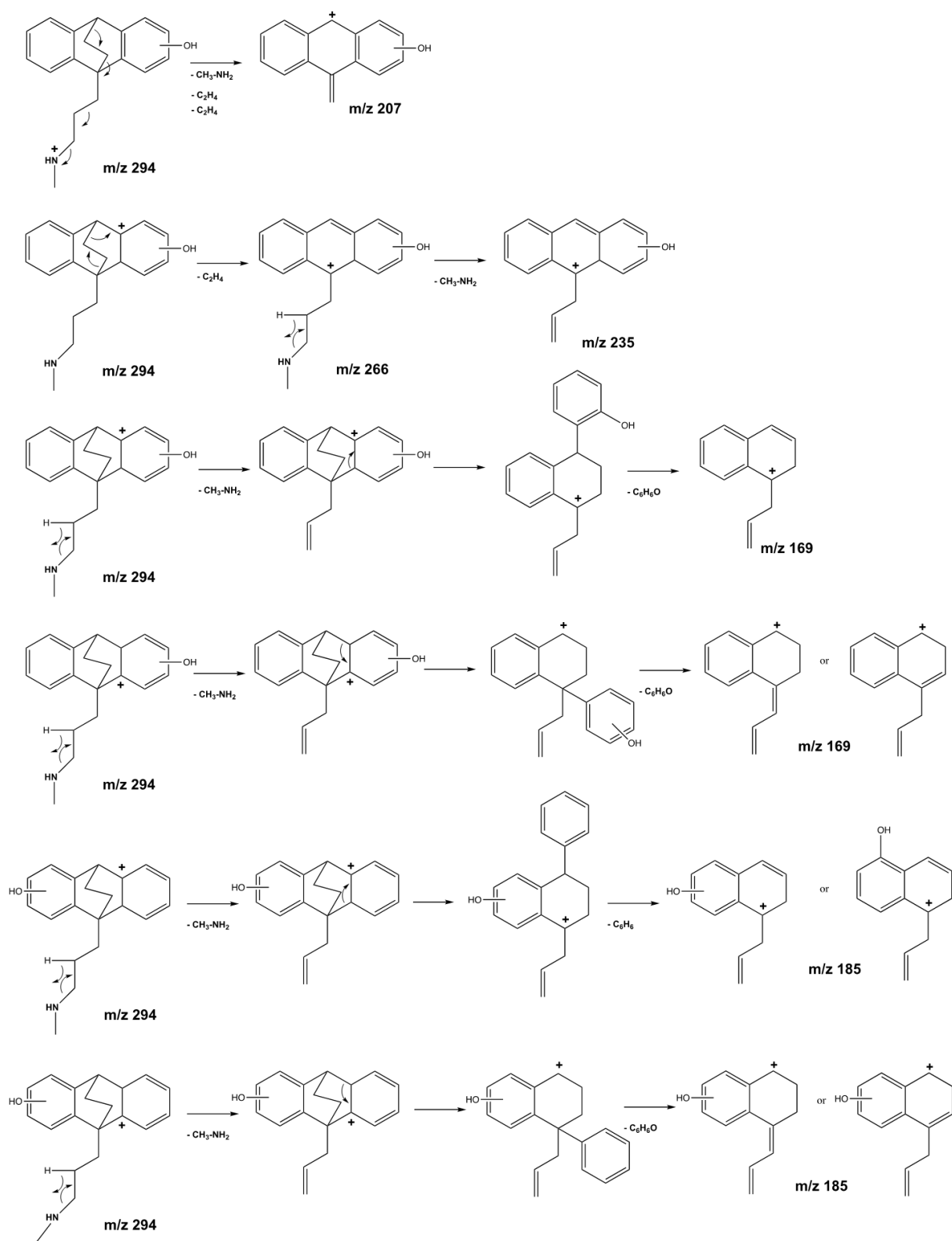


Figure 4.3.5: Suggested dissociation pathways for photoproducts resulting from hydroxylation of maprotiline on an aromatic ring

Table 4.3.1: Ions detected in CID experiments for maprotiline main degradation products

m/z	Ion formula	294				
		A	B	C	D	E
294.1852	$C_{20}H_{24}NO^+$	+		+	+	+
276.1747	$C_{20}H_{22}N^+$	+	+		+	
266.1539	$C_{18}H_{20}NO^+$	+		+	+	+
263.1447	$C_{19}H_{19}O^+$				+	
250.1606 ^a	$C_{18}H_{20}N^+$		+			
245.1341	$C_{19}H_{17}^+$		+		+	
235.1132	$C_{15}H_{15}O^+$	+		+	+	+
219.1182 ^a	$C_{17}H_{15}^+$		+			
207.0804	$C_{15}H_{11}O^+$	+		+	+	+
191.0868 ^a	$C_{15}H_{11}^+$		+			
185.0973	$C_{13}H_{13}O^+$	+		+	+	+
169.1023 ^a	$C_{13}H_{13}^+$	+		+	+	+
157.0658	$C_{11}H_9O^+$					+

m/z	Ion formula	292				
		A	B	C	D	E
292.1713	$C_{20}H_{24}NO^+$	+	+	+	+	+
250.1605 ^a	$C_{18}H_{20}N^+$	+	+	+	+	
246.1292	$C_{18}H_{16}N^+$					+
243.1183	$C_{15}H_{15}O^+$			+	+	
219.1182 ^a	$C_{17}H_{15}^+$	+	+	+	+	
217.1025	$C_{15}H_{11}O^+$	+	+	+	+	
191.0867 ^a	$C_{15}H_{11}^+$	+	+	+	+	
183.0816	$C_{13}H_{13}O^+$					+

^aProduct ions observed also in the maprotiline fragmentation.

Dehydrogenation is possible to create a double bond between C7 and C8 or C8 and C9, the first hypothesis leading to a more stable species regarding mesomeric effects. This is confirmed by CID mechanisms. Considering for example the molecule 292-B, the formation of ions at m/z 250 and m/z 119 from MH^+ is only possible if the new double bond created is located between C7 and C8 (See Figure S4.3.7). Based on these considerations, the four ions at m/z 292 that dissociate to provide ions at m/z 250, m/z 243, m/z 219 and m/z 191 were assumed to result from the formation of a double bond between carbon atoms C7 and C8 from the photoproducts with MH^+ ions at m/z 294. The photoproduct 292-E displays a different CID pathway with product ions at m/z 246 and m/z 183, which show that in this case the double bond was created on the alkyl chain. It has been assumed to be formed between C12 and C13 because: i) it is thus conjugated with the free doublet of the nitrogen atom, ii) this localization allows the C_2H_4 elimination depicted in Figure S4.3.8. Localization of the hydroxyl group on C9 permits to explain the same mechanism. This last conclusion allowed assigning the structure of the compound 294-B as displayed

in Figure S4.3.9 (see Supplementary information).

Considering the molecular symmetry of maprotiline and the fact that water loss induced by CID does not allow to attribute the exact position of the corresponding hydroxyl group, it was not always possible to accurately elucidate the structures of the poly hydroxylated species. However, it is reasonable to assume that the second, third and fourth consequent hydroxylations took place on the aromatic ring or the ethylene bridge of species with molecular ions at m/z 294 and 292.

Six products with MH^+ at m/z 310 resulting from the dihydroxylation of maprotiline were detected between 8.4 and 11.3 min. As suggested above, it can be expected that these substances resulted from the hydroxyl addition to the generated monohydroxylated species m/z 294. Table S4.3.3 summarizes the common ions observed in CID experiments of different isomers and the main dissociation pathways are shown in Figure S4.3.10. In the case of the photoproduct 310-F, CID experiments provided common ions with those resulting from CID of protonated maprotiline: m/z 250 and m/z 191, which show evidence that hydroxylation of this compound occurred on the bridge, i.e. on C9 and C8 (Figure S4.3.11). The CID experiments of the photoproduct 310-E provided the ions m/z 280 and 101, allowing to postulate the hydroxyl group addition in the C2 and C5 (Figure S4.3.12). As evidenced in Figure S4.3.2, this was the most abundant dihydroxylated compound, what can be explained the probability of the second hydroxyl group addition in the most abundant photoproducts, also formed from the hydroxylation in the C2 (294-E) and C5 (294-D), besides the ortho/para director effect. However, this structure could not be demonstrated due to the lack of product ions. The CID experiments of 310-A, 310-C and 310-D do not permit to elucidate the structure of the isomer. However, the generated ion at m/z 251 from 310-C and 310-D species allowed to confirm that the hydroxylation does not occurred on the bridge, i.e. on C8 and C9, while the ion m/z 201 from 310-D endorsed to ascertain the dihydroxylation in the same aromatic ring (Figure S4.3.10). The ion m/z 266 obtained from CID experiments of compound 310-B evidenced the hydroxyl addition to the bridge, i.e. on C9 if considering this species to result from the hydroxyl group addition to the 294-B. The formation of ions m/z 123 and 89 allowed to postulate the hydroxyl group addition on C11, as suggested in Figure S4.3.13. However, the formed ions do not allow demonstrating the suggested structure.

Additionally, three compounds with MH^+ at m/z 284 were detected with retention times between 8.0 and 9.5 min; they result from ethylene loss and hydroxylation with ring-opening. In the case of 284-A, CID experiments lead to the formation of the fragment at m/z 225 through consecutive losses of methylamine and carbon monoxide. The compound 284-C generated the product ion at m/z 256 from the loss of ethylene bridge and at m/z 225 through the loss of methylamine. The structures were postulated based on these eliminations (Figs. S13 and S14) but the lack of other product ions does not allow their

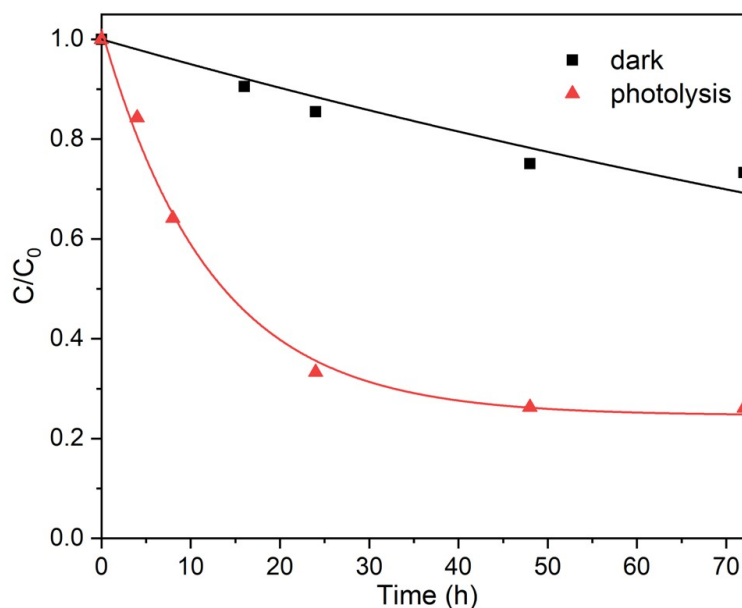


Figure 4.3.6: Maprotiline ($10 \mu\text{gL}^{-1}$) removal over time in a river water sample, in the dark and under UVA irradiation

conclusive elucidation. The 284-B generated a single ion at m/z 89, allowing speculating the oxygen addition on C3 and C4 with the loss of the ethylene bridge, as proposed in Figure S4.3.16.

A compound with MH^+ at m/z 258 ($\text{C}_{16}\text{H}_{20}\text{NO}_2^+$) elutes at 7.3 min. The fact that no other isobaric species are detected suggests that it does not result from further oxidation of one of the aforementioned hydroxylated species. Only two product ions are detected in CID experiments and correspond to subsequent losses of water and carbon monoxide, which is typical of protonated carboxylic acids. That is why the structure displayed in Figure S4.3.17 is that of a carboxylic acid. Opening of an aromatic ring with the formation of a carboxylic acid is quite frequent in photochemistry [39]. Unfortunately, the structure postulated in Figure S4.3.17 was not demonstrated due to the lack of product ions in CID experiments; although its high polarity is in agreement with relatively short retention time.

Simulated and real environmental conditions

The environmental fate of the drug was investigated in natural river water by searching for the TPs detected in the photocatalytic simulation, but also for potential new TPs not observed before. For such, a river water sample was spiked with maprotiline ($10 \mu\text{g L}^{-1}$) at a concentration similar to those previously reported in the environment [14]. It should be pointed out that, as detailed in Methods, the samples were pre-concentrated by freeze-drying before analysis. During degradation experiments, the pH value was measured and compared the initial pH with that measured at the end of the degradation no significant

change over time was observed ($\Delta\text{pH} \leq 0.1$).

As evidenced in Figure 4.3.6, experiments performed in the dark showed around 20% of maprotiline removal within 72 h, so implying a limited effect of the biotic components on drug fate. In the dark, the drug degradation leads to the formation of the byproducts 294-D and 284-C, observed after 24 h and 16 h, respectively, and still present after 72 h, as shown in Figure 4.3.7a. The monohydroxylated species matches with one of the most abundant TPs observed in ultrapure water, while the species with m/z 284, was previously observed in low abundance.

Under irradiation, the maprotiline degradation kinetic increased following a pseudo first-order decay until 24 h, achieving 65% of drug removal (Figure 4.3.6), while the appearance of TPs is also favored compared to dark conditions. In detail, 12 out of the 32 TPs previously identified (see Table S4.3.4) were found in spiked river water and all were still present after 72 h irradiation. All the 5 isomeric forms of the monohydroxylated species (MH^+ at m/z 294) were observed, 294-C, 294-D and 294-E in significantly larger amounts (Figure 4.3.7). It is interesting to note the slower formation of 294-B, the only isomer resulting from hydroxylation on the bridge and not on an aromatic ring. From the literature, it is possible to realize that besides maprotiline degradation, the species 294-A (2-hydroxymaprotiline) and 294-C (3-hydroxymaprotiline) can reach the environment also from drug metabolism; hydroxylated products represent 4–8% of the dose being excreted in human urine, with 3-hydroxymaprotiline and the corresponding N-demethylated specie reported as major human metabolites [22]. Additionally, the study identifies metabolites resulting from hydroxylation on the C8 atom (ethylene bridge) and the corresponding demethylation product, besides the metabolite resulted from the di-hydroxylation in C3 and C4.

The species 292-B, 292-C and 292-D, issued from dehydrogenation of the most abundant 294 isomers, (with the formation of a double bond between atoms C7 and C8) show distinct evolutions over time. 292-C showed its maximum intensity at 4 h and was completely removed within 48 h, 292-D reached its maximum intensity at 48 h and was still present at 72 h, while 292-B appeared after 24 h and decreased until the end of the experiment.

Only one species formed by the addition of more than one hydroxyl group was detected. Resulting from the addition of two hydroxyl groups, the compound 310-E was formed after 24 h irradiation with increasing abundance until the end of the experiment. As stated before this compound was the most abundant dihydroxylated observed in photocatalytic experiments in ultrapure water and resulted from a second hydroxyl group addition into the most abundant monohydroxylated species (294-D and 294-E).

Additionally, the 3 species at m/z 284 resulting from the ringopening were also formed with maximum intensity at 24 h, showing a slow degradation profile and still present at the end of the experiment. One could argue that the species MH^+ at m/z 284 resulted

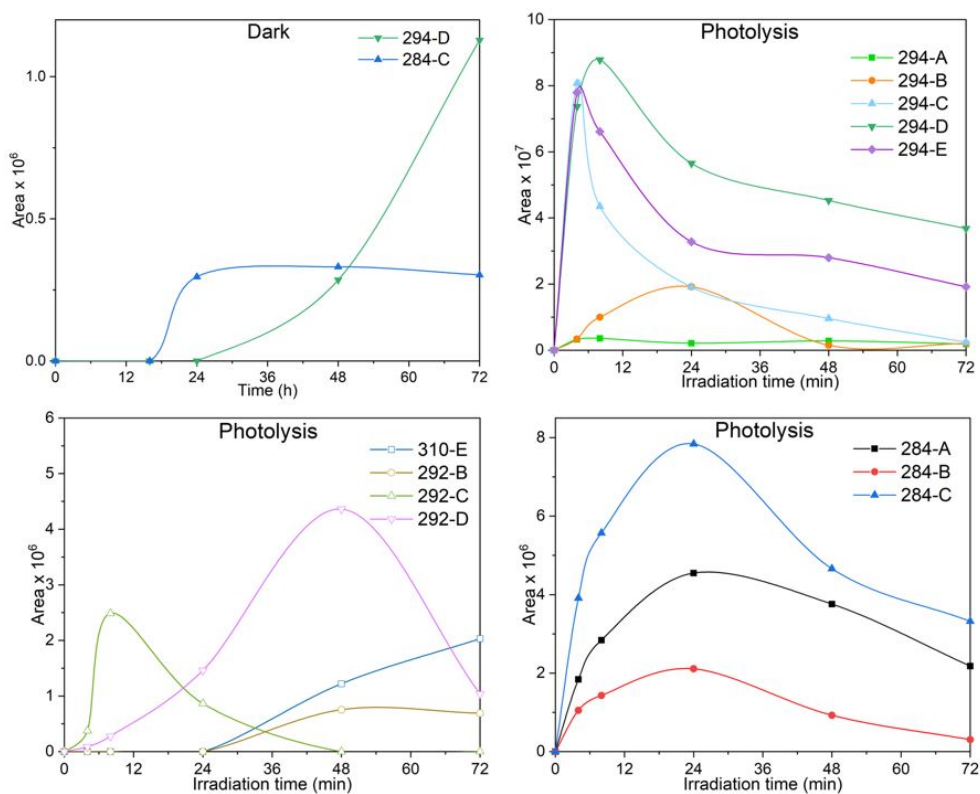


Figure 4.3.7: Profile over time of maprotiline degradation products observed in a river water sample over time: a) in the dark; b, c and d) under irradiation

from the degradation through ring-opening of the dihydroxylated compounds (MH^+ at m/z 310), particularly the 284-A resulting from the degradation of the compound 310-E. However, as evidenced in Figure 4.3.7, the species MH^+ at m/z 284 are formed at the early steps of maprotiline degradation, while the compound 310-E was observed only after 24 h, so implying that ring-opening pathway occurs from maprotiline molecule. Figure 4.3.8 displays the proposed maprotiline degradation pathways in river water.

All the TPs observed in river water experiments matched with those previously identified in the photocatalytic experiments performed in ultrapure water, as previously observed for other pollutants [40, 41].

Additionally, the faster photodegradation rate observed in river water experiments relative to the degradation in ultrapure water indicated that indirect photolysis played an important role in the drug removal. Faster photodegradation of organic pollutants in wastewater has been reported by other authors [42–44], while nitrate and dissolved organic matter have been identified as photosensitizers responsible for the generation of reactive species [42, 45, 46].

The results of the retrospective suspect screening presented in Table S4.3.4 indicate that the elucidated TPs by laboratory-scale experiments are formed in real waters. 16 TPs were detected in at least one effluent wastewater sample with maprotiline 308-B showing the

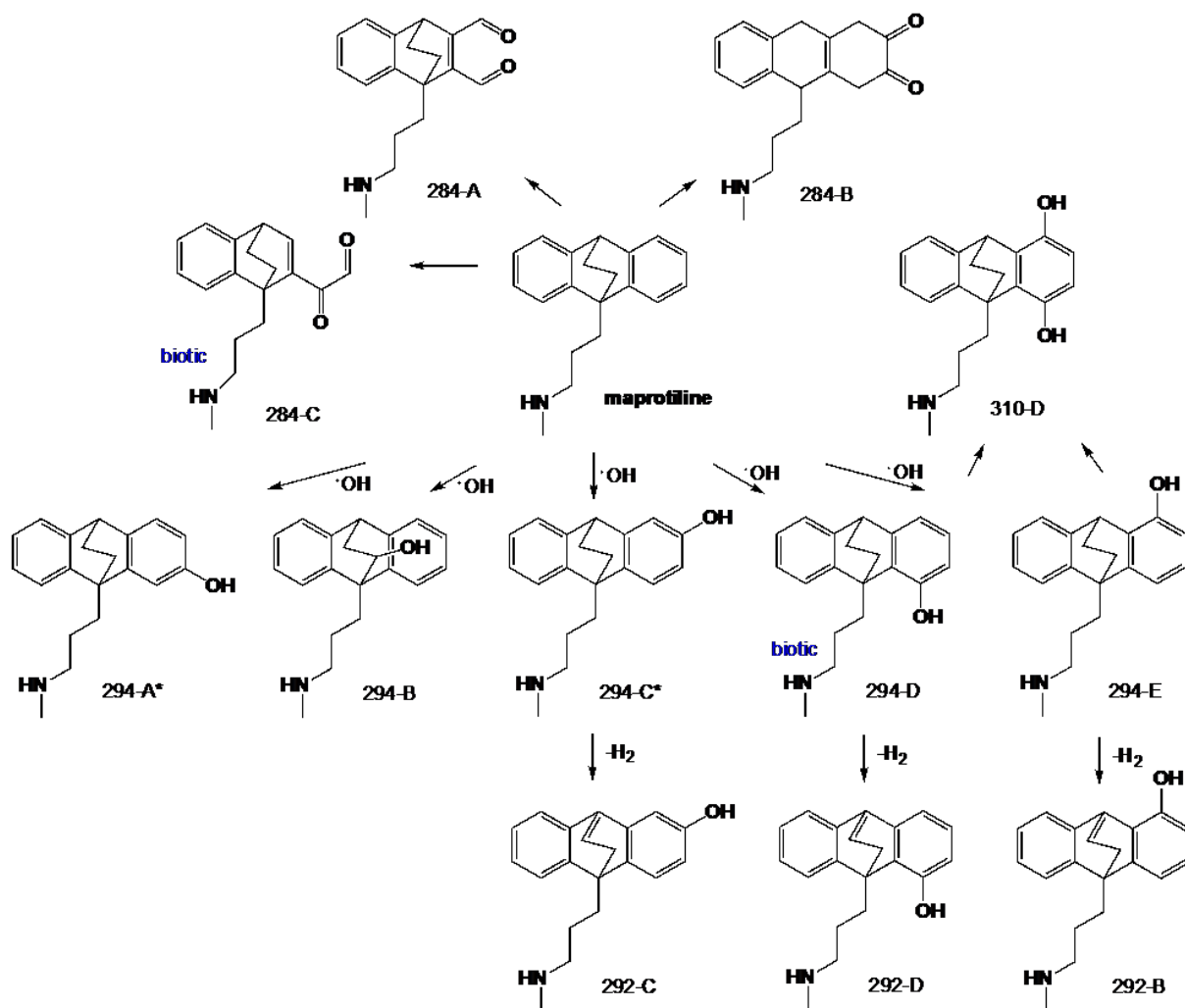


Figure 4.3.8: Proposed maprotiline degradation pathways in river water in the dark (biotic) and under irradiation (abiotic) *indicated TPs also resulted from human metabolic transformation.

highest frequency of appearance (FoA 56.9%). This fact creates concerns about the toxicity of the formed chemical mixture in wastewaters. Despite the formation and the detection of numerous TPs in real wastewater, most of the TPs remained undetectable in river water samples. Maprotiline and three TPs (308-B, 326-C, 234) were the only TPs that were scarcely detected in river waters (FoA below 2.8%), which indicates that the substance is further degraded in the environment and the concentration of the substance and its TPs becomes lower than the limit of the detection of the applied sample preparation and instrumental methods.

Conclusions

The degradation of maprotiline in spiked river water led to the formation of twelve TPs, structurally elucidated through LC/HRMS. The degradation pathways in natural water

were proposed for the first time, which results from monohydroxylation in several positional isomers and the corresponding dehydrogenated molecules, besides dihydroxylation and ring-opening. Some of these TPs, 2-hydroxymaprotiline and 3-hydroxymaprotiline matched with described maprotiline metabolites, that can be released in the environment by drug excretion.

Moreover, photocatalytic experiments led to the formation of a higher number of TPs, mostly resulting from similar chemical transformation in multiple positions.

Additionally, retrospective suspect screening of wastewater effluents and river water samples indicate that the elucidated TPs by laboratory-scale experiments are formed in real waters. *Vibrio fischeri* Microtox assay allowed estimating that maprotiline photocatalytic degradation leads to the formation of slightly more toxic TPs than the parent compound. Therefore, future research should focus on evaluating the toxicity of the formed TPs in wastewater treatment plants.

Acknowledgements

This work is part of a project that has received funding from the European Union's Horizon 2020 - Research and Innovation Framework Programme under the Marie Skłodowska-Curie Grant Agreement No 765860 (AQUALity).

Supplementary information

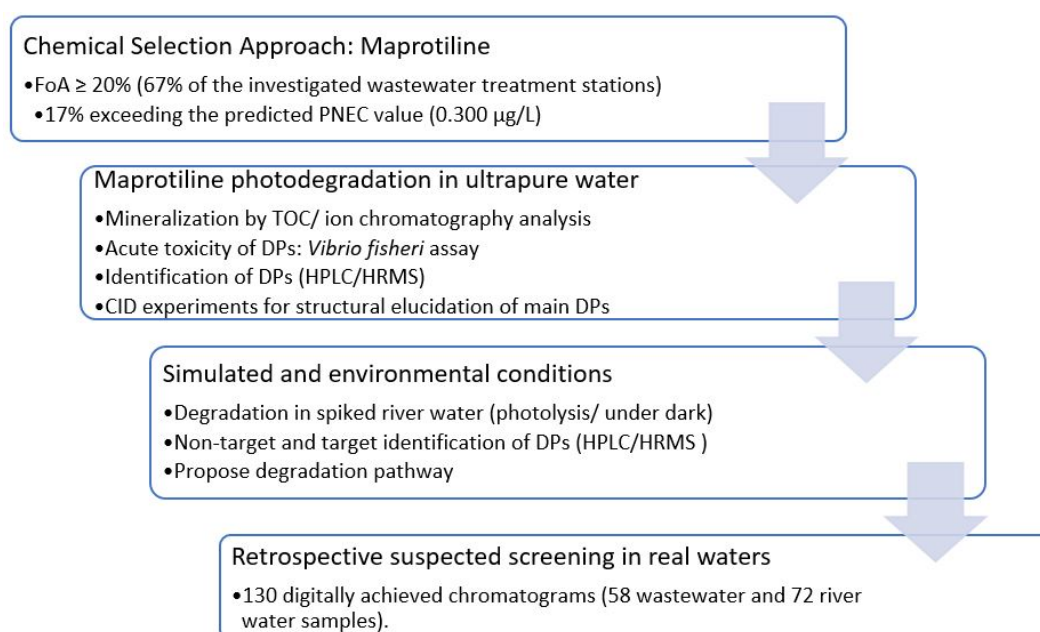


Figure S4.3.1: Schematic view of the workflow for maprotiline degradation pathway

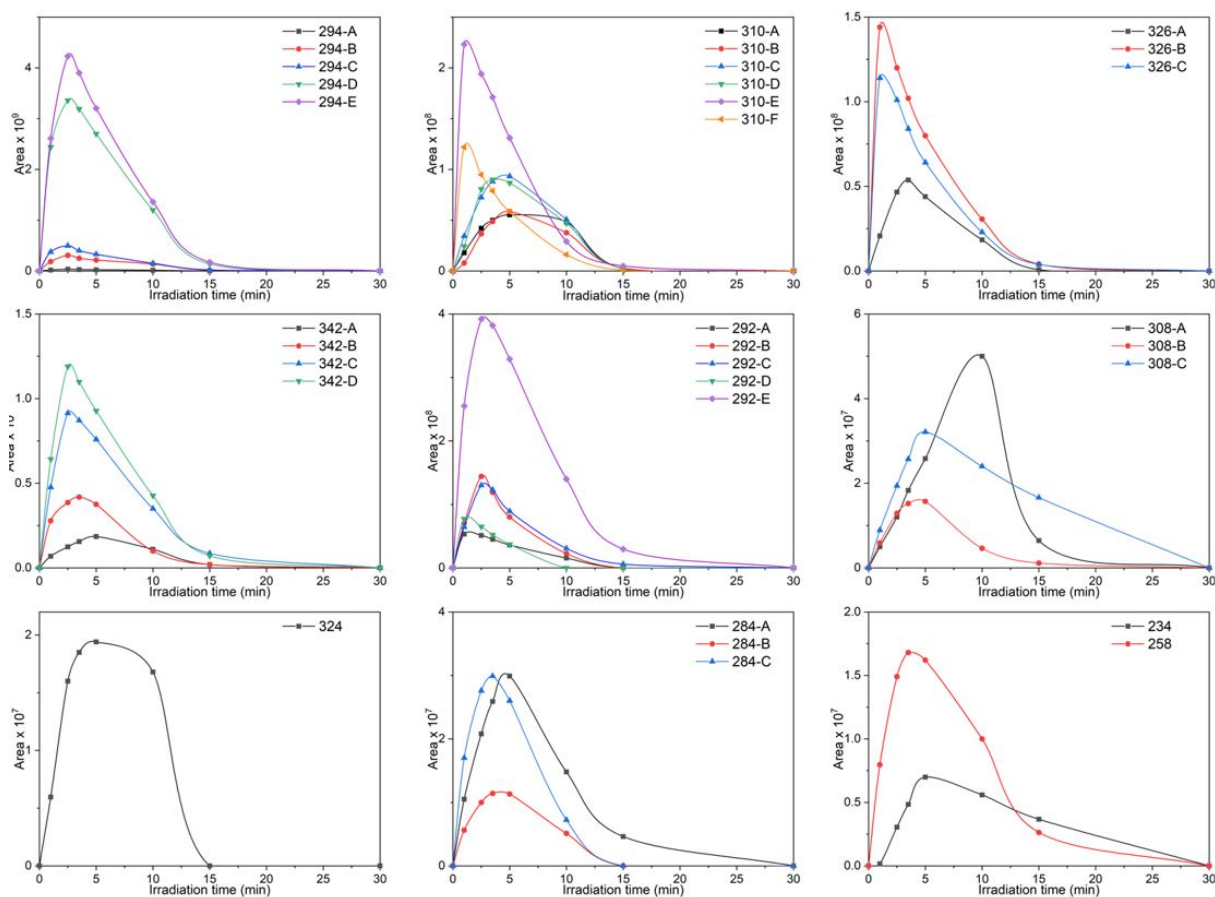


Figure S4.3.2: Profiles over time of maprotiline TPs observed in ultrapure water in the presence of TiO_2

Table S4.3.1: Summary of $[\text{M}+\text{H}]^+$ ions and main product ions from CID experiments

Compound	$[\text{M}+\text{H}]^+$	Empirical formula	r.t. (min)	MS^2			
				(m/z)	Empirical formula	$\Delta(\text{ppm})$	Theoretical m/z
Maprotiline	278.1911	$\text{C}_{20}\text{H}_{24}\text{N}$	12.5	278.1943	$\text{C}_{20}\text{H}_{24}\text{N}(16)$	0.45	278.1903
				250.1594	$\text{C}_{18}\text{H}_{20}\text{N}(100)$	-0.66	250.1590
				247.1489	$\text{C}_{19}\text{H}_{19}(1)$	0.91	247.1482
				219.1173	$\text{C}_{17}\text{H}_{15}(66)$	-0.48	219.1168
				191.0850	$\text{C}_{15}\text{H}_{11}(13)$	-5.26	191.0855
				169.1013	$\text{C}_{13}\text{H}_{13}(8)$	-2.76	169.1012
294-A	294.1858	$\text{C}_{20}\text{H}_{24}\text{NO}$	9.0	294.1871	$\text{C}_{20}\text{H}_{24}\text{NO}(8)$	-6.4	294.1852
				266.1556	$\text{C}_{18}\text{H}_{20}\text{NO}(100)$	-6.2	266.1539
				235.1132	$\text{C}_{17}\text{H}_{15}\text{O}(42)$	-6.3	235.1117
				217.1026	$\text{C}_{17}\text{H}_{13}(35)$	-6.4	217.1012
				207.0818	$\text{C}_{15}\text{H}_{11}\text{O}(55)$	-6.4	207.0804
				191.0868	$\text{C}_{15}\text{H}_{11}(25)$	-6.4	191.0855

		157.0658	C ₁₁ H ₉ O(6)	-6.5	157.0648
		117.0706	C ₉ H ₉ (6)	-6.4	117.0699
		91.0548	C ₇ H ₇ (10)	-6.3	91.0542
294-B	9.7	276.1765	C ₂₀ H ₂₂ N(100)	-6.5	276.1747
		250.1606	C ₁₈ H ₂₀ N(59)	-6.3	250.1590
		245.1340	C ₁₉ H ₁₇ (31)	-6.0	245.1325
		219.1182	C ₁₇ H ₁₅ (78)	-6.4	219.1168
		217.1026	C ₁₇ H ₁₃ (40)	-6.4	217.1012
		191.0868	C ₁₅ H ₁₁ (6)	-6.4	191.0855
		141.0708	C ₁₁ H ₉ (7)	-6.8	141.0699
		129.0707	C ₁₀ H ₉ (30)	-6.6	129.0699
		91.0548	C ₇ H ₇ (21)	-6.3	91.0542
294-C	10.0	294.1871	C ₂₀ H ₂₄ NO(5)	-6.4	294.1852
		266.1556	C ₁₈ H ₂₀ NO(54)	-6.3	266.1539
		235.1132	C ₁₇ H ₁₅ O(100)	-6.3	235.1117
		209.0974	C ₁₅ H ₁₃ O(3)	-6.4	209.0961
		207.0818	C ₁₅ H ₁₁ O(21)	-6.4	207.0804
		185.0973	C ₁₃ H ₁₃ O(20)	-6.5	185.0961
		169.1023	C ₁₃ H ₁₃ (8)	-6.4	169.1012
		147.0814	C ₁₀ H ₁₁ O(6)	-6.3	147.0804
		143.0865	C ₁₁ H ₁₁ (7)	-6.7	143.0855
		133.0657	C ₉ H ₉ O(14)	-6.5	133.0648
		117.0706	C ₉ H ₉ (15)	-6.4	117.0699
		107.0498	C ₇ H ₇ O(9)	-6.2	107.0491
		91.0548	C ₇ H ₇ (5)	-6.3	91.0542
294-D	10.5	294.1871	C ₂₀ H ₂₄ NO(16)	-6.2	294.1852
		266.1556	C ₁₈ H ₂₀ NO(59)	-6.2	266.1539
		263.1447	C ₁₉ H ₁₉ O(9)	-6.3	263.1430
		245.1340	C ₁₉ H ₁₇ (9)	-6.4	245.1325
		235.1132	C ₁₇ H ₁₅ O(100)	-6.3	235.1117
		221.0975	C ₁₆ H ₁₃ O(19)	-6.4	221.0961
		217.1026	C ₁₇ H ₁₃ (14)	-6.4	217.1012
		209.0974	C ₁₅ H ₁₃ O(11)	-6.4	209.0961
		207.0818	C ₁₅ H ₁₁ O(16)	-6.5	207.0804
		185.0973	C ₁₃ H ₁₃ O(19)	-6.5	185.0961
		169.1023	C ₁₃ H ₁₃ (51)	-6.5	169.1012
		143.0865	C ₁₁ H ₁₁ (32)	-6.5	143.0855
		141.0708	C ₁₁ H ₉ (40)	-6.5	141.0699
		133.0657	C ₉ H ₉ O(24)	-6.5	133.0648
		129.0707	C ₁₀ H ₉ (15)	-6.5	129.0699
		117.0706	C ₉ H ₉ (16)	-6.5	117.0699
		107.0498	C ₇ H ₇ O(24)	-6.4	107.0491
		91.0548	C ₇ H ₇ (5)	-6.3	91.0542
294-E	11.3	294.1871	C ₂₀ H ₂₄ NO(11)	-6.2	294.1852
		276.1764	C ₂₀ H ₂₂ N(6)	-6.3	276.1747
		266.1556	C ₁₈ H ₂₀ NO(98)	-6.2	266.1539

				235.1132	C ₁₇ H ₁₅ O(100)	-6.3	235.1117
				217.1026	C ₁₇ H ₁₃ (11)	-6.4	217.1012
				207.0818	C ₁₅ H ₁₁ O(72)	-6.4	207.0804
				185.0973	C ₁₃ H ₁₃ O(26)	-6.5	185.0961
				169.1023	C ₁₃ H ₁₃ (19)	-6.5	169.1012
				157.0658	C ₁₁ H ₉ O(13)	-6.5	157.0648
				141.0708	C ₁₁ H ₉ (19)	-6.5	141.0699
				133.0657	C ₉ H ₉ O(21)	-6.5	133.0648
				117.0706	C ₉ H ₉ (23)	-6.5	117.0699
				107.0498	C ₇ H ₇ O(17)	-6.4	107.0491
				91.0548	C ₇ H ₇ (7)	-6.3	91.0542
310-A	310.1807	C ₂₀ H ₂₄ NO ₂	8.4	310.1820	C ₂₀ H ₂₄ NO ₂ (100)	-6.1	310.1802
				292.1714	C ₂₀ H ₂₂ NO(63)	-6.2	292.1696
				279.1397	C ₁₉ H ₁₉ O ₂ (67)	-6.2	279.1380
				261.1290	C ₁₉ H ₁₇ O(31)	-6.3	261.1274
				217.1026	C ₁₇ H ₁₃ (70)	-6.4	217.1012
				191.0867	C ₁₅ H ₁₁ (81)	-6.5	191.0855
				185.0973	C ₁₃ H ₁₃ O(34)	-6.5	185.0961
				159.0815	C ₁₁ H ₁₁ O(15)	-6.5	159.0804
				133.0657	C ₉ H ₉ O(9)	-6.5	133.0648
310-B			9.0	310.1820	C ₂₀ H ₂₄ NO ₂ (45)	-6.1	310.1802
				292.1714	C ₂₀ H ₂₂ NO(86)	-6.1	292.1696
				266.1556	C ₁₈ H ₂₀ NO(15)	-6.3	266.1539
				261.1290	C ₁₉ H ₁₇ O(100)	-6.3	261.1274
				233.0976	C ₁₇ H ₁₃ O(45)	-6.4	233.0961
				207.0818	C ₁₅ H ₁₁ O(21)	-6.5	207.0804
				169.1023	C ₁₃ H ₁₃ (53)	-6.5	169.1012
				141.0708	C ₁₁ H ₉ (20)	-6.5	141.0699
				123.0449	C ₇ H ₇ O ₂ (14)	-6.5	123.0441
				89.0603	C ₄ H ₉ O ₂ (9)	-6.2	89.0597
310-C			9.4	310.1820	C ₂₀ H ₂₄ NO ₂ (99)	-6.1	310.1802
				282.1506	C ₁₈ H ₂₀ NO ₂ (100)	-6.2	282.1489
				279.1397	C ₁₉ H ₁₉ O ₂ (23)	-6.2	279.1380
				251.1082	C ₁₇ H ₁₅ O ₂ (39)	-6.3	251.1067
				185.0973	C ₁₃ H ₁₃ O(80)	-6.5	185.0961
				159.0815	C ₁₁ H ₁₁ O(21)	-6.5	159.0804
				145.0657	C ₁₀ H ₉ O(8)	-6.6	145.0648
				133.0657	C ₉ H ₉ O(17)	-6.5	133.0648
				107.0498	C ₇ H ₇ O(10)	-6.4	107.0491
310-D			10.1	310.1820	C ₂₀ H ₂₄ NO ₂ (96)	-6.1	310.1802
				282.1506	C ₁₈ H ₂₀ NO ₂ (100)	-6.2	282.1489
				251.1082	C ₁₇ H ₁₅ O ₂ (27)	-6.3	251.1067
				233.0976	C ₁₇ H ₁₃ O(8)	-6.3	233.0961
				201.0923	C ₁₃ H ₁₃ O ₂ (11)	-6.4	201.0910
				169.1023	C ₁₃ H ₁₃ (65)	-6.5	169.1012
				143.0865	C ₁₁ H ₁₁ (14)	-6.5	143.0855

				141.0708	C ₁₁ H ₉ (16)	-6.5	141.0699
310-E			10.6	310.1821	C ₂₀ H ₂₄ NO ₂ (50)	-6.1	310.1802
				292.1714	C ₂₀ H ₂₂ NO(100)	-6.1	292.1696
				280.1349	C ₁₈ H ₁₈ NO ₂ (26)	-6.2	280.1332
				233.0976	C ₁₇ H ₁₃ O(24)	-6.5	233.0961
				101.0604	C ₅ H ₉ O ₂ (14)	-6.5	101.0597
310-F			11.3	310.1820	C ₂₀ H ₂₄ NO ₂ (4)	-6.1	310.1802
				250.1606	C ₁₈ H ₂₀ N(100)	-6.2	250.1590
				217.1026	C ₁₇ H ₁₃ (23)	-6.4	217.1012
				191.0868	C ₁₅ H ₁₁ (42)	-6.5	191.0855
326-A	326.1757	C ₂₀ H ₂₄ NO ₃	7.2	326.1770	C ₂₀ H ₂₄ NO ₃ (100)	-6.0	326.1751
				308.1664	C ₂₀ H ₂₂ NO ₂ (42)	-6.2	308.1645
				298.1456	C ₁₈ H ₂₀ NO ₃ (23)	-6.0	298.1438
				185.0973	C ₁₃ H ₁₃ O(8)	-6.5	185.0961
				89.0603	C ₄ H ₉ O ₂ (2)	-6.2	89.05971
326-B			8.4	326.1770	C ₂₀ H ₂₄ NO ₃ (99)	-6.0	326.1751
				308.1664	C ₂₀ H ₂₂ NO ₂ (37)	-6.0	308.1645
				298.1456	C ₁₈ H ₂₀ NO ₃ (100)	-6.0	298.1438
				267.1032	C ₂₀ H ₁₃ N(23)	3.8	267.1043
				191.0867	C ₁₅ H ₁₁ (23)	-6.4	191.0855
				185.0973	C ₁₃ H ₁₃ O(62)	-6.4	185.0961
326-C			9.3	326.1770	C ₂₀ H ₂₄ NO ₃ (21)	-5.9	326.1751
				308.1664	C ₂₀ H ₂₂ NO ₂ (55)	-6.0	308.1645
				298.1456	C ₁₈ H ₂₀ NO ₃ (59)	-6.0	298.1438
				280.1349	C ₁₈ H ₁₈ NO ₂ (100)	-6.1	280.1332
				267.1032	C ₂₀ H ₁₃ N(25)	3.9	267.1043
				249.0926	C ₁₇ H ₁₃ O ₂ (86)	-6.2	249.0910
342-A	342.1707	C ₂₀ H ₂₄ NO ₄	6.5	342.1720	C ₂₀ H ₂₄ NO ₄ (75)	-5.9	342.1700
				324.1613	C ₂₀ H ₂₂ NO ₃ (54)	-5.9	324.1594
				275.1084	C ₁₉ H ₁₅ O ₂ (53)	-6.2	275.1067
				247.0769	C ₁₇ H ₁₁ O ₂ (100)	-6.3	247.0754
				183.0816	C ₁₃ H ₁₁ O(47)	-6.4	183.0804
342-B			7.1	342.1720	C ₂₀ H ₂₄ NO ₄ (100)	-5.9	342.1700
				324.1613	C ₂₀ H ₂₂ NO ₃ (47)	-5.9	324.1594
				306.1507	C ₂₀ H ₂₀ NO ₂ (37)	-6.0	306.1489
				216.1397	C ₁₄ H ₁₈ NO(51)	-6.3	216.1383
				185.0973	C ₁₃ H ₁₃ O(57)	-6.4	185.0961
				167.0866	C ₁₃ H ₁₁ (46)	-6.5	167.0855
				157.0658	C ₁₁ H ₉ O(50)	-6.5	157.0648
342-C			7.5	342.1720	C ₂₀ H ₂₄ NO ₄ (100)	-5.8	342.1700
				324.1614	C ₂₀ H ₂₂ NO ₃ (36)	-6.0	324.1594
				296.1663	C ₁₉ H ₂₂ NO ₂ (48)	-6.1	296.1645
				240.1398	C ₁₆ H ₁₈ NO(16)	-6.3	240.1383
				133.0868	C ₆ H ₁₃ O ₃ (22)	-6.4	133.0859
				89.0603	C ₄ H ₉ O ₂ (17)	-6.1	89.0597
342-D			8.5	342.1720	C ₂₀ H ₂₄ NO ₄ (100)	-5.8	342.1700

				324.1614	C ₂₀ H ₂₂ NO ₃ (30)	-6.0	324.1594
				296.1663	C ₁₉ H ₂₂ NO ₂ (22)	-6.1	296.1645
				240.1398	C ₁₆ H ₁₈ NO(16)	-6.3	240.1383
				212.1447	C ₁₅ H ₁₈ N(8)	-6.4	212.1434
292-A	292.1701	C ₂₀ H ₂₂ NO	9.4	292.1714	C ₂₀ H ₂₂ NO(31)	-6.3	292.1696
				250.1606	C ₁₈ H ₂₀ N(14)	-6.3	250.1590
				217.1026	C ₁₇ H ₁₃ (94)	-6.3	217.1012
				191.0868	C ₁₅ H ₁₁ (100)	-6.5	191.0855
282-B			9.9	292.1714	C ₂₀ H ₂₂ NO(100)	-6.1	292.1696
				250.1606	C ₁₈ H ₂₀ N(11)	-6.3	250.1590
				219.1182	C ₁₇ H ₁₅ (12)	-6.1	219.1168
				191.0867	C ₁₅ H ₁₁ (13)	-6.3	191.0855
282-C			10.7	292.1714	C ₂₀ H ₂₂ NO(67)	-6.1	292.1696
				250.1606	C ₁₈ H ₂₀ N(58)	-6.2	250.1590
				243.1183	C ₁₉ H ₁₅ (23)	-6.2	243.1168
				219.1182	C ₁₇ H ₁₅ (100)	-6.3	219.1168
				191.0867	C ₁₅ H ₁₁ (22)	-6.4	191.0855
282-D			11.3	292.1713	C ₂₀ H ₂₂ NO(27)	-6.0	292.1696
				243.1183	C ₁₉ H ₁₅ (20)	-6.2	243.1168
				217.1026	C ₁₇ H ₁₃ (31)	-6.3	217.1012
				191.0868	C ₁₅ H ₁₁ (100)	-6.4	191.0855
282-E			11.6	292.1714	C ₂₀ H ₂₂ NO(36)	-6.3	292.1696
				246.1292	C ₁₈ H ₁₆ N(66)	-6.0	246.1277
				183.0816	C ₁₃ H ₁₁ O(100)	-6.4	183.0804
308-A	308.1651	C ₂₀ H ₂₂ NO ₂	7.5	308.1664	C ₂₀ H ₂₂ NO ₂ (3)	-6.2	308.1645
				233.0976	C ₁₇ H ₁₃ O(100)	-6.3	233.0961
				215.0869	C ₁₇ H ₁₁ (28)	-6.4	215.0855
				207.0818	C ₁₅ H ₁₁ O(16)	-6.4	207.0804
				203.0868	C ₁₆ H ₁₁ (9)	-6.4	203.0855
308-B			8.4	308.1664	C ₂₀ H ₂₂ NO ₂ (86)	-6.0	308.1645
				265.1478	C ₁₈ H ₁₉ NO(25)	-6.2	265.1461
				233.0976	C ₁₇ H ₁₃ O(91)	-6.3	233.0961
				215.0869	C ₁₇ H ₁₁ (18)	-6.3	215.0855
				207.0818	C ₁₅ H ₁₁ O(100)	-6.4	207.0804
				178.0789	C ₁₄ H ₁₀ (24)	-6.4	178.0777
308-C			9.6	308.1663	C ₂₀ H ₂₂ NO ₂ (14)	-5.9	308.1645
				280.1349	C ₁₈ H ₁₈ NO ₂ (100)	-6.1	280.1332
284-A	284.1650	C ₁₈ H ₂₂ NO	8.0	284.1662	C ₁₈ H ₂₂ NO ₂ (100)	-6.1	284.1645
				266.1557	C ₁₈ H ₂₀ NO (3)	-6.1	266.1539
				253.1239	C ₁₇ H ₁₇ O ₂ (6)	-6.3	253.1223
				225.1288	C ₁₆ H ₁₇ O (3)	-6.4	225.1274
				207.1182	C ₁₆ H ₁₅ (4)	-6.4	207.1168
284-B			9.1	284.1664	C ₁₈ H ₂₂ NO ₂ (100)	-6.5	284.1645
				89.0603	C ₄ H ₉ O ₂ (5)	-6.2	89.0597
284-C			9.5	284.1662	C ₁₈ H ₂₂ NO ₂ (100)	-6.1	284.1645
				256.1348	C ₁₆ H ₁₈ NO ₂ (15)	-6.2	256.1332

				225.0924	C ₁₅ H ₁₃ O ₂ (7)	-6.3	225.0910
234	234.1492	C ₁₄ H ₂₀ NO ₂	5.4	216.1396	C ₁₄ H ₁₈ NO(21)	-6.0	216.1383
				185.0972	C ₁₃ H ₁₃ O(53)	-6.1	185.0961
				167.0866	C ₁₃ H ₁₁ (100)	-6.2	167.0855
				157.0658	C ₁₁ H ₉ O(27)	-6.1	157.0648
				141.0707	C ₁₁ H ₉ (14)	-6.1	141.0699
				129.0707	C ₁₀ H ₉ (26)	-6.1	129.0699
258	258.1493	C ₁₆ H ₂₀ NO ₂	7.3	258.1505	C ₁₆ H ₂₀ NO ₂ (100)	-6.2	258.1489
				240.1398	C ₁₆ H ₁₈ NO(4)	-6.3	240.1383
				212.1447	C ₁₅ H ₁₈ N(4)	-6.4	212.1434

Table S4.3.2: Ions in common detected in CID experiments for m/z 310 transformation products

m/z	Ion formula	310					
		A	B	C	D	E	F
310.1820	C ₂₀ H ₂₄ NO ₂ ⁺	+	+	+	+	+	+
292.1714	C ₂₀ H ₂₂ NO ⁺	+	+			+	
282.1506	C ₁₈ H ₂₀ NO ₂ ⁺			+	+		
279.1397	C ₁₉ H ₁₉ O ₂ ⁺	+		+			
261.1290	C ₁₉ H ₁₇ O ₃ ⁺	+	+				
251.1082	C ₁₇ H ₁₅ O ₂ ⁺			+	+		
233.0976	C ₁₇ H ₁₃ O ₂ ⁺		+		+	+	
217.1026	C ₁₇ H ₁₃ ⁺	+					+
191.0867	C ₁₅ H ₁₁ ⁺	+					+
185.0973	C ₁₃ H ₁₃ O ⁺	+		+			
169.1023	C ₁₃ H ₁₃ ⁺		+		+		
159.0815	C ₁₁ H ₁₁ O ⁺	+		+			
133.0657	C ₉ H ₉ ⁺	+		+			

Table S4.3.3: Maprotiline TPs observed in river water in the dark and under irradiation; (+) observed, (-) non observed

TPs	Dark	Photolysis
294-A	-	+
294-B	-	+
294-C	-	+
294-D	+	+
294-E	-	+
310-A	-	-
310-B	-	-
310-C	-	-
310-D	-	-
310-E	-	-

310-E	-	-
326-A	-	-
326-B	-	-
326-C	-	-
342-A	-	-
342-B	-	-
342-C	-	-
342-D	-	-
292-A	-	-
292-B	-	+
292-C	-	+
292-D	-	+
310-E	-	-
308-A	-	-
308-B	-	-
308-C	-	-
324	-	-
284-A	-	+
284-B	-	+
284-C	+	+
234	-	-
258	-	-

Table S4.3.4: Investigation of maprotiline and its TPs in digitally archived wastewater and river water samples. Results are expressed as percentage of frequency of appearance (FoA). Substances that were not detected are marked as “N.D.”.

Compounds	FoA treated waste water (n=58)	FoA river water (n=72)
Maprotiline	65.5	1.4
294-A	15.5	N.D.
294-B	6.9	N.D.
294-C	17.2	N.D.
294-D	N.D.	N.D.
294-E	N.D.	N.D.
310-A/B/C/D/E/F	N.D.	N.D.
326-A	N.D.	N.D.
326-B	3.4	N.D.
326-C	5.2	2.8
342-A	13.8	N.D.
342-B	5.2	N.D.
342-C	12.1	N.D.
342-D	N.D.	N.D.
292-A	N.D.	N.D.
292-B	1.7	N.D.

292-C	1.7	N.D.
292-D	N.D.	N.D.
292-E	N.D.	N.D.
308-A	1.7	N.D.
308-B	56.9	2.8
308-C	19.0	N.D.
324	1.7	N.D.
284-A	N.D.	N.D.
284-B	N.D.	N.D.
284-C	1.7	N.D.
234	1.7	1.4
258	N.D.	N.D.

Table S4.3.5: Description of the river water and wastewater samples used in the retrospective analysis

Name (Format: Name, Region, Country, Sampling date (DD/MM/YYYY), Project, Unique ID)	Country	Matrix	Date of sampling	Latitude	Longitude
Procedural Blank JDS4.Ulm_Germany_29.06.2019_JDS4_40703	Germany	River water	6/29/2019	48.424005	10.026232
Procedural blank surface water Dni- ester_Chisinau_Moldova_26.05.2019_Dniester Monitoring_38612	Moldova	River water	5/26/2019	47.03	28.83
Blank for water samples_Vesele_Ukraine_24.09.2018_Siverskyi Donets Monitoring_31438	Ukraine	River water	9/24/2018	47.01	34.91
Procedural Blank wastewater from Ger- many_Gottingen_Germany_03.05.2018_ITN ANSWER_28513	Germany	Wastewater	5/3/2018	51.53	9.92
Effluent wastewater Field Blank_Amstetten_Austria_28.08.2017 _SOLUTIONS & ITN ANSWER_26146	Austria	Wastewater	8/28/2017	48.11	14.89
River water 51 Vilkova - Chilia arm Kilia arm_Vylkove_Ukraine_29.06.2019_JDS4_40819	Ukraine	River water	6/29/2019	45.39702	29.582076
River water 50 Reni_Reni_Ukraine_30.06.2019_JDS4_40817	Ukraine	River water	6/30/2019	45.460721	28.252591
River water 49 Giurgiulesti_Galati_Romania_ 30.06.2019_JDS4_40815	Romania	River water	6/30/2019	45.471361	28.196357
River water 48 Chiciu - Silis- tra_Silistra_Bulgaria_01.07.2019_JDS4_40813	Bulgaria	River water	7/1/2019	44.134297	27.057112
River water 47 Downstream Ruse - Giurgiu Marten_Ruse_Bulgaria_02.07.2019_JDS4_40811	Bulgaria	River water	7/2/2019	43.91083	26.06696

River water 46 Russenski Lom mouth_Ruse_Bulgaria_01.07.2019_JDS4_40809	Bulgaria	River water	7/1/2019	43.835077	25.93106
River water 45 Jantra mouth_Svistov_Bulgaria_03.07.2019_JDS4_40806	Bulgaria	River water	7/3/2019	43.627561	25.56477
River water 44 Iskar mouth_Pleven_Bulgaria_03.07.2019_JDS4_40804	Bulgaria	River water	7/3/2019	43.702484	24.45541
River water 43 Pristol - Novo Selo Har- bour_Vidin_Bulgaria_04.07.2019_JDS4_40802	Bulgaria	River water	7/4/2019	44.16883	22.77937
River water 42 Timok mouth_Vidin_Bulgaria_05.07.2019_JDS4_40800	Bulgaria	River water	7/5/2019	44.213244	22.67083
River water 41 Upstream Timok Rudujevac - Gruia_Zajecar_Serbia_05.07.2019_JDS4_40798	Serbia	River water	7/5/2019	44.261977	22.680131
River water 40 Banatska Palanka - Bazias_Pozarevac_Serbia_06.07.2019_JDS4_40796	Serbia	River water	7/6/2019	44.804779	21.380162
River water 39 Velika Morava mouth_Pozarevac_Serbia_05.07.2019_JDS4_40794	Serbia	River water	7/5/2019	44.7114	21.035472
River water 38 Var- varin_Krusevac_Serbia_06.07.2019_JDS4_40792	Serbia	River water	7/6/2019	43.739599	21.368847
River water 37 Downstream Pancevo_Pancevo_Serbia_07.07.2019_JDS4_41933	Serbia	River water	7/7/2019	44.812138	20.644889
River water 36 Jamena Sava mouth_Belgrade_Serbia_08.07.2019_JDS4_40790	Serbia	River water	7/8/2019	44.795293	20.420803
River water 35 Jamena.Sremska Mitrovica_Serbia_10.07.2019_JDS4_40788	Serbia	River water	7/10/2019	44.877767	19.083919
River water 34 Jesenice na Dolen- jskem_Zapresic_Croatia_10.07.2019_JDS4_40773	Croatia	River water	7/10/2019	45.86157	15.692091
River water 33 Tisza mouth_Zrenjanin_Serbia_09.07.2019_JDS4_40770	Serbia	River water	7/9/2019	45.145604	20.282187
River water 32 Tiszasziget - Martonos_Szeged_ Hungary_10.07.2019_JDS4_40768	Hungary	River water	7/10/2019	46.186105	20.106786
River water 31 Ilok - Backa Palanka_Ilok_Croatia_08.07.2019_JDS4_40766	Croatia	River water	7/8/2019	45.233948	19.380969
River water 30 Drava 5 km upstream Danube conflu- ence_Mohacs_Hungary_10.07.2019_JDS4_40764	Hungary	River water	7/10/2019	45.55221	18.86517
River water 29 Hercegszanto - Batina - Bez- dan_Mohacs_Hungary_08.07.2019_JDS4_40762	Hungary	River water	7/8/2019	45.914079	18.801928
River water 28 Baja_Baja_Hungary_09.07.2019_JDS4_40760	Hungary	River water	7/9/2019	46.201182	18.925556
River water 27 Paks_Paks_Hungary_08.07.2019_JDS4_40758	Hungary River	water	7/8/2019	46.633827	18.877346
River water 26 Dunafoldvar_Dunafoldvar_ Hungary_08.07.2019_JDS4_40756	Hungary	River water	7/8/2019	46.815543	18.924702

River water 25 Tass_Dunaujvaros_ Hungary_07.07.2019_JDS4_40754	Hungary	River water	7/7/2019	46.033748	18.977803
River water 24 Budapest downstream - M0 bridge_Budapest_ Hungary_07.07.2019_JDS4_40752	Hungary	River water	7/7/2019	47.386701	19.010416
River water 23 Budapest upstream - Megyeri Bridge_Budapest_ Hungary_06.07.2019_JDS4_40750	Hungary	River water	7/6/2019	47.606306	19.095476
River water 22 Szob_Esztergom_Hungary_06.07.2019_JDS4_40748	Hungary	River water	7/6/2019	47.815262	18.861795
River water 21 Salka_Sturovo_Slovakia_05.07.2019_JDS4_40746	Slovakia	River water	7/5/2019	47.88596	18.76256
River water 20 Ka-menica_Sturovo_Slovakia_05.07.2019_JDS4_40743	Slovakia	River water	7/5/2019	47.827052	18.72107
River water 19 Ko-marno_Komarno_Slovakia_04.07.2019_JDS4_40741	Slovakia	River water	7/4/2019	47.76091	18.14233
River water 18 Gonyu_Komarno_Slovakia_04.07.2019_JDS4_40739	Slovakia	River water	7/4/2019	47.746329	17.853306
River water 17 Venek_Komarno_Slovakia_04.07.2019_JDS4_40737	Slovakia	River water	7/4/2019	47.745198	17.807639
River water 16 Medvedov Medve_Vel'ky Meder_Slovakia_03.07.2019_JDS4_40735	Slovakia	River water	7/3/2019	47.794793	17.659407
River water 15 Cunovo, Gabcikovo re-sevoir_Samorin_Slovakia_03.07.2019_JDS4_40733	Slovakia	River water	7/3/2019	48.035975	17.23098
River water 14 Bratislava_Bratislava_ Slovakia_05.07.2019_JDS4_40731	Slovakia	River water	7/5/2019	48.13948	17.104089
River water 13 Devin_Stupava_Slovakia_05.07.2019_JDS4_40729	Slovakia	River water	7/5/2019	48.191051	16.976016
River water 12 Lanzhot_Breclav_Czech Republic_04.07.2019_JDS4_40727	Czech Republic	River water	7/4/2019	48.687035	16.988535
River water 11 Pohansko_Breclav_Czech Republic_04.07.2019_JDS4_40725	Czech Republic	River water	7/4/2019	48.723556	16.884981
River water 10 Hainburg, upstream Morava_Vienna_Austria_03.07.2019_JDS4_40722	Austria	River water	7/3/2019	48.151363	16.943437
River water 09 Klosterneuburg_Vienna_ Austria_03.07.2019_JDS4_40720	Austria	River water	7/3/2019	48.329499	16.332155
River water 08 Ober-loiben_Vienna_Austria_02.07.2019_JDS4_40718	Austria	River water	7/2/2019	48.385326	15.533342
River water 07 Engha-gen_Linz_Austria_02.07.2019_JDS4_40716	Austria	River water	7/2/2019	48.241034	14.513545
River water 06 Jochen-stein_Passau_Germany_01.07.2019_JDS4_40714	Germany	River water	7/1/2019	48.5216425	13.7038264
River water 05 Inn at Passau-Ingling below power station _Passau_Germany_01.07.2019_JDS4_40712	Germany	River water	7/1/2019	48.557238	13.436065

River water 04 Niederalteich - Muh-lau_Deggendorf_Germany_30.06.2019_JDS4_40710	Germany	River water	6/30/2019	48.772996	13.009893
River water 03 Kelheim_Kelheim_Germany_30.06.2019_JDS4_40708	Germany	River water	6/30/2019	48.916176	11.866875
River water 02 Bittenbrunn 700m below power station_Oberhausen_Germany_29.06.2019_JDS4_40706	Germany	River water	6/29/2019	48.7347	11.144794
River water 01 Boefinger Halde_Ulm_Germany_29.06.2019_JDS4_40704	Germany	River water	6/29/2019	48.424005	10.026232
Station 13 Hradenytsi_Odesa_Ukraine_25.05.2019_Dniester Monitoring_38632	Ukraine	River water	5/25/2019	46.60638889	29.98361111
Station 12 Ustia_Chisinau_Moldova_26.05.2019_Dniester Monitoring_38631	Moldova	River water	5/26/2019	47.25222222	29.13527778
Station 11 Bulboaca_Chisinau_Moldova_25.05.2019_Dniester Monitoring_38629	Moldova	River water	5/25/2019	46.89055556	29.30333333
Station 10 Vasyliv_Chernivtsi_Ukraine_26.05.2019_Dniester Monitoring_38628	Ukraine	River water	5/26/2019	48.62138889	25.85777778
Station 09 Mohyliv-Podilskyi_Mohyliv-Podil's'kyi_Ukraine_26.05.2019_Dniester Monitoring_38627	Ukraine	River water	5/26/2019	48.45333333	27.7725
Station 08 Pochajevychi_Drohobych_Ukraine_28.05.2019_Dniester Monitoring_38626	Ukraine	River water	5/28/2019	49.36194444	23.57638889
Station 07 Poberezhzha_Ivano-Frankivs'k_Ukraine_28.05.2019_Dniester Monitoring_39312	Ukraine	River water	5/28/2019	49.03527778	24.80888889
Station 06 Shabo_Bilhorod-Dnistrovs'kyi_Ukraine_25.05.2019_Dniester Monitoring_38619	Ukraine	River water	5/25/2019	46.13444444	30.37111111
Station 05 Cioburciu_Ribnita_Moldova_25.05.2019_Dniester Monitoring_38617	Moldova	River water	5/25/2019	46.60027778	29.72138889
Station 04 Rezina_Ribnita_Moldova_26.05.2019_Dniester Monitoring_38616	Moldova	River water	5/26/2019	47.74388889	28.97694444
Station 03 Soroca_Soroca_Moldova_26.05.2019_Dniester Monitoring_38615	Moldova	River water	5/26/2019	48.14083333	28.30388889
Station 02 Zalishchyky Park_Zalishchyky_Ukraine_27.05.2019_Dniester Monitoring_38614	Ukraine	River water	5/27/2019	48.63444444	25.73555556

Station 01 Vovche_Turka_Ukraine_28.05.2019_Dniester Monitoring_38613	Ukraine	River water	5/28/2019	49.205	22.91916667
Station Lysychansk (428 km)_Lysychans'k_Ukraine_25.09.2018_Siverskyi Donets Monitoring_31427	Ukraine	River water	9/25/2018	48.91665	38.453586
Bakhmutka river_Kostyantynivka_Ukraine_25.09.2018_Siverskyi Donets Monitoring_31426	Ukraine	River water	9/25/2018	48.559532	38.023995
Kryvyi Torets river at Karlivska dam_Druzhkivka_Ukraine_24.09.2018_Siverskyi Donets Monitoring_31425	Ukraine	River water	9/24/2018	48.602686	37.561002
Kazannyi Torets river at Raygorodok vil- lage_Slov'yanoserbs'k_Ukraine_25.09.2018_Siverskyi Donets Monitoring_31424	Ukraine	River water	9/25/2018	48.917078	37.733307
Station Raygorodska dam (522 km)_Borova_Ukraine_24.09.2018_Siverskyi Donets Monitoring_31422	Ukraine	River water	9/24/2018	49.341563	37.548651
Oskil river at Chervonyi Oskil village_Kharkiv_Ukraine_26.09.2018_Siverskyi Donets Monitoring_31420	Ukraine	River water	9/26/2018	49.170724	37.437593
Udy river at Eskhar village_Eskhar_Ukraine_26.09.2018_Siverskyi Donets Monitoring_31420	Ukraine	River water	9/26/2018	49.788775	36.594185
Station Ohurtsovo village (944 km)_Rubizhne_Ukraine_26.09.2018_Siverskyi Donets Monitoring_31419	Ukraine	River water	9/26/2018	50.176532	36.844251
SPEDEX effluent wastewater Amstet- ten_Amstetten_Austria_28.08.2017_SOLUTIONS & ITN ANSWER_24766	Austria	Wastewater	8/28/2017	48.108815	14.895335
SPEDEX effluent wastewater Brno_Brno_Czech Republic_29.08.2017_SOLUTIONS & ITN ANSWER_24764	Czech Republic	Wastewater	8/29/2017	49.130863	16.631645
SPEDEX effluent wastewater Augsburg_Augsburg_ Germany_30.08.2017_SOLUTIONS & ITN ANSWER_24768	Germany	Wastewater	8/30/2017	48.40873	10.8854748
SPEDEX effluent wastewater Varazdin_Varazdin_ Croatia_20.08.2017_SOLUTIONS & ITN ANSWER_24754	Croatia	Wastewater	8/20/2017	46.309679	16.395325
SPEDEX effluent wastewater Za- greb_Zagreb_Croatia_21.08.2017_SOLUTIONS & ITN ANSWER_24752	Croatia	Wastewater	8/21/2017	45.78972	16.087301

SPEDEX effluent wastewater Budapest_Budapest_ Hungary_24.08.2017_SOLUTIONS & ITN ANSWER_24758	Hungary	Wastewater	8/24/2017	47.4563852	19.071257
SPEDEX effluent wastewater Bucharest_Bucharest_ Romania_18.08.2017_SOLUTIONS & ITN ANSWER_24746	Romania	Wastewater	8/18/2017	44.39546	26.23222
SPEDEX effluent wastewater Cluj-Napoca_Cluj- Napoca_Romania_19.08.2017_SOLUTIONS & ITN ANSWER_24748	Romania	Wastewater	8/19/2017	46.79319	23.68284
SPEDEX effluent wastewater Ljubl- jana_Ljubljana_Slovenia_24.08.2017_SOLUTIONS & ITN ANSWER_24756	Slovenia	Wastewater	8/24/2017	46.070851	14.6208963
SPEDEX effluent wastewater Krsko_Krsko_Slovenia_31.08.2017_SOLUTIONS & ITN ANSWER_24760	Slovenia	Wastewater	8/31/2017	45.97	15.47
SPEDEX effluent wastewater Zilina_Sabac_Serbia_18.08.2017_SOLUTIONS & ITN ANSWER_24762	Serbia	Wastewater	8/18/2017	49.247315	18.645833
SPEDEX effluent wastewater Sabac_Sabac_Serbia_31.08.2017_SOLUTIONS & ITN ANSWER_24750	Serbia	Wastewater	8/31/2017	44.743972	19.726941
Effluent wastewater Brno_Brno_Czech Republic_29.08.2017_SOLUTIONS & ITN ANSWER_26136	Czech Republic	Wastewater	8/29/2017	49.130863	16.631645
Effluent wastewater Amstet- ten_Amstetten_Austria_28.08.2017_SOLUTIONS & ITN ANSWER_26138	Austria	Wastewater	8/28/2017	48.10882	14.89534
Effluent wastewater Varazdin_Varazdin_ Croatia_20.08.2017_SOLUTIONS & ITN ANSWER_26122	Croatia	Wastewater	8/20/2017	46.30968	16.39533
Effluent wastewater Za- greb_Zagreb_Croatia_21.08.2017_SOLUTIONS & ITN ANSWER_26124	Croatia	Wastewater	8/21/2017	45.78972	16.0873
Effluent wastewater Budapest_Budapest_ Hungary_24.08.2017_SOLUTIONS & ITN ANSWER_26128	Hungary	Wastewater	8/24/2017	47.45639	19.07126
Effluent wastewater Bucharest_Bucharest_ Romania_18.08.2017_SOLUTIONS & ITN ANSWER_26116	Romania	Wastewater	8/18/2017	44.39546	26.23222
Effluent wastewater Cluj-Napoca_Cluj- Napoca_Romania_19.08.2017_SOLUTIONS & ITN ANSWER_26126	Romania	Wastewater	8/19/2017	46.79319	23.68284

Effluent wastewater Ljubljana_Ljubljana_Slovenia_24.08.2017_SOLUTIONS & ITN ANSWER_26126	Slovenia	Wastewater	8/24/2017	46.07085	14.6209
Effluent wastewater Krsko_Krsko_Slovenia_31.08.2017_SOLUTIONS & ITN ANSWER_26132	Slovenia	Wastewater	8/31/2017	45.97	15.47
Effluent wastewater Zilina_Zilina_Slovakia_18.08.2017_SOLUTIONS & ITN ANSWER_26134	Slovakia	Wastewater	8/18/2017	49.24732	18.64583
Effluent wastewater Sabac_Sabac_Serbia_31.08.2017_SOLUTIONS & ITN ANSWER_26120	Serbia	Wastewater	8/31/2017	44.74397	19.72694
Effluent wastewater Augsburg_Augsburg_Germany_16.11.2017_SOLUTIONS & ITN ANSWER_26142	Germany	Wastewater	11/16/2017	48.40873	10.88547
Effluent wastewater *****_Stuttgart_Germany_03.05.2018_ITN ANSWER_28543	Germany	Wastewater	5/3/2018	Confidential	Confidential
Effluent wastewater *****_Herrenberg_Germany_03.05.2018_ITN ANSWER_28545	Germany	Wastewater	5/3/2018	Confidential	Confidential
Effluent wastewater *****_Neustadt_Germany_03.05.2018_ITN ANSWER_28541	Germany	Wastewater	5/3/2018	Confidential	Confidential
Effluent wastewater *****_Grevenbroich_Germany_03.05.2018_ITN ANSWER_28539	Germany	Wastewater	5/3/2018	Confidential	Confidential
Effluent wastewater *****_Amberg_Germany_03.05.2018_ITN ANSWER_28537	Germany	Wastewater	5/3/2018	Confidential	Confidential
Effluent wastewater *****_Berlin_Germany_03.05.2018_ITN ANSWER_28535	Germany	Wastewater	5/3/2018	Confidential	Confidential
Effluent wastewater *****_Wurzburg_Germany_03.05.2018_ITN ANSWER_28533	Germany	Wastewater	5/3/2018	Confidential	Confidential
Effluent wastewater *****_Hattingen_Germany_03.05.2018_ITN ANSWER_28531	Germany	Wastewater	5/3/2018	Confidential	Confidential
Effluent wastewater *****_Amberg_Germany_03.05.2018_ITN ANSWER_28529	Germany	Wastewater	5/3/2018	Confidential	Confidential
Effluent wastewater *****_Geldern_Germany_03.05.2018_ITN ANSWER_28527	Germany	Wastewater	5/3/2018	Confidential	Confidential

Effluent wastewater *****_Augsburg_Germany_03.05.2018_ITN ANSWER_28525	Germany	Wastewater	5/3/2018	Confidential	Confidential
Effluent wastewater *****_Landsberg_Germany_03.05.2018_ITN ANSWER_28523	Germany	Wastewater	5/3/2018	Confidential	Confidential
Effluent wastewater *****_Bergheim_Germany_03.05.2018_ITN ANSWER_28521	Germany	Wastewater	5/3/2018	Confidential	Confidential
Effluent wastewater *****_Erlangen_Germany_03.05.2018_ITN ANSWER_28519	Germany	Wastewater	5/3/2018	Confidential	Confidential
Effluent wastewater *****_Memmingen_ Germany_27.03.2018_ITN ANSWER_28517	Germany	Wastewater	3/27/2018	Confidential	Confidential
Effluent wastewater *****_Wedel_Germany_27.03.2018_ITN ANSWER_28515	Germany	Wastewater	3/27/2018	Confidential	Confidential
Effluent wastewater *****_Dortmund_ Germany_27.03.2018_ITN ANSWER_28592	Germany	Wastewater	3/27/2018	Confidential	Confidential
Effluent wastewater *****_Krefeld_Germany_27.03.2018_ITN ANSWER_28590	Germany	Wastewater	3/27/2018	Confidential	Confidential
Effluent wastewater *****_Sinsheim_Germany_27.03.2018_ITN ANSWER_28588	Germany	Wastewater	3/27/2018	Confidential	Confidential
Effluent wastewater *****_Berlin_Germany_27.03.2018_ITN ANSWER_28586	Germany	Wastewater	3/27/2018	Confidential	Confidential
Effluent wastewater *****_Jena_Germany_27.03.2018_ITN ANSWER_28584	Germany	Wastewater	3/27/2018	Confidential	Confidential
Effluent wastewater *****_Reichenbach_ Germany_27.03.2018_ITN ANSWER_28582	Germany	Wastewater	3/27/2018	Confidential	Confidential
Effluent wastewater *****_Markkleeberg_ Germany_27.03.2018_ITN ANSWER_28580	Germany	Wastewater	3/27/2018	Confidential	Confidential
Effluent wastewater *****_Chemnitz_Germany_27.03.2018_ITN ANSWER_28578	Germany	Wastewater	3/27/2018	Confidential	Confidential
Effluent wastewater *****_Dessau_Germany_27.03.2018_ITN ANSWER_28576	Germany	Wastewater	3/27/2018	Confidential	Confidential

Effluent wastewater *****_Osnabruck_ Germany_27.03.2018_ITN ANSWER_28574	Germany	Wastewater	3/27/2018	Confidential	Confidential
Effluent wastewater *****_Schwerin_Germany_27.03.2018_ITN ANSWER_28572	Germany	Wastewater	3/27/2018	Confidential	Confidential
Effluent wastewater *****_Marburg_Germany_27.03.2018_ITN ANSWER_28570	Germany	Wastewater	3/27/2018	Confidential	Confidential
Effluent wastewater *****_Bremen_Germany_27.03.2018_ITN ANSWER_28568	Germany	Wastewater	3/27/2018	Confidential	Confidential
Effluent wastewater *****_Traunreut_Germany_27.03.2018_ITN ANSWER_28566	Germany	Wastewater	3/27/2018	Confidential	Confidential
Effluent wastewater *****_Hockenheim_ Germany_27.03.2018_ITN ANSWER_28564	Germany	Wastewater	3/27/2018	Confidential	Confidential
Effluent wastewater *****_Frankfurt_Germany_27.03.2018_ITN ANSWER_28562	Germany	Wastewater	3/27/2018	Confidential	Confidential
Effluent wastewater *****_Neuruppin_Germany_27.03.2018_ITN ANSWER_28560	Germany	Wastewater	3/27/2018	Confidential	Confidential
Effluent wastewater *****_Kaiserslautern_ Germany_05.03.2018_ITN ANSWER_28673	Germany	Wastewater	3/5/2018	Confidential	Confidential

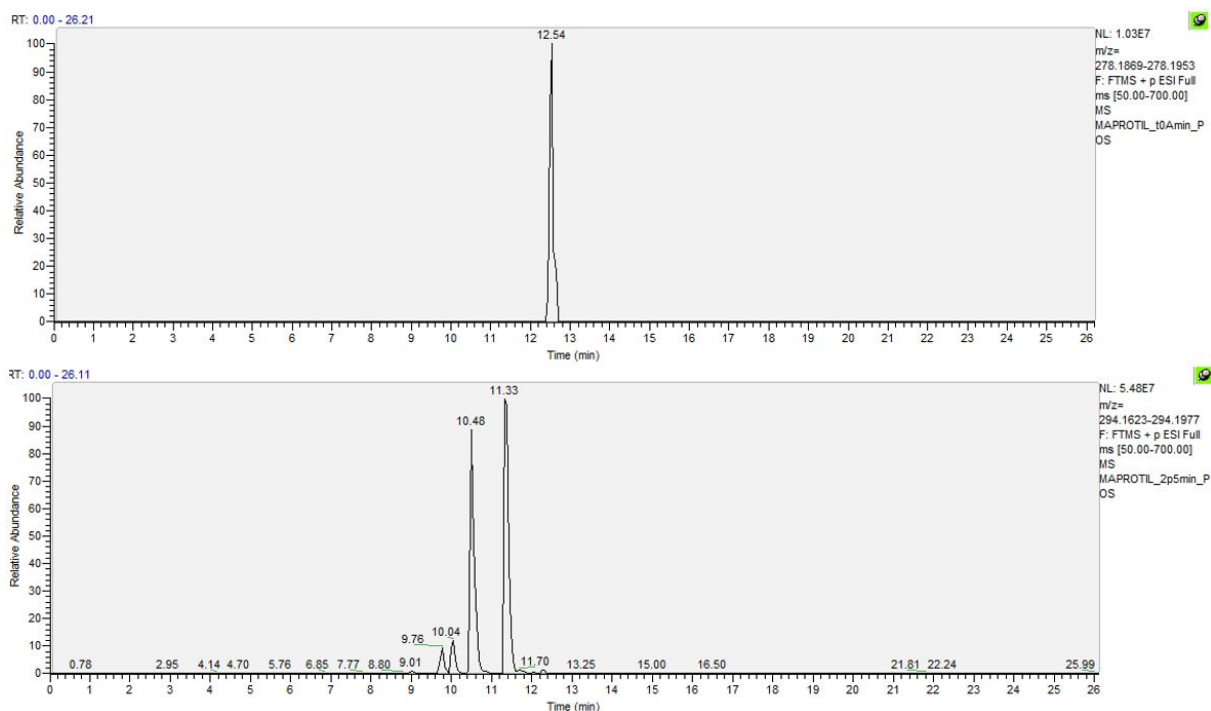


Figure S4.3.3: HPLC/HRMS chromatogram of maprotiline (top) and m/z 294 (bottom)

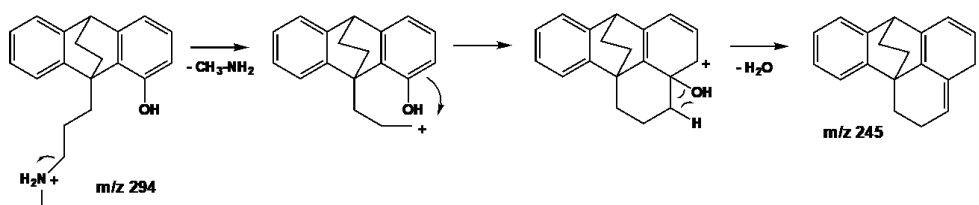


Figure S4.3.4: Specific CID mechanisms for the compound 294-D

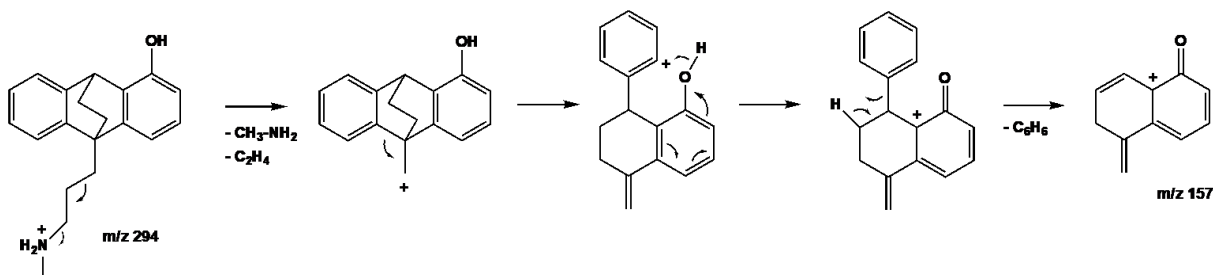


Figure S4.3.5: Specific CID mechanisms for the compound 294-E

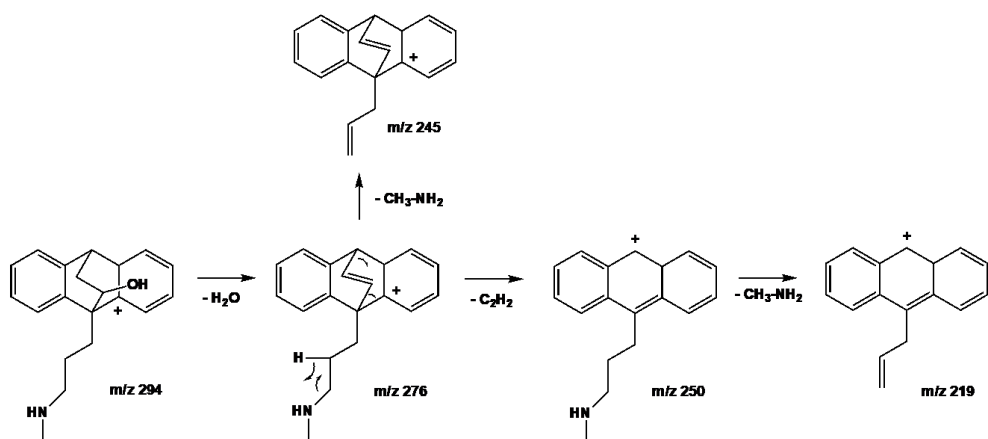


Figure S4.3.6: Specific CID mechanisms for the compound 294-B

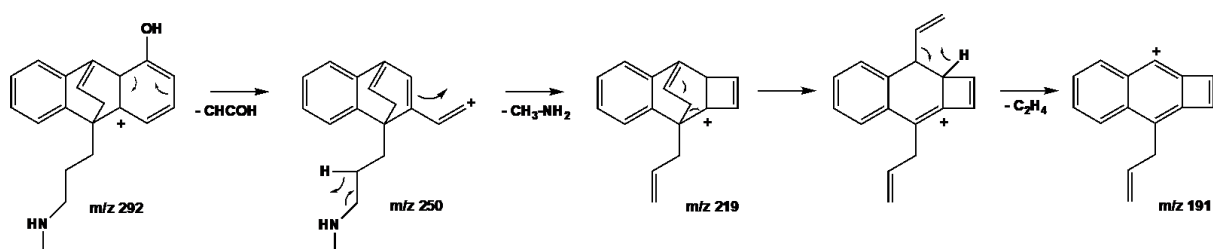


Figure S4.3.7: CID mechanisms for the compound 292-B issued from dehydrogenation of 294-E

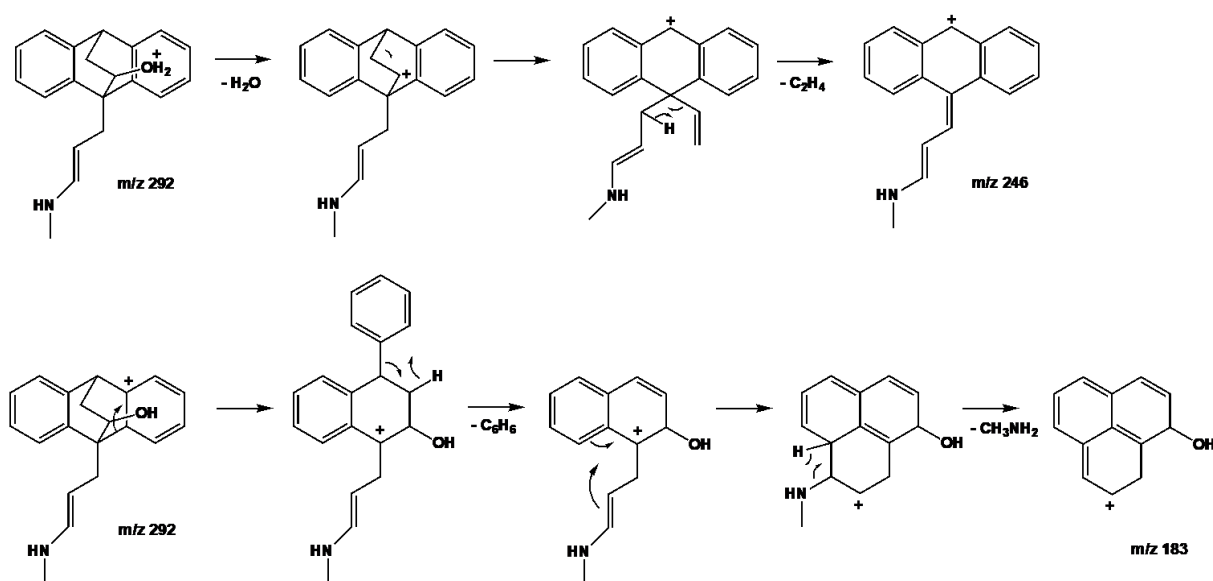


Figure S4.3.8: CID mechanism for the compound 292-E

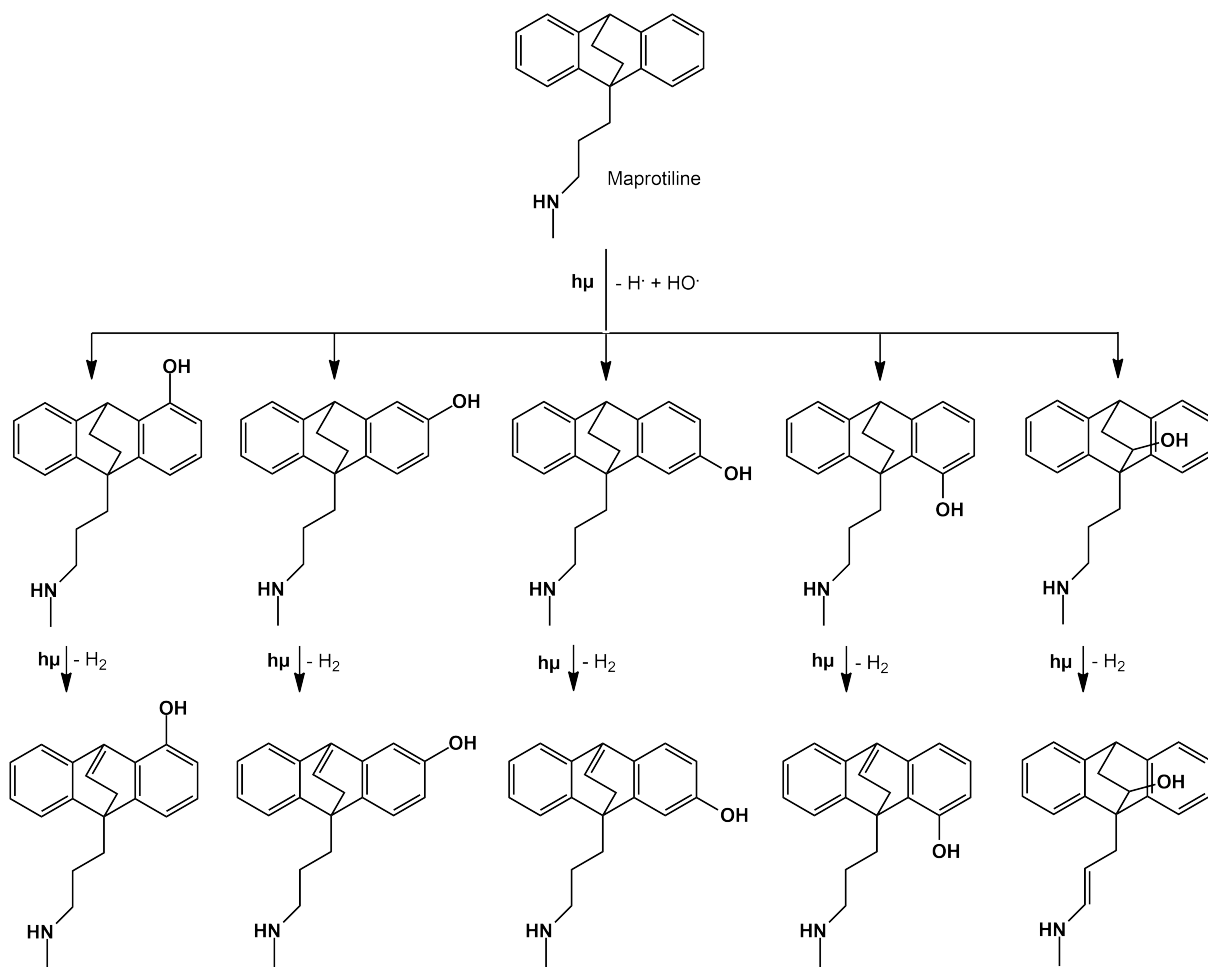


Figure S4.3.9: Dehydrogenation of species with MH^+ at m/z 294

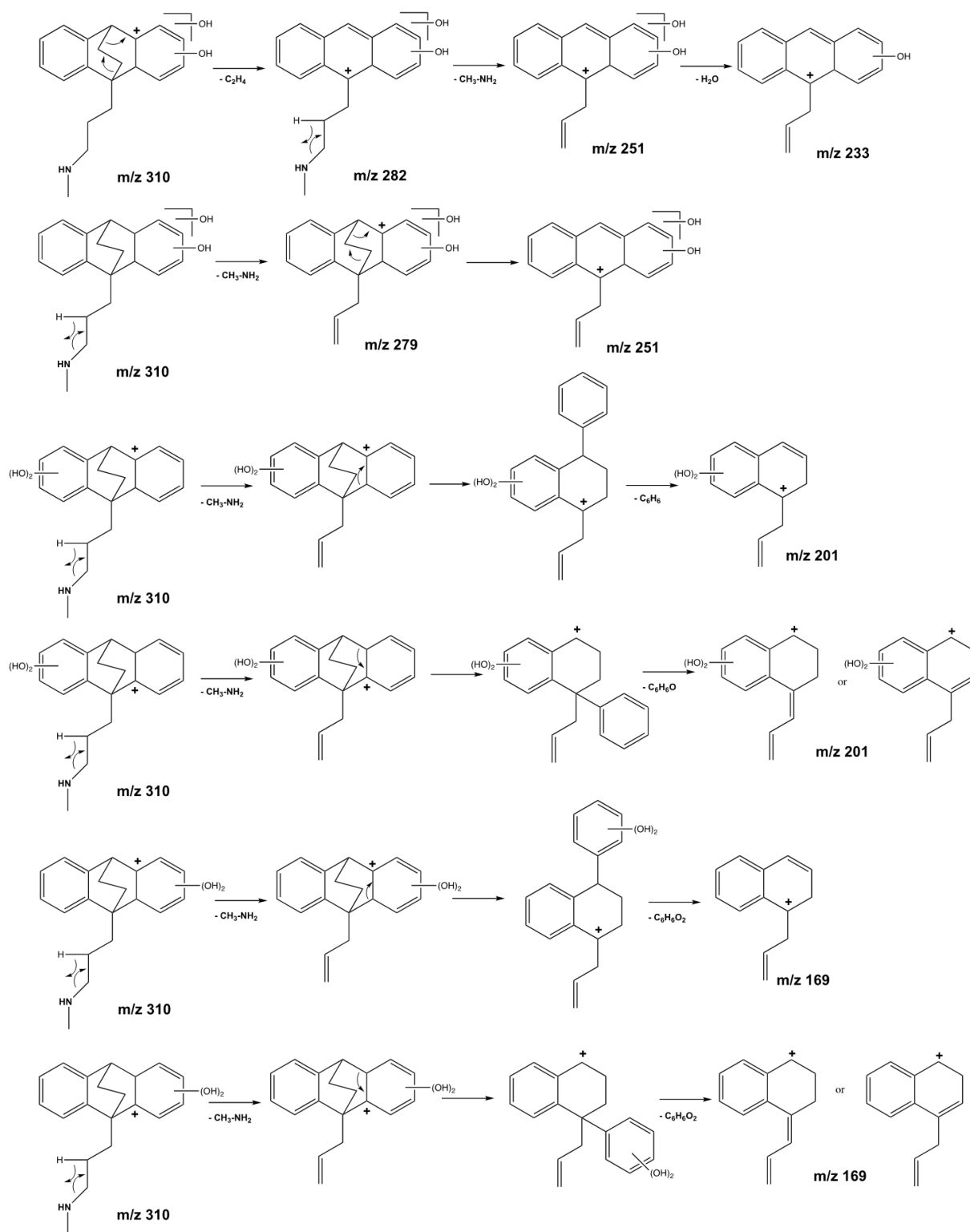


Figure S4.3.10: Suggested dissociation pathways for m/z 310 photoproducts

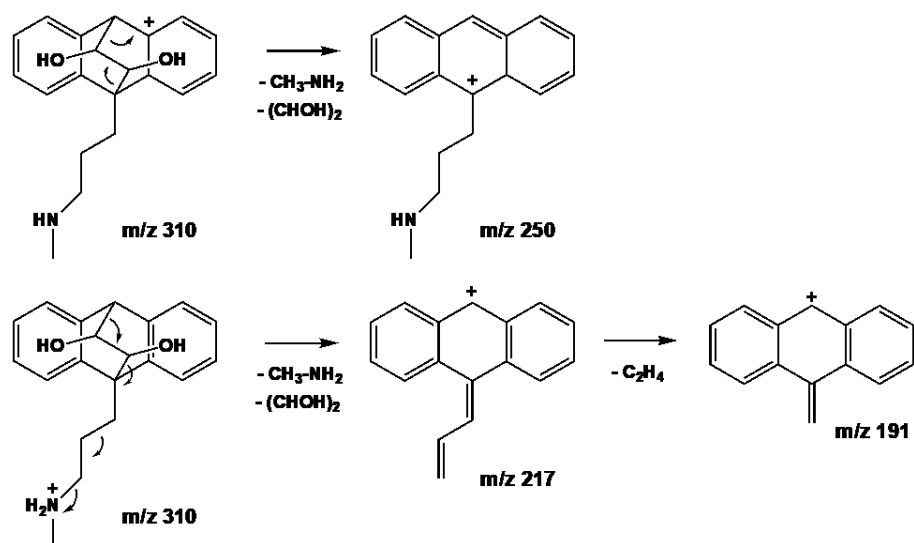


Figure S4.3.11: CID mechanisms for the compound 310-F

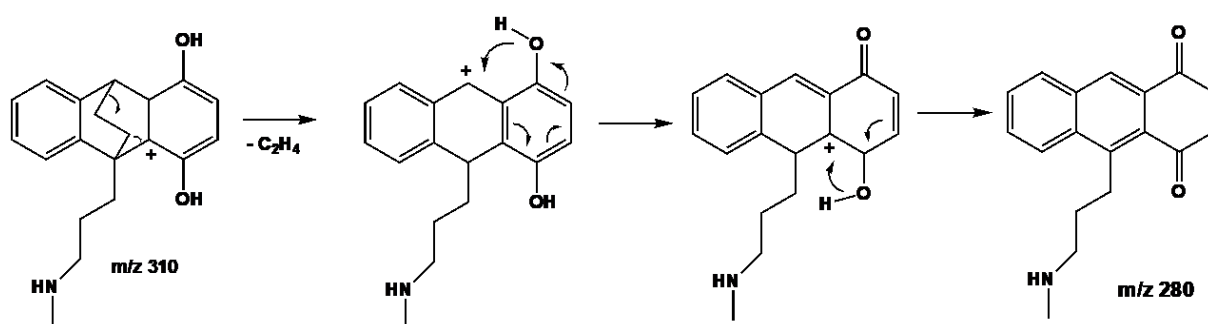
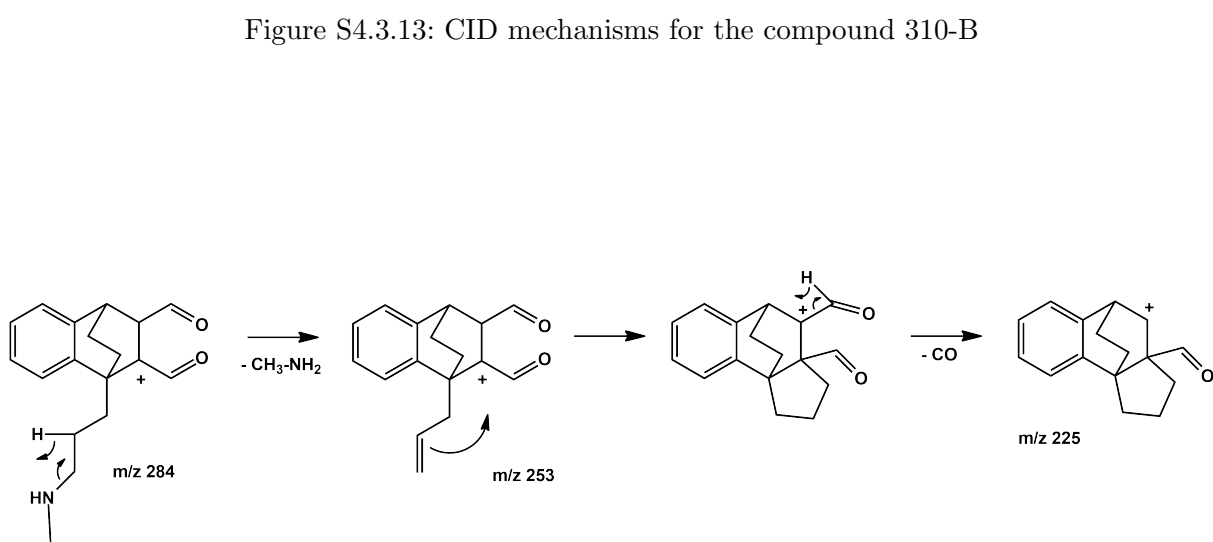
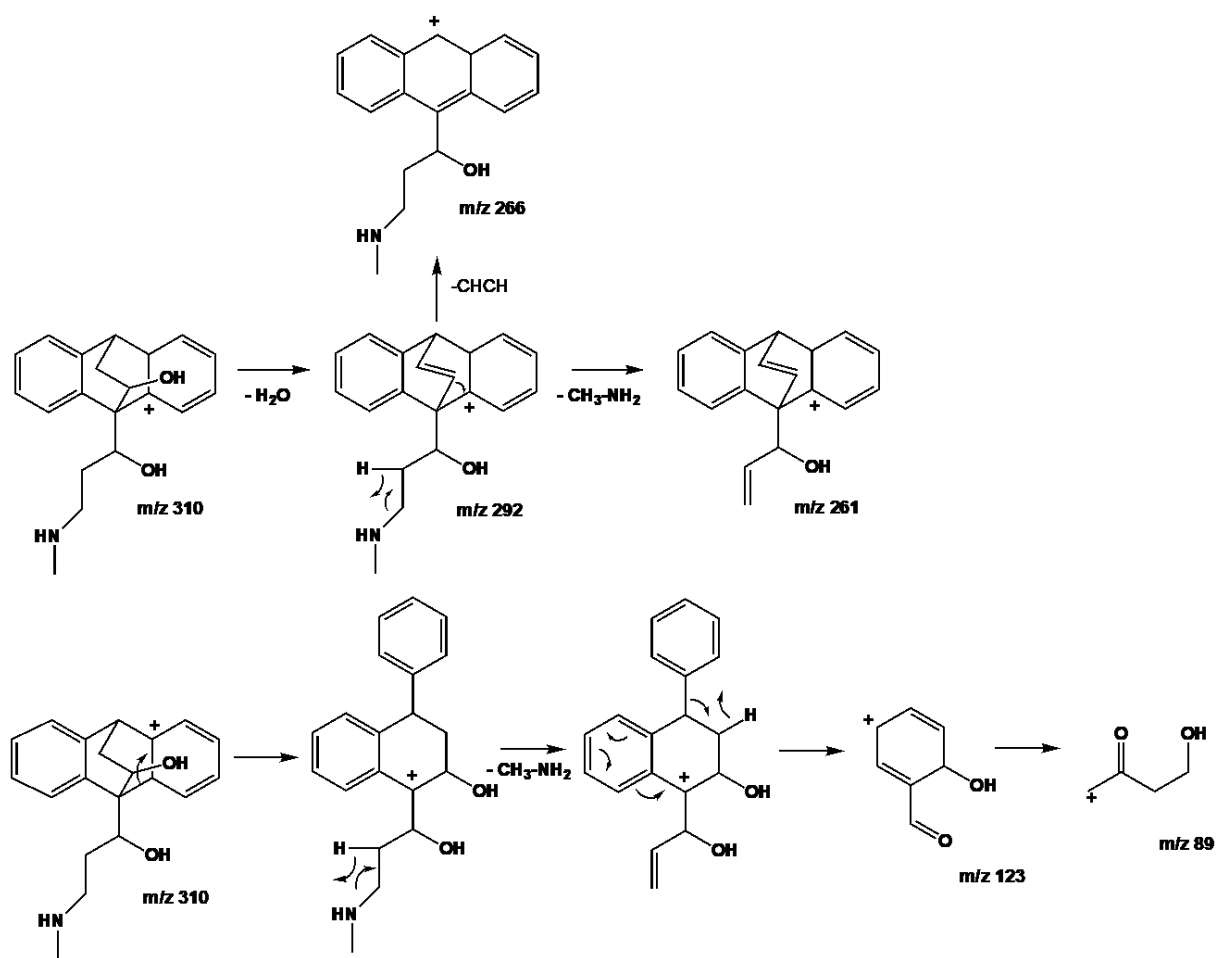


Figure S4.3.12: CID mechanisms for the compound 310-E



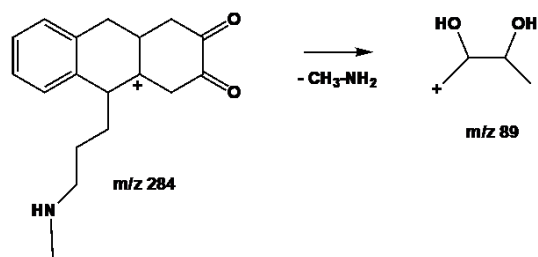


Figure S4.3.15: CID mechanisms for the compound 284-B

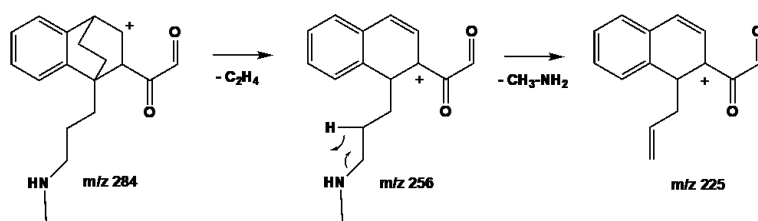


Figure S4.3.16: CID mechanisms for the compound 284-C

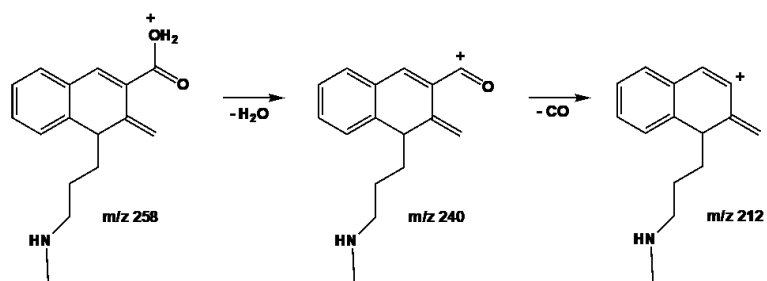


Figure S4.3.17: CID mechanisms for the compound 258

References

- [1] UNESCO. *World Water Assessment Programme (Paris)*. 2019. URL: <http://www.unesco.org/new/en/natural-sciences/environment/water/wwap/about/>.
- [2] *NORMAN Databases*. 2005. URL: <https://www.norman-network.net/?q=node/24>.
- [3] J Hollender, B van Bavel, V Dulio, E Farmen, K Furtmann, J Koschorreck, U Kunkel, M Krauss, J Munthe, M Schlabach, J Slobodnik, G Stroomberg, T Ternes, NS Thomaidis, A Togola, and V Tornero. “High resolution mass spectrometrybased non-target screening can support regulatory environmental monitoring and chemicals management.” In: *Environ Sci Eur* 31 (2019), p. 42. DOI: 10.1186/s12302-019-0225-x.
- [4] T Nawaz and S Sengupta. *Chapter 4 - Contaminants of Emerging Concern: Occurrence, Fate, and Remediation, Advances in Water Purification Techniques: Meeting the Needs of Developed and Developing Countries*. Elsevier Inc, 2018. DOI: 10.1016/B978-0-12-814790-0.00004-1.
- [5] W Brack, S Ait-Aissa, R Altenburger, I Cousins, V Dulio, B Escher, A Focks, A Ginebreda, D Hering, K Hilscherová, J Hollender, H Hollert, A Kortenkamp, ML de Alda, L Posthuma, E Schymanski, H Segner, and J Slobodnik. “Let us empower the WFD to prevent risks of chemical pollution in European rivers and lakes.” In: *Environ Sci Eur* 31.47 (2019), pp. 10–12. DOI: 10.1186/s12302-019-0228-7.
- [6] S Sauvé and M Desrosiers. “A review of what is an emerging contaminant.” In: *Chem Cent J* 8 (2014), pp. 1–7. DOI: 10.1186/1752-153X-8-15.
- [7] T aus der Beek, FA Weber, A Bergmann, S Hickmann, I Ebert, A Hein, and A Küster. “Pharmaceuticals in the environment-global occurrences and perspectives.” In: *Environ Toxicol Chem* 35.4 (2016), pp. 823–835. DOI: 10.1002/etc.3339.
- [8] AJ Ebele, M Abou-Elwafa Abdallah, and S Harrad. “Pharmaceuticals and personal care products (PPCPs) in the freshwater aquatic environment.” In: *Emerg Contam* 3.1 (2017), pp. 1–16. DOI: 10.1016/j.emcon.2016.12.004.
- [9] WWP Lai, YC Lin, HH Tung, SL Lo, and AYC Lin. “Occurrence of pharmaceuticals and perfluorinated compounds and evaluation of the availability of reclaimed water in Kinmen.” In: *Emerg Contam* 2.3 (2016), pp. 135–144. DOI: 10.1016/j.emcon.2016.05.001.

- [10] G Vandermeersch, HM Lourenço, D Alvarez-Muñoz, S Cunha, J Diogène, G CanoSancho, JJ Sloth, C Kwadijk, D Barcelo, W Allegaert, K Bekaert, JO Fernandes, A Marques, and J Robbens. “Environmental contaminants of emerging concern in seafood - European database on contaminant levels.” In: *Environ Res* 143 (2015), pp. 29–45. DOI: 10.1016/j.envres.2015.06.011.
- [11] A Küster and N Adler. “Pharmaceuticals in the environment: scientific evidence of risks and its regulation.” In: *Philos Trans R Soc B Biol Sci* 369.1656 (2014). DOI: 10.1098/rstb.2013.0587.
- [12] A Gogoi, P Mazumder, V Kumar, GGT Chaminda, A Kyoungjin, and M Kumar. “Occurrence and fate of emerging contaminants in water environment: a review.” In: *Groundw Sustain Dev* 6 (2018), pp. 169–180. DOI: 10.1016/j.gsd.2017.12.009.
- [13] P Krzeminski, MC Tomei, P Karaolia, A Langenhoff, CMR Almeida, E Felis, F Gritten, HR Andersen, T Fernandes, CM Manaia, L Rizzo, and D Fatta-Kassinos. “Performance of secondary wastewater treatment methods for the removal of contaminants of emerging concern implicated in crop uptake and antibiotic resistance spread: a review.” In: *Sci Total Environ* 648 (2019), pp. 1052–1081. DOI: 10.1016/j.scitotenv.2018.08.130.
- [14] HELCOM UNESCO. *Pharmaceuticals in the Aquatic Environment of the Baltic Sea Region – A Status Report. UNESCO Emerging Pollutants in Water Series – No. 1, Report*. UNESCO Publishing, Paris, 2017. URL: <https://helcom.fi/action-areas/industrial-municipal-releases/pharmaceuticals/status-report/>.
- [15] V Abbing-Karahagopian, C Huerta, PC Souverein, F De Abajo, HGM Leufkens, J Slattery, Y Alvarez, M Miret, M Gil, B Oliva, U Hesse, G Requena, F De Vries, M Rottenkolber, S Schmiedl, R Reynolds, RG Schlienger, MCH De Groot, OH Klungel, TP Van Staa, L Van Dijk, ACG Egberts, H Gardarsdottir, and ML De Bruin. “Antidepressant prescribing in five European countries: application of common definitions to assess the prevalence, clinical observations, and methodological implications.” In: *Eur J Clin Pharmacol* 70 (2014), pp. 849–857. DOI: 10.1007/s00228-014-1676-z.
- [16] L Pratt, D Brody, and Q Gu. “Antidepressant Use among Persons Aged 12 and Over: United States”. In: *NCHS Data Brief* 283 (2017), pp. 2011–2014. URL: <https://www.cdc.gov/nchs/products/databriefs/db283.htm>.
- [17] AT Ford and H Herrera. “‘Prescribing’ psychotropic medication to our rivers and estuaries.” In: *BJPsycho Bull* 43.4 (2019), pp. 147–150. DOI: 10.1192/bjb.2018.72.

- [18] A David, A Lange, CR Tyler, and EM Hill. “Concentrating mixtures of neuroactive pharmaceuticals and altered neurotransmitter levels in the brain of fish exposed to a wastewater effluent.” In: *Sci Total Environ* 621 (2018), pp. 782–790. DOI: 10.1016/j.scitotenv.2017.11.265.
- [19] P Sehonova, Z Svobodova, P Dolezelova, P Vosmerova, and C Faggio. “Effects of waterborne antidepressants on non-target animals living in the aquatic environment: a review.” In: *Sci Total Environ* 631–632 (2018), pp. 789–794. DOI: 10.1016/j.scitotenv.2018.03.076.
- [20] T Brodin, J Fick, M Jonsson, and J Klaminder. “Dilute concentrations of a psychiatric drug alter behavior of fish from natural populations.” In: *Science* 339.6121 (2013), pp. 814–815. DOI: 10.1126/science.1226850.
- [21] JK Aronson. *Meyler’s Side Effects of Drugs: The International Encyclopedia of Adverse Drug Reactions and Interactions*. Elsevier Science, 2016. URL: <https://www.elsevier.com/books/meylers-side-effects-of-drugs/aronson/978-0-444-53717-1>.
- [22] U Breyer-Pfaff, M Kroeker, T Winkler, and P Kriemler. “Isolation and identification of hydroxylated maprotiline metabolites.” In: *Xenobiotica* 15.1 (1985), pp. 57–66. DOI: 10.3109/00498258509045335.
- [23] R Loos, R Carvalho, D.C António, S Comero, G Locoro, S Tavazzi, B Paracchini, M Ghiani, T Lettieri, L Blaha, B Jarosova, S Voorspoels, K Servaes, P Haglund, J Fick, RH Lindberg, D Schwesig, and BM Gawlik. “EU-wide monitoring survey on emerging polar organic contaminants in wastewater treatment plant effluents.” In: *Water Res* 47.17 (2013), pp. 6475–6487. DOI: 10.1016/j.watres.2013.08.024.
- [24] S Das, NM Ray, J Wan, A Khan, and MB Chakraborty T Ray. “Micropollutants in wastewater: Fate and removal processes. Physico-Chemical Wastewater Treatment and Resource Recovery.” In: (2017), pp. 75–107. DOI: 10.5772/65644.
- [25] NA Alygizakis, P Oswald, NS Thomaidis, EL Schymanski, R Aalizadeh, T Schulze, M Oswaldova, and J Slobodnik. “NORMAN digital sample freezing platform: a European virtual platform to exchange liquid chromatography high resolution-mass spectrometry data and screen suspects in “digitally frozen” environmental samples.” In: *Trends Anal Chem* 115 (2019), pp. 129–137. DOI: 10.1016/j.trac.2019.04.008.
- [26] F Freeling, NA Alygizakis, PC von der Ohe, J Slobodnik, P Oswald, R Aalizadeh, L Cirka, NS Thomaidis, and M Scheurer. “Occurrence and potential environmental risk of surfactants and their transformation products discharged by wastewater treatment plants.” In: *Sci Total Environ* 681 (2019), pp. 475–487. DOI: 10.1016/j.scitotenv.2019.04.445.

- [27] NA Alygizakis, H Besselink, GK Paulus, P Oswald, LM Hornstra, M Oswaldova, G Medema, Thomaidis NS, PA Behnisch, and J Slobodnik. “Characterization of wastewater effluents in the Danube River Basin with chemical screening, in vitro bioassays and antibiotic resistant genes analysis.” In: *Environ Int* 127 (2019), pp. 420–429. DOI: 10.1016/j.envint.2019.03.060.
- [28] KS Diamanti, NA Alygizakis, MC Nika, M Oswaldova, P Oswald, NS Thomaidis, and J Slobodnik. “Assessment of the chemical pollution status of the Dniester River basin by wide-scope target and suspect screening using mass spectrometric techniques.” In: *Anal Bioanal Chem* 412 (2020), pp. 4893–4907. DOI: 10.1007/s00216-020-02648-y.
- [29] PC von der Ohe and V Dulio. *NORMAN Prioritisation Framework for Emerging Substances*. 2013. URL: <https://www.norman-network.net/?q=Publications>.
- [30] *NORMAN Database System*. 2005. URL: <https://www.norman-network.com/nds/>.
- [31] *NORMAN Substance Database*. 2005. URL: <https://www.norman-network.com/nds/susdat/>.
- [32] *NORMAN Ecology Database*. 2005. URL: <https://www.norman-network.com/nds/ecotox/>.
- [33] NA Alygizakis, J Urík, VG Beretsou, I Kampouris, A Galani, M Oswaldova, T Berendonk, P Oswald, NS Thomaidis, J Slobodnik, B Vrana, and D Fatta-Kassinou. “Evaluation of chemical and biological contaminants of emerging concern in treated wastewater intended for agricultural reuse.” In: *Environ Int* 138.105597 (2020). DOI: 10.1016/j.envint.2020.105597.
- [34] R Aalizadeh, PC von der Ohe, and NS Thomaidis. “Prediction of acute toxicity of emerging contaminants on the water flea *Daphnia magna* by Ant Colony Optimization-Support Vector Machine QSTR models.” In: *Environ Sci Process Impacts* 19 (2017), pp. 438–448. DOI: 10.1039/c6em00679e.
- [35] SK Suh and JB Smith. “Maprotiline hydrochloride.” In: *Anal Profiles Drug Subst* 15 (1986), pp. 393–426. DOI: 10.1016/S0099-5428(08)60420-7.
- [36] R Frank and W Klöpffer. “Spectral solar photon irradiance in Central Europe and the adjacent North Sea.” In: *Chemosphere* 17 (1988), pp. 985–994. DOI: 10.1016/0045-6535(88)90069-0.
- [37] GKC Low, SR McEvoy, and RW Matthews. “Formation of nitrate and ammonium ions in titanium dioxide mediated photocatalytic degradation of organic compounds containing nitrogen atoms.” In: *Environ Sci Technol* 25.3 (1991), pp. 460–467. DOI: 10.1021/es00015a013.

- [38] TO Nicolescu. *Interpretation of mass spectra. Mass Spectrometry*. InTech, 2017. DOI: 10.5772/intechopen.68595.
- [39] WM Horspool and F Lenci. “RC Handbook of Organic Photochemistry and Photobiology, Volumes 1 and 2.” In: *CRC Press* (2003). DOI: 10.1201/9780203495902.
- [40] T Katagi. “Direct photolysis mechanism of pesticides in water.” In: *J Pestic Sci* 43.2 (2018), pp. 57–72. DOI: 10.1584/jpestics.D17-081.
- [41] C Sirtori, A Agüera, W Gernjak, and S Malato. “Effect of water-matrix composition on trimethoprim solar photodegradation kinetics and pathways.” In: *Water Res* 44.9 (2010), pp. 2735–2744. DOI: 10.1016/j.watres.2010.02.006.
- [42] MM Dong, R Trenholm, and FL Rosario-Ortiz. “Photochemical degradation of atenolol, carbamazepine, meprobamate, phenytoin and primidone in wastewater effluents.” In: *J Hazard Mater* 282 (2015), pp. 216–223. DOI: 10.1016/j.jhazmat.2014.04.028.
- [43] C Rering, K Williams, M Hengel, and R Tjeerdema. “Comparison of direct and indirect photolysis in imazosulfuron photodegradation.” In: *J Agric Food Chem* 65.15 (2017), pp. 3103–3108. DOI: 10.1021/acs.jafc.7b00134.
- [44] Y Wang, FA Roddick, and L Fan. “Direct and indirect photolysis of seven micropollutants in secondary effluent from a wastewater lagoon.” In: *Chemosphere* 185 (2017), pp. 297–308. DOI: 10.1016/j.chemosphere.2017.06.122.
- [45] LC Bodhipaksha, CM Sharpless, YP Chin, and AA MacKay. “Role of effluent organic matter in the photochemical degradation of compounds of wastewater origin.” In: *Water Res* 110 (2017), pp. 170–179. DOI: 10.1016/j.watres.2016.12.016.
- [46] C Minero, S Chiron, G Falletti, V Maurino, E Pelizzetti, R Ajassa, M.E Carlotti, and D Vione. “Photochemical processes involving nitrite in surface water samples.” In: *Aquat Sci* 69 (2007), pp. 71–85. DOI: 10.1007/s00027-007-0881-6.

4.4 Role of iron in the photodegradation of enrofloxacin

A collaboration project on the elucidation of photodegradation products of enrofloxacin antibiotic was carried out with one of the early stage researchers of the AQUALity project, Iván Sciscenko. The project was exhaustive and contained theoretical photochemistry approaches. The part concerning the influence of the parameters on the formation of the photoproducts and their structural elucidation was carried out by the LCM group.

Significant role of iron on the fate and photodegradation of enrofloxacin

Iván Sciscenko^b, Antonio Arques^b, Zsuzsanna Varga^c, Stéphane Bouchonnet^c, Olivier Monfort^{a,d}, Marcello Brigante^a, Gilles Mailhot^a

^a*Université Clermont Auvergne, CNRS, SIGMA Clermont, Institut de Chimie de Clermont-Ferrand, 63000, Clermont-Ferrand, France*

^b*Departamento de Ingeniería Textil y Papelera, Universitat Politècnica de Valencia, Alcoy, Spain*

^c*Laboratoire de Chimie Moléculaire, CNRS / Ecole Polytechnique, Institut Polytechnique de Paris, 91128, Palaiseau, France*

^d*Comenius University in Bratislava, Faculty of Natural Sciences, Department of Inorganic Chemistry, Ilkovicova 6, Mlynska Dolina, 84215, Bratislava, Slovakia*

Abstract

Enrofloxacin (ENR) belongs to the fluoroquinolone (FQ) antibiotics family, which are contaminants of emerging concern frequently found in effluents. Although many works studying photo-Fenton process for FQ degradation have been reported, there are no reports analysing in deep the effect of iron complexation, as well as other metals, towards FQs' photolysis, which, evidently, also contributes in the overall degradation of the pollutant. Therefore, in this work, we report a comparative study between the photochemical fate of ENR and its complex with Fe(III) under simulated sunlight irradiation. In addition, the effect of dissolved oxygen, self-sensitization process, and H₂O₂ addition on the studied photochemical systems are also investigated. Results indicate that, for free and iron-complexed ENR, singlet oxygen (¹O₂) is generated from the interaction of its triplet state with ground state oxygen. Half-life time (t_{1/2}) of ENR under sun simulated conditions is estimated to be around 22 minutes, while complexation with iron enhances its photostability, leading to a t_{1/2} of 2.1 hours. Such finding indicates that at least the presence of iron, might notably increases the residence time of these pollutants in the environment. Eventually, only with the addition of H₂O₂, the FQ-iron complex is efficiently degraded due to photo-Fenton process even at circumneutral pH values due to the high stability of the formed complex. Finally, after LC/FT-ICR MS analysis, 39 photoproducts

ucts are detected, of which the 14 most abundant ones are identified. Results indicate that photoproducts formation is pH and iron dependent.

Introduction

Antibiotics are among the substances considered as contaminants of emerging concern; they are present in urban wastewater and they persist even after treatment in conventional wastewater treatment plants (WWTPs), this being an entry route into the environment [1–3]. Within this category, fluoroquinolones (FQs), are one of the most consumed antibiotics of the world [4].

FQs can absorb light within the range of solar radiation ($\lambda > 300$ nm), and due to their abundance in natural effluents, photodegradation of these molecules had been thoroughly studied in order to have further insights related to their fate and photoproduct formation in surface waters [5–7]. Besides, these compounds can easily interact with humic-like substances [8], soil [9], and even WWTP sludge, where they can accumulate [10]. In this regard, another water constituent to take into consideration are metals. FQs present high affinity to metal complexation. They can act as mono or bidentate ligands, as well as bridging ligand, being the most common coordination mode via carbonyl and carboxyl groups in adjacent positions [11].

To date, however, there is a lack of information about the FQ-metal environmental behaviour, recently collected in the review of [12], where they reported significant changes towards their toxicity, soil-water mobility, WWTP degradation efficiencies and photochemistry. Regarding the latter, DFT calculations have shown that the complex formed between one of the most frequently found FQ in natural effluents, the enrofloxacin (ENR), with Mg^{+2} , presented higher activation energies for the most direct photolysis pathways than ENR itself [13]. Similarly for ciprofloxacin, another highly consumed FQ, which is also the main photoproduct of ENR [14], in presence of Cu(II) exhibited a strong photolytic inhibition, only recovered in presence of ethylenediaminetetraacetic acid (EDTA) [15]. On the contrary, Cu(II) increased by a factor of 2.4 the photolytic rate constant of moxifloxacin [16], thus indicating that FQ-metal photochemical behaviour could also be dependent on the antibiotic molecular structure.

Advanced oxidation processes (AOPs) had long been studied and proposed for tertiary wastewater treatment, as they are able to degrade these emerging pollutants [17]. In one of the most common AOP, the Fenton process, the highly reactive species $\bullet\text{OH}$ and $\text{HO}_2\bullet$ involved in the contaminants abatement, are formed in the elementary reactions of H_2O_2 disproportionation catalyzed by Fe(II)/Fe(III) (and other transition metals) and enhanced by the action of light (photo-Fenton) [18], which could be also photogenerated in situ in the natural environment [19]. In these cases, when the pollutant is also photolabile, photolysis degradation contribution must be also considered. However, although many

studies of FQs oxidation by photo-Fenton had been published [20], the individual effect of iron towards FQs' photochemical fate is practically unexplored. For instance [21], when treated two FQs and another type of antibiotic by UV/Fe(III), it can be seen that for the tested FQs, its removal rate was much more sensitive to the iron concentration variation compared to the other non-FQ antibiotic. According to the above mentioned statements, this could have been most likely related to the downplayed FQ-iron interaction, not present in the case of the other compound. In this regard, FQs Fenton degradation has been reported as effective even at mild pH conditions due to iron chelation by the pollutant itself [22].

In this work, we decided to compare the photochemical fate under sun-simulated conditions of a model FQ (ENR) alone and as Fe(III)-complex. First, spectroscopic characterization and stability of the complex between ENR and Fe(III) was assessed, secondly, photochemical degradation of ENR and its Fe(III)-complex was evaluated with and without addition of hydrogen peroxide. Finally, the main photoproducts were characterized, and a schematic degradation pathway was proposed. Besides the environmental aspect, we believe that these results will be useful to better comprehend the behaviour of FQs degradation by photo-Fenton and analogues processes.

Materials and methods

Reagents and chemical analysis

Reagents, chemical analysis and kinetics methods are described in the Supporting Information. For further information about transition absorption experiments using laser flash photolysis system, this equipment and procedure have been described in previously published papers [23, 24]. When specified, filtration was performed employing Chromafil Xtra PTFE 0.45 μm filters and no significant ENR retention (i.e. adsorption on the filter) was determined. All the solutions were prepared with ultrapure water (18.2 $\text{M}\Omega\text{ cm}$).

Fe-ENR complex characterization

The complex formation between Fe(III) and ENR was studied by analysing its stoichiometry and pH-stability. Fe-ENR stoichiometry was obtained by applying the method of continuous variation [25], acquiring the UV-vis spectra of fixed 100 μM Fe(III) solution at pH 3.0 with different ENR concentrations in the range 100–600 μM . For pH-stability analysis, the complex between ENR and Fe(III) was firstly prepared at pH 3.0, and afterwards, pH was increased until the desired value and leaving each solution for 10 h in the dark with magnetic stirring.

Irradiation experiments and analysis

Photochemical experiments were carried out in a thermostat cylindrical open glass reactor (total volume of 50 mL) at 20°C loaded with 25 mL of the testing solution containing ENR 300 μM , with and without Fe(III) 100 μM . Irradiations were performed with

a solar simulator (Lot-Oriel LS0306) equipped with a high-pressure Xe short arc lamp (Ushio UXL-302-O) and a Pyrex filter to avoid wavelengths < 290 nm. Iron-ENR complex solutions were always prepared and left with stirring for at least 10 h to assure full complexation prior to irradiation experiments. All assays were performed for 2 h, withdrawing 1 mL of sample in time-intervals and filtered with PTFE 0.45 μm Chromafil Xtra filters. When needed, 200 μM H_2O_2 were employed as source of $\bullet\text{OH}$. Two initial pH were studied, 3.0 where Fenton-(like) processes are optimal, and 7.0, relevant towards realistic natural/wastewater scenario. All samples (1 mL) were filtered with PTFE 0.45 μm filters and mixed with 100 μL of methanol in order to stop the reaction before analysis (i.e. to quench possible hydroxyl radical formation through Fenton reaction). Experiments were performed at least twice.

The oxygen effect was studied by bubbling solution with pure N_2 and O_2 for 10 min before and during the photochemical experiment, thus assuring negligible and high O_2 concentrations, respectively. Formation of reactive oxygen species (ROS) was studied employing isopropyl alcohol (IPA) ($\bullet\text{OH}$ scavenger, $k(\bullet\text{OH}) = 1.9 \times 10^9 \text{ M}^{-1} \text{ s}^{-1}$) and furfuryl alcohol (FFA) ($\bullet\text{OH}$ and $^1\text{O}_2$ scavenger, $k(\bullet\text{OH}) = 1.5 \times 10^{10} \text{ M}^{-1} \text{ s}^{-1}$ and $k(^1\text{O}_2) = 1.2 \times 10^8 \text{ M}^{-1} \text{ s}^{-1}$, respectively) [26, 27]. IPA was employed in a concentration of 5 mM whereas FFA of 300 μM . The chosen concentrations were based on other related works [28–30], ROS being able to react much faster with the probes than with ENR at 300 μM . It is important to highlight that FFA was chosen over NaN_3 as $^1\text{O}_2$ probe since this last one is highly pH dependent ($k(^1\text{O}_2)(\text{N}_3^-) = 5 \times 10^8 \text{ M}^{-1} \text{ s}^{-1}$ and $k(^1\text{O}_2)(\text{HN}_3) \approx 1 \times 10^6 \text{ M}^{-1} \text{ s}^{-1}$, with $\text{pK}_a = 4.6$, being also HN_3 strongly partitioned to the gas phase) [31], whereas FFA is not [32], thus being better when comparing assays at pH 3.0 with pH 7.0.

Results and discussion

Complexation with ferric ions

When iron (III) perchlorate is added to an ENR solution (both colourless) at pH 3.0, the mixture changed into a yellow-colour solution. Indeed, an absorbance shoulder after 400 nm and up to 540 nm appears in the UV–vis spectrum of ENR-iron mixture (Figure 4.4.1A). Such absorption suggests that a charge-transfer transition between the ENR and Fe(III) occurs, corresponding to the formation of a coordination complex [33]. In Figure 4.4.1B, the absorbance at 430 nm as a function of different ENR/Fe(III) ratios is depicted. Absorbance increases from 0.23 to about 0.43 when ENR/ Fe(III) ratio grows up to 3, and then reaches a plateau at higher ratios. Such finding is in agreement with an octahedral complex employing the FQ carbonyl and carboxyl moieties to bind Fe(III) with a ratio 3:1, which has been previously reported [34]. Then, the ENR-iron complex ($\text{Fe}^{\text{III}}\text{-ENR}_3$) stability was investigated in the range of pH 3.0 to 9.0 with measuring the total iron concentration in solution. Figure 4.4.1C shows that dissolved Fe(III) concentration

remained constant for pH values below 7.5, while for $\text{pH} \geq 8.0$, a decay due to precipitation of its (oxy)hydroxides was observed [35]. However, measurements without filtration have shown that Fe(III) concentration remained at ca. $100 \mu\text{M}$ even until $\text{pH} 9.0$, indicating that ENR is also capable of stabilizing Fe(III) in the colloidal state.

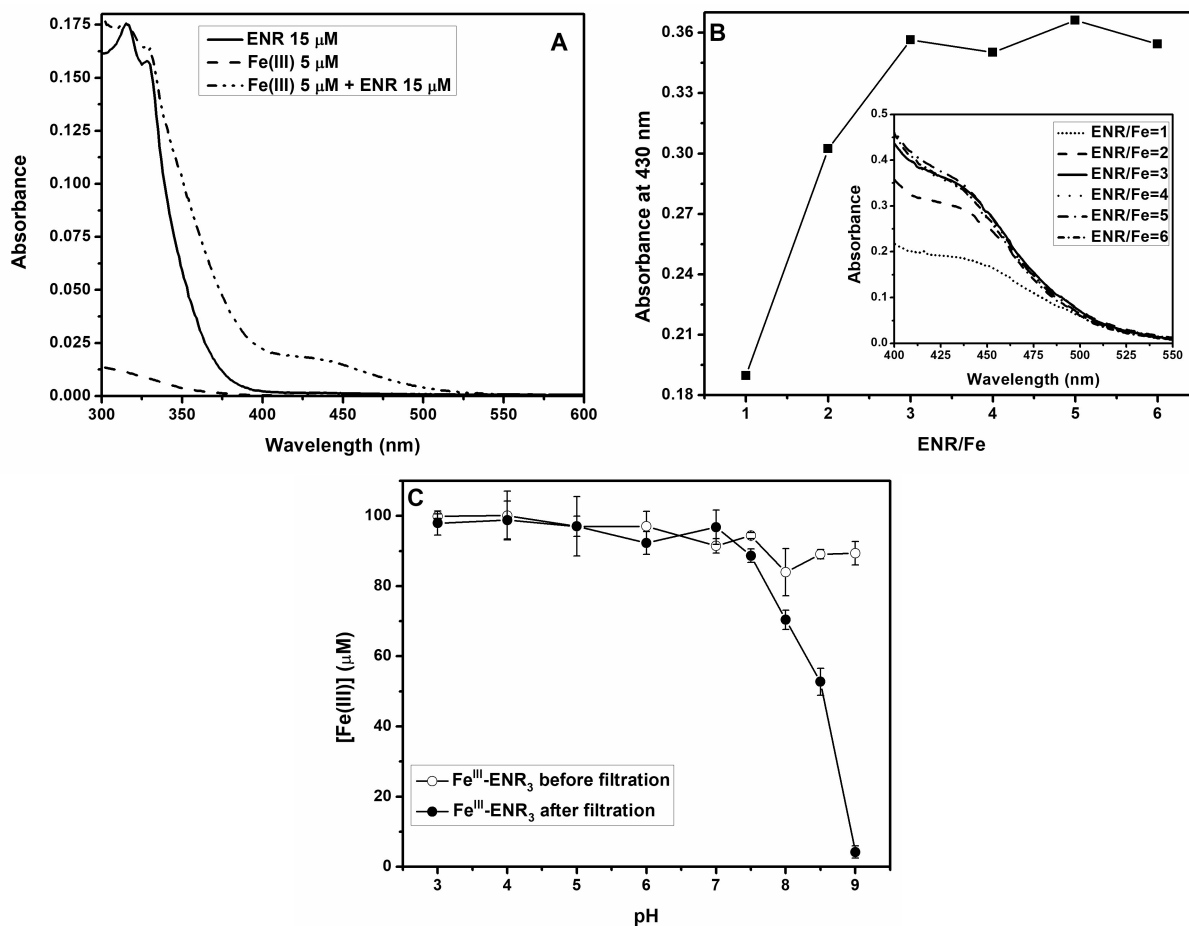


Figure 4.4.1: (A) Absorption spectra for ENR, Fe(III) and $\text{Fe}^{\text{III}}\text{-ENR}_3$ at $\text{pH} 3.0$; (B) Method of continuous variation for a fixed amount of Fe(III) $100 \mu\text{M}$ and varying ENR concentration from 100 to $600 \mu\text{M}$. Insert represent the UV-vis spectra of different ENR/ Fe(III) ratio solutions at $\text{pH} 3.0$. (C) Fe(III) concentration from $100 \mu\text{M}$ $\text{Fe}^{\text{III}}\text{-ENR}_3$ complex at different pH values measured 24 h after preparation. PTFE filters $0.45 \mu\text{m}$ were used to filter solutions. Values represent the average of two measurements, and the error bar gives the associated uncertainty.

In addition, $\text{Fe}^{\text{III}}\text{-ENR}_3$ solutions from $\text{pH} 3.0$ to 7.5 proved to be stable at least for one month in the dark and at room temperature since Fe(III) remained in solution all time. In fact, the formation constant of $\text{Fe}^{\text{III}}\text{-ENR}_3$ complex is reported to have its highest value at acidic pH , $\log K(\text{Fe}^{\text{III}}\text{-ENR}_3) \approx 45$, and it decreases with increasing pH , being equal to 25 at neutral conditions (Urbaniak and Kokot, 2009). These values are comparable with other stable Fe(III) -organic ligand complexes such as EDTA ($\log K(\text{Fe}^{\text{III}}\text{-EDTA}) \approx 25$) [36]. Preparation of analogous solutions containing Fe(II) instead of Fe(III) did not evidence the complex signal at 430 nm , thus indicating that the ENR-ferrous complex is

not formed [37].

Photodegradation experiments

– Effect of pH

In order to investigate the degradation of the antibiotic, in free form or as iron-complex, the same concentration of ENR was considered for all the experiments (300 μM of ENR or 100 μM of $\text{Fe}^{\text{III}}\text{-ENR}_3$) in acidic (pH 3.0) and neutral (pH 7.0) solutions (Figure 4.4.2A). In this way, even though the pollutant concentration was higher than the environmental related levels, this allowed us to also study the $\text{Fe}(\text{III})/\text{Fe}(\text{II})$ behaviour (see later Figure 4.4.3B and S4.4.5). In addition, the concentrations of the complex $\text{Fe}^{\text{III}}\text{-ENR}_3$ between 1 and 100 mg L^{-1} has no effect on the photochemical process. Besides, some studies propose the use of photo-Fenton to treat the concentrate stream from membrane processes, hence, dealing with higher concentration of pollutants [38].

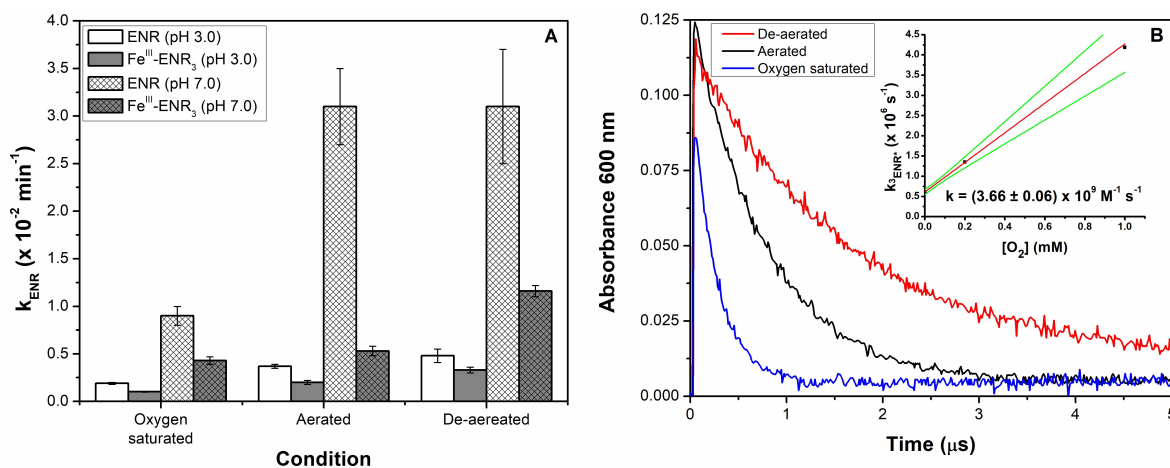


Figure 4.4.2: (A) Photolytic rate constants for ENR 300 μM and $\text{Fe}^{\text{III}}\text{-ENR}_3$ 100 μM at all tested conditions (error bars were calculated from the deviation from linear fit and experimental data); (B) $^3\text{ENR}^*$ relaxation kinetics from ENR 280 μM at pH 7.0 by laser flash photolysis measurements at de-aerated, aerated and oxygen saturated conditions. In the insert, $^3\text{O}_2$ quenching kinetic rate constant determination from obtained relaxation fitting curves.

Under irradiation at pH 3.0, the pseudo-first order photolysis rate constants of ENR and as iron-complex were 3.7×10^{-3} and $2.0 \times 10^{-3} \text{ min}^{-1}$, respectively. Therefore, even though $\text{Fe}^{\text{III}}\text{-ENR}_3$ exhibited greater absorbance within the visible region, we can assume that this complex could present higher activation energy for most of the photodegradation pathways of ENR, hence, being more stable against light irradiation than the pollutant alone, as it has been reported for other FQ-metal complexes [13, 15]. At pH 7.0, where the zwitterionic form of ENR becomes predominant ($\text{pK}_{\text{a}1} \approx 6.0$ and $\text{pK}_{\text{a}2} \approx 8.5$, Figure S4.4.1), the photolysis rate constant was one order of magnitude higher than at acidic conditions ($k_{\text{ENR}} = 3.1 \times 10^{-2} \text{ min}^{-1}$), which is in agreement with the higher photolysis quantum yields of FQs for zwitterionic forms associated to changes in functional groups reactivity with the ionic forms [39]. After 2 h of irradiation, the pH decreased to 6.0

due to decarboxylation of the molecule, as confirmed by mass spectrometry analysis. Interestingly, in the case of iron-complex, the photolysis enhancement was clearly less marked than for free antibiotic, being its kinetic rate constant $5.3 \times 10^{-3} \text{ min}^{-1}$, only 2.7 times more than at pH 3.0.

It is important to highlight that photolysis results at pH 3.0 could have also been well explained by zero order fitting (see Figures S4.4.2A–B). However, this is opposed to the consensus of photolytic pseudo-first order kinetic fitting for FQs in all previously cited related works employing ca. $5 \mu\text{M}$ [30], $120 \mu\text{M}$ [40] or even $2.78 \times 10^3 \mu\text{M}$ [21].

– ROS generation and effect of dissolved oxygen

In order to understand the degradation mechanisms, different photochemical experiments were performed in the presence of ROS scavengers, such as IPA and FFA, or in oxygen saturated and deaerated solutions. As shown in Figure S4.4.2, the presence of IPA (5 mM) and FFA (300 μM) did not significantly modify the degradation of ENR or $\text{Fe}^{\text{III}}\text{-ENR}_3$, indicating that generation of $\bullet\text{OH}$ or $^1\text{O}_2$ by the self-sensitization process should not be relevant for ENR degradation in any of the studied cases. However, $^1\text{O}_2$ generation was confirmed when observing FFA degradation (Figure S4.4.3). At both studied pH, a 40% FFA removal was obtained after 120 min with ENR, whereas for $\text{Fe}^{\text{III}}\text{-ENR}_3$, 10% and 25% was obtained at pH values 3.0 and 7.0, respectively. Therefore, $^1\text{O}_2$ formation should be reduced when ENR is chelating Fe(III), which is in agreement with other FQ-metal complexes that showed a decrease in singlet oxygen overall production [41]. Nevertheless, this could be also linked to the slower photolysis degradation in the case of the complex, resulting also in a lower singlet oxygen production. Therefore, we can conclude that Fe(III) complexation by ENR should affect more its direct photolysis pathways rather than its photosensitized ones.

Although singlet oxygen is formed through the interaction of dissolved oxygen ($^3\text{O}_2$) with the excited states of other molecules [42], ENR photodegradation was slower when increasing the amount of dissolved oxygen in the system. For instance, at pH = 3.0 and with the antibiotic alone, a photolytic rate constant of $4.8 \times 10^{-3} \text{ min}^{-1}$ was determined under de-aerated conditions, whereas with an oxygen-saturated solution was $1.9 \times 10^{-3} \text{ min}^{-1}$ (Figure 4.4.2A). In line with these observations, faster quenching of ENR triplet state (ENR^*) was obtained when increasing the dissolved oxygen concentration (Figure 4.4.2B). Therefore, even though ENR could be oxidized by photogenerated $^1\text{O}_2$, the reactivity between them is estimated to be around $10^6 \text{ M}^{-1} \text{ s}^{-1}$ [41], which is considerably lower than the $^3\text{O}_2$ quenching by ENR^* , determined to be 4.7 and $3.7 \times 10^9 \text{ M}^{-1} \text{ s}^{-1}$ at pH 3 (Figure S4.4.4A) and 7 (Figure 4.4.2B), respectively. For $\text{Fe}^{\text{III}}\text{-ENR}_3$, the same counterproductive effect of ground state dissolved oxygen was observed, with the difference that the obtained removals were proportionally slower than the antibiotic in free form, in agreement with the higher photochemical stability of the FQ-metal complex

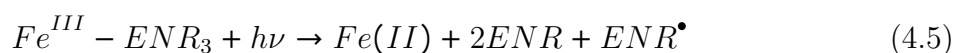
At pH 7.0, dissolved oxygen inhibitory effect for ENR was observed when comparing aerated/de-aerated conditions ($k_{\text{ENR}} = 3.1 \times 10^{-2} \text{ min}^{-1}$ in both cases) against oxygen-saturated ones ($k_{\text{ENR}} = 9 \times 10^{-3} \text{ min}^{-1}$). On the contrary, for $\text{Fe}^{\text{III}}\text{-ENR}_3$, the tendency remained as at acidic conditions, observing decreasing photolytic rate constants when going from de-aerated towards aerated, and oxygen saturated conditions (Figure 4.4.2A).

Fe(II) formation due to ligand to metal charge transfer (LMCT) within the photolysis of $\text{Fe}^{\text{III}}\text{-ENR}_3$ at pH 3.0, followed the same tendency, de-aerated > aerated > oxygen saturated (Figure S4.4.5), obtaining after 60 min irradiation, a reduction of 100% from Fe(III) to Fe(II) with N_2 bubbling, 87% in aerated conditions, and 36% with O_2 bubbling.

Based on these results, a plausible reaction mechanism can be proposed as following: after absorption of light, an electron of ENR can be promoted to the excited state ($^1\text{ENR}^*$) followed by intersystem crossing and generation of ENR triplet state ($^3\text{ENR}^*$) (Eq (4.1)). The excited triplet state can lead to the formation of degradation product (Eq (4.2)) or can be quenched by molecular oxygen ($^3\text{O}_2$) through energy transfer reaction leading to the formation of singlet oxygen ($^1\text{O}_2$) and ENR ground state (Eq (4.3)). Photogenerated $^1\text{O}_2$ can also slightly contribute to the oxidation of ENR (Eq (4.4)).



For $\text{Fe}^{\text{III}}\text{-ENR}_3$, the first photoinduced reaction is the LMCT reaction, leading to the formation of ferrous ions (Fe(II)), 2 molecules of ENR, and ENR radical (ENR^\bullet) in solution (Eq (4.5)). ENR^\bullet can start different degradation pathways in which water and oxygen can be involved (Eq (4.6)).



– Time-course absorbance spectra changes

Analysing the changes in absorbance spectra with light irradiation for ENR and $\text{Fe}^{\text{III}}\text{-ENR}_3$ at pH 3.0, a signal formation at 535 nm was observed (Figure 4.4.3A and B), also evidenced by a final light pink colour of the solutions after the 120 min of irradiation, which could probably be related to the formation of poly-conjugated products [43]. Secondly, analysing the iron complex (Figure 4.4.3B) two additional issues have been seen: 1) there is a decay in 430 nm complex signal, which is related to the Fe(III) reduction to Fe(II)

due to LMCT process, and 2) an isosbestic point at 516 nm was obtained, which suggests the conversion of $\text{Fe}^{\text{III}}\text{-ENR}_3$ into one main absorbing photoproduct.

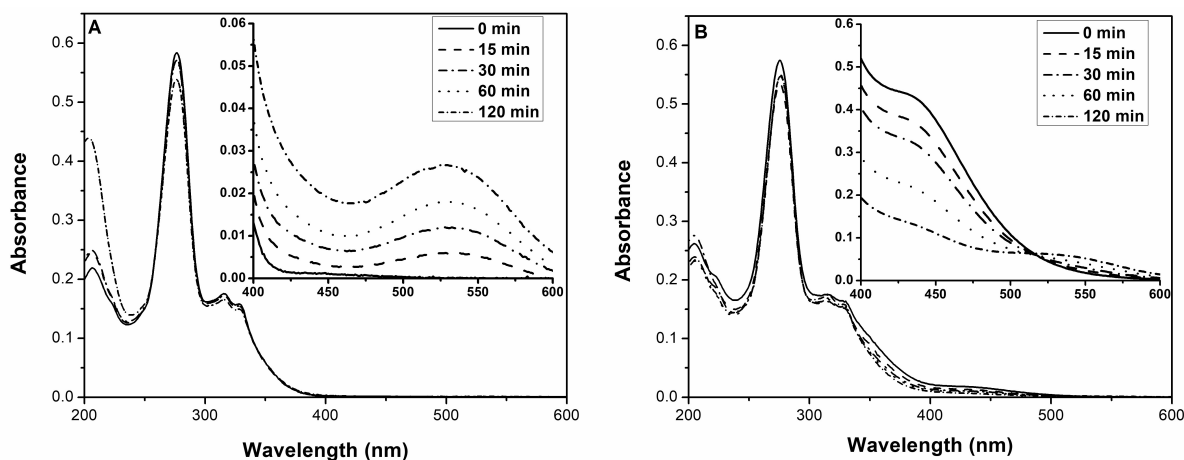


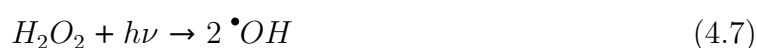
Figure 4.4.3: Time-course absorbance spectra changes during irradiation experiments at pH 3.0. Full spectra were recorded by 20 times dilution of the original sample (in the insert). (A) ENR 300 μM ; (B) $\text{Fe}^{\text{III}}\text{-ENR}_3$ 100 μM .

Analogous results for pH 7.0 are shown in Figures S4.4.6A–B, where pink colourization of the solution after irradiation was also observed, thus, with signal formation at 535 nm (however, not as pronounced as at acidic conditions). As expected, no complex absorbance signal decay was observed for $\text{Fe}^{\text{III}}\text{-ENR}_3$ due to fast reoxidation of Fe(II) at neutral pH. In addition, there was only a negligible dissolved total iron loss within $\text{Fe}^{\text{III}}\text{-ENR}_3$ irradiations at pH 7.0 (5–10% after 2 h), indicating that the by-product formation should be of the FQ-type structure, hence still being capable of binding iron and keeping it in aqueous solution even at neutral pH [22].

Impact of H_2O_2 addition

In the frame of water treatment, the effect of H_2O_2 addition (200 μM) was also studied. In this case, higher amounts of $\bullet\text{OH}$ are produced in situ due to H_2O_2 photolysis observed using the same irradiation setup (Eq (4.7)) [44] as well as Fenton-like and Fenton reactions (Eqs (4.8) and (4.9)), strongly enhanced by the photo-generated Fe(II) in the presence of the complex $\text{Fe}^{\text{III}}\text{-ENR}_3$ (Eq (4.5)) [18].

Due to this reason, under light at pH 3.0, $\text{Fe}^{\text{III}}\text{-ENR}_3$ was even more reactive than ENR, obtaining 60% removal in 60 min, compared to the 40% of the free antibiotic (Figure 4.4.4). By comparison to the photochemical system without H_2O_2 , ENR removal effectiveness was increased by a factor of 2, while for $\text{Fe}^{\text{III}}\text{-ENR}_3$, this increment reached approximately a factor of 4.



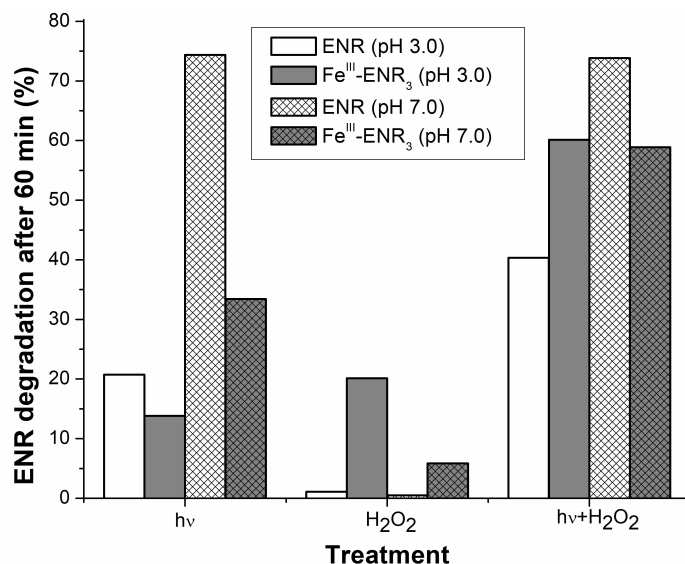
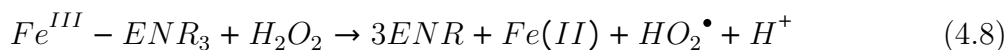


Figure 4.4.4: Degradation percentages after 60 min at both studied pH in aerated conditions, under sunlight irradiation ($h\nu$), with H_2O_2 200 μM without irradiation (dark control), and the combination of both, $h\nu+H_2O_2$ 200 μM , for 300 μM of ENR and 100 μM of Fe^{III} -ENR₃. Error bars were calculated as the associated standard deviation between respective duplicates.



At pH 7.0 under light, even though the antibiotic removal was slightly higher without Fe(III) (74% for the free form, and 59% for the iron complexed one in 60 min), H_2O_2 did not enhance ENR degradation, thus, the contribution of the low concentration of photo-generated $\bullet OH$ from H_2O_2 photolysis was negligible for the already fast ENR photolytic degradation. On the contrary, the addition of H_2O_2 to the analogous system containing Fe(III), represented a removal increment for almost the double than the one without it. Therefore, it can be hypothesized that photo-Fenton process was running even at pH 7.0, bearing in mind that is usually no longer effective in these conditions without the addition of any chelating agent due to the precipitation of iron oxides [45–47].

No significant differences were obtained for Fe^{III} -ENR₃ under light and in the presence of H_2O_2 for the both studied pH values (c.a. 60% in 60 min in both cases). However, since photolytic degradation was lower at pH 3.0 than at pH 7.0 (14% and 33% in 60 min, respectively), photo-Fenton contribution to the overall pollutant removal should have been lower at neutral conditions, as expected.

Within dark controls, the greater reactivity of Fe^{III} -ENR₃ against H_2O_2 was even more evident. While for ENR no degradation was observed in any case, for the iron-complex form, 20% degradation was achieved at pH 3.0, and 6% at pH 7.0.

Photoproduct identification and formation pathways

A total of 39 photoproducts were detected under the different reaction conditions, exact molecular formulae were determined for all of them, based on accurate mass measurements. The 14 most abundant ones were successfully isolated and fragmented to obtain structural information (Table S4.4.1), and a schematic degradation pathway was proposed (Figure 4.4.5). Results for the whole 39 photoproducts are shown in Figure S4.4.7.

Observing Figure 4.4.6, since complexation reduced the direct photolysis of the FQ, lower photoproduct formation was obtained in the case of the iron-complex form at both studied pH without H₂O₂. Analysing pH 3.0, photodegradation pathways did not differ significantly between ENR and Fe^{III}-ENR₃, observing in both cases that the main reaction was ethyl loss from piperazinyl ring, forming photoproduct A, ciprofloxacin (another commercial FQ), which is in agreement with related studies that have indicated it as the common path for ENR photolytic degradation [14, 40]. Similarly, photoproduct C, still with no modification on the FQ core, presents rupture on the piperazinyl ring. Only in the cases of B, D, E and M, oxidation of chromophoric part of ENR became relevant. In addition, the use of IPA showed the expected decrease in formation of hydroxylated photoproducts (Figure S4.4.7c), even though it had not significantly affected the pollutant degradation kinetics (Figures S4.4.2a–b).

In sharp contrast with acidic conditions, at pH 7.0 without H₂O₂, photoproduct formation was notably distinctive when ENR was chelating iron compared to when it was not. In both cases, a higher variety of photoproducts were observed than the ones obtained at pH 3.0, presenting more defluorinated compounds (H, J, K, and N) and also decarboxylated (G, I and L). These reactions have been reported in the literature as common paths for FQ photolysis for zwitterionic chemical speciation form rather than for the cationic one [30, 48]. Moreover, in the case of Fe^{III}-ENR₃, fluorine substitution by hydroxyl group (photoproduct E) has been observed as the favored path, in contrast with the prevalent ciprofloxacin (photoproduct A) formation at pH 3.0. Without Fe(III) complexation, there was no formation of a single major photoproduct, but a wider variety of transformation products were detected in lower quantities.

It is well known that photo-induced decarboxylation reactions occur on Fe(III)-carboxylate complexes under sun-simulated irradiation [18, 49, 50]. However, in this case, lower decarboxylation was observed in the case of Fe^{III}-ENR₃ than ENR, which is in agreement with previous observations reported, describing no significant iron loss during the 120 min of Fe^{III}-ENR₃ irradiation at pH 7.0. This trend could be probably explained by the chelation mode between ENR and Fe(III) between the carbonyl and carboxyl groups of FQs, hence being an overall protection of the carboxylic acidic group. Nevertheless, the difference between the decarboxylation of ENR and Fe^{III}-ENR₃ is the same as for the other photoproducts, obtaining maybe higher photoproduct formation for the

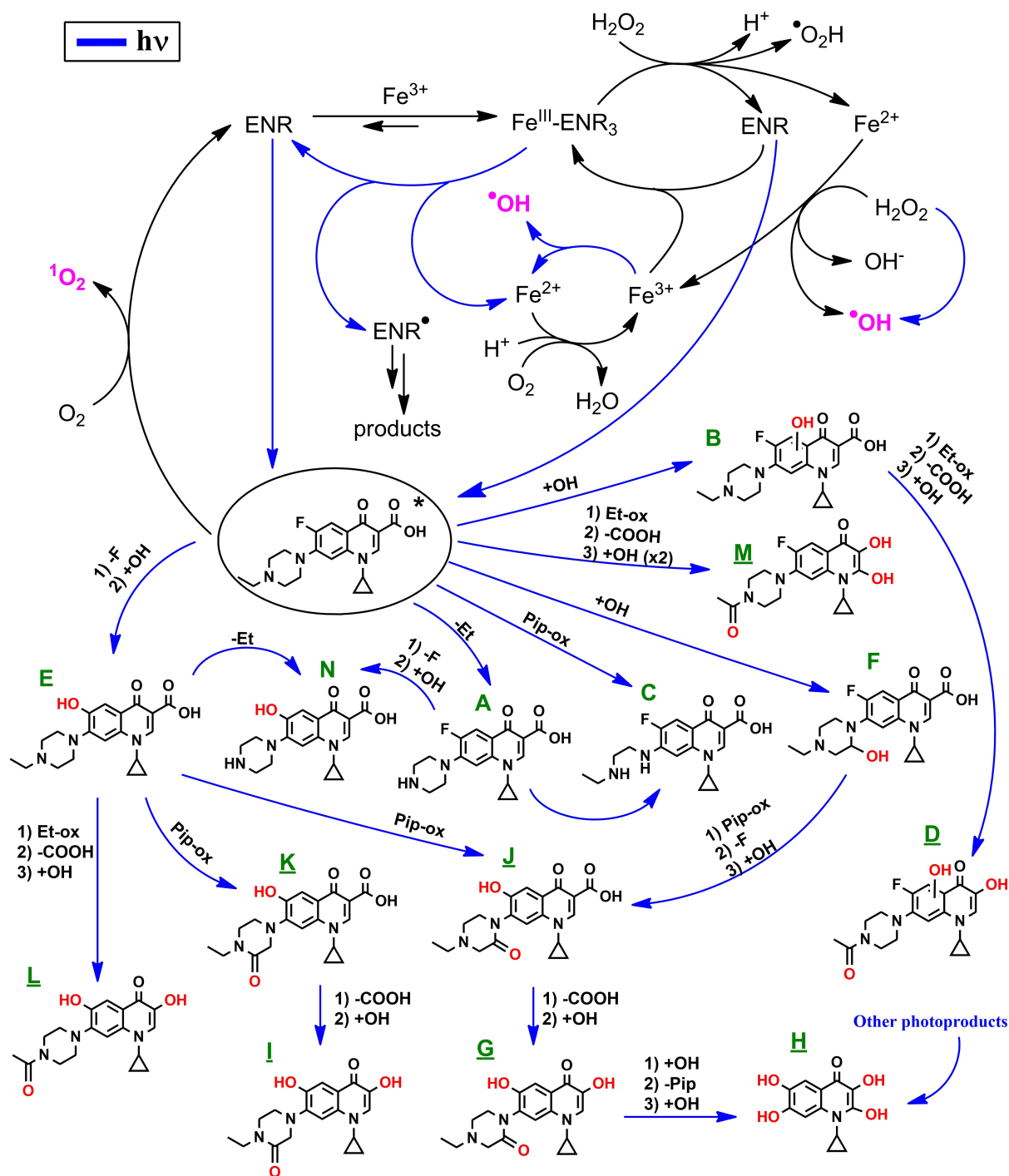


Figure 4.4.5: Summary of the studied reactions and photoproduct formation mechanism proposal. Underlined photoproducts were found for the first time in this work. Reactions include defluorination (-F), decarboxylation (-COOH), hydroxylation (+OH), piperazine cleavage and oxidation (-Pip and Pip-ox, respectively), and ethyl moiety cleavage and oxidation (-Et and Et-ox, respectively).

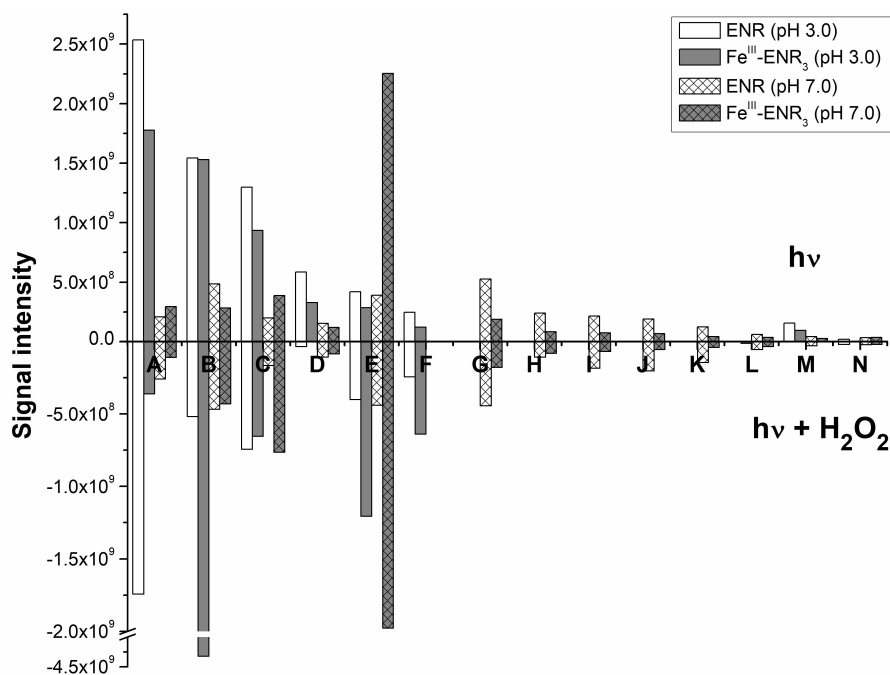


Figure 4.4.6: Obtained photoproducts formation after 120 min for ENR 300 μM and $\text{Fe}^{\text{III}}\text{-ENR}_3$ 100 μM , pH 3.0 and 7.0. Above with only light irradiation ($h\nu$), and below with $h\nu + \text{H}_2\text{O}_2$ 200 μM .

noncomplexed pollutant. Therefore, no conclusion can be taken from an enhancement or inhibition of decarboxylation between ENR and $\text{Fe}^{\text{III}}\text{-ENR}_3$.

When H_2O_2 was added, at pH 3.0, formation of hydroxylated byproducts (B, E and F) occurred at a higher extent in the case of $\text{Fe}^{\text{III}}\text{-ENR}_3$, which is in agreement with the higher $\bullet\text{OH}$ production due to the photo-Fenton process. These differences are clearer when analysing the respective obtained photoproduct formation kinetics (Figures S4.4.8a–b), noticing that not only the order of formation was different, but the rates as well. Interestingly, decarboxylation was negligible compared to direct photolysis (without H_2O_2), where D and M were obtained in higher amounts.

In the case of pH 7.0, the addition of H_2O_2 did not alter the photodegradation mechanism of ENR compared to the results without the addition of it. On the other hand, despite the fact that with $\text{Fe}^{\text{III}}\text{-ENR}_3$ differences were not as clear as the ones at pH 3.0, when analysing Figures S4.4.7e–f, enhanced oxidized products were formed when H_2O_2 was added, results that are in agreement with the ones shown in the previous section.

Conclusions

Our results demonstrate that iron, ubiquitous metal in water compartment as well as catalyst reagent in photo-Fenton type processes, can strongly affect the photochemical processes of ENR also frequently found in aqueous media. Indeed, when iron, coexist

with ENR, they form a stable complex within a wide pH range, affecting each other's photochemistry, in particular, decreasing ENR photolytic rate constant, thus probably enhancing their persistence in the environment. Photoproduct formation pathway is also affected by metal chelation. The FQ-Fe(III) complex was efficiently removed from water only with the addition of H₂O₂, due to photoFenton process. In this sense, even though FQs could be photochemically stabilized in the presence of Fe(III), this coexistence could represent an advantage when achieving Fenton-type treatment at circumneutral pH for the degradation of more recalcitrant pollutants.

Acknowledgement

This paper is part of a project that has received funding from the European Union's Horizon 2020 research and innovation programme under the Marie Skłodowska-Curie grant agreement No. 765860 (AQUALity). The paper reflects only the authors' view and the Agency is not responsible for any use that may be made of the information it contains. M.B. and G. M. acknowledge financial support from the CAP 20–25 I-site project.

Supplementary information

Reagents and chemical analysis

1. Reagents

High purity (> 99%) enrofloxacin (ENR), Fe(ClO₄)₃·xH₂O, NaOH, ferrozine, ascorbic acid and furfuryl alcohol (FFA) were purchased from Sigma-Aldrich. Isopropyl alcohol (IPA), formic acid 98%, H₂SO₄ 98%, and HPLC grade, methanol and acetonitrile, were obtained from VWR Chemicals.

When needed, pH was adjusted with H₂SO₄ 0.05 M or NaOH 0.1 M. Fe(III) 2 mM stock solutions were prepared from Fe(ClO₄)₃·xH₂O solid each day. Stock solution of ENR was prepared in acidic water at pH 2.0. Iron-ENR solutions were prepared 10 h before each experiment. All the solutions were kept in dark conditions and final preparations were performed just before experiments.

2. Chemical analysis and kinetics

ENR concentration was monitored by a Shimadzu Nexera DGU-20A5R high performance liquid chromatography (HPLC) coupled with a photodiode array (PDA) detector. A C18 Macherey-Nagel column Nucleodur- π^2 5 μm was used with a 0.25 mL min⁻¹ isocratic flow of 85% formic acid 0.1 M and 15% acetonitrile. The oven was set at 40°C and detection of ENR and FFA were performed at 278 and 227 nm, respectively. ENR in presence or absence of Fe(III) has exhibited the same retention time in all cases.

Total iron and Fe(II) concentrations, were measured by Ferrozine method [51]. All UV-vis spectra were acquired using a Varian Cary 3 UV-Visible spectrophotometer.

LC-MS and LC-MS/MS measurements were performed on a Bruker SolarixXR FT-ICR 9.4T ultrahigh-resolution mass spectrometer coupled to a Waters Acquity HPLC system. For the separation an Agilent Pursuit XR_sULTRA C18 (length 50 mm, diameter 2 mm, particle size 2.8 μm) column was used with a flow of 0.2 mL min^{-1} . Gradient elution was used starting with 95% of water with 0.1% formic acid and 5% of acetonitrile with 0.1% formic acid (95-5%). This ratio was held up to 3 minutes, after that it was gradually changed to 50-50% up to 12 minutes, and altered to 5-95% until 17 minutes of elution. Electrospray ionization source was used in positive mode, the capillary voltage was set at 4000 V and spray shield at -500 V. Nitrogen was used both as nebulizer gas at 1 bar, and drying gas at 8 L min^{-1} and 250°C. The sample injection volumes were 2 μL for LC-MS and 10 μL for LC-MS/MS experiments. The m/z detection range was between 57.7 and 1000 m/z . Data acquisition size was 4 Mpts in broadband mode, with a data reduction of 97%. For MS^2 experiments the isolation was performed at 1 m/z window and collision induced dissociation experiments were carried out with collision energies of 15 and 20 V. The data were processed with Bruker Compass Data Analysis software. For the molecular ions sub-ppm accuracy was achieved, while for the collision induced dissociation experiments the detected fragment mass accuracy was below 10 ppm. Molecular structures were proposed based on the mass spectrometry fragmentation patterns, expected photochemical reactions and existing literature data.

Pseudo-first order apparent constant of ENR degradation (k_{ENR}) was determined from the slope of $\ln(C_t/C_0)$ vs irradiation time (t) where C_0 was the initial ENR concentration and C_t the remaining concentration at time t . k_{ENR} were calculated from the fitting within 0-120 min, except in some cases where it was only considered with the first 30 min irradiation (ENR alone at pH 3.0 aerated, pH 7.0 aerated, pH 7.0 de-aerated and pH 7.0 oxygen saturated) due to deviation of the linear tendency at longer periods of time attributed to the competition effect of photogenerated products in solution. The emission spectrum of the lamp was recorded using a charge-coupled device (CCD) spectrophotometer (Ocean Optics USD 2000CUV-VIS) equipped with an optical fibre. Over the wavelength range of 260 – 600 nm, a total photon flux of 157 W m^{-2} was determined.

The determination of the second-order rate constants between triplet ENR excited state ($^3\text{ENR}^*$) and ground state oxygen ($^3\text{O}_2$) was carried out with the nanosecond laser flash photolysis apparatus from Applied Photophysics-LKS60. The equipment and procedure employed for transition absorption experiments using laser flash photolysis system, has been previously described [23, 24].

Error bars were calculated as the standard deviation between replicates, except for kinetic rate constant calculation, where they were obtained from the deviation from linear fit and experimental data (average between replicates).

Dimer formation was confirmed for photolysis at pH 3.0 through direct infusion mass

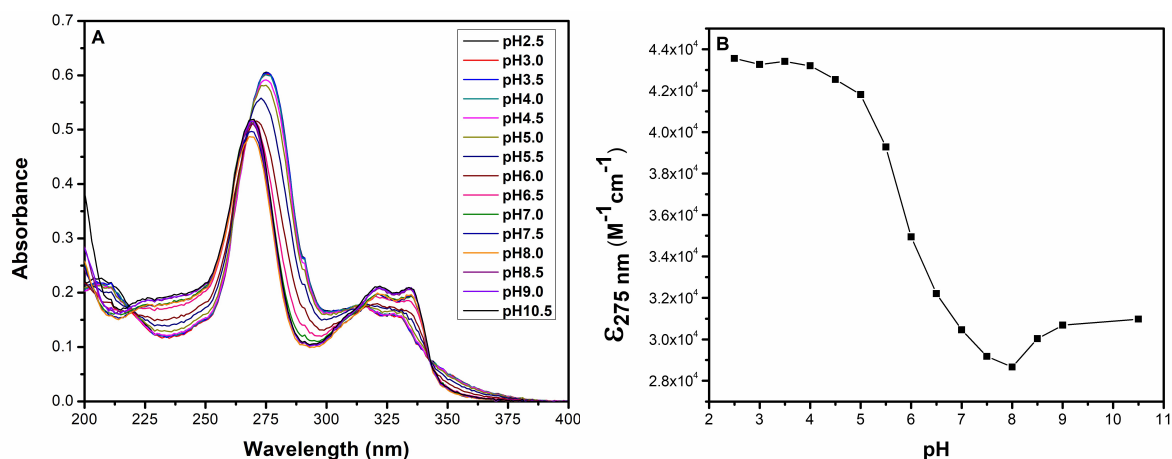


Figure S4.4.1: ENR pKa determination ($[\text{ENR}] = 15 \mu\text{M}$). A) Different spectra as function of pH (pH 2.5 to 10.5), B) Molar absorption coefficient (ϵ) at 275 nm as function of pH

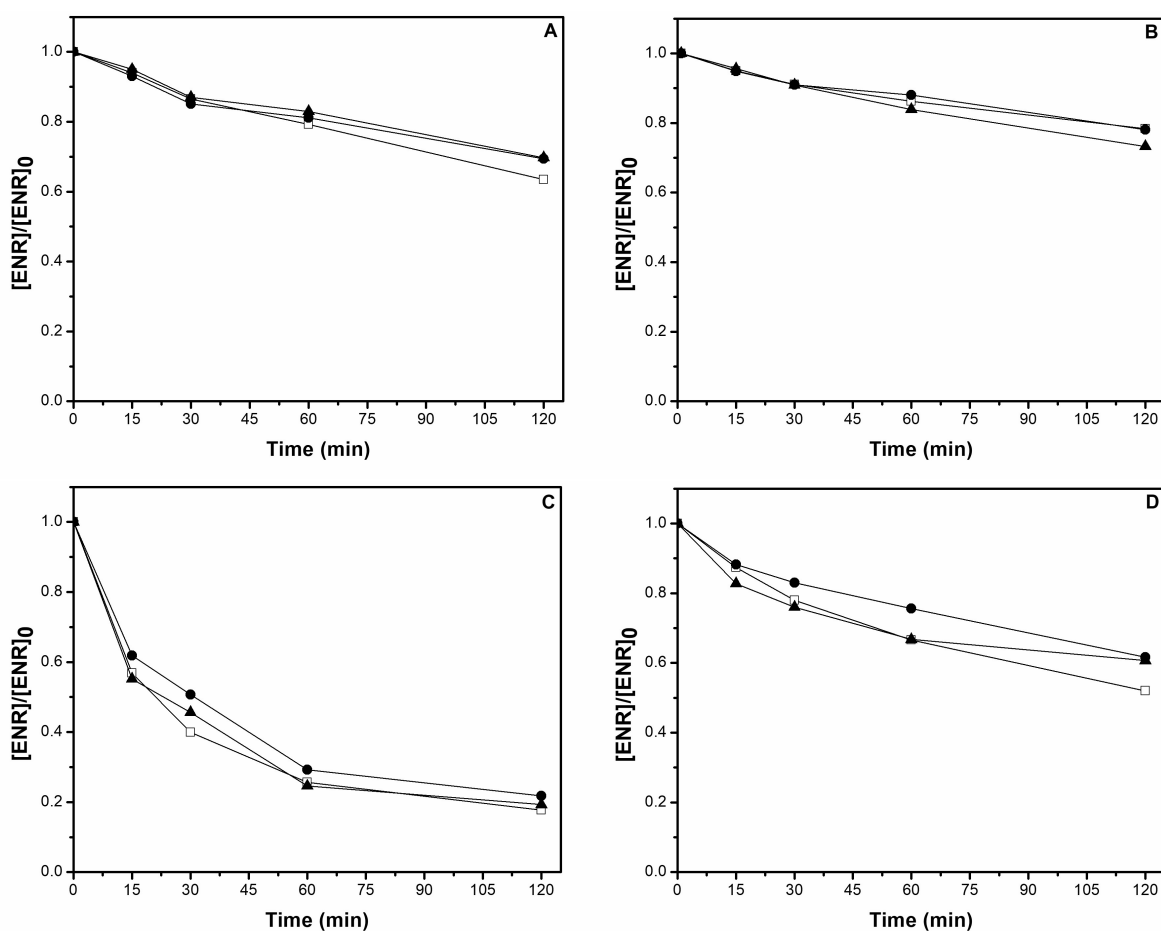


Figure S4.4.2: Effect of ROS scavenger addition (IPA 5 mM and FFA 300 μM) at aerated conditions. ENR degradation without scavenger addition (\square), with IPA (\bullet) and with FFA (\blacktriangle). A) ENR 300 μM pH 3.0; B) $\text{Fe}^{\text{III}}\text{-ENR}_3$ 100 μM pH 3.0; C) ENR 300 μM pH 7.0; D) $\text{Fe}^{\text{III}}\text{-ENR}_3$ 100 μM pH 7.0

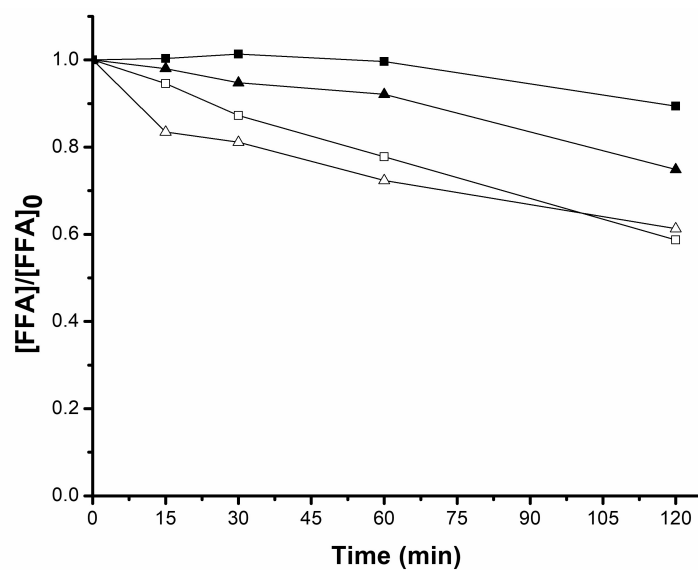


Figure S4.4.3: FFA 300 μM removal by $^1\text{O}_2$ generation at different tested conditions: ENR 300 μM pH 3.0 (\square), Fe^{III} -ENR₃ 100 μM pH 3.0 (\blacksquare), ENR 300 μM pH 7.0 (\triangle), Fe^{III} -ENR₃ 100 μM pH 7.0 (\blacktriangle). Control: FFA photodegradation alone at both studied pH was negligible (1-3% in 120 min).

spectrometry, which is in agreement with the spectral changes observed during photolysis of ENR and its complex (Figure 4.4.3A-B). However, this has not been detected at pH 7.0, whereas similar signal increase at 535 nm, but with lower intensity and resolution, had been seen. Dimer formation via FQ-radical coupling as a product of self-sensitization process has been also reported by other authors[30, 43, 52]

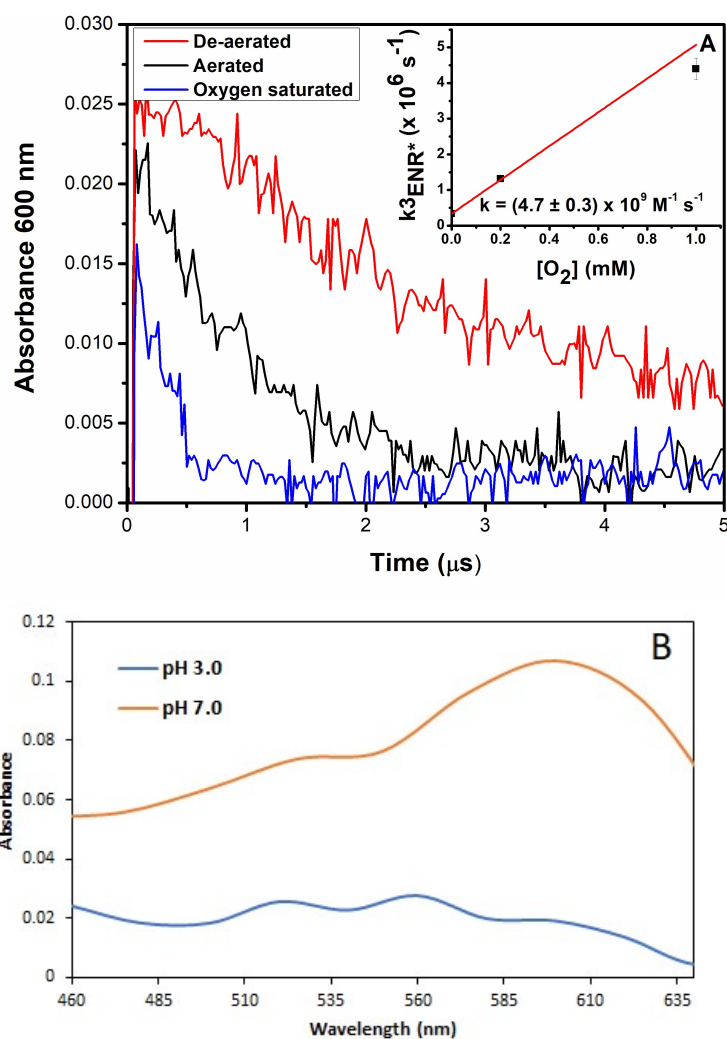
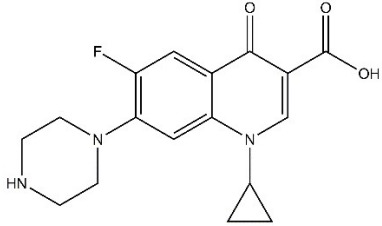
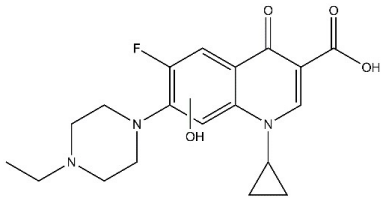
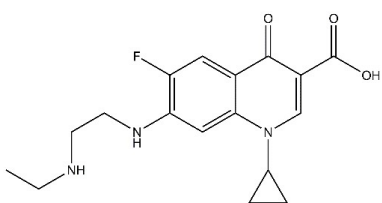
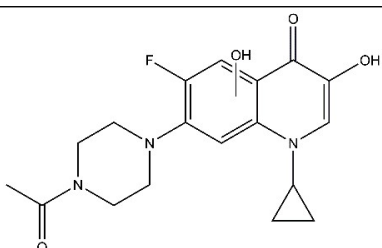
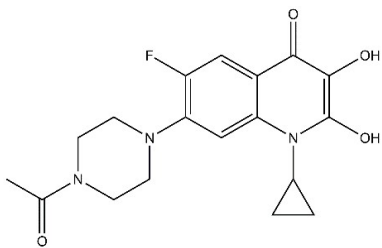
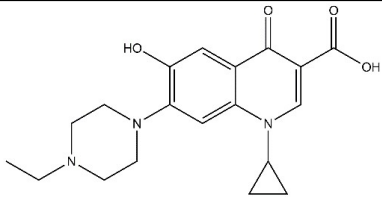
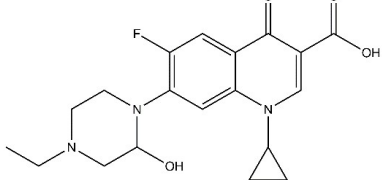
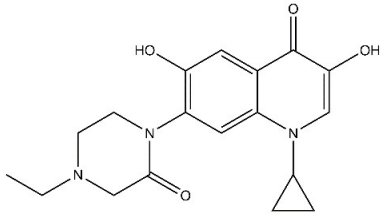
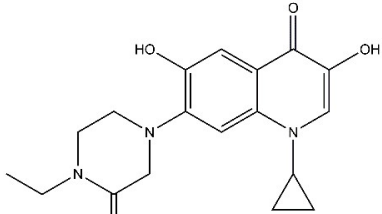
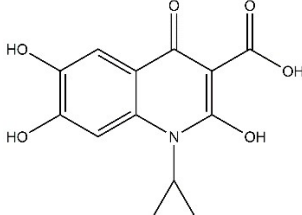
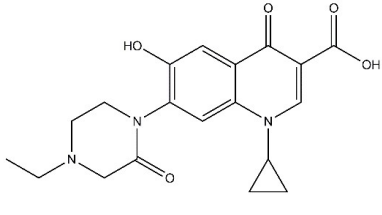
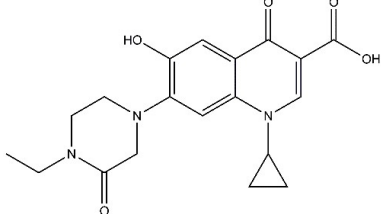
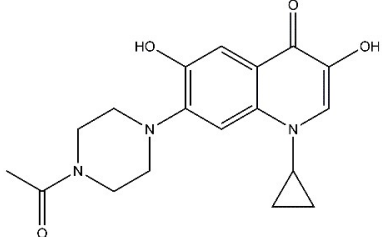


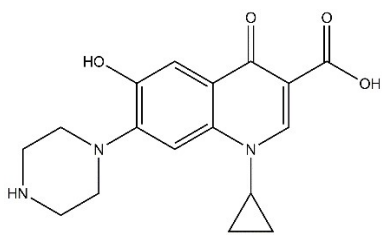
Figure S4.4.4: ENR 280 μM laser flash photolysis measurements: A) ${}^3\text{ENR}^*$ relaxation kinetics at pH 3.0 at de-aerated, aerated and oxygen saturated conditions, with ${}^3\text{O}_2$ quenching kinetic rate constant determination (inserted graph); B) ${}^3\text{ENR}^*$ absorbance spectra at both studied pH (measured at 0.09 μs)

Table S4.4.1: Elucidated major photoproducts in both systems ENR and $\text{Fe}^{\text{III}}\text{-ENR}_3$ and at both studied pHs. *not found

Name	Ret. Time (min)	m/z for $[\text{M}+\text{H}]^+$	Empirical formula of the neutral form	Fragment ion mass $[\text{F}+\text{H}]^+$	Raw formulas of fragment ions	Elucidated structure	Literature data
ENR	7.0	360.17207	$\text{C}_{19}\text{H}_{23}\text{FN}_3\text{O}_3$	342.165 316.184 314.169 245.110	$\text{C}_{19}\text{H}_{21}\text{FN}_3\text{O}_2$ $\text{C}_{14}\text{H}_{14}\text{FN}_2\text{O}$ $\text{C}_{18}\text{H}_{21}\text{FN}_3\text{O}$ $\text{C}_{18}\text{H}_{23}\text{FN}_3\text{O}$		

A	6.8	332.14072	$C_{17}H_{19}FN_3O_3$	288.153 268.147 245.110	$C_{16}H_{19}FN_3O$ $C_{16}H_{18}N_3O$ $C_{14}H_{14}FN_2O$		[14, 53–55]
B	7.0	376.16705	$C_{19}H_{23}FN_3O_4$	358.156 332.180 305.097 301.125 287.109 261.106 233.074	$C_{19}H_{21}FN_3O_3$ $C_{18}H_{23}FN_3O_2$ $C_{15}H_{14}FN_2O_4$ $C_{16}H_{16}FN_3O_2$ $C_{15}H_{14}FN_3O_2$ $C_{14}H_{14}FN_2O_2$ $C_{12}H_{10}FN_2O_2$		Analogous [30, 56]
C	6.7	334.15629	$C_{17}H_{21}FN_3O_3$	314.159 296.142 289.099 263.085 245.109 219.094 203.062	$C_{17}H_{20}N_3O_3$ $C_{17}H_{18}N_3O_2$ $C_{15}H_{14}FN_2O_3$ $C_{13}H_{12}FN_2O_3$ $C_{14}H_{14}FN_2O$ $C_{12}H_{12}FN_2O$ $C_{11}H_8FN_2O$		[48]
D	9.6	362.15137	$C_{18}H_{21}FN_3O_4$	344.143 316.111 263.084 248.061 230.050	$C_{18}H_{19}FN_3O_3$ $C_{16}H_{15}FN_3O_3$ $C_{13}H_{12}FN_2O_3$ $C_{12}H_9FN_2O_3$ $C_{12}H_7FN_2O_2$		*
M	10.3	362.15137	$C_{18}H_{21}FN_3O_4$	344.143 342.146 316.111 314.152 263.084 248.061 245.110 230.050	$C_{18}H_{19}FN_3O_3$ $C_{18}H_{20}N_3O_4$ $C_{16}H_{15}FN_3O_3$ $C_{17}H_{20}N_3O_3$ $C_{13}H_{12}FN_2O_3$ $C_{12}H_9FN_2O_3$ $C_{14}H_{14}FN_2O$ $C_{12}H_7FN_2O_2$		*
E	6.3	358.17624	$C_{19}H_{24}N_3O_4$	314.189 243.115 217.099	$C_{18}H_{24}N_3O_2$ $C_{14}H_{15}N_2O_2$ $C_{12}H_{13}N_2O_2$		[7, 48, 56–58]
F	6.8	376.16705	$C_{19}H_{24}N_3O_4$	358.159 314.169 285.129 257.111 229.079	$C_{19}H_{21}FN_3O_3$ $C_{18}H_{21}FN_3O$ $C_{16}H_{16}FN_3O$ $C_{15}H_{14}FN_2O$ $C_{13}H_{10}FN_2O$		Analogous [30]

G	9.2	344.16071	$C_{18}H_{22}N_3O_4$	326.152	$C_{18}H_{20}N_3O_3$		*
				316.168	$C_{17}H_{22}N_3O_3$		
				298.120	$C_{16}H_{16}N_3O_3$		
				230.070	$C_{11}H_7N_2O_2$		
				199.051	$C_{11}H_7N_2O_2$		
I	9.6	344.16071	$C_{18}H_{22}N_3O_4$	326.152	$C_{18}H_{20}N_3O_3$		*
				316.168	$C_{17}H_{22}N_3O_3$		
				298.120	$C_{16}H_{16}N_3O_3$		
				245.093	$C_{12}H_{10}N_2O_3$		
				230.070	$C_{11}H_7N_2O_2$		
				212.059	$C_{12}H_8N_2O_2$		
				199.051	$C_{11}H_7N_2O_2$		
H	8.7	278.06611	$C_{13}H_{12}NO_6$	260.057	$C_{13}H_{10}NO_5$		*
				237.029	$C_{10}H_7NO_6$		
				232.062	$C_{12}H_{10}NO_4$		
				219.018	$C_{10}H_5NO_5$		
				191.023	$C_9H_5NO_4$		
J	8.6	372.15576	$C_{19}H_{22}N_3O_5$	344.163	$C_{18}H_{22}N_3O_4$		*
				281.094	$C_{16}H_{13}N_2O_3$		
				273.089	$C_{14}H_{13}N_2O_4$		
				259.073	$C_{13}H_{11}N_2O_4$		
				241.062	$C_{13}H_9N_2O_3$		
				100.076	$C_5H_{10}NO$		
K	9.1	372.15576	$C_{19}H_{22}N_3O_5$	344.163	$C_{18}H_{22}N_3O_4$		*
				281.094	$C_{16}H_{13}N_2O_3$		
				273.089	$C_{14}H_{13}N_2O_4$		
				259.073	$C_{13}H_{11}N_2O_4$		
				241.062	$C_{13}H_9N_2O_3$		
				100.076	$C_5H_{10}NO$		
L	6.2	344.16071	$C_{18}H_{22}N_3O_4$	316.168	$C_{17}H_{22}N_3O_3$		*
				255.115	$C_{15}H_{15}N_2O_2$		
				227.120	$C_{14}H_{15}N_2O$		
				186.080	$C_{11}H_{10}N_2O$		
				100.076	$C_5H_{10}NO$		

N	6.1	330.14510	$C_{17}H_{20}N_3O_4$	312.136	$C_{17}H_{18}N_3O_3$		[7, 48, 59]
				287.104	$C_{15}H_{15}N_2O_4$		
				286.157	$C_{16}H_{20}N_3O_2$		
				261.089	$C_{13}H_{13}N_2O_4$		
				243.114	$C_{14}H_{15}N_2O_2$		
				229.098	$C_{13}H_{13}N_2O_2$		
				217.099	$C_{12}H_{13}N_2O_2$		
				202.075	$C_{11}H_{10}N_2O_2$		
				200.072	$C_{12}H_{10}NO_2$		

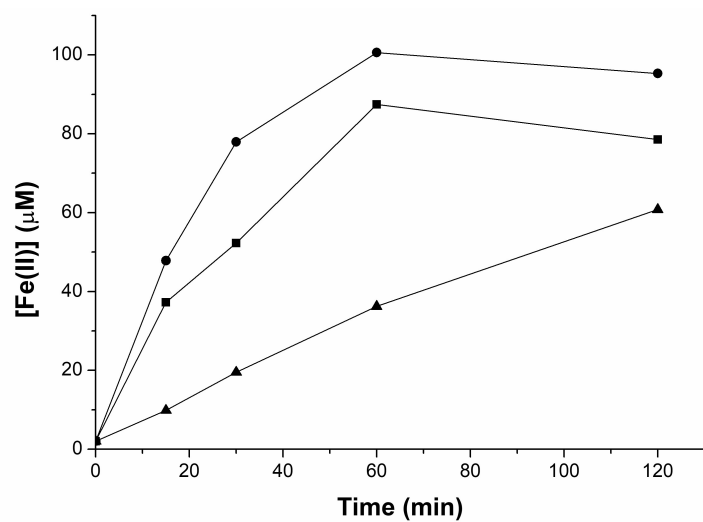


Figure S4.4.5: Fe(II) formation from Fe^{III} -ENR₃ ($[\text{Fe}(\text{III})]_0 = 100 \mu\text{M}$, $[\text{ENR}]_0 = 300 \mu\text{M}$) at pH 3.0 under irradiations in de-aerated (\bullet), aerated (\blacksquare) and oxygen saturated conditions (\blacktriangle)

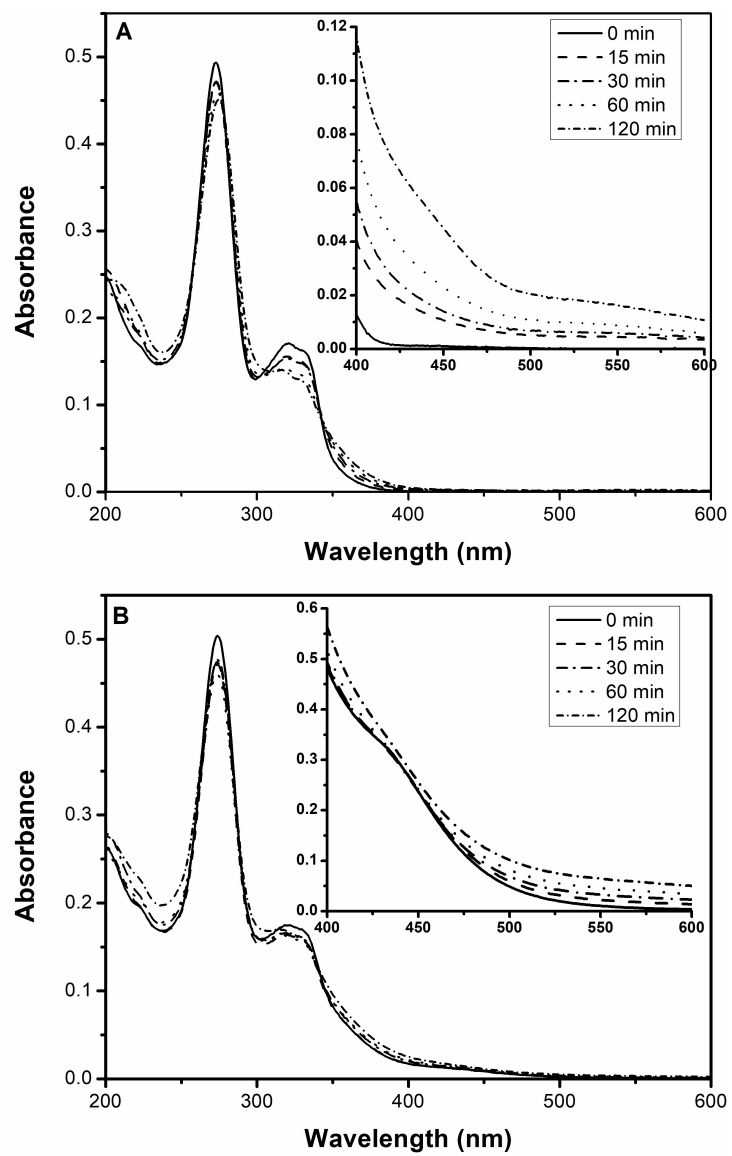


Figure S4.4.6: Changes on absorbance spectra during direct photolysis at pH 7.0 for (A) ENR 300 μ M and (B) Fe^{III}-ENR₃ 100 μ M. Full spectra were recorded by 20 times dilution of the original sample (inserted in the graph).

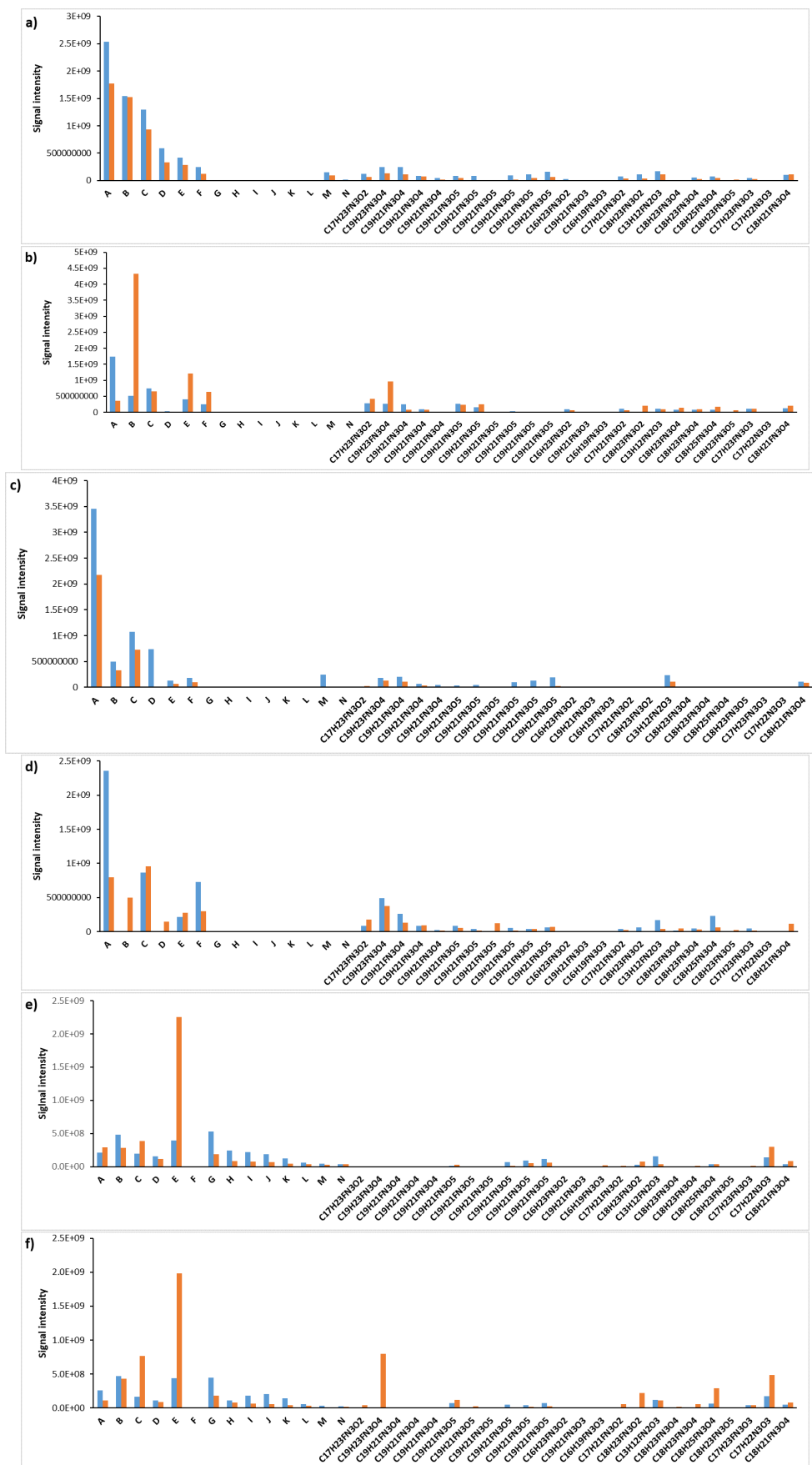


Figure S4.4.7: All detected photoproducts for ENR 300 μ M (blue) and Fe^{III}-ENR₃ 100 μ M (orange) after 120 min of: a) $h\nu$ pH 3.0; b) $H_2O_2 + h\nu$ pH 3.0; c) $h\nu + IPA$ pH 3.0; d) $h\nu + H_2O_2 + IPA$ pH 3.0; e) $h\nu$ pH 7.0; f) $H_2O_2 + h\nu$ pH 7.0

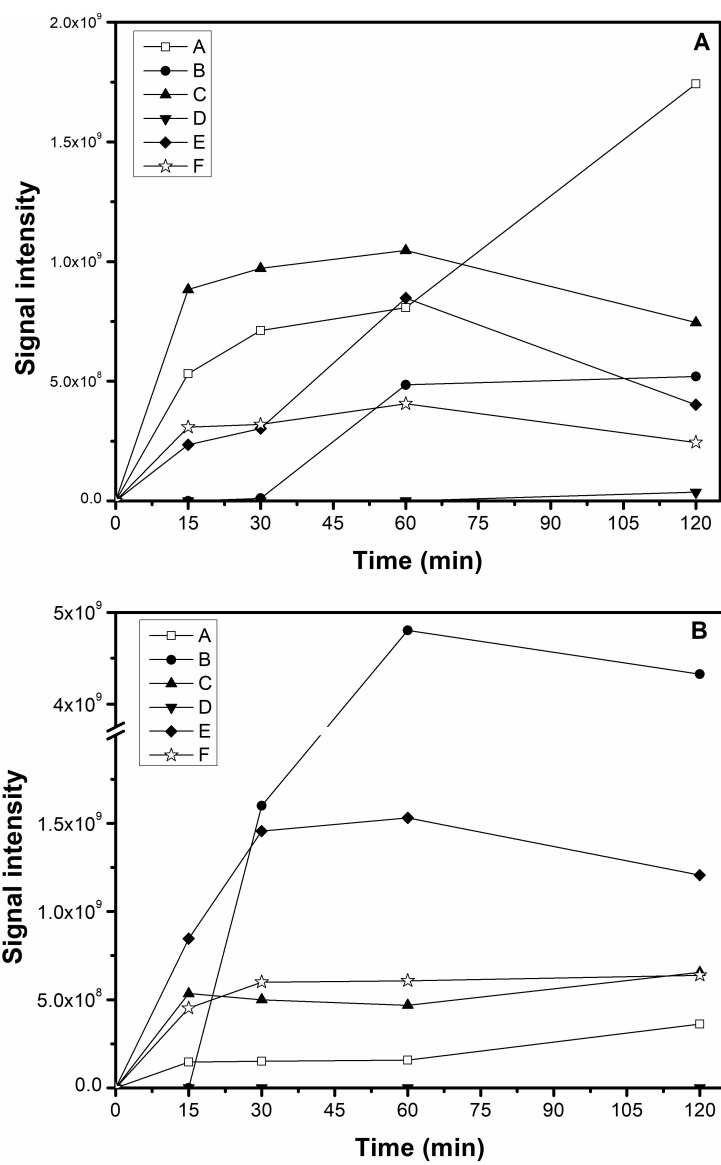


Figure S4.4.8: Photoproduct formation kinetics when H₂O₂ 200 μM was added at pH 3.0 to: A) ENR 300 μM , B) Fe^{III}-ENR₃ 100 μM

References

- [1] K Kümmerer. “The presence of pharmaceuticals in the environment due to human use - present knowledge and future challenges.” In: *J Environ Manag* 90.8 (2009), pp. 2354–2366. DOI: 10.1016/j.jenvman.2009.01.023.
- [2] BF Silva, A Jelic, R López-Serna, AA Mozeto, M Petrovic, and D Barceló. “Occurrence and distribution of pharmaceuticals in surface water, suspended solids and sediments of the Ebro river basin, Spain.” In: *Chemosphere* 85 (2011), pp. 1331–1339. DOI: 10.1016/j.chemosphere.2011.07.051.
- [3] P Verlicchi, M Al Aukidy, and E Zambello. “Occurrence of pharmaceutical compounds in urban wastewater: removal, mass load and environmental risk after a secondary treatment-A review.” In: *Sci Total Environ* 429 (2012), pp. 123–155. DOI: 10.1016/j.scitotenv.2012.04.028.
- [4] B Hamad. “The antibiotics market”. In: *Nat Rev Drug Discov* 9 (2010), pp. 675–676. DOI: 10.1038/nrd3267.
- [5] SR Batchu, VR Panditi, KE O’Shea, and PR Gardinali. “Photodegradation of antibiotics under simulated solar radiation: implications for their environmental fate.” In: *Sci Total Environ* 470–471 (2014), pp. 299–310. DOI: 10.1016/j.scitotenv.2013.09.057.
- [6] L Ge, G Na, S Zhang, K Li, P Zhang, H Ren, and Z Yao. “New insights into the aquatic photochemistry of fluoroquinolone antibiotics: direct photodegradation, hydroxyl-radical oxidation, and antibacterial activity changes.” In: *Sci Total Environ* 527–528 (2015), pp. 12–17. DOI: 10.1016/j.scitotenv.2015.04.099.
- [7] T Haddad and K Kümmerer. “Characterization of photo-transformation products of the antibiotic drug Ciprofloxacin with liquid chromatography-tandem mass spectrometry in combination with accurate mass determination using an LTQ-Orbitrap.” In: *Chemosphere* 115 (2014), pp. 40–46. DOI: 10.1016/j.chemosphere.2014.02.013.
- [8] L Aristilde and G Sposito. “Binding of ciprofloxacin by humic substances: a molecular dynamics study.” In: *Environ Toxicol Chem* 29.1 (2010), pp. 90–98. DOI: 10.1002/etc.19.
- [9] L Riaz, T Mahmood, A Khalid, A Rashid, MB Ahmed Siddique, A Kamal, and MS Coyne. “Fluoroquinolones (FQs) in the environment: a review on their abundance, sorption and toxicity in soil.” In: *Chemosphere* 191 (2018), pp. 704–720. DOI: 10.1016/j.chemosphere.2017.10.092.

- [10] X Van Doorslaer, J Dewulf, H Van Langenhove, and K Demeestere. “Fluoroquinolone antibiotics: an emerging class of environmental micropollutants.” In: *Sci Total Environ* 500–501 (2014), pp. 250–269. DOI: 10.1016/j.scitotenv.2014.08.075.
- [11] V Uivarosi. “Metal complexes of quinolone antibiotics and their applications: an update.” In: *Molecules* 18.19 (2013), pp. 11153–11197. DOI: 10.3390/molecules180911153.
- [12] A Cuprys, R Pulicharla, SK Brar, P Drogui, M Verma, and RY Surampalli. “Fluoroquinolones metal complexation and its environmental impacts.” In: *Coord Chem Rev* 376 (2018), pp. 46–61. DOI: 10.1016/j.ccr.2018.05.019.
- [13] S Wang, Z Wang, C Hao, and WJGM Peijnenburg. “DFT/TDDFT insights into effects of dissociation and metal complexation on photochemical behavior of enrofloxacin in water.” In: *Environ Sci Pollut Res* 25 (2018), pp. 30609–30616. DOI: 10.1007/s11356-018-3032-9.
- [14] S Snowberger, H Adejumo, K He, KP Mangalgiri, M Hopanna, AD Soares, and L Blaney. “Direct photolysis of fluoroquinolone antibiotics at 253.7 nm: specific reaction kinetics and formation of equally potent fluoroquinolone antibiotics.” In: *Environ Sci Technol* 50.17 (2016), pp. 9533–9542. DOI: 10.1021/acs.est.6b01794.
- [15] X Wei, J Chen, Q Xie, S Zhang, Y Li, Y Zhang, and H Xie. “Photochemical behavior of antibiotics impacted by complexation effects of concomitant metals: a case for ciprofloxacin and Cu(II)”. In: *Environ Sci Process Impacts* 17 (2015), pp. 1220–1227. DOI: 10.1039/c5em00204d.
- [16] U Hubicka, J Krzek, B Zuromska, M Walczak, M Zylewski, and D Pawłowski. “Determination of photostability and photodegradation products of moxifloxacin in the presence of metal ions in solutions and solid phase. Kinetics and identification of photoproducts,” in: *Photochem Photobiol Sci* 11 (2012), pp. 351–357. DOI: 10.1039/c1pp05259d.
- [17] M Salimi, A Esrafil, M Gholami, A Jonidi Jafari, R Rezaei Kalantary, M Farzadkia, M Kermani, and HR Sobhi. “Contaminants of emerging concern: a review of new approach in AOP technologies.” In: *Environ Monit Assess* 189.414 (2017). DOI: 10.1007/s10661-017-6097-x.
- [18] JJ Pignatello, E Oliveros, and A MacKay. “Advanced oxidation processes for organic contaminant destruction based on the fenton reaction and related chemistry.” In: *Crit Rev Environ Sci Technol* 36 (2006), pp. 1–84. DOI: 10.1080/10643380500326564.
- [19] AW Vermilyea and BM Voelker. “Photo-fenton reaction at near neutral pH.” In: *Environ Sci Technol* 43.18 (2009), pp. 6927–6933. DOI: 10.1021/es900721x.

- [20] Y Gou, P Chen, L Yang, S Li, L Peng, S Song, and Y Xu. “Degradation of fluoroquinolones in homogeneous and heterogeneous photo-Fenton processes: a review.” In: *Chemosphere* 270 (2020), p. 129481. DOI: 10.1016/j.chemosphere.2020.129481.
- [21] W Qiu, M Zheng, J Sun, Y Tian, M Fang, Zheng Y., Zhang T., and C Zheng. “Photolysis of enrofloxacin, pefloxacin and sulfaquinoxaline in aqueous solution by UV/H₂O₂, UV/Fe(II), and UV/H₂O₂/Fe(II) and the toxicity of the final reaction solutions on zebrafish embryos.” In: *Sci Total Environ* 651 (2019), pp. 1457–1468. DOI: 10.1016/j.scitotenv.2018.09.315.
- [22] I Sciscenko, S Garcia-Ballesteros, C Sabater, MA Castillo, C Escudero-Oñate, I Oller, and A Arques. “Monitoring photolysis and (solar photo)-Fenton of enrofloxacin by a methodology involving EEM-PARAFAC and bioassays: role of pH and water matrix.” In: *Sci Total Environ* 719 (2020), p. 137331. DOI: 10.1016/j.scitotenv.2020.137331.
- [23] W Huang, A Bianco, M Brigante, and G Mailhot. “UVA-UVB activation of hydrogen peroxide and persulfate for advanced oxidation processes: efficiency, mechanism and effect of various water constituents.” In: 347 (2018), pp. 279–287. DOI: 10.1016/j.jhazmat.2018.01.006.
- [24] Y Tao, M Brigante, H Zhang, and G Mailhot. “Phenanthrene degradation using Fe(III)-EDDS photoactivation under simulated solar light: a model for soil washing effluent treatment.” In: *Chemosphere* 236 (2019), p. 124366. DOI: 10.1016/j.chemosphere.2019.124366.
- [25] JS Renny, LL Tomasevich, EH Tallmadge, and DB Collum. “Method of continuous variations: applications of job plots to the study of molecular associations in organometallic chemistry.” In: *Angew Chem Int Ed* 52.46 (2013), pp. 11998–12013. DOI: 10.1002/anie.201304157.
- [26] GV Buxton, CL Greenstock, WP Helman, and AB Ross. “Critical Review of rate constants for reactions of hydrated electrons, hydrogen atoms and hydroxyl radicals ($\cdot\text{OH}/\cdot\text{O}$ -) in Aqueous Solution.” In: *J Phys Chem Ref Data* 17 (1988), pp. 513–886. DOI: 10.1063/1.555805.
- [27] WR Haag, J Hoigné, E Gassman, and AM Braun. “Singlet oxygen in surface waters - Part I: furfuryl alcohol as a trapping agent.” In: *Chemosphere* 13.5-6 (1984), pp. 631–640. DOI: 10.1016/0045-6535(84)90199-1.
- [28] AD Bokare and W Choi. “Singlet-oxygen generation in alkaline periodate solution.” In: *Environ Sci Technol* 49.24 (2015), pp. 14392–14400. DOI: 10.1021/acs.est.5b04119.

- [29] DE Latch, BL Stender, JL Packer, WA Arnold, and K McNeill. “Photochemical fate of pharmaceuticals in the environment: cimetidine and ranitidine.” In: *Environ Sci Technol* 37.15 (2003), pp. 3342–3350. DOI: 10.1021/es0340782.
- [30] Z Zhang, X Xie, Z Yu, and H Cheng. “Influence of chemical speciation on photochemical transformation of three fluoroquinolones (FQs) in water: kinetics, mechanism, and toxicity of photolysis products.” In: *Water Res* 148 (2019), pp. 19–29. DOI: 10.1016/j.watres.2018.10.027.
- [31] WR Haag and T Mill. “Rate constants for interaction of $^1\text{O}_2(^1\Delta_g)$ with azide ion in water.” In: *Photochem Photobiol* 45.3 (1987), pp. 317–321. DOI: 10.1111/j.1751-1097.1987.tb05381.x.
- [32] E Appiani, R Ossola, DE Latch, PE Erickson, and K McNeill. “Aqueous singlet oxygen reaction kinetics of furfuryl alcohol: effect of temperature, pH, and salt content.” In: *Environ Sci Process Impacts* 19 (2017), pp. 507–516. DOI: 10.1039/c6em00646a.
- [33] EK Efthimiadou, A Karaliota, and G Psomas. “Mononuclear metal complexes of the second-generation quinolone antibacterial agent enrofloxacin: synthesis, structure, antibacterial activity and interaction with DNA.” In: *Polyhedron* 27.6 (2008), pp. 1729–1738. DOI: 10.1016/j.poly.2008.02.006.
- [34] B Urbaniak and ZJ Kokot. “Analysis of the factors that significantly influence the stability of fluoroquinolone-metal complexes.” In: *Anal Chim Acta* 647 (2009), pp. 54–59. DOI: 10.1016/j.aca.2009.05.039.
- [35] A Stefánsson. “Iron(III) hydrolysis and solubility at 25°C.” In: *Environ Sci Technol* 41.17 (2007), pp. 6117–6123. DOI: 10.1021/es070174h.
- [36] M Bucheli-Witschel and T Egli. “Environmental fate and microbial degradation of aminopolycarboxylic acids.” In: *FEMS Microbiol Rev* 25.1 (2001), pp. 69–106. DOI: 10.1016/S0168-6445(00)00055-3.
- [37] Y Chen, A Wang, Y Zhang, R Bao, X Tian, and J Li. “Electro-Fenton degradation of antibiotic ciprofloxacin (CIP): formation of Fe^{3+} -CIP chelate and its effect on catalytic behavior of $\text{Fe}^{2+}/\text{Fe}^{3+}$ and CIP mineralization.” In: *Electrochim Acta* 256 (2017), pp. 185–195. DOI: 10.1016/j.electacta.2017.09.173.
- [38] S Miralles-Cuevas, I Oller, JAS Pérez, and S Malato. “Removal of pharmaceuticals from MWTP effluent by nanofiltration and solar photo-Fenton using two different iron complexes at neutral pH.” In: *Water Res* 64 (2014), pp. 23–31. DOI: 10.1016/j.watres.2014.06.032.

- [39] L Ge, C Halsall, CE Chen, P Zhang, Q Dong, and Z Yao. “Exploring the aquatic photodegradation of two ionisable fluoroquinolone antibiotics – gatifloxacin and balofloxacin: degradation kinetics, photobyproducts and risk to the aquatic environment.” In: *Sci Total Environ* 633 (2018), pp. 1192–1197. DOI: 10.1016/j.scitotenv.2018.03.279.
- [40] Y Li, J Niu, and W Wang. “Photolysis of Enrofloxacin in aqueous systems under simulated sunlight irradiation: kinetics, mechanism and toxicity of photolysis products.” In: *Chemosphere* 85.18 (2011), pp. 892–897. DOI: 10.1016/j.chemosphere.2011.07.008.
- [41] A Albini and S Monti. “Photophysics and photochemistry of fluoroquinolones.” In: *Chem Soc Rev* 32 (2003), pp. 238–250. DOI: 10.1039/b209220b.
- [42] XZ Niu, EG Moore, and JP Croué. “Excited triplet state interactions of fluoroquinolone norfloxacin with natural organic matter: a laser spectroscopy study.” In: *Environ Sci Technol* 52 (2018), pp. 10426–10432. DOI: 10.1021/acs.est.8b02835.
- [43] M Sturini, A Speltini, F Maraschi, A Profumo, L Pretali, E Fasani, and A Albini. “Photochemical degradation of marbofloxacin and enrofloxacin in natural waters.” In: *Environ Sci Technol* 44.12 (2010), pp. 4564–4569. DOI: 10.1021/es100278n.
- [44] A Bianco, M Passananti, H Perroux, G Vyard, C Mouchel-Vallon, N Chaumerliac, G Mailhot, L Deguillaume, and M. “Brigante A better understanding of hydroxyl radical photochemical sources in cloud waters collected at the puy de Dôme station - experimental versus modelled formation rates.” In: *Atmos Chem Phys* 15 (2015), pp. 9191–9202. DOI: 10.5194/acp-15-9191-2015.
- [45] A De Luca, RF Dantas, and S Esplugas. “Assessment of iron chelates efficiency for photo-Fenton at neutral pH.” In: *Water Res* 61 (2014), pp. 232–242. DOI: 10.1016/j.watres.2014.05.033.
- [46] W Huang, M Brigante, F Wu, C Mousty, K Hanna, and G Mailhot. “Assessment of the Fe(III)-EDDS complex in Fenton-like processes: from the radical formation to the degradation of bisphenol A.” In: *Environ Sci Technol* 47.4 (2013), pp. 1952–1959. DOI: 10.1021/es304502y.
- [47] L Santos-Juanes, AA Amat, and A Arques. “Strategies to drive photo-fenton process at mild conditions for the removal of xenobiotics from aqueous systems.” In: *Curr Org Chem* 21 (2017), pp. 1074–1083. DOI: 10.2174/1385272821666170102150337.
- [48] M Sturini, A Speltini, F Maraschi, A Profumo, L Pretali, EA Irastorza, E Fasani, and A Albini. “Photolytic and photocatalytic degradation of fluoroquinolones in untreated river water under natural sunlight.” In: *Appl Catal B Environ* 119–120 (2012), pp. 32–39. DOI: 10.1016/j.apcatb.2012.02.008.

- [49] O Abida, G Mailhot, M Litter, and M Bolte. “Impact of iron-complex (Fe(III)-NTA) on photoinduced degradation of 4-chlorophenol in aqueous solution.” In: *Photochem Photobiol Sci* 5.4 (2006), pp. 395–402. DOI: 10.1039/b518211e.
- [50] M Passananti, V Vinatier, AM Delort, G Mailhot, and M Brigante. “Siderophores in cloud waters and potential impact on atmospheric chemistry: photoreactivity of iron complexes under sun-simulated conditions.” In: *Environ Sci Technol* 50.17 (2016), pp. 9324–9332. DOI: 10.1021/acs.est.6b02338.
- [51] E Viollier, PW Inglett, K Hunter, AN Roychoudhury, and P Van Cappellen. “The Ferrozine method revisited.” In: *Appl Geochemistry* 15.6 (2000), pp. 785–790. DOI: 10.1016/S0883-2927(99)00097-9.
- [52] T Araki and H Kitaoka. “ESR Detection of Free Radical and Active Oxygen Species Generated during Photolysis of Fluoroquinolones.” In: *Chem Pharm Bull* 46.6 (1998), pp. 1021–1026. DOI: 10.1248/cpb.46.1021.
- [53] S Babić, M Periša, and I Škorić. “Photolytic degradation of norfloxacin, enrofloxacin and ciprofloxacin in various aqueous media.” In: *Chemosphere* 91.11 (2013), pp. 1635–1642. DOI: 10.1016/j.chemosphere.2012.12.072.
- [54] L Ge, J Chen, W Xiaoxuan, S Zhang, X Qiao, C Xiyun And, and X Qing. “Aquatic photochemistry of fluoroquinolone antibiotics: kinetics, pathways, and multivariate effects of main water constituents.” In: *Environ Sci Technol* 44.7 (2010), pp. 2400–2405. DOI: 10.1021/es902852v.
- [55] KH Wammer, AR Korte, RA Lundeen, JE Sundberg, K McNeill, and WA Arnold. “Direct photochemistry of three fluoroquinolone antibacterials: Norfloxacin, ofloxacin, and enrofloxacin.” In: *Water Res* 47.1 (2013), pp. 439–448. DOI: 10.1016/j.watres.2012.10.025.
- [56] T An, H Yang, G Li, W Song, WJ Cooper, and X Nie. “Kinetics and mechanism of advanced oxidation processes (AOPs) in degradation of ciprofloxacin in water.” In: *Appl Catal B Environ* 94.3-4 (2010), pp. 288–294. DOI: 10.1016/j.apcatb.2009.12.002.
- [57] J Porras, C Bedoya, J Silva-Agreto, A Santamaría, JJ Fernández, and RA Torres-Palma. “Role of humic substances in the degradation pathways and residual antibacterial activity during the photodecomposition of the antibiotic ciprofloxacin in water.” In: *Water Res* 94 (2016), pp. 1–9. DOI: 10.1016/j.watres.2016.02.024.
- [58] P Villegas-Guzman, S Oppenheimer-Barrot, J Silva-Agreto, and RA Torres-Palma. “Comparative Evaluation of Photo-Chemical AOPs for Ciprofoxacin Degradation: Elimination in Natural Waters and Analysis of pH Effect, Primary Degradation By-Products, and the Relationship with the Antibiotic Activity.” In: *Water Air Soil Pollut* 228 (2017), pp. 209–224. DOI: 10.1007/s11270-017-3388-3.

- [59] TG Vasconcelos, DM Henriques, A König, AF Martins, and K Kümmerer. “Photodegradation of the antimicrobial ciprofloxacin at high pH: Identification and biodegradability assessment of the primary by-products.” In: *Chemosphere* 76.4 (2009), pp. 487–493. DOI: 10.1016/j.chemosphere.2009.03.022.

4.5 Photodegradation of enrofloxacin in a pilot plant

During the project, a 3 months secondment was carried at a WWTP operated by the Spanish company Facsa in Alhama de Murcia. The aim was to optimize a pilot plant for different AOPs and direct photolysis to achieve efficient photodegradation of contaminants of emerging concern.

The optimization of the pilot plant was realized by monitoring the decoloration of an industrial dye, Rhodamine B. The decoloration was quantified based on the decay of a local absorption maximum of the dye at 554 nm, measured with UV-Vis spectroscopy. The optimized parameters were: water flow, airflow, catalyst, and hydrogen peroxide concentrations.

Different AOPs were tested in the pilot plant regarding their degradation efficiency on the artificial dye Rhodamine B (Figure 4.5.1). This was measured as the normalized absorption maximum of RhB, which is proportional to the concentration. It does not consider the possible mixture effect of potential photoproducts and serves as an indicator of efficiency.

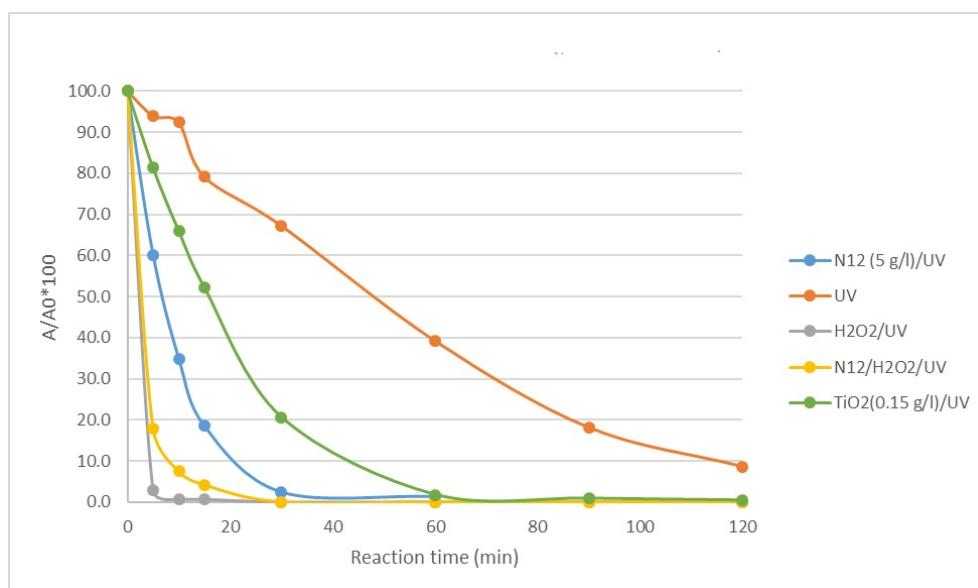


Figure 4.5.1: Efficiency of AOPs on the decoloration of Rhodamine B

The most efficient process under these conditions was the peroxide/UV system. This process has been extensively studied in the literature, and it is known that hydroxyl radicals are formed under such conditions, which react with the dye and degrade it. Adding TiO_2 coated magnetic nanoparticles (Magnox) in a mixture with H_2O_2 and irradiating it with UV light slightly slowed down the reaction. This can be explained by a competition mechanism or a Magnox particles' screening effect; no positive synergistic effect could be observed. The reaction with Magnox was faster than the reaction with TiO_2 alone. Both

conditions were optimized for their best performances, with a higher amount of catalyst in the process with Magnox (5 g/l). With TiO₂ alone (0.15 g/l), increasing further the catalyst concentration yielded a suspension of the nanoparticles in the water, resulting in a strong screening effect. There was no such issue with Magnox, which is made of TiO₂ suspended on magnetic microparticles.

After optimizing and comparing the different AOP processes, the photodegradation of different pharmaceutical compounds was realized; the example of enrofloxacin removal is reported in this section. In the article presented below, the applicability of the AOPs is discussed, considering the secondary treated wastewater effect on the removal efficiency.

Is the efficiency of a pilot plant advanced oxidation process strongly affected by matrix effects?

Zsuzsanna Varga^a, Iván Sciscenko^b, Francisco Valero^c, Stéphane Bouchonnet^a,

^a*Laboratoire de Chimie Moléculaire, CNRS / Ecole Polytechnique, Institut Polytechnique de Paris, 91128, Palaiseau, France*

^b*Departamento de Ingeniería Textil y Papelera, Universitat Politècnica de Valencia, Alcoy, Spain*

^c*Sociedad Fomento Agrícola Castellonense S.A. (FACSA), Alhama de Murcia, Spain*

Abstract

The setting up of a pilot plant equipped with an ultraviolet light (UV) lamp for various advanced oxidation processes (AOPs) has been previously reported. The present work aims at expanding this study by investigating the effect of a wastewater matrix on their performances. Firstly, the comparison of degradation efficiencies of different AOPs on Rhodamine B dye was performed in tapwater and secondary treated wastewater matrices. Wastewater matrix proved to strongly decrease Rhodamine B degradation when a TiO₂-based photocatalyst was used, whereas for H₂O₂-UV system this difference was slight, hence, the latter is less dependent on water matrix effect. Finally, the H₂O₂-UV system, was selected and applied to the degradation of an emerging contaminant, enrofloxacin. The degradation of this pollutant was followed by LC-MS and UV-Vis spectroscopy, and its mineralization by total organic carbon (TOC).

Introduction

Pharmaceuticals, flame retardants, plasticizers, among others, represent thousands of harmful or potentially toxic compounds that are commonly known as contaminants of emerging concern. These substances were detected in various wastewater treatment plants effluents, as they are resistant to conventional activated sludge treatments. As their mineralization is usually incomplete, their degradation frequently leads to by-products whose toxicity is not or poorly studied [1]. For most of these compounds, regulatory limits do

not exist and the toxicity of pollutant mixtures, with plausible synergism, as well as the effect of chronic exposures remains not well known [2, 3].

Antibiotics constitute a sub-class of compounds of particular concern, as their increasing presence in the environment leads to the formation of antibiotic-resistant strains [4]. Fluoroquinolones (FQs) rise a growing interest due to their high global consumption. Only in France, 3.6 tons of FQs are sold every year [5]. This class of antibiotics was widely detected in surface waters and wastewater treatment effluents [6, 7]. Their photodegradation mechanisms were investigated with emphasis towards the effect of common water constituents, such as natural organic matter (NOM), anions, and metals, on photolytic rates [8–11]. FQs are significantly adsorbed onto the activated sludge of wastewater treatment plants, which constitutes an additional potential way for their transport into the environment. Additionally, they have been shown to be toxic towards aquatic organisms [12]. The elimination of such micropollutants requires the development of novel water treatment processes or implementation of some existing ones.

Advanced oxidation processes (AOPs) are increasingly popular for the elimination of pollutants in water treatment plants. They rely on the generation of extremely reactive species, mainly hydroxyl radicals ($\bullet\text{OH}$). The high reactivity and low selectivity of $\bullet\text{OH}$ radicals make them ideal to remove various contaminants. Irradiation-based processes occupy a large place among AOPs [13]. Pollutants can be degraded using only ultraviolet (UV) light, but the various elements present in wastewater can exert both enhancing and hindering effects on the photodegradation of a contaminant. The photolysis process can be direct and/or indirect. For the latter, natural organic matter (NOM), nitrites, and nitrates when present, usually act as photosensitizers, as they contribute to generate reactive oxygen species (ROS) [14–16]. However, NOM can also decrease the photodegradation rate by producing light screening effect, reacting with ROS, or quenching the pollutant excited states [17]. In this case the polluting load should be lowered, to achieve efficient process with lower amount of added chemicals, thus achieving cost-effectiveness [18]. In addition, chloride, bromide, and phosphates can also impact the photolysis process, for example by scavenging the aforementioned ROS [19, 20]. Since it is difficult to determine all the components of an aqueous matrix and to determine the extent of the opposing contributing factors to the photodegradation, the overall effect of the aqueous matrix was measured on the degradation of enrofloxacin. The tested AOPs were carried out with a UVC lamp in a pilot plant previously described in detail [21] and presented in SI-2 and Figure S4.5.2. Tested AOPs were based on the use of UVC, UVC/ H_2O_2 , and heterogeneous photocatalysis.

Materials and methods

Rhodamine B (AppliChem PanReac, Barcelona, Spain) and enrofloxacin (Sigma Aldrich, Madrid, Spain) were used to test the efficiency of the various water treatment processes. A 33% w/v solution of H₂O₂ technical grade (VWR chemicals, Barcelona, Spain) and 5 mg/L starting concentration of dye and enrofloxacin were used to test the H₂O₂/UV system in the pilot plant. Peroxide amounts were added based on the stoichiometry of expected reactions (See eq. 4.11 and 4.12), so that mineralization should be theoretically achieved. Secondary treated wastewater was obtained from direct pipeline connection to the Alhama de Murcia wastewater treatment plant, it was mainly of industrial origin and went through the following steps before reaching the reactor: pretreatment (screening, sand, and grease removal), biological treatment, decantation, and filtration. The wastewater was characterized over a period of 4 months by measuring turbidity, chemical oxygen demand (COD), biochemical oxygen demand (BOD₅), total organic carbon (TOC), and nitrogen content; results are reported in Table S4.5.1.

UV-Vis analyses were performed on a DR6000 benchtop spectrophotometer (Hach-Lange, Colorado, USA). Measurements were carried out using a 1 cm cell and normalized based on the absorbance of the reference matrix. Spectra of the solution were recorded using UV-Vis spectroscopy, on a wavelength range from 190 to 500 nm. Rhodamine B discoloration was monitored in single wavelength mode and its absorption maximum wavelength (554 nm, see Figure S4.5.1) was selected for quantification. TOC measurements were carried out on a Shimadzu TOC-V instrument (Kyoto, Japan), the sampling was done at the beginning of the experiment (t₀) and after 2 hours of reaction. Degradation of enrofloxacin was monitored by LC-HRMS using an Acquity HPLC system (Waters Technologies, Guyancourt, France) coupled with a Bruker SolarixXR FT-ICR 9.4 T MS instrument (Bruker Daltonics, Bremen, Germany) (see parameters in SI-3).

In one of the applied AOPs Magnox were utilized as photocatalyst, these are magnetic microparticles, coated with TiO₂. Information about the pilot plant used, working conditions, and Magnox photocatalyst characterization has been previously described by Sciscenko et al [21]. A brief description of the plant and the applied working parameters are presented in the supplementary information SI-2. Efficiencies of the various AOPs were estimated based on the discoloration of Rhodamine B dye. The approach consisting in using a dye to monitor an AOP is affordable, fast, and suitable for industrial applications [22, 23]. Discoloration is an indicator of the efficiency of degradation of the dye as it is correlated with structural changes in the molecule. However, it is not suitable to measure mineralization as potential transformation products may be produced.

Results and discussion

Matrix effect

Figure 4.5.2 shows the kinetics of Rhodamine B in tapwater and wastewater under three different treatment processes: UVC, UVC/H₂O₂, and heterogeneous photocatalysis using Magnox. Decolorization rate of Rhodamine B was the least efficient under UV irradiation alone in tapwater. Combining UV irradiation with hydrogen-peroxide or Magnox significantly improved the degradation efficiency: it takes about 50 minutes to remove half of the initial amount of Rhodamine B from tapwater with UV, against 10 and 5 minutes with UV/Magnox and UVC/H₂O₂, respectively. The UVC/H₂O₂ system showed the best efficiency on both tapwater and wastewater reaction even if its performance is slightly decreased in wastewater. On the contrary, the efficiency of heterogeneous photocatalysis with Magnox was considerably decreased in wastewater treatment: 40 minutes are needed to degrade by half the initial amount of Rhodamine in wastewater against 10 minutes in tapwater. The strong difference between the results obtained with UV/H₂O₂ and heterogeneous photocatalysis suggest that the available reactive surface of Magnox might be decreased due to possible absorption/adsorption of matrix molecules on it, and consequently, reducing the •OH generation. More generally these results indicate that a UVC/H₂O₂-type treatment can be efficiently applied in a complex matrix, whereas the application of heterogeneous photocatalysis with Magnox should be conducted after removing as many interferents as possible via filtration. Following global changes in wastewater, such as the formation of undesired by-products, remains a great analytical challenge as the complexity of the matrix makes the assessment very difficult. There is a limited number of studies related to the formation of potentially harmful by-products as a result of treatment with AOPs. This aspect requires further investigation combining high-resolution mass spectrometry with advanced data processing.

Degradation of enrofloxacin

The UVC/H₂O₂ system proved to be the most simple and efficient method for the decolorization of Rhodamine B; its efficiency was thus tested on the removal of enrofloxacin in both tapwater and wastewater matrices. Here again, the main goal of these experiments was to study a potential matrix effect on the degradation efficiencies of this process regarding enrofloxacin degradation. The reaction was carried under UV irradiation as well, to prove the potential benefits of adding hydrogen peroxide to the mixture.

In all cases, enrofloxacin was not detected by LC-MS after 60 minutes of reaction (Figure 4.5.3). The UVC/H₂O₂ process allowed to reach 100% of removal after only 7.5 minutes of reaction in tapwater. There is an improvement yielded by the addition of peroxide, that shows the strong oxidizing power and low selectivity of hydroxyl radicals. The UVC/H₂O₂ process was not significantly impacted by the nature of the aqueous matrix. Considering the aforementioned strong matrix effect, it can be suggested that this apparent lack of

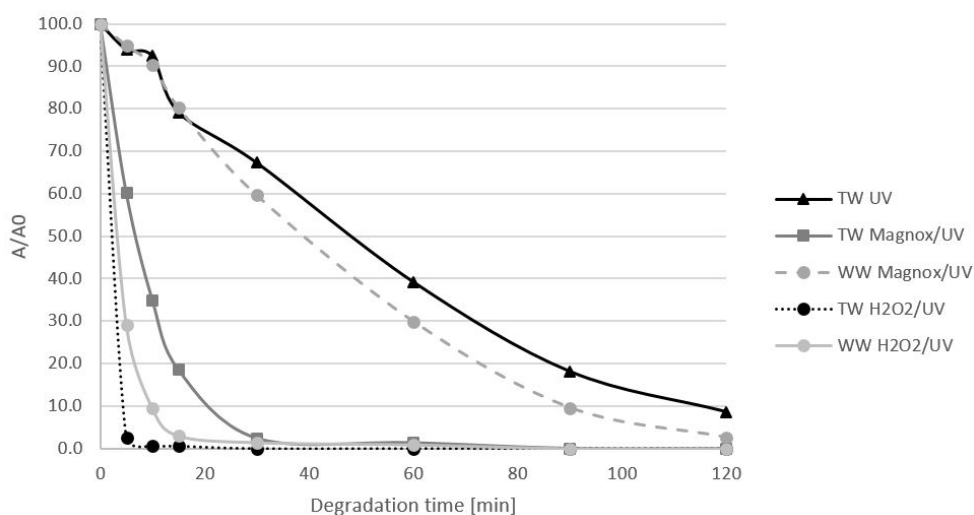


Figure 4.5.2: Degradation kinetics of Rhodamine B in tapwater (TW) and wastewater (WW) matrices, under three different treatment processes: UVC alone, UVC/H₂O₂ and UVC with heterogeneous photocatalysis using Magnox

effect would actually be the result of opposing effects in balance. Looking at the parameters of the secondary treated wastewater (see Table S4.5.1), an assessment can be made about such potential effects. On one hand, reactive species can react competitively with the components of wastewater and enrofloxacin. For instance, chlorides and phosphates, which are present in the wastewater, were shown to scavenge reactive oxygen species [13, 20]. The turbidity of the water can also induce a filtering effect. On the other hand, natural organic matter can improve reaction rates by acting as photosensitizer. The result of TOC analysis reveals a partial loss in total organic carbon content in the wastewater (from 29.3 mg/L to 12.2 mg/L with the UVC/H₂O₂ system) - indicating that organic compounds present in the wastewater were mineralized - while the TOC remained constant in tapwater. Therefore, enrofloxacin mineralization is negligible in both cases and photoproducts formation likely occurred, as previously reported [9]. In the UV-Vis spectra evolution, the typical absorbance bands decrease considerably at all wavelengths (see Figure S4.5.3). The three local maxima, observed at 270, 322, and 334 nm belong to enrofloxacin. These specific features all disappear after the process, meaning that there are considerable differences between the structure of enrofloxacin and that of the potential photoproducts, and no highly conjugated aromatic system remains.

Conclusion

Three AOPs were compared in terms of discoloration of Rhodamine B in tapwater and wastewater matrices. The process with the highest overall discoloration rate was the one associating UVC/H₂O₂, which was efficient even in a highly complex wastewater matrix, whereas the activity of the Magnox catalyst was hindered under such conditions. The applicability of photocatalysts appears to be restricted by potential water constituents

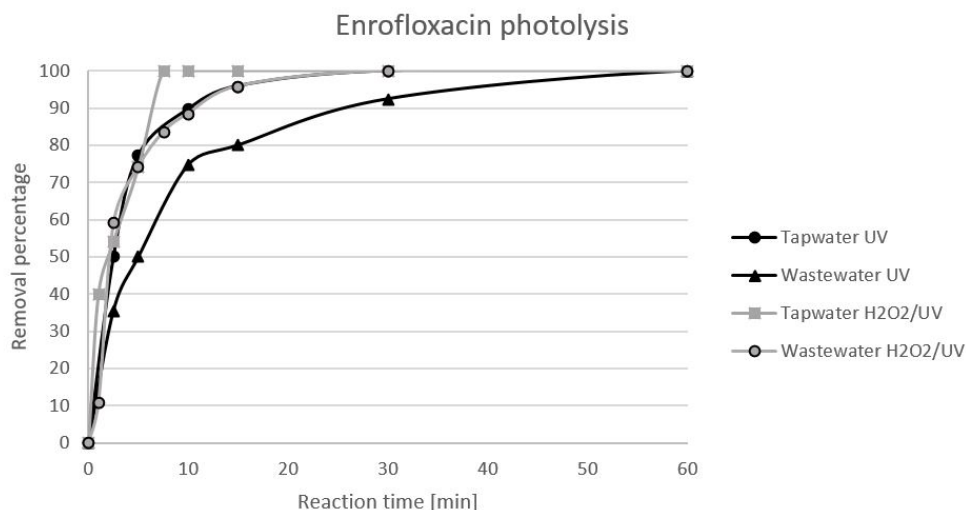


Figure 4.5.3: LC-MS monitoring of enrofloxacin removal using a peroxide/UV AOP

absorption or adsorption phenomena; a screening effect of the wastewater components could be involved in a lesser extent. The use of heterogeneous photocatalysis should be restricted to wastewater partly purified in natural organic matter content by previous filtration. The UVC/H₂O₂ process was tested on enrofloxacin; it permitted a total elimination of this antibacterial drug in less than half an hour in both tapwater and wastewater matrices.

Supplementary information

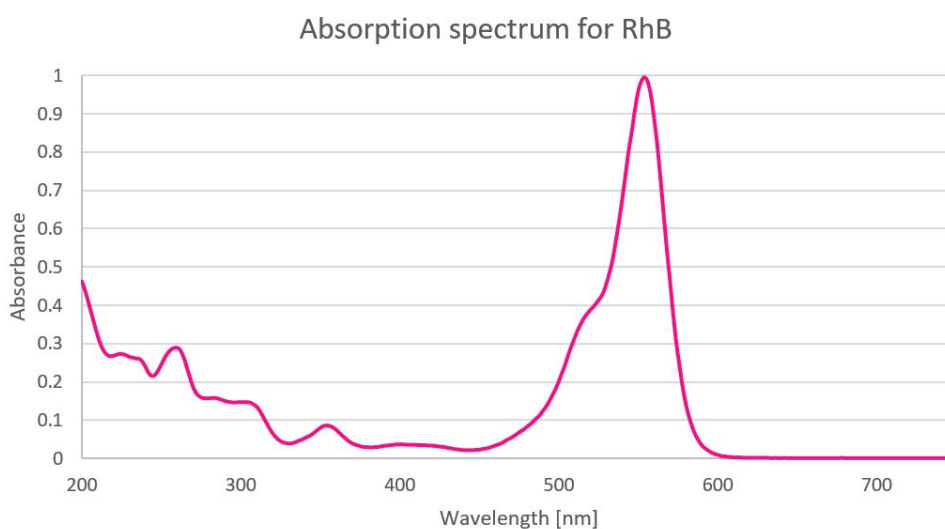


Figure S4.5.1: UV-Vis absorption spectrum of Rhodamine B

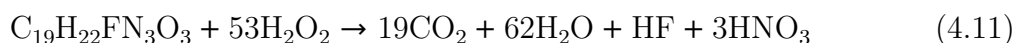
Table S4.5.1: Wastewater characterization

Sampling date	pH	Conductivity μS/cm	Turbidity FNU	COD mg/L	BOD5 mg/L	TOC mg/L	Total nitrogen mg/L	Total phosphorus mg/L
19/11/19	7.4	2337.9	6	46	<5	15.8	2.3	3.6
11/12/19	7.4	2640.2	4.5	42	7	14.3	3.1	3.6
18/12/19	7.4	2933.6	4.4	36	<5	15.0	2.9	3.5
08/01/20	7.4	2712.5	4.2	33	<5	12.0	2.1	0.7
29/01/20	7.4	2742.7	4.1	38	<5	14.6	0	0.5
13/02/20	7.4	3221.5	7.3	60	8	16.3	0	3.5

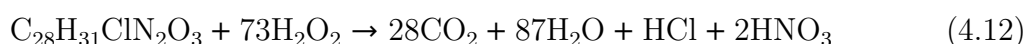
Sampling date	Sulfates mg/L	Chloride mg/L	Nitrites mg/L	Total calcium mg/L	Total Magnesium mg/L	Total Sodium mg/L	Total Iron mg/L	
19/11/19	353.2	368.4	0.4	95.9	65.4	253.5	0.08	
11/12/19	429.8	432.5	0.3	102.5	77.6	317.2	0.08	
18/12/19	483.0	494.1	0.7	105.2	72.8	388.9	0.08	
08/01/20	435.5	479.9	0.2	97.4	72.2	372.0	0.04	
29/01/20	492.0	472.0	0.4	110.6	89.3	329.0	0.09	
13/02/20	3.5	583.5	566.4	0.2	114.2	94.1	429.3	0.28

1. Chemical reactions for the calculations of peroxide stoichiometry

Reaction of enrofloxacin with peroxide:



Reaction of Rhodamine B with peroxide:



2. Pilot plant description

The pilot plant included a tank for mixing with a stirrer, a UV lamp reactor, a model UVLA-325-4 controlled by a Synergy 3 control panel (atg UV Technology, Wigan, United Kingdom), a pump for water circulation, a rotameter to assess the water flow, and a compressor (metabo Basic 250-50 W. Nürtingen, Germany) to provide airflow in the reactor. The use of air in the photoreactor was especially useful to keep the solid catalysts suspended and for more efficient mixing. The total volume of the reactor system was approximately 45 liters, this was the volume of the added water. The variables in the reactor were optimized as follows: water flow 400 l/h, airflow 28 l/min, contaminant concentration 5 mg/L each, Magnox concentration 5 g/L, and water matrix (tap water or wastewater). The pH was not altered; it remained in the range of 7.5-8.5 over all the experiments. The reaction time was 2 hours for every cycle, with a higher sampling



Figure S4.5.2: Pilot plant

frequency at the beginning of the reaction.

3. LC-MS analysis

LC-MS measurements were performed on an Acquity HPLC system (Waters Technologies, Guyancourt, France) coupled with a Bruker SolarixXR FT-ICR 9.4 T MS instrument (Bruker Daltonics, Bremen, Germany). For hyphenated methods, an Agilent Pursuit XR-SULTRA C18 (length 50 mm, diameter 2 mm, particle size 2.8 μm) column was used with an Agilent HPLC MetaGuard (Pursuit XRs C18, 3 μm , 2,0 mm) guard column (Agilent Technologies, Les Ulis, France). The flow was set to 0.2 mL/min, the total run time was 22 minutes with an acquisition time of 15 minutes. Solvent A was water with 0.1% formic acid and solvent B was acetonitrile with 0.1% formic acid. The gradient started and was kept until 3 minutes at 95% of solvent A, then this was lowered and reached 50% at 12 minutes. From 12.1 until 17.1 minutes the amount of solvent A was lowered to 5%, and then switched back to the starting conditions. The injection volume was 1 μl , each sample was prepared for the analysis by adding 10% volume of a mixture of acetonitrile/formic acid (0.1%). Electrospray ionization was used as the ion source in positive mode with a sample flow of 0.2 mL/min. The capillary voltage was 4000 V and the spray shield was set at -500 V. Nitrogen was used as nebulizer gas (1 bar) and drying gas (8 L/min, 250 $^{\circ}\text{C}$). The detection range was 57.7 – 1000 m/z, in broadband mode, with a data acquisition size of 4 Mpts and a data reduction of noise of 97%.

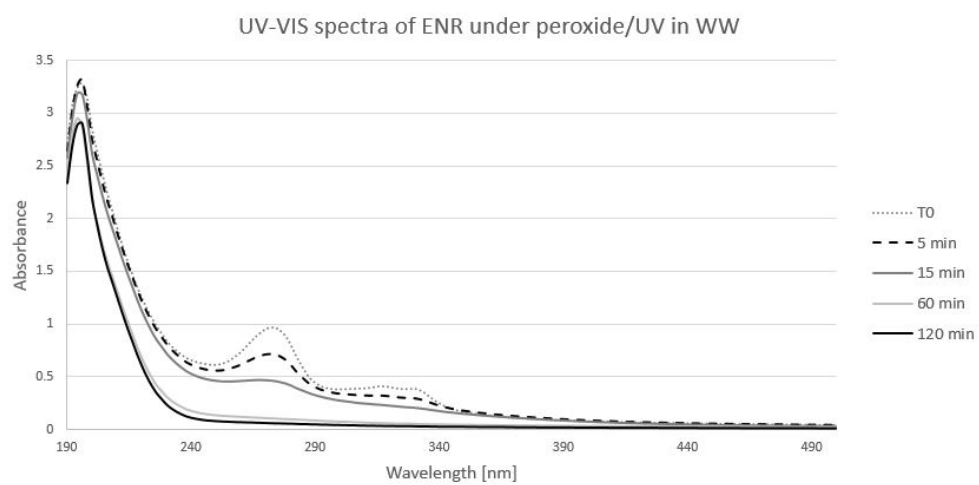


Figure S4.5.3: Degradation of enrofloxacin in wastewater with UV-VIS spectroscopy

References

- [1] K. Kummerer. In: *Pharmaceuticals in the Environment: Sources, fate, effects and risks*. Vol. 17. Berlin, Heidelberg: Springer Verlag, 2001. DOI: 10.1007/978-3-540-74664-5.
- [2] PE Stackelberg, ET Furlong, MT Meyer, SD Zaugg, AK Henderson, and DB Reissman. “Persistence of pharmaceutical compounds and other organic wastewater contaminants in a conventional drinking-water-treatment plant”. In: *Sci Total Environ* 329.1-3 (2004), pp. 99–113. DOI: 10.1016/j.scitotenv.2004.03.015.
- [3] KM Blum, PL Andersson, G Renman, L Ahrens, M Gros, K Wiberg, and P Haglund. “Non-target screening and prioritization of potentially persistent, bioaccumulating and toxic domestic wastewater contaminants and their removal in on-site and large-scale sewage treatment plants”. In: *Sci Total Environ* 575 (2017), pp. 265–275. DOI: 10.1016/j.scitotenv.2016.09.135.
- [4] SD Richardson and TA Ternes. “Water analysis: emerging contaminants and current issues”. In: *Anal Chem* 77.12 (2005), pp. 3807–3838. DOI: 10.1021/ac058022x.
- [5] T Trouchon and S Lefebvre. “A Review of Enrofloxacin for Veterinary Use”. In: *Open J Vet Med* 6 (2016), pp. 40–58. DOI: 10.4236/ojvm.2016.62006.
- [6] H Nakata, K Kannan, PD Jones, and JP Giesy. “Determination of fluoroquinolone antibiotics in wastewater effluents by liquid chromatography-mass spectrometry and fluorescence detection”. In: *Chemosphere* 58.6 (2005), pp. 759–766. DOI: 10.1016/j.chemosphere.2004.08.097.
- [7] Y Xiao, H Chang, A Jia, and J Hu. “Trace analysis of quinolone and fluoroquinolone antibiotics from wastewaters by liquid chromatography-electrospray tandem mass spectrometry”. In: *J Chromatogr A* 1214.1-2 (2008), pp. 100–108. DOI: 10.1016/j.chroma.2008.10.090.
- [8] M Sturini, A Speltini, F Maraschi, L Pretali, A Profumo, E Fasani, A Albini, E Nucleo, and R Migliavacca. “Photodegradation of fluoroquinolones in surface water and antimicrobial activity of the photoproducts”. In: *Water Research* 46.17 (2012), pp. 5575–5582. DOI: 10.1016/j.watres.2012.07.043.
- [9] I Sciscenko, A Arques, Z Varga, S Bouchonnet, O Monfort, M Brigante, and G Mailhot. “Significant role of iron on the fate and photodegradation of enrofloxacin”. In: *Chemosphere* 270 (2021), p. 129791. DOI: 10.1016/j.chemosphere.2021.129791.
- [10] L Aristilde and G Sposito. “Binding of ciprofloxacin by humic substances: a molecular dynamics study”. In: *Environ Toxicol Chem* 29.1 (2010), pp. 90–98. DOI: 10.1002/etc.19.

- [11] EM Golet, I Xifra, H Siegrist, AC Alder, and W Giger. “Environmental exposure assessment of fluoroquinolone antibacterial agents from sewage to soil”. In: *Environ Sci Technol* 37.15 (2003), pp. 3243–3249. DOI: 10.1021/es0264448.
- [12] AA Robinson, JB Belden, and MJ Lydy. “Toxicity of fluoroquinolone antibiotics to aquatic organisms”. In: *Environ Toxicol Chem* 24.2 (2005), pp. 423–430. DOI: 10.1897/04-210r.1.
- [13] S Babić, M Periša, and I Škorić. “Photolytic degradation of norfloxacin, enrofloxacin and ciprofloxacin in various aqueous media”. In: *Chemosphere* 91.11 (2013), pp. 1635–1642. DOI: 10.1016/j.chemosphere.2012.12.072.
- [14] D Fatta-Kassinos, MI Vasquez, and K Kümmerer. “Transformation products of pharmaceuticals in surface waters and wastewater formed during photolysis and advanced oxidation processes - degradation, elucidation of byproducts and assessment of their biological potency”. In: *Chemosphere* 85.5 (2011), pp. 693–709. DOI: 10.1016/j.chemosphere.2011.06.082.
- [15] JP Hassett. “Dissolved natural organic matter as a microreactor”. In: *Science* 311.5768 (2006), pp. 1723–1724. DOI: 10.1126/science.1123389.
- [16] J Mack and JR Bolton. “Photochemistry of nitrite and nitrate in aqueous solution: a review”. In: *J Photochem Photobiol A* 128.1-3 (1999), pp. 1–13. DOI: 10.1016/S1010-6030(99)00155-0.
- [17] XZ Niu, EG Moore, and JP Croué. “Excited Triplet State Interactions of Fluoroquinolone Norfloxacin with Natural Organic Matter: A Laser Spectroscopy Study”. In: *Environ Sci Technol* 52.18 (2018), pp. 10426–10432. DOI: 10.1021/acs.est.8b02835.
- [18] R Andreozzi, V Caprio, A Insola, and M Raffaele. “Advanced oxidation processes (AOP) for water purification and recovery”. In: *Catal Today* 53.1 (1999), pp. 51–59. DOI: 10.1016/S0920-5861(99)00102-9.
- [19] R Andreozzi, M Raffaele, and P Nicklas. “Pharmaceuticals in STP effluents and their solar photodegradation in aquatic environment”. In: *Chemosphere* 50.10 (2003), pp. 1319–1330. DOI: 10.1016/s0045-6535(02)00769-5.
- [20] E Fasani, M Mella, S Monti, and A Albini. “Unexpected Photoreactions of Some 7-Amino-6-fluoroquinolones in Phosphate Buffer”. In: *Eur J Org Chem* 2001.2 (2001), pp. 391–397. DOI: 10.1002/1099-0690(200101)2001:2<391::AID-EJOC391>3.0.CO;2-R.
- [21] I Sciscenko, S Mestre, J Climent, F Valero, C Escudero-Oñate, I Oller, and A Arques. “Magnetic Photocatalyst for Wastewater Tertiary Treatment at Pilot Plant Scale: Disinfection and Enrofloxacin Abatement”. In: *Water* 13.3 (2021), p. 329. DOI: 10.3390/w13030329.

- [22] E Basturk and M Karatas. “Decolorization of antraquinone dye Reactive Blue 181 solution by UV/H₂O₂ process”. In: *J Photochem Photobiol A* 299 (2015), pp. 67–72. DOI: 10.1016/j.jphotochem.2014.11.003.
- [23] MS Lucas and JA Peres. “Decolorization of the azo dye Reactive Black 5 by Fenton and photo-Fenton oxidation”. In: *Dyes Pigm* 71.3 (2006), pp. 236–244. DOI: 10.1016/j.dyepig.2005.07.007.



Chapter 5

Untargeted approach using SPIX

5.1 Introduction of Spix

With the development and evolution of HRMS techniques and instrumentation performance, the amount of data obtained from each measurement is sharply increasing. It is of high interest to combine data analysis with mass spectrometry to extract the maximum amount of pertinent information from each spectrum or series of spectra. Both commercial and open-source data analysis tools are being developed to meet the analytical needs. In the framework of a collaboration with the Institut national de recherche en sciences et technologies du numérique (INRIA) and Centre de Mathématiques Appliquées de l'École polytechnique (CMAP), we aimed to develop a new software, SPIX. The concept behind this software is novel, as it aims to model reaction kinetics in complex mixtures. It is a unique feature and helps with understanding chemical changes through a holistic approach. This software's development was driven by our data analysis needs, but as software undergo continuous development and updates, SPIX is no different; therefore, various future features are envisaged.

The software shows the statistically relevant changes between two sets of spectra or models the changes through a series of conditions. In this project, as the aim was to study the photochemical reactions of contaminants of emerging concern, SPIX became a valuable tool to model the kinetics of degradation of the parent compound and detect the molecular ions that undergo change over time, thus aiding in the rapid identification of photoproducts. This result chapter is divided into three parts. The first part introduces general considerations and features of the software, such as data formats and interface. Secondly, a research article presents SPIX, detailing in-depth the work performed so far, explaining the mathematical background of the software, and showing its potential application on two complex environmental datasets. The third part presents the latest developments proposed for the processing of 3D LC-MS datasets.

Development of the software

As presented in chapter 3, the photodegradation of benzisothiazolinone (BIT) was studied using a laboratory modeling approach. In parallel, the samples from the same experiment were analyzed via direct infusion (DI) high-resolution mass spectrometry (in ESI mode), and the obtained spectra were used for the development and testing of the software. The reasons behind starting the development on 2D DI-MS datasets were twofold. Firstly the analytical gains were considered: analyzing complex mixtures via DI-MS can provide a vast amount of information, as avoiding chromatographic separation permits to decrease selectivity (potential ion suppression must nevertheless be taken into consideration). Secondly, processing 2D data files aligned well with the development goals and constituted a preliminary step to data pre-processing.

Format of the files

One of the first challenges of mass spectrometry data analysis is the handling of various file formats. Different vendors market and make available differently encoded datasets. The multitude of these proprietary binary output formats cause great issues in data processing, as well as data sharing. However, there are some efforts to develop universal formats, such as the open XML-based format, mzML [1]. Our work was performed on a Bruker FT-ICR MS instrument, using its own processing software, Bruker DataAnalysis; the available export formats are shown in Table 5.1.1.

Table 5.1.1: Available exporting formats with Bruker DataAnalysis software

Export format for spectra	Export format for chromatogram
.xml	.mzXML
.d	.mzML
.ascii	.mzData
.xy	.cdf
.bsc	.dx
.spectrum	.d
.mgf	.ascii
.asc	

The first format chosen to process with SPIX was the .xy format, a simple x-y ASCII file, converting the mass spectrum only into x-y values. This format is easy to process, as it encompasses the m/z -intensity pair values without encoding. Moreover, it was of high interest to look at all the data without *a priori* choice. This is not true for all formats, as during data-exporting, only peaks above a default threshold are retained in some of the available formats. Therefore, all the recorded points are present in these files: approximately 4 Mpts (395 2122) per spectrum in the set of experiments carried out on benzisothiazolinone photodegradation. In the first version of SPIX, alignment of the data was not achieved before data processing, therefore the m/z values had to match exactly between sets of spectra. In this case, the measurements were performed on the same day, within the same calibration because a new calibration would have caused a slight shift in the m/z values.

Photodegradation mechanisms are studied in-depth by our group, so the first approach was to determine if SPIX could extract the m/z values of the known photoproducts from mass spectra of an irradiated solution. The data was generated by analyzing three replicates for each sampling time. Using replicates is not mandatory but it has been shown that it strongly improves fitting to the models, so that higher statistical significance can be obtained.

Uploading data to SPIX

To upload the data, the spectra have to be arranged in separate folders per condition. A CSV file has to be created to indicate the type of data analysis: continuous, referring to kinetics mode or categorical, referring to the comparison of two conditions. Table 5.1.2 shows an example for such a CSV file, this was used to summarize the spectra of interest in the experiment related to benzisothiazolinone degradation. The software will convert the .xy files into one .mat file for each condition. This method was used because the software was initially programmed in Matlab. However, since then it was developed to run without Matlab; this step is used only to convert and combine the spectra for each condition. After this, the user selects the converted files in the framework of a new project.

Table 5.1.2: Describing the data files in a .csv file

data_xy	Time (min)	0_90
folder	continuous	categorical
0 min	0	0 min
10 min	10	.
20 min	20	.
30 min	30	.
40 min	40	.
50 min	50	.
60 min	60	.
70 min	70	.
80 min	80	.
90 min	90	90 min

The interface of the software

After converting and uploading the data, the data-processing parameters are shown at the interface of the software. Firstly, in the covariates, it can be selected the comparison of two conditions or the kinetics of a series of conditions, which was set at the previous step during data uploading.

In the case of comparison of two conditions, the analysis section will provide whether the data should be represented according to the difference in mean values in the intensity between the two datasets or the p-value (Figure 5.1.1). In the case of the kinetics, the data can be shown based again on the p-value, or the R^2 , which represents the goodness of fitting of the kinetic models (Figure 5.1.2). A color-coding can be selected for better visualization of the data. For the segmentation, the threshold of intensity can be set, above which the dataset will be processed. Parameters regarding blank subtraction can be selected. In the case of two conditions, the statistical approach of Wilcoxon or t-test is available.

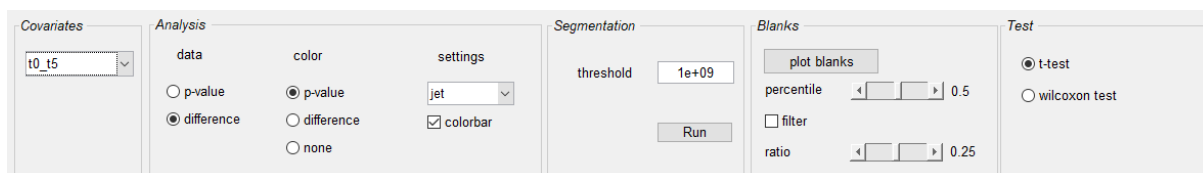


Figure 5.1.1: Interface displaying the parameters of SPIX in the case of comparison of two conditions (explained from left to right)

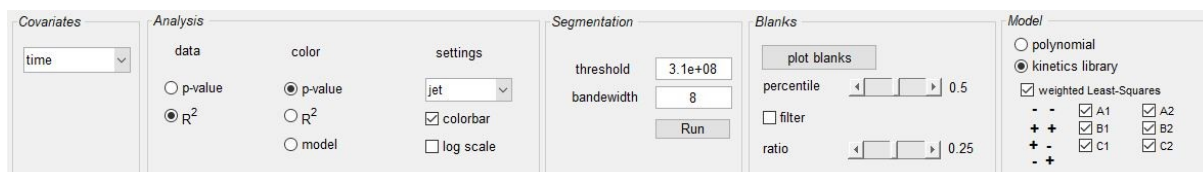


Figure 5.1.2: Interface displaying the parameters of SPIX in the case of kinetic modeling (explained from left to right).

For the kinetics, models from the kinetics library proposed by our group or polynomial fitting are applicable. The latter is selected to achieve mathematically the best fit, with a potentially high polynomial degree, which reduces significance. Therefore, the pseudo exponential fit is mostly selected, representing the nature of chemical reactions, for example, the exponential decay of a contaminant under irradiation. There are 8 types of exponential models proposed by our library. Table 5.1.3 shows the trends in the proposed library models to help identifying molecules undergoing increasing or decreasing changes or reaching a plateau. The models can be visualized using a linear or logarithmic scale.

Table 5.1.3: Available exponential kinetic model types in the SPIX library

Model	Type	Explanation
A1	- -	Decreasing exponential
A2	- -	Decreasing exponential + reaching a plateau
B1	+ +	Increasing exponential
B2	+ +	Increasing exponential + reaching a plateau
C1	+ -	Increase then decrease
C2	+ -	Increase then decrease + reaching a plateau
D1	- +	Decrease then increase
D2	- +	Decrease then increase + reaching a plateau

Outcome of the processing

After processing the data, the outcome is demonstrated by showing the example of BIT photodegradation. Using the t-test and a threshold value (3.1×10^8 in the present case),

the data will appear as in Figure 5.1.3. The generated spectrum can be seen on the left side, showing all the ions that undergo significant intensity change between the two conditions. On the upper side of these simulated spectra are displayed the peaks that show a decrease in intensity between the first and the second condition, while the lower side shows the ones that increase. After clicking on an ion of interest, the ionic current changes between the two conditions (red vs. blue), and the error boxes will materialize on the right-hand. This example shows the decrease in BIT molecular ion intensity before and after 20 minutes of irradiation.

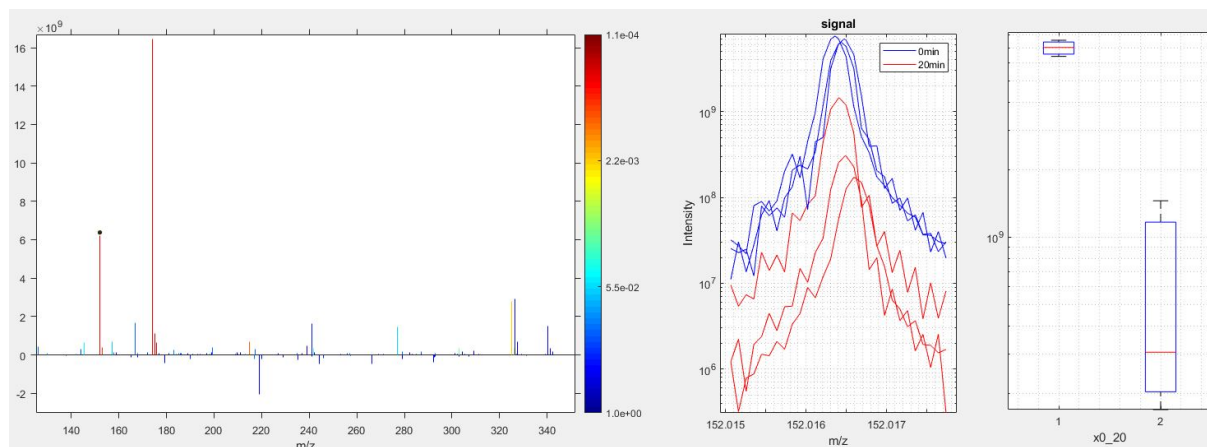


Figure 5.1.3: Change in the intensity of the benzisothiazolinone pseudomolecular ion $[M+H]^+$ between 0 and 20 minutes of irradiation

In the kinetic studies, the generated spectrum will encompass all the ions that can be modeled according to the given criteria. Again, by selecting one ion, its model will be presented as in Figure 5.1.4. In this example, the model of the parent compound is shown. As a result of the irradiation experiment, exponential decay was expected, and indeed the exponential kinetics model matched this tendency well.

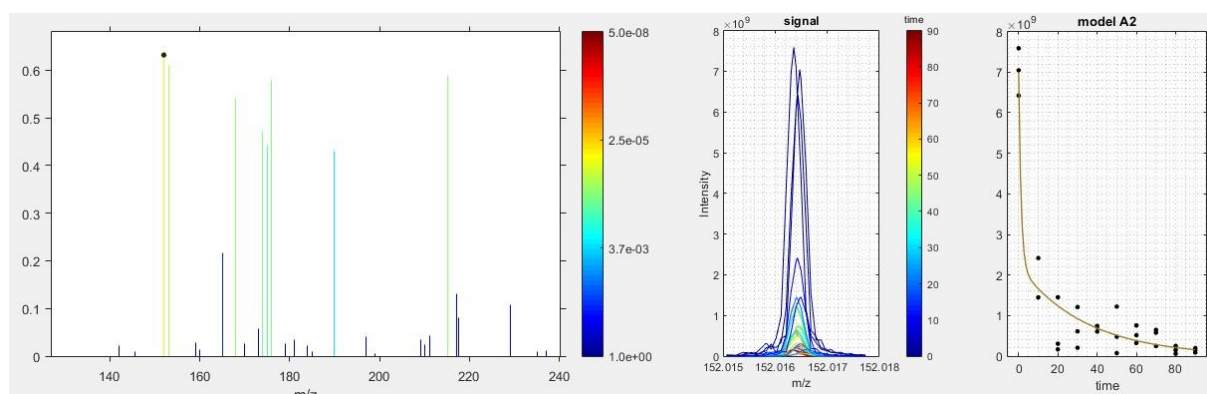


Figure 5.1.4: Kinetic model of benzisothiazolinone, exponential fit

Exporting the data

This approach aimed not only to discuss the photoproducts individually but to extract the maximum amount of statistically relevant information as quickly as possible. For this purpose, the data can be exported to a CSV file. This way, all the possible m/z values are summarized, which are found by SPIX. It is important to rank and filter them by p-value or R^2 value and select the ones that indeed show a good fit. Further data processing can be performed after obtaining the list of ions that undergo statistically relevant changes.

References

- [1] EW Deutsch. “Mass spectrometer output file format mzML”. In: *Methods Mol Biol* 604 (2010), pp. 319–331. DOI: 10.1007/978-1-60761-444-9_22.

5.2 SPIX software

SPIX: A new software package to reveal chemical reactions at trace amounts in very complex mixtures from high-resolution mass spectra dataset

Edith Nicol^{a*}, Yao Xu^{b,c}, Zsuzsanna Varga^a, Said Kinani^d, Stéphane Bouchonnet^a, Marc Lavielle^{b,c}

^a*Laboratoire de Chimie Moléculaire, CNRS / Ecole Polytechnique, Institut Polytechnique de Paris, 91128, Palaiseau, France*

^b*Centre de Mathématiques Appliquées, CNRS – IP Paris, Ecole polytechnique, Route de Saclay, Palaiseau, 91128 France*

^c*Inria, École polytechnique, 1 Rue Honoré d’Estienne d’Orves, Palaiseau, 91120 France*

^d*Laboratoire National d’Hydraulique et Environnement (LNHE), Division Recherche et Développement, Electricité de France (EDF), 6 Quai de Watier, Chatou Cedex 01, 78401 France*

Funding information: European Union’s Horizon 2020 research and innovation program, Grant/Award Number: Marie Skłodowska-Curie Grant Agreement No 765860; Inria (Institut national de recherche en informatique et en automatique); National FT-ICR network (FR 3624 CNRS)

Abstract

Rationale

High-resolution mass spectrometry based non-targeted screening has a huge potential for applications in environmental sciences, engineering and regulation. However, it produces large datasets for which full appropriate processing is a real challenge; the development of processing software is the last building-block to enable large-scale use of this approach.

Methods

A new software application, SPIX, has been developed to extract relevant information from high-resolution mass spectral datasets. Dealing with intrinsic sample variability and reducing operator subjectivity, it opens up opportunities and promising prospects in many areas of analytical chemistry. SPIX is freely available at: <http://spix.webpopix.org>.

Results

Two features of the software are presented in the field of environmental analysis. An example illustrates how SPIX reveals photodegradation reactions in wastewater by fitting kinetic models to significant changes in ion abundance over time. A second example shows the ability of SPIX to detect photoproducts at trace amounts in river water, through comparison of datasets from samples taken before and after irradiation.

Conclusions

SPIX has shown its ability to reveal relevant modifications between two series of large

datasets, allowing, for instance, the study of the consequences of a given event on a complex substrate. Most of all – and it is to our knowledge the only software currently available allowing this – it can reveal and monitor any kind of reaction in all types of mixture.

Introduction

High-resolution mass spectrometry (HRMS) is now experiencing unprecedented growth. It appeared in the early 1970s with dual-focus devices combining magnetic and electrostatic fields, and continued its development with the introduction of time-of-flight (TOF), Orbitrap and Fourier transform ion cyclotron resonance (FT-ICR) analyzers. While FT-ICR mass spectrometers remain the most accurate today, high-end QTOFs and QEx Orbitraps provide accuracies below 3 ppm. The resolution of an analyzer reflects its ability to separate ions with close m/z values. High-resolution analyzers can thus differentiate isobaric ions: i.e. ions with the same nominal mass but different exact masses, and therefore different chemical formulae, such as $\text{N}_2^{+\bullet}$ (m/z 28.0056) and $\text{CO}^{+\bullet}$ (m/z 27.9944). High resolution is a very valuable asset: it not only greatly improves the selectivity and specificity of “traditional” detection and quantification methods (in comparison with low-resolution analyzers), but also greatly facilitates structural elucidation by assigning raw formulae to the detected ions [1].

More recent use of high resolution takes advantage of its ability to separate isobaric ions, in an attempt to break free from separation methods – mainly gas (GC) or liquid chromatography (LC), or more rarely capillary electrophoresis or ion mobility – so as to expand the range of molecules detectable in a single analysis. This is particularly interesting in the context of non-targeted analyses – in which the operator does not know which molecules are likely to be present in a sample – because the choice of a chromatographic system focuses the analysis of certain classes of compounds based on their properties (volatile or not, polar or apolar, large or small, etc.) and thereby introduces a bias attributable to the subjectivity of the analyst. Direct introduction into the ion source without prior pretreatment or chromatographic separation was shown to be a useful alternative for rapid and comprehensive diagnosis of environmental samples, but this approach remains very challenging due to the extreme complexity of environmental matrices and the large number of contaminants likely to be present [2]. On direct introduction of a mixture, various molecules are simultaneously ionized, resulting in mass spectra yielded by the overlapping of spectra of the detectable species. Thus, complex mixture analyses provide mass spectra that can contain tens or hundreds of thousands of ions, even with soft ionization techniques such as electrospray ionization, atmospheric pressure ionization or atmospheric pressure photoionization; these spectra are of no possible use to the operator without the help of adapted software. Finding a molecule showing significant change between two con-

ditions (upstream/downstream or after treatment, for instance) in its trace amounts in an environmental sample is like looking for a needle in a haystack. Being able to quickly evaluate all the chemical consequences of an industrial accident on the biotope can be crucial to decision-making. In these situations, non-targeted HRMS-based screening is one of the last resorts for identifying unexpected or unknown contaminants [3–7]. This approach has recently been evaluated in a comprehensive collaborative study organized by the NORMAN association, in which a total of 18 institutes from 12 European countries analyzed an extract of the same water sample collected from the Danube River. The results revealed that non-targeted analytical techniques were already widespread and that practices were substantially harmonized between the participants, but that data processing remained complicated and time-consuming [8]. Among the main recommendations formulated to improve the non-targeted approach is the development of robust user-friendly processing software. Likewise, AQUAREF – the French national reference laboratory for aquatic environment monitoring, which works in close concert with other European reference laboratories – published guidelines for HRMS untargeted analysis, for which SPIX could be a powerful tool [9].

The first part of this article discusses the notions of uncertainty and subjectivity related to untargeted analysis. The second part presents the general working principle of SPIX software. The third part is dedicated to the presentation of results obtained on real samples. It discusses the strengths and limitations of the software and its specificities compared with the few programs currently commercially available. A brief overview of current computational and statistical approaches to extract relevant information from the *big data* of mass spectrometry analyses is provided in SI-1 (supporting information); it describes the approaches of Kendrick [10, 11] and van Krevelen [12–14], as well as multivariate statistical analysis [15–21]. Multivariate analysis tools enable global understanding of many concomitant variables and of their inter-correlations. Metabolomics processing pipelines often include univariate and multivariate statistical approaches. Univariate analysis is usually used as a pre-processing step, while multivariate analysis is used for classification of samples or features. For example, principal component analysis is used to characterize differences of two groups of metabolomics GC/MS data for the diagnosis of gastric cancer. The Wilcoxon rank sum test showed the marker metabolites specific to the tumor group. Multivariate analysis, specifically principal component analysis, successfully divided the two groups of samples of normal and malignant gastric tissue [22]. A comprehensive workflow for univariate analysis of LC/HRMS data was developed to follow human adult urinary metabolome variations. Univariate analysis was used as a preprocessing step: nonparametric hypothesis testing was used to assess correlations with covariables and the Wilcoxon test was used to calculate the median differences between genders. The univariate p-value results together with multivariate importance in projection evidenced that there were 108 urine metabolites whose concentrations varied with either age, body

mass index or gender [23]. Concerning direct infusion mass spectrometry, a comprehensive workflow for data processing and quality control was developed for metabolomics analysis of cardiac tissue extract. It can be used for different metabolomics analyses as it focuses on the correction of intra- and inter-batch variations and offers best-practice workflows and rigorous quality assessment. The data processing steps include the Wilcoxon test and multivariate analysis [24]. These applications could be extended to environmental samples; however, no approach has been reported using univariate or multivariate analysis which focuses on the kinetics of compounds in HRMS datasets. The concept behind multivariate analysis is different from that of the SPIX software: the latter aims at observing all statistically relevant variables individually. Examples of SPIX applications are given below.

Notions of uncertainty and subjectivity in modern untargeted analytical approaches, and introduction to spix

To illustrate the functionality of the SPIX software, it is necessary to address the notions of uncertainty and subjectivity that are fundamental in analytical chemistry. We propose to take an example in environmental chemistry. Consider a plant located on the bank of a river; it may be a treatment plant or, on the contrary, a source of pollution. The question is whether its presence significantly alters the composition of the water. The question seems simple enough, but providing a relevant answer is much less so. The conventional approach is to take water samples upstream and downstream of the plant, analyze them chemically and compare the results. This approach, while scientifically reasonable, nevertheless raises many questions at each step of the process. How many samples are needed to take account of the spatial and temporal variability of upstream and downstream water composition? Where, when and how to sample? What sample preparation to adopt, given that each choice of solvent, filter, solid-phase extraction column, chromatographic protocol and mass spectrometry ionization mode conditions the results of the analysis by favoring detection of certain molecules based on their size or polarity? Every single step in the analytical process introduces metrological uncertainties related to the measuring instruments used (balances, pipettes, etc.), but also to the so-called “matrix effect”: i.e. the matrix of the reference used to validate the method is generally not rigorously identical to the matrix being analyzed. Stochastic biases and uncertainties are also caused by adsorption, evaporation, etc. The proliferation of sources of error obliges analysts to use internal standards to reduce the overall uncertainty of the results and try to conform to industry-specific standards. Limiting the subjectivity in a method needs to make no assumptions at all, which is in contradiction with the use of an internal standard; thus, the analytical scientist is left with choosing between limiting subjectivity or limiting uncertainties. To the problem of uncertainties must be added that of operator subjectivity, at two main levels. As mentioned above, this subjectivity comes into play before

measurement: when the operator establishes the analytical protocol, choices are made, conditioned by assumptions – the operator’s own or those of third parties – as to what might have contaminated the water of the river. Even if the method is not “targeted” (i.e. specifically designed for the selective detection of given analytes), it cannot be considered totally “non-targeted” as there is no effective protocol capable of extracting and detecting everything simultaneously (e.g. both polar and apolar molecules) and any selected protocol effectively excludes some potential analytes. This will lead the analyst to try to minimize sample preparation, with the dual objective of limiting uncertainties and of reducing operator-induced subjectivity; an immediate consequence of this simplification is to increase the complexity of the data. For example, mass spectra recorded from environmental samples will be much more complex if the sample is introduced directly into the mass spectrometer without prior purification and separation. A point that is generally much less considered is operator subjectivity in interpreting results, especially when the data are complex and voluminous, when it comes to manually integrating a peak or comparing two chromatograms or two mass spectra, for example.

In 2019, a visual trial devoted to subjectivity evaluation was carried out during a European winter school on mass spectrometry, on a panel of 37 people with a strong scientific background in analytical chemistry. It consisted of a series of one-minute projections of two images with 5 to 22 differences; panelists were asked to note the number of differences that they were able to spot. Some images were quite simple (pictures with modified areas) while others were very complex (fractals containing very small differences within complex areas). A set of simulated mass spectra containing 15 differences (variations in peak intensity, addition and removal of peaks) was presented to the panel – in triplicate and not consecutively – without prior notice. The variability between the results of these triplicates gave an average standard deviation of 2.3 observed differences per individual, with mean and median values of 9.6 and 9.7, respectively, and a range of 0–19. Considering the variability between panelists, a standard deviation of 20.6 differences was determined over the whole dataset, with mean and median values of 85.6 and 90, respectively, for a total 148 differences to be identified. The number of observed differences ranged from 31 to 122. The number of differences identified varied to the point that one operator would conclude that two spectra were almost identical while another would consider them significantly different! [25]

The problem is substantially more complicated when comparing not only spectra but series of spectra corresponding, for example, to samples taken upstream and downstream of a treatment plant. A large variation in an ion count between upstream and downstream spectra may not be significant if the magnitude of variation is equal within and between the downstream and upstream populations; changes in the abundance of this ion reflect only the intrinsic chemical variability of the environment and are not a relevant marker

of the impact of the plant. On the other hand, a slight change in the abundance of an ion between “upstream and downstream spectra” may be significant if the abundance is almost constant within each population; it then reflects a real effect of the plant on water quality. The SPIX software was created to remedy the observed fact that it is impossible for an operator to determine what makes sense based on simple observation of complex datasets, especially since the data are subject to intrinsic variability. The aim is to extract relevant information from numerous complex datasets. As explained below, the software can identify significant differences between mass spectra series and track the kinetic evolution of reagents, unknown reaction intermediates and reaction products at low concentrations in complex mixtures.

Materials and methods

The SPIX software

SPIX was developed in Matlab 2018a (MathWorks, Natick, MA, USA). A stand-alone version is freely available on the website (<http://spix.webpopix.org>). The source code can be made available on request. Prior to performing any statistical analysis of the data, pre-processing is required to identify and align significant peaks in the data. The method used for detection and alignment actually depends on the type of data available:

- When the device provides data in xml format, these data have already been filtered and contain only the most significant peaks. These peaks are then aligned by using the `malign` function of the Bioinformatics Toolbox (Matlab) with the “shortest-path” option.
- When the data obtained are raw data (e.g. xy Bruker format in the present study), i.e. intensities measured on a fine and regular grid, the following algorithm is used: considering K series to analyze, the approximate positions of the significant peaks are first roughly determined by building a single series, consisting of the maximum intensities of the K series at all data points, and by thresholding this series. This procedure is used to determine disjoint segments in which the peaks of each of the K series are located.

The position and intensity of each of these peaks are then estimated for each spectrum by fitting a model of the form $A \exp(-\alpha(x-m))$ for which the maximum value A is reached for $x = m$.

SPIX can be used in essentially two situations. The first one allows evidencing some modifications in the composition of a complex mixture over time. The focus here is on how the abundance of certain species varies as a function of a given parameter (time, pH, reagent, etc.). The objective is twofold: to detect ions with significantly varying abundance (in

terms of statistical relevance), and to describe how the abundance varies by kinetic modeling. After aligning the peaks as previously described, different kinetic models, including various patterns associated with compound degradation and formation and reaction intermediates, are fitted to the data. A library including seven typical kinetics profiles is currently available; examples of graphical representations are provided in Table S5.2.1 and Figure S5.2.1. The selected model minimizes the Bayesian information criterion. The coefficient of determination r^2 is calculated to quantify the part of the variability of the data explained by the model and an ANOVA assesses whether this part of explained variability is statistically significant. The p value of the F-test and the r^2 value are represented graphically so as to easily visualize ions with abundance accurately fitting a kinetic model.

SPIX also permits two series of samples collected under two experimental conditions to be compared. The objective is to identify the ions with significant differences in intensity and to quantify these differences. The algorithm first consists of identifying the peaks considered significant: i.e. present and above a given threshold in at least one of the two conditions. For an ion detected in this way, the procedure is as follows. First, the series are locally shifted so that all the peaks are aligned. The maximum intensity at the peak is estimated for each spectrum by fitting a model of the form $A \exp(-\alpha(x-m))$ for which the maximum value A is reached when $x = m$. This provides two series of values that can be compared on statistical tests. A t -test detects differences in the mean while a nonparametric Wilcoxon test more generally detects whether the peak intensity tends to be higher in one condition than in the other. A graphical representation of the p values obtained for all the peaks detected, as well as of the size effects (i.e. differences in mean values between the two conditions), provides quick visualization of the chemically significant differences and the statistical relevance of the differences.

Blank correction can be done as follows. The user chooses as a threshold, a ratio and a percentile. By default, the median of intensities is used for the calculations ($p = 0.5$). For the given percentile, the ratio is defined as:

$$r_p(m/z) = \frac{B_p(m/z)}{S_p(m/z)} \quad (5.1)$$

with $B_p(m/z)$ being the percentile of order p of the blank intensities' maximum and $S_p(m/z)$ the percentile of order p of the experimental data intensities' maximum. If the peak intensity is higher than $S_p(m/z)$ (as a threshold value) in at least one of the experiment spectra, it will be kept as a peak; if not it will be ignored.

With `.mat` or `.xml` files, SPIX occupies about 500 MB (it is the Matlab runtime that takes up all the space). With `.xy` formats the `.mat` conversion stage has to be added (sequentially): if a sub-repository (time_0 for example) is 25 MB, then SPIX occupies about 750 MB of memory. It does not represent the total volume of all sub-repositories

because SPIX loads them and converts them one by one. In all cases, it works very well on a standard PC.

Chemicals, reagents, irradiation processes and analysis

The ability of SPIX to extract relevant information from sets of complex high-resolution mass spectra is illustrated in two experiments. The first concerned peroxide-photocatalyzed degradation of maprotiline (an antidepressant drug) in a wastewater treatment pilot plant. In this case, the comparison aimed at revealing reagents, intermediates and products using kinetic models, from mass spectra recorded at different irradiation times. The second experiment concerned UV irradiation of acetamiprid (a neonicotinoid insecticide) in a complex mixture of aqueous fulvic acid to simulate river water; it aimed at revealing acetamiprid photoproducts at trace levels and evaluating the impact of UV treatment on dissolved organic matter. The comparison covers two datasets, for spectra recorded before and after irradiation. The chemical structures of maprotiline and acetamiprid are shown in Figure 5.2.1. File SI-2 (supporting information) describes the chemicals, sampling and irradiation processes used for the two experiments.

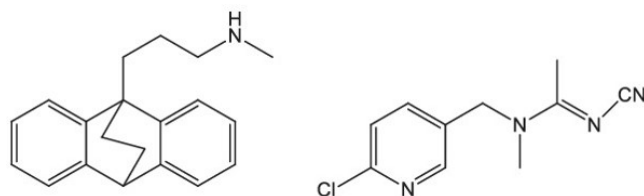


Figure 5.2.1: Chemical structures of maprotiline (left) and acetamiprid (right)

An ultrahigh-resolution mass spectrometer (FT-ICR SolarixXR 9.4 T; Bruker Daltonics, Bremen, Germany) was used for direct infusion mass spectrometry analysis. The electrospray ionization (ESI) source was set in positive mode and solutions were injected using an automated Acquity HPLC system (Waters, Saint Quentin en Yvelines, France). The injection volume was 10 μL . Elution was carried out using a 0.002 mL/min flow of water/acetonitrile/formic acid ($\text{H}_2\text{O}/\text{ACN}/\text{FA}$; 50/50/0.1). Nitrogen was used as nebulizer and as drying gas, set at 1 bar pressure and 4 L/min flow rate, respectively. The drying gas temperature was set at 180°C. The capillary voltage and endplate offset potential were set at -4500 and -500 V, respectively. Ions were accumulated for 0.2 s in the collision cell, and 50 scans were summed. The resolution was set at 4 Mpt (million data points) on a scan range from m/z 57 to m/z 1000 in order to obtain a resolution greater than 400 000 at m/z 200. A tune mix (Agilent Technologies, Les Ulis, France) was used for mass calibration. Exact formulae were assigned with error < 1 ppm.

Results and discussion

Highlighting chemical reactions in complex mixtures

Degradation of maprotiline in wastewater under an advanced oxidation process (peroxide/UV) was carried out in a pilot plant, with the aim of testing the ability of SPIX to follow the degradation of contaminants and the evolution of their transformation products. This pilot plant was set up by FACSA, a Spanish company operating water treatment plants, to design, optimize and compare novel water treatment processes; the operational parameters and analytical conditions are given in SI-2 (supporting information). Considering that the abundances of reagents, intermediates and products of a chemical reaction are not expected to evolve stochastically, an original way to extract relevant information from untargeted analysis consists of filtering the results based on ion abundance trends. Briefly, A-type models are selected to detect molecules with decreasing abundance during the reaction while B-type and C-type models detect the products and intermediates, respectively. The software detects all significant changes over time and provides a kinetic model; statistical data can be exported for further analysis in the table format described in Table S5.2.2. As a first example, from one set of samples using the software default threshold (1.2×10^8), SPIX automatically extracted the m/z 278.19056 signal (protonated maprotiline) for each irradiation time, and associated the fitting model referred to as A1 in SPIX with $r^2 > 0.99$ (Figure 5.2.2).

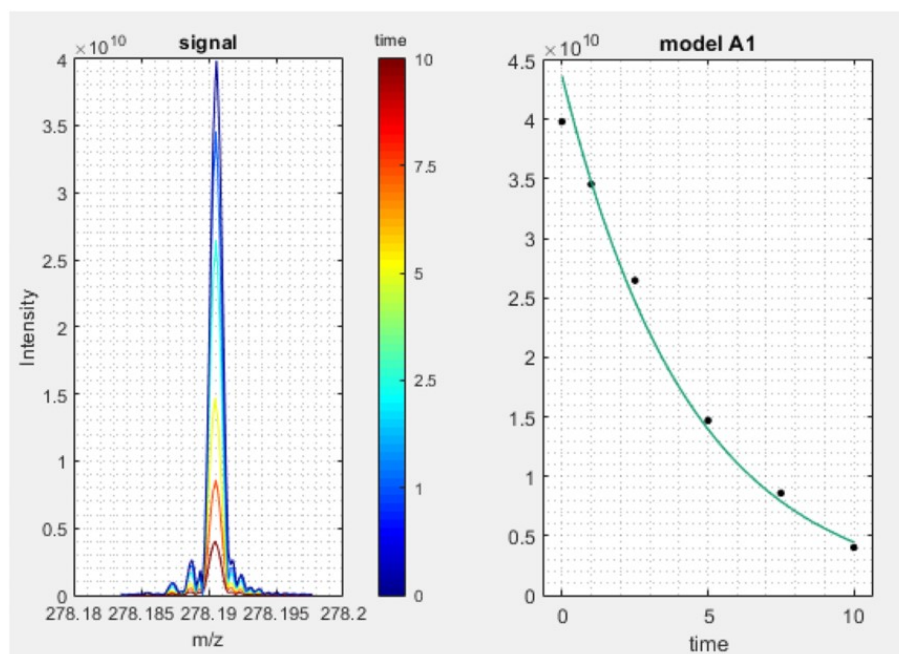


Figure 5.2.2: m/z 278.19056 signal (protonated maprotiline) extracted for each irradiation time and fitting model associated with degradation kinetics: $8.19 \times 10^5 + 4.37 \times 10^{10} \times \exp(0.23x)$; $r^2 = 0.991$

A first attempt to extract transformation products from the background noise, conducted on the basis of one set of measurements, gave a few maprotiline-related peaks, but a

thorough study of the raw data showed that using data from duplicate measurements yielded a kinetic model better fitting ion intensity evolution. The aim was to maximize the relevant data obtained while minimizing the number of parallel measurements, to gain valuable analysis time. Using two parallel measurements for each irradiation time, 88 ions fitting one of the SPIX kinetic models were extracted with default threshold intensity 1.2×10^8 ; this list was reduced to 12 ions keeping m/z fitting a kinetic model with $r^2 > 0.9$ (Table 5.2.1), these fittings being also those corresponding to the lowest p values.

Table 5.2.1: Ions extracted and associated kinetic models related to the photodegradation of maprotiline in wastewater with $r^2 > 0.9$ (data ordered by decreasing intensity).

m/z	r^2	p value	Model ^a	Maprotiline-related	Ion formula	Intensity	Relative intensity (%)
With intensity $> 1.2 \times 10^8$							
278.19054	0.93	5.25×10^{-6}	A1	Yes	$C_{20}H_{24}N^+$	8350669911	100.0
279.19386	0.94	3.82×10^{-6}	A1	Yes	$C_{19}H_{24}N^{13}C^+$	1643233281	19.7
294.18552	0.98	3.91×10^{-7}	C1	Yes	$C_{20}H_{24}NO^+$	1126960171	13.5
276.17486	0.92	7.58×10^{-5}	C1	Yes	$C_{20}H_{22}N^+$	451170002	5.4
292.16992	0.94	2.73×10^{-5}	B2	Yes	$C_{20}H_{22}NO^+$	352390361	4.2
92.73055	0.92	1.48×10^{-5}	A1	Yes	^b	339591819	4.1
310.18038	0.94	4.09×10^{-6}	B1	Yes	$C_{20}H_{24}NO_2^+$	228987461	2.7
295.18881	0.97	2.30×10^{-6}	C1	Yes	$C_{19}H_{24}NO^{13}C^+$	218499045	2.6
280.19727	0.94	3.44×10^{-6}	A1	Yes	$C_{18}H_{24}N^{13}C_2^+$	157067516	1.9
308.16472	0.91	1.69×10^{-4}	B2	Yes	$C_{20}H_{22}NO_2^+$	140798543	1.7
344.18594	0.95	1.52×10^{-5}	B2	Yes	$C_{20}H_{26}NO_4^+$	135672030	1.6
342.17029	0.95	1.50×10^{-5}	B2	Yes	$C_{20}H_{24}NO_4^+$	112723518	1.3
With intensity $1.2 \times 10^8 > 6 \times 10^7$							
360.18088	0.96	8.69×10^{-6}	B2	Yes	$C_{20}H_{26}NO_5^+$	95678296	1.1
312.19604	0.94	2.71×10^{-5}	C1	Yes	$C_{20}H_{26}NO_2^+$	84376971	1.0
328.19096	0.94	2.74×10^{-5}	C1	Yes	$C_{20}H_{26}NO_3^+$	79243551	0.9
318.17025	0.94	2.46×10^{-5}	B2	Yes	$C_{18}H_{24}NO_4^+$	75240290	0.9
302.1753	0.98	6.44×10^{-5}	C1	Yes	$C_{18}H_{24}NO_3^+$	66900122	0.8
93.06499	0.92	9.63×10^{-6}	A1	Yes	^b	66023322	0.8
242.15416	0.95	1.34×10^{-5}	B2	Yes	$C_{16}H_{20}NO^+$	63982463	0.8
326.17543	0.92	8.04×10^{-5}	C1	Yes	$C_{20}H_{24}NO_3^+$	50496456	0.6
300.17259	0.95	1.27×10^{-6}	A1	Yes	$C_{20}H_{23}NNa^+$	20928662	0.2
139.09569	0.91	9.43×10^{-4}	C2	Yes	$[C_{20}H_{24}N]_2^+$	7061477	0.1
336.14927	0.91	1.76×10^{-5}	A1	No	$C_{23}H_{18}N_3^+$	104081459	1.2

^aCurrently available SPIX kinetic models are given in SI-2 (supporting information)

^b m/z 93.06499 and m/z 92.73055 signals correspond to artifact peaks related to the harmonics of the m/z 278.19054 and m/z 279.19386 ions, respectively; they resulted from signal digitization [26].

The formulae were assigned using Bruker software based on accurate mass measurements (sub-ppm accuracy) and isotopic pattern-matching. All the extracted m/z values were

related to maprotiline or its photoproducts (oxidized compounds); they corresponded to singly charged ions with ^{12}C and ^{13}C isotopic contributions. One signal (m/z 92.73055) corresponded to an artifact related to the harmonics of the m/z 278.19054 signal, resulting from signal digitization and Fourier transformation, a phenomenon previously described and explained by Mathur and O'Connor [26]. To study the threshold effect and determine whether additional photoproducts would be found if more peaks were considered, the threshold was halved (6×10^7) and the same methodology was applied. Thus 197 peaks were selected by SPIX and the data were ordered according to statistical relevance. Then 23 peaks were selected on the criterion $r^2 > 0.9$ (see Table 5.2.1). Here again, the m/z values were all related to maprotiline and its photoproducts; a second artifact (m/z 93.06499) was found and attributed to the harmonics of m/z 279.19386.

Using the selection parameters referred to above, one protonated species was detected at m/z 336.14927. Considering the “seven golden rules” of Kind and Fiehn and selecting atoms C, H, N, O, P, S, F, Cl, Br, Si, Na and K, the only matching formula was $\text{C}_{23}\text{H}_{18}\text{N}_3^+$ [27]. This species is logically assumed not to be related to maprotiline; it could correspond to a contaminant in high concentration in wastewater, degrading under UV radiation. According to the kinetics revealed by SPIX, some photoproducts were present in detectable abundance after 2.5 min irradiation. To estimate the relevance of the results provided by SPIX, one of the spectra recorded at this reaction time was selected. After blank subtraction (the blank consisting of wastewater matrix without maprotiline), the spectrum was exported in .csv format (Bruker’s FTICR-MS file format). The spectra were recorded using 8 Mpt, and as the experiments were carried out using secondary treated wastewater, 4479 peaks were exported by the Bruker software which were above the signal-to-noise ratio threshold of 4. Out of these 4479 peaks, the 11 most abundant ions in the selected spectrum corresponded to the 11 most statistically relevantly changing m/z values extracted by SPIX. The two m/z signals corresponding to harmonics of major ions were also extracted with good fit, and ranked 18th and 115th in the original file (overall blank-subtracted spectrum). The photoproducts showing the highest significance (lowest p values) were those corresponding to m/z 294.18552 and m/z 302.17530 (protonated molecules); the fitting is presented in Figure 5.2.3 for the former. One of the maprotiline-related peaks that was not in the list of the highest intensities was not found in the spectrum recorded at 2.5 min of irradiation: it was removed by the blank subtraction process, since the wastewater matrix was very complex. It is thus noteworthy that SPIX does not require blank subtraction to provide valuable information, allowing relevant peaks that coincidentally overlap with some of the matrix peaks not to be removed. The experiment conducted on photodegradation of maprotiline showed that the SPIX software efficiently revealed the most relevant changes in the composition of the irradiated mixture on the basis of only 12 mass spectra. It was able to automatically detect reagents, intermediates and products at trace levels. Most extracted ions were related

either to maprotiline or to its photoproducts. Only one compound was found which was assumed not to be related to maprotiline on the basis of its molecular formula ($C_{23}H_{17}N_3$); no significant change in the composition of the dissolved organic matter was found, although of course only electrospray-ionized species were considered. The photodegradation pathways of maprotiline have been reported in a study more oriented toward structural elucidation [28].

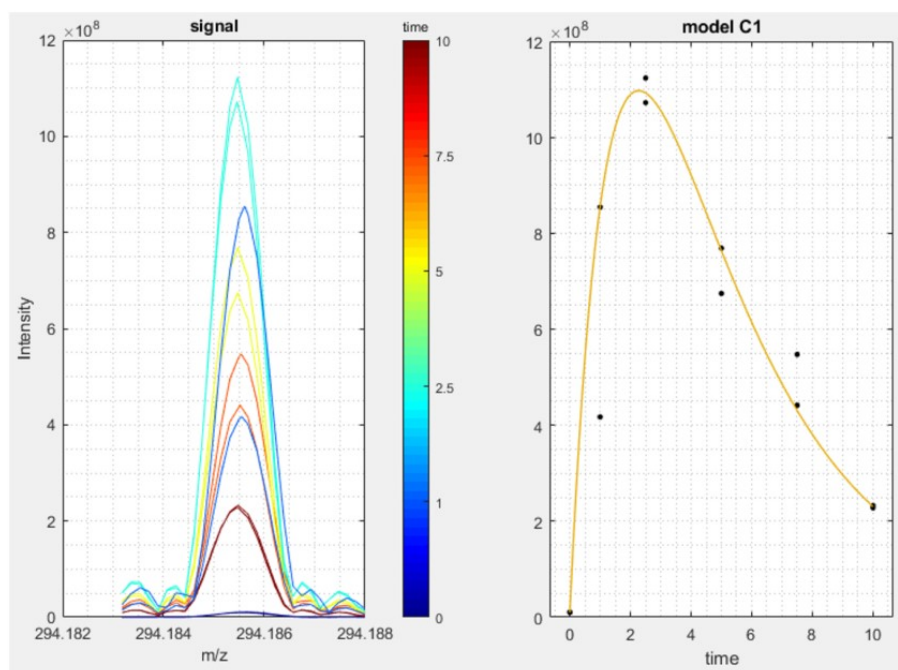


Figure 5.2.3: m/z 294.18552 signal extracted for each irradiation time and associated kinetic model

Comparison of two conditions: example of photodegradation of acetamiprid in aqueous solution of fulvic acid

This example demonstrates the ability of the SPIX software to point out relevant changes between two conditions from changes in low-abundance ions within a complex matrix. We studied the effect of UV radiation on acetamiprid in a complex mixture, simulating river water. A prior photolysis study of acetamiprid in ultrapure water identified acetamiprid degradation products in ultrapure water and demonstrated that the presence of other substances in the matrix leads to the formation of different degradation products [29]. These results led us to study the effect of dissolved organic matter on the photodegradation of acetamiprid as may happen under real environmental conditions. The peak intensity of acetamiprid represented 9.2% of the base peak of the mass spectrum before photolysis and only 1.9% after 30 min irradiation. A sodium adduct, originating from the use of glassware during sample preparation, impurity in solvents or electrospray ionization needle for instance, was detected with a relative intensity of 10.4% in the spectrum recorded before and 2.4% after photolysis. These differences, not detectable looking at the whole

spectrum, are obvious when zooming on the region from m/z 223.00 to 223.20 (Figure 5.2.4).

Table 5.2.2: m/z values for which the intensity significantly varied between series of spectra recorded before and after 30 min of irradiation ($n = 6$). Ions are listed by increasing p value.

m/z	Difference in intensity	p value	Ion formula	Related to acetamidrid ^a
224.07792	10523197	1.47×10^{-6}	$C_9H_{12}ClN_4^{13}C^+$	Yes
223.07459	103518217	3.20×10^{-6}	$C_{10}H_{12}ClN_4^+$	Yes
225.07161	24820606	1.08×10^{-5}	$C_{10}H_{12}N_4^{37}Cl^+$	Yes
246.05988	10966361	1.30×10^{-5}	$C_9H_{11}ClN_4Na^{13}C^+$	Yes
247.05358	30754403	2.86×10^{-5}	$C_{10}H_{11}N_4Na^{37}Cl^+$	Yes
245.05653	107329585	4.50×10^{-5}	$C_{10}H_{11}ClN_4Na^+$	Yes
201.03705	3542730	1.84×10^{-2}	$C_6H_{10}NaO_6^+$	No
205.10847	28497851	2.11×10^{-2}	$C_{10}H_{13}N_4O^+$	Yes
251.05269	7062764	2.71×10^{-2}	$C_{12}H_{11}O_6^+$	No
297.05819	5696496	2.72×10^{-2}	$C_{11}H_{14}NaO_8^+$	No
267.04760	5586613	2.99×10^{-2}	$C_{10}H_{12}NaO_7^+$	No
283.04253	4479881	3.20×10^{-2}	$C_{10}H_{12}NaO_8^+$	No
237.03704	4871105	3.25×10^{-2}	$C_9H_{10}NaO_6^+$	No
253.03194	4495727	3.33×10^{-2}	$C_9H_{10}NaO_7^+$	No
245.10095	14590229	3.65×10^{-2}	$C_{10}H_{14}N_4NaO_2^+$	Yes
211.02138	5849796	3.65×10^{-2}	$C_7H_8NaO_6^+$	No
227.09036	38558966	3.70×10^{-2}	$C_{10}H_{12}N_4NaO^+$	Yes
239.05270	7601354	3.77×10^{-2}	$C_9H_{12}NaO_6^+$	No
213.03705	8698910	4.00×10^{-2}	$C_7H_{10}NaO_6^+$	No
275.05267	3822758	4.02×10^{-2}	$C_{12}H_{12}NaO_6^+$	No
284.12725	12781460	4.41×10^{-2}	$C_{12}H_{19}ClN_5O^+$	Yes
253.06834	7132886	4.57×10^{-2}	$C_{10}H_{14}NaO_6^+$	No
255.08400	3840684	4.60×10^{-2}	$C_{10}H_{16}NaO_6^+$	No
325.05308	3163824	4.66×10^{-2}	$C_{12}H_{14}NaO_9^+$	No
241.03195	4410055	4.98×10^{-2}	$C_8H_{10}NaO_7^+$	No

^a Assumption based on the ion chemical formula.

Sets of spectra recorded before and after photolysis were compared using the SPIX software. Given the intensity of acetamidrid within the mixture, a peak detection limit was set at only three times the average intensity of spectral noise (average noise at 1×10^6 , detection threshold set at 3×10^6). This threshold was set as low as possible so as to identify acetamidrid degradation products in small amounts. Blank spectra were subtracted to eliminate any interference from solvents or instruments. Exported from SPIX, Table 5.2.2 lists the ions the abundance of which underwent significant change after irradiation. Here, only ions with a probability of $\geq 95\%$ ($p \leq 0.05$) were retained, i.e. with significant difference in intensity between the two conditions. In this example, results are organized

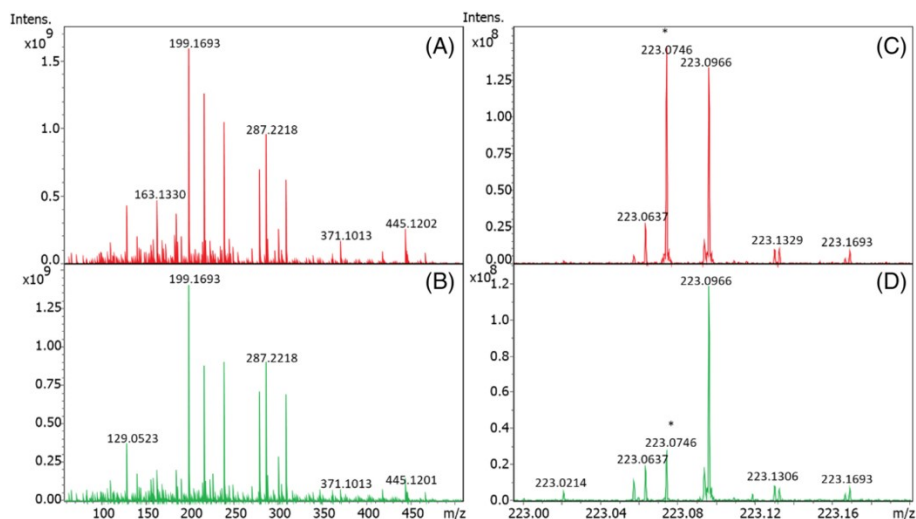


Figure 5.2.4: Mass spectra of acetamiprid in mixture with fulvic acid. A, Mass spectrum before photolysis; B, mass spectrum after 30 min photolysis; C, zoom on the protonated acetamiprid peak (m/z 223.0746) in (A); D, zoom on the protonated acetamiprid peak in (B).

by increasing p value, but any parameter can be chosen for presentation of the results. A negative value in the “Difference” column indicates that the ion abundance increased after photolysis. Visual comparison (Figure 5.2.5) confirms the results displayed in Table 5.2.2: the greatest change in intensity – and with the highest significance – was the concomitant decrease of the m/z 223 (MH^+) and m/z 245 (MNa^+) ions. Many other peaks decreased or increased after photolysis, but with lower p values for the difference in intensity; some were related to acetamiprid photodegradation, others to changes in dissolved organic matter. The ions at m/z 205.10847 ($C_{10}H_{13}N_4O^+$) and m/z 227.09036 ($C_{10}H_{12}N_4NaO^+$) shown here correspond to the protonated and cationized forms of a photoproduct previously described, the structure of which was elucidated in a study of the UV irradiation of acetamiprid in pure water [22]. This photoproduct was the major one. Thus, it is not possible to say whether others which were previously described were not detected here due to too high detection thresholds or because they are not formed in the presence of fulvic acid. It is interesting to note that SPIX revealed two ions, m/z 284.12725 ($C_{12}H_{19}ClN_5O^+$) and m/z 245.10095 ($C_{10}H_{14}N_4NaO_2^+$) – resulting from ionization of acetamiprid photoproducts based on their formulae – that were not detected by LC/MS in pure water. With a relative intensity below 1% in infusion mode, these two molecules could not have been revealed without SPIX. Fifteen ions with abundance significantly varying before and after UV irradiation were indicated. Based on their chemical formulae, they were assumed not to be related to acetamiprid or to its photoproducts; they all included a large number of oxygen atoms (≥ 6) and probably resulted from oxidation of dissolved organic matter. This is of great interest because it opens a way to investigate the global consequences of a depollution treatment, evaluating the treatment - apart from its ability to efficiently degrade pollutants - in terms of biotope preservation.

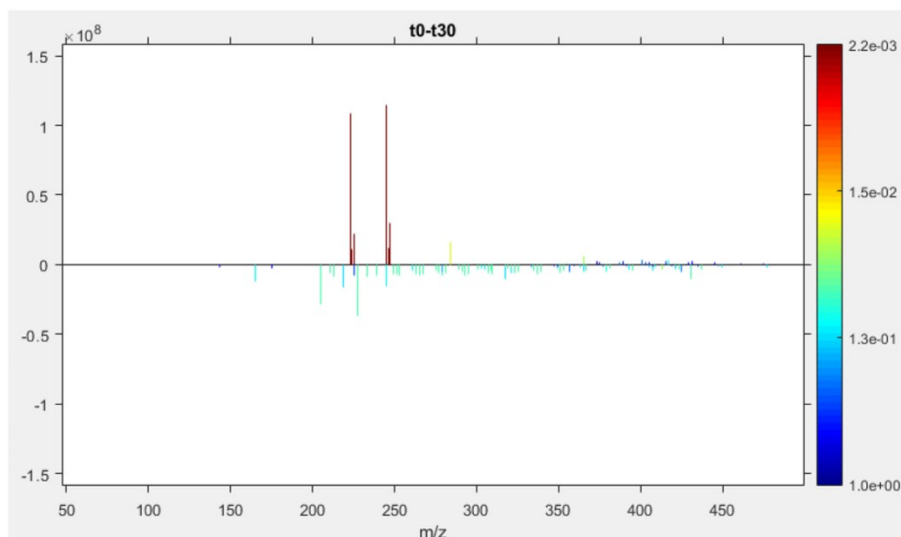


Figure 5.2.5: Visual result provided by the SPIX software after processing of mass spectra series recorded from samples taken before and after 30 min photolysis. The differences in ion intensities are given on the y -axis, positive values corresponding to decreased intensity after irradiation. The associated p value is given by the color scale: the more the color tends toward red, the more statistically significant the difference.

Conclusions

The SPIX software aims at extracting relevant data from mass spectra datasets. User-friendly and totally free, it is available for all at: <http://spix.webpopix.org>. Two features of SPIX are presented in this article, based on examples taken from the field of environmental analysis. The first example showed how SPIX revealed photodegradation reactions by correlating significant changes in ion abundance over time with kinetic models. Thus, the software revealed the reagents, products and intermediate species in a very complex mixture (wastewater). This functionality can be extended to monitor any kind of reaction – even unknown – in all types of mixtures. Some features of the SPIX software are still under development. One aims at extending compatibility with many more file formats (wiff, .d, .pkl, .qgd, etc.), in order to be used with most marketed mass spectrometers. Another focus of development – already running but requiring some improvements – concerns the extension of SPIX to three-dimensional datasets from hyphenated techniques such as GC/MS, LC/MS or IM-MS. Some commercial software applications allow comparison of chromatograms but, to our knowledge, an approach consisting of extracting relevant data from hyphenated techniques based on fitting with kinetic models has never been reported. The second example showed the ability of SPIX to detect photoproducts at trace amounts in an aqueous solution containing dissolved organic matter, through comparison of datasets for two conditions (before/after photolysis in the present case). Regarding this example, the ability of SPIX to deal with intrinsic variability and reduce operator subjectivity opens up promising prospects in all areas of analytical chemistry. It could, in particular, be a very useful tool to assess fragrance and flavor counterfeits,

where assessment is very challenging due to the normal variations in abundance of natural substances featuring at low levels in their composition. This feature can also be used to estimate the global consequences of a given treatment on the treated medium, for example to monitor the oxidation of dissolved organic matter and its consequences on biotope preservation.

Acknowledgements

Financial support from the National FT-ICR network (FR 3624 CNRS) and from Inria (Institut national de recherche en informatique et en automatique) for conducting the research is gratefully acknowledged. This work is part of a project that has received funding from the European Union's Horizon 2020 research and innovation program under Marie Skłodowska-Curie Grant Agreement No. 765860 (AQUALity).

Supporting information

SI-1. State of the art of modern approaches in managing high-resolution mass spectrometry data

In mass spectrometry, the emergence of high-resolution analyzers has enabled analysis of samples of ever-increasing complexity. Whether in direct infusion or with hyphenated techniques (LC/MS and GC/MS couplings), the amount of information issuing from high-resolution analysis of complex mixtures requires computer processing and simplified data representation. Direct infusion of a sample can thus provide a mass spectrum including several thousands of distinct ions. Various representations are commonly used to simplify the visualization and comparison of samples analyzed by mass spectrometry. As the approaches are so diverse, this section does not seek to be exhaustive, but restricts itself to presenting the Kendrick and Van Krevelen diagrams and the multivariate statistical analyses most commonly used by high-resolution mass spectrometry specialists.

– Kendrick diagrams

The Kendrick diagram allows easy identification, from a mass spectrum, of series of compounds that include the same number of heteroatoms and unsaturations but differ from each other by the number of -CH₂- groups [10]. The diagram is built by plotting the Kendrick mass defect (KMD) for each ion (eq. 5.2) as a function of the Kendrick mass (KM) (eq. 5.3).

$$KMD = (Nominal Kendrick Mass - Exact Kendrick Mass) \quad (5.2)$$

$$KM = IUPAC\ mass * \frac{14}{14.01565} \quad (5.3)$$

Compounds in the same series (i.e., with the same number of heteroatoms and degrees of unsaturation) will have the same KMD. In the diagram, each series is aligned horizontally with a deviation of 14 that reflects a difference of one -CH₂- pattern. A shift of 0.01340 on the vertical axis corresponds to implementation of 1 unsaturation. Originally reported for the investigation of petroleomics-type samples in the early 2000s [30, 31], the use of the Kendrick diagram has been extended and adapted over the years for complex environmental samples [32–34] metabolomic studies [35, 36] and proteomics on phosphopeptides [37]. As needs differ between environmental chemistry and petroleomics, many studies have focused on modification of the mass defect [11] in order to characterize reaction products such as oxidation or chlorination [38, 39]. Even with a mass measurement accuracy of 1 ppm, a compound with a mass of 200 Da is assigned only 1 raw formula, while one with a mass of 500 Da is assigned 21 [40]. Regarding this issue, the Kendrick diagram can significantly increase the number of single raw formulae that can be assigned from m/z values in a mass spectrum. From the raw formula of the first compound, the identification of homologous series aids in assigning the raw formulae of other compounds in the series regardless of their mass. This allows a complex spectrum to be recalibrated, to obtain the best possible accuracy and thus assign as many raw formulae as possible (e.g., prior to a principal component analysis) [41, 42].

– Van Krevelen diagrams

The van Krevelen diagram, originally used in petroleomics to control oil and kerosene quality, represents the H/C ratio as a function of the O/C or N/C ratio for each ion of a complex mixture [12]. This allows the composition of a sample to be quickly estimated based on constituent molecular families (lipids, proteins, sugars, carbohydrates, lignin, tannins, etc.) [13]. Today, this representation is commonly used for environmental samples to track their evolution following an event such as treatment or pollution [43–47]. Some studies have extended the van Krevelen diagram over 3 dimensions to achieve better classification of compounds and better differentiation between complex mixtures. In some cases, this approach is associated with other t-test type statistical tests [14, 48].

– Multivariate statistical analysis

Multivariate statistical analysis is a versatile tool for dealing with high-dimensional datasets, and many methods can be used to extract valuable information, perform data compression, assess subclasses and compare groups of samples assessing relationships between variables. For quantitative datasets, two categories of model can be distinguished in terms of the relationship between variables and response, according to the parameters: linear and non-linear. An example is UV-Vis absorbance analysis of a complex mixture, where the absorbance depends on the concentrations of all the compounds present in the mixture, based on a linear relationship; in this case, multivariate linear regression can describe the correlations [15]. On the other hand, supervised and unsupervised methods

are applied for qualitative datasets [16, 49]. Principal component analysis, an unsupervised method, is usually implemented as a first approach for visualization, dimensionality reduction, classification, and finding patterns of similarities in the dataset [17, 50]. Supervised methods require *a priori* information, meaning that classes, determined by specific qualitative properties, are known in advance, and this information is used to sharpen the distinction between the given classes. A subclass of these methods, discriminant analysis, studies why the classes are different and which variables drive their separation, bearing the largest discriminatory power (e.g., Partial Least Squares Discriminant Analysis) [51]. The main areas of application in mass spectrometry data interpretation include food analysis and authentication [52–55], environmental sample analysis [56, 57], proteomics [58, 59], metabolomics in diagnostics and biology [60–62], and imaging [63, 64]. However, when dealing with high-dimensionality data (e.g., direct infusion HRMS) it is difficult to assess and visualize which variables account for the differences. Usually, variable selection [65] or sparse methods [20] must be applied, which are able to remove or suppress variables that are irrelevant to response prediction or classification [21]. These methods proved their efficiency but have to be used with caution to avoid losing valuable information, to prevent overfitting, and to handle chance correlations correctly. In summary, multivariate analysis tools enable global understanding of many concomitant variables and of their inter-correlations. The concept behind multivariate analysis is different from that of the SPIX software: the latter aims at observing all statistically relevant variables individually.

Table S5.2.1: Current kinetic models in SPIX - equations

Model	Theoretical equation	Experimental equations for the examples shown
A1	$f=f_0+A*\exp(-k*t); k>0$	$1.18E+06 + 1.70E+08 * \exp(-5.50E-02 * t)$
A2	$f=f_0+A1*\exp(-k1*t)+A2*\exp(-k2*t); k1>0 ; k2>0$	$8.22E+05 + 1.89E+06 * \exp(-9.61E-01 * t) + 1.25E+06 * \exp(-6.93E-02 * t)$
B1	$f=f_0+B*(1-\exp(-k*t)); k>0$	$4.69E+06 - 3.91E+06 * \exp(-3.17E-02 * t)$
B2	$f=A+B/(1+C*\exp(-k*t)); k>0$	$1.21E-12 + 1.47E+07 / (1 + \exp(-4.83E-02 * (t - 65.23)))$
C1	$f=f_0+A*(\exp(-k1*t)-\exp(-k2*t)); k2>k1>0$	$1.90E+07 + 3.25E+08 * (\exp(-1.00E-01 * t) - \exp(-1.06E-01 * t))$
C2	$f=f_0+A1*\exp(-k1*t)-A2*\exp(-k2*t); k2>k1>0; A1>A2$	$3.64E+07 + 3.70E+08 * \exp(-3.96E-02 * t) - 3.52E+08 * \exp(-4.29E-02 * t)$
D1	$f=f_0+A1*\exp(-k1*t)-A2*\exp(-k2*t); k1>k2>0 ; A2>A1$	$1.01E+09 + 6.22E+05 * \exp(-2.14E-01 * t) - 1.01E+09 * \exp(-5.12E-05 * t)$

SI-2. Chemicals, reagents, irradiation processes and sample preparation

– Chemicals and reagents

Acetamiprid ((E)-N-(6-chloro-3-pyridylmethyl)-N'-cyano-N-methylacetamide), maprotiline hydrochloride (N-methyl-3-(1-tetracyclo[6.6.2.02,7.09,14]hexadeca-2,4,6,9,11,13-hexaenyl) propan-1-amine;hydrochloride), acetonitrile (ACN) and formic acid (FA)

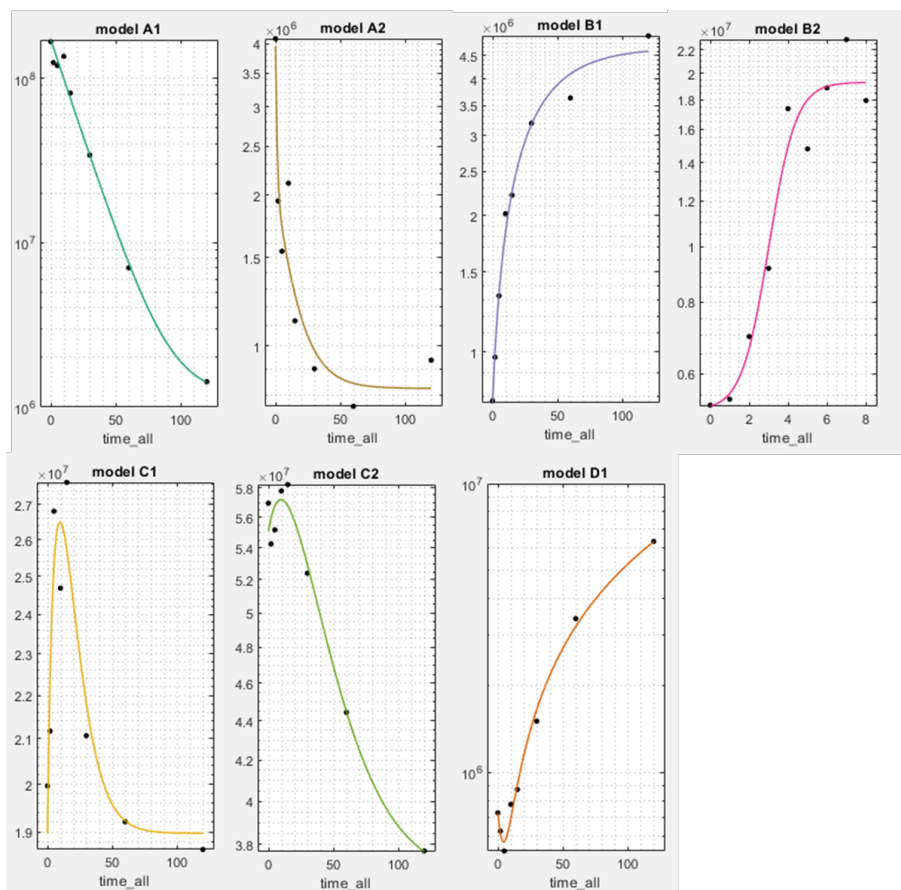


Figure S5.2.1: Current kinetic models in SPIX

(chromatographic grade purity > 99.99% for both) were purchased from Sigma-Aldrich (Saint Quentin Fallavier, France). Suwannee River Fulvic Acid Standard was purchased from International Humic Substances Society (Denver, CO, USA). Ultrapure water (specific resistance, 18 M Ω cm⁻¹ at 25 °C) was produced by a Purelab Chorus 1 water purification system purchased from Veolia Water Technologies (Wissous, France).

– Sample preparation

a.) Peroxide/UV photodegradation of maprotiline in wastewater

The UV photocatalyzed degradation of maprotiline was carried out in a 45-L pilot plant with continuous flow at a wastewater treatment plant operated by the FACSA company in Alhama de Murcia, Spain. The molecule was submitted to peroxide/UV advanced oxidation process. The pilot plant included a tank for mixing with a stirrer, a reactor with UV lamp (model UVLA-325-4, controlled by a Synergy 3 control panel - ATG UV Technology, Wigan, UK), a pump for water circulation, a rotameter to assess the water flow, and a compressor (Metabo Basic 250-50 W, Metabowerke, Nürtingen, Germany) to provide airflow in the rotameter equipped-reactor. The wastewater, secondary treated water originating from municipal and industrial sources, was transferred into the pilot plant after undergoing preliminary treatment (screening, sand and grease removal): decantation, biological treatment and sand filtration, before the chlorination step. At this point

there were still bacteria in the mixture as well as micropollutants, which the traditional wastewater treatment methods are not able to remove. The wastewater was spiked with Maprotiline hydrochloride at 5 ppm, and the total organic carbon content of the mixture was measured as 37.2 mg/L. 4 mL of hydrogen peroxide of technical grade (33 v/w%, VWR chemicals, Llinars del Vallès, Spain) were added to the pilot plant; this corresponds to the stoichiometric amount needed for maprotiline mineralization. Since the reaction with peroxide radical is usually fast, the reaction time was 10 minutes and the sampling for HRMS (2 x 1 mL) was done at the following times: t0 (3 samples), 1 min, 2.5 min, 5 min, 7.5 min and 10 min. The only sample preparation before direct infusion mass spectrometry analysis was the addition of 0.1 mL of acetonitrile and 0.1% of formic acid to the 1-mL samples, to achieve better ionization and solubility. Direct infusion HRMS was aimed at suppressing many sample preparation steps, to gain a considerable amount of time and avoid too much variability and operator subjectivity.

b.) UV irradiation of acetamiprid in an aqueous solution of humic acid

Acetamiprid has been detected in agriculture water samples at concentrations of up to 44 µg/L [66]. Therefore, a 40 µg/L acetamiprid solution was prepared using an aqueous solution of fulvic acid at 20 mg/L, a mean value corresponding to the amount usually found in natural waters [67]. Six glass tubes of the solution were simultaneously irradiated for 30 minutes in a laboratory-made reactor equipped with a UV-Vis high-pressure mercury lamp HPL-N125W/542 E27 SC (Philips, Ivry-sur-Seine, France) emitting light at wavelengths ranging from 200 nm to 650 nm, with a maximum irradiation wavelength at 254 nm and a radiation flux of 6200 lm. Each tube contained 50 mL of solution to ensure good surface irradiation. 1 mL of solution was taken twice from each tube before and after irradiation. Samples were analyzed by electrospray ionization-MS using automated direct infusion with a solvent made up of 50% H₂O/AF (0.1%) and 50% ACN/AF (0.1%) at a flow rate of 0.002 mL/min. The six replicates and blanks (H₂O/ACN 50/50 v/v) were randomly analyzed and data were extracted in a «.xy» text format so that they could be treated with the SPIX software.

Table S5.2.2: Exported data from the SPIX software after assignation of a kinetic model to a *m/z* ratio.

Segment	<i>m/z</i>	Intensity	Time	File
65	278.19055	3.53E+10	0.0	Maprotiline WW H2O2 0min B.xy
65	278.19057	3.39E+10	1.0	Maprotiline WW H2O2 1min B.xy
65	278.19050	8.34E+09	2.5	Maprotiline WW H2O2 2min B.xy
65	278.19052	3.74E+09	5.0	Maprotiline WW H2O2 5min B.xy
65	278.19057	1.95E+09	7.5	Maprotiline WW H2O2 7min B.xy
65	278.19053	8.84E+08	10.0	Maprotiline WW H2O2 10min B.xy

m/z	r^2	p-value	model
278.19053	0.99	0.000776	A1

References

- [1] J Hollender, B van Bavel, V Dulio, E Farmen, K Furtmann, J Koschorreck, U Kunkel, M Krauss, J Munthe, M Schlabach, J Slobodnik, G Stroomberg, T Ternes, NS Thomaidis, A Togola, and V Tornero. “High resolution mass spectrometry-based non-target screening can support regulatory environmental monitoring and chemicals management.” In: *Environ Sci Eu* 31.42 (2019), pp. 62–67. DOI: 10.1186/s12302-019-0225-x.
- [2] C Giorio, C Bortolini, I Kourtchev, A Tapparo, S Bogialli, and M Kalberer. “Direct target and non-target analysis of urban aerosol sample extracts using atmospheric pressure photoionisation high-resolution mass spectrometry”. In: *Chemosphere* 224 (2019), pp. 786–795. DOI: 10.1016/j.chemosphere.2019.02.151.
- [3] NG Hoh Eand Dodder, SJ Lehotay, KC Pangallo, C M Reddy, and KA Maruya. “Nontargeted Comprehensive Two-Dimensional Gas Chromatography/Time-of-Flight Mass Spectrometry Method and Software for Inventorying Persistent and Bioaccumulative Contaminants in Marine Environments”. In: *Environ Sci Technol* 46.15 (2012), pp. 8001–8008. DOI: 10.1021/es301139q.
- [4] J Guo, D Chen, D Potter, KJ Rockne, NC Sturchio, JP Giesy, and A Li. “Polyhalogenated Carbazoles in Sediments of Lake Michigan: A New Discovery”. In: *Environ Sci Technol* 48.21 (2014), pp. 12807–12815. DOI: 10.1021/es503936u.
- [5] EL Schymanski, HP Singer, P Longrée, M Loos, M Ruff, MA Stravs, C Ripollés Vidal, and J Hollender. “Strategies to Characterize Polar Organic Contamination in Wastewater: Exploring the Capability of High Resolution Mass Spectrometry”. In: *Environ Sci Technol* 48.3 (2014), pp. 1811–1818. DOI: 10.1021/es4044374.
- [6] P Gago-Ferrero, EL Schymanski, AA Bletsou, R Aalizadeh, J Hollender, and NS Thomaidis. “Extended Suspect and Non-Target Strategies to Characterize Emerging Polar Organic Contaminants in Raw Wastewater with LC-HRMS/MS”. In: *Environ Sci Technol* 49.20 (2015), pp. 12333–12341. DOI: 10.1021/acs.est.5b03454.
- [7] A Kinani, S Kinani, and S Bouchonnet. “Formation and determination of organohalogen by-products in water. Part III. Characterization and quantitative approaches”. In: *Trends Anal Chem* 85 (2016), pp. 295–305. DOI: 10.1016/j.trac.2016.09.013.

- [8] EL Schymanski, HP Singer, J Slobodnik, IM Ipolyi, P Oswald, M Krauss, T Schulze, P Haglund, T Letzel, S Grosse, NS Thomaidis, A Bletsou, C Zwiener, M Ibanez, T Portoles, R de Boer, MJ Reid, M Onghena, U Kunkel, W Schulz, A Guillon, N Noyon, G Leroy, P Bados, S Bogialli, D Stipanicev, P Rostkowski, and J Hollender. “Non-target screening with high-resolution mass spectrometry: critical review using a collaborative trial on water analysis.” In: *Anal Bioanal Chem* 407 (2015), pp. 6237–6255. DOI: 10.1007/s00216-015-8681-7.
- [9] A Togola, C Soulier, F Lestremau, V Dulio, C Margoum, C Miège, S Lardy-Fontan, and J Cabilic. *Positionnement et actions d’AQUAREF sur l’analyse non ciblée pour la surveillance des milieux aquatiques*. 2018. URL: https://www.ineris.fr/sites/ineris.fr/files/contribution/Documents/AQUAREF_Togola_NTS.pdf.
- [10] E Kendrick. “A Mass Scale Based on $\text{CH}_2 = 14.0000$ for High Resolution Mass Spectrometry of Organic Compounds.” In: *Anal Chem* 35.13 (1963), pp. 2146–2154. DOI: 10.1021/ac60206a048.
- [11] L Sleno. “The use of mass defect in modern mass spectrometry.” In: *J Mass Spectrom* 47.2 (2012), pp. 226–236. DOI: 10.1002/jms.2953.
- [12] DW Van Krevelen. “Graphical-statistical method for the study of structure and reaction processes of coal.” In: *Fuel* 29 (1950), pp. 228–269.
- [13] W Kew, JWT Blackburn, DJ Clarke, and D Uhrin. “Inter-active van Krevelen diagrams: Advanced visualisation of mass spectrometry data of complex mixtures.” In: *Rapid Commun Mass Spectrom* 31.7 (2017), pp. 658–669. DOI: 10.1002/rcm.7823.
- [14] Z Wu, RP Rodgers, and AG Marshall. “Two- and Three-Dimensional van Krevelen Diagrams: A Graphical Analysis Complementary to the Kendrick Mass Plot for Sorting Elemental Compositions of Complex Organic Mixtures Based on Ultrahigh-Resolution Broadband Fourier Transform Ion Cyclotron Resonance Mass Measurements”. In: *Anal Chem* 76.9 (2004), pp. 2511–2516. DOI: 10.1021/ac0355449.
- [15] DL Massart, BGM Vandeginste, SM Deming, Y Michotte, and L Kaufman. *Regression Methods in Chemometrics: A Textbook*. Amsterdam: Elsevier, 1988, pp. 165–182. DOI: 10.1002/cem.1180020409.
- [16] PC Jurs. “Pattern recognition used to investigate multivariate data in analytical chemistry.” In: *Science* 232.4755 (1986), pp. 1219–1224. DOI: 10.1126/science.3704647.
- [17] H Abdi and LJ Williams. “Principal component analysis.” In: *WIREs Comput Stat* 2.4 (2010), pp. 433–459. DOI: 10.1002/wics.101.

- [18] M Rantalainen, O Cloarec, JK Nicholson, E Holmes, and J Trygg. “OPLS discriminant analysis: Combining the strengths of PLS-DA and SIMCA classification.” In: *J Chemom* 20.8-10 (2006), pp. 341–351. DOI: 10.1002/cem.1006.
- [19] F Araujo, P Peres, and FS Fogliatto. “Variable selection methods in multivariate statistical process control: A systematic literature review.” In: *Comput Ind Eng* 115 (2017), pp. 603–611. DOI: 10.1016/j.cie.2017.12.006.
- [20] H Zou, T Hastie, and R Tibshirani. “Sparse principal component analysis.” In: *J Comput Graph Stat* 15 (2006), pp. 265–286. DOI: 10.1198/106186006X113430.
- [21] P Filzmoser, M Gschwandtner, and V Todorov. “Review of sparse methods in regression and classification with application to chemometrics.” In: *J Chemometr* 26.3-4 (2012), pp. 42–51. DOI: 10.1002/cem.1418.
- [22] H Wu, R Xue, Z Tang, C Deng, T Liu, H Zeng, Y Sun, and X Shen. “Metabolomic investigation of gastric cancer tissue using gas chromatography/mass spectrometry.” In: *Anal Bioanal Chem* 396 (2010), pp. 1385–1395. DOI: 10.1007/s00216-009-3317-4.
- [23] EA Thevenot, A Roux, Y Xu, E Ezan, and C Junot. “Analysis of the human adult urinary metabolome variations with age, body mass index, and gender by implementing a comprehensive workflow for univariate and OPLS statistical analyses.” In: *J Proteome Res* 14.8 (2015), pp. 3322–3335. DOI: 10.1021/acs.jproteome.5b00354.
- [24] JA Kirwan, RJM Weber, DI Broadhurst, and MR Viant. “Direct infusion mass spectrometry metabolomics dataset: A benchmark for data processing and quality control.” In: *Sci Data* 1.140012 (2014). DOI: 10.1038/sdata.2014.12.
- [25] E Nicol, Y Xu, Z Varga, R Grosshans, M Lavielle, and S Bouchonnet. “Variability and subjectivity in analytical chemistry.” In: *International Winter School on Mass Spectrometry (Palaiseau, France)* (2019).
- [26] R Mathur and PB O’Connor. “Artifacts in Fourier transform mass spectrometry.” In: *Rapid Commun Mass Spectrom* 23.4 (2009), pp. 523–529. DOI: 10.1002/rcm.3904.
- [27] T Kind and O Fiehn. “Seven golden rules for heuristic filtering of molecular formulas obtained by accurate mass spectrometry.” In: *BMC Bioinform* 8.105 (2007). DOI: 10.1186/1471-2105-8-105.
- [28] NPF Gonçalves, Z Varga, S Bouchonnet, V Dulio, N Alygizakis, F Dal Bello, C Medana, and P Calza. “Study of the photoinduced transformations of maprotiline in river water using liquid chromatography high-resolution mass spectrometry.” In: *Sci Total Environ* 755.2 (2020), p. 143556. DOI: 10.1016/j.scitotenv.2020.143556.

- [29] E Nicol, Z Varga, S Vujovic, and S Bouchonnet. “Laboratory scale UV–visible degradation of acetamiprid in aqueous marketed mixtures – Structural elucidation of photoproducts and toxicological consequences.” In: *Chemosphere* 248 (2020), p. 126040. DOI: 10.1016/j.chemosphere.2020.126040.
- [30] AG Marshall and RP Rodgers. “Petroleomics: The Next Grand Challenge for Chemical Analysis”. In: *Acc Chem Res* 37.1 (2004), pp. 53–59. DOI: 10.1021/ar020177t.
- [31] CA Hughey, CL Hendrickson, RP Rodgers, AG Marshall, and K Qian. “Kendrick mass defect spectrum: a compact visual analysis for ultrahigh-resolution broadband mass spectra.” In: *Anal Chem* 73.19 (2001), pp. 4676–4681. DOI: 10.1021/ac010560w.
- [32] FL Chu, L Pirastru, R Popovic, and L Sleno. “Carotenogenesis up-regulation in *Scenedesmus* sp. using a targeted metabolomics approach by liquid chromatography – high-resolution mass spectrometry.” In: *J Agric Food Chem* 59.7 (2011), pp. 3004–3013. DOI: 10.1021/jf105005q.
- [33] RL Sleighter and PG Hatcher. “The application of electrospray ionization coupled to ultrahigh resolution mass spectrometry for the molecular characterization of natural organic matter.” In: *J Mass Spectrom* 42.5 (2007), pp. 559–574. DOI: 10.1002/jms.1221.
- [34] R.W Kramer, EB Kujawinski, and PG Hatcher. “Identification of black carbon derived structures in a volcanic ash soil humic acid by Fourier transform ion cyclotron resonance mass spectrometry.” In: *Environ Sci Technol* 38.12 (2004), pp. 3387–3395. DOI: 10.1021/es030124m.
- [35] S Ni, Qian D, J Duan, J Guo, E-X Shang, Y Shu, and C Xue. “UPLC-QTOF/MS-based screening and identification of the constituents and their metabolites in rat plasma and urine after oral administration of *Glechoma longituba* extract.” In: *J Chromatogr B* 878.28 (2010), pp. 2741–2750. DOI: 10.1016/j.jchromb.2010.08.014.
- [36] H Zhang, D Zhang, K Ray, and M Zhu. “Mass defect filter technique and its applications to drug metabolite identification by high-resolution mass spectrometry.” In: *J Mass Spectrom* 44.7 (2009), pp. 999–1016. DOI: 10.1002/jms.1610.
- [37] C Bruce, P Shifman MA Miller, and EE Gulcicek. “Probabilistic enrichment of phosphopeptides by their mass defect.” In: *Anal Chem* 78.13 (2006), pp. 4374–4382. DOI: 10.1021/ac060046w.

- [38] KJ Jobst, L Shen, EJ Reiner, VY Taguchi, PA Helm, R McCrindle, and S Backus. “The use of mass defect plots for the identification of (novel) halogenated contaminants in the environment.” In: *Anal Bioanal Chem* 405 (2013), pp. 3289–3297. DOI: 10.1007/s00216-013-6735-2.
- [39] VY Taguchi, RJ Nieckarz, RE Clement, S Krolik, and R Williams. “Dioxin analysis by gas chromatography-Fourier transform ion cyclotron resonance mass spectrometry (GC-FTICRMS).” In: *J Am Soc Mass Spectrom* 21 (2010), pp. 1918–1921. DOI: 10.1016/j.jasms.2010.07.010.
- [40] T Kind and O Fiehn. “Metabolomic database annotations via query of elemental compositions: Mass accuracy is insufficient even at less than 1 ppm.” In: *BMC Bioinform* 7 (2006), p. 234. DOI: 10.1186/1471-2105-7-234.
- [41] C Ajaero, Dena W. McMartin, KM Peru, J Bailey, M Haakensen, V Friesen, R Martz, SA Hughes, C Brown, H Chen, AM McKenna, YE Corilo, and JV Headley. “Fourier Transform Ion Cyclotron Resonance Mass Spectrometry Characterization of Athabasca Oil Sand Process-Affected Waters Incubated in the Presence of Wetland Plants.” In: *Energy Fuels* 31.2 (2017), pp. 1731–1740. DOI: 10.1021/acs.energyfuels.6b02643.
- [42] C Ajaero, KM Peru, SA Hughes, H Chen, AM McKenna, YE Corilo, DW McMartin, and JV Headley. “Atmospheric pressure photoionization fourier transform ion cyclotron resonance mass spectrometry characterization of oil sand process-affected water in constructed wetland treatment.” In: *Energy Fuels* 33.5 (2019), pp. 4420–4431. DOI: 10.1021/acs.energyfuels.9b00469.
- [43] EC Minor, MM Swenson, BM Mattson, and AR Oyler. “Structural characterization of dissolved organic matter: a review of current techniques for isolation and analysis.” In: *Environ Sci - Proc Imp* 16 (2014), pp. 2064–2079. DOI: 10.1039/C4EM00062E.
- [44] J D’Andrilli, CM Foreman, AG Marshall, and DM McKnight. “Characterization of IHSS Pony Lake fulvic acid dissolved organic matter by electrospray ionization Fourier transform ion cyclotron resonance mass spectrometry and fluorescence spectroscopy.” In: *Org Geochem* 65 (2013), pp. 19–28. DOI: 10.1016/j.orggeochem.2013.09.013.
- [45] AS Wozniak, JE Bauer, RL Sleighter, RM Dickhut, and PG Hatcher. “Technical Note: Molecular characterization of aerosol-derived water-soluble organic carbon using ultrahigh resolution electrospray ionization Fourier transform ion cyclotron resonance mass spectrometry.” In: *Atmos Chem Phys* 8 (2008), pp. 5099–5111. DOI: 10.5194/acp-8-5099-2008.

- [46] N Hertkorn, R Benner, M Frommberger, P Schmitt-Kopplin, M Witt, K Kaiser, A Kettrup, and JI Hedges. “Characterization of a major refractory component of marine dissolved organic matter.” In: *Geochim Cosmochim Acta* 70.12 (2006), pp. 2990–3010. DOI: 10.1016/j.gca.2006.03.021.
- [47] S Kim, RW Kramer, and PG Hatcher. “Graphical method for analysis of ultrahigh-resolution broadband mass spectra of natural organic matter.” In: *Anal Chem* 75.20 (2003), pp. 5336–5344. DOI: 10.1021/ac034415p.
- [48] N Martins, NT Jiménez-Morillo, F Freitas, R Garcia, M Gomez da Silva, and MJ Cabrita. “Revisiting 3D van Krevelen diagrams as a tool for the visualization of volatile profile of varietal olive oils from Alentejo region, Portugal.” In: *Talanta* 207 (2020), pp. 120276–120285. DOI: 10.1016/j.talanta.2019.120276.
- [49] EK Kemsley. “Discriminant analysis of high-dimensional data: a comparison of principal components analysis and partial least squares data reduction methods”. In: *Chemom Intell Lab Syst* 33.1 (1996), pp. 47–61. DOI: 10.1016/0169-7439(95)00090-9.
- [50] M Ringnér. “What is principal component analysis?” In: *Nat Biotechnol* 26 (2008), pp. 303–304. DOI: 10.1038/nbt0308-303.
- [51] M Bylesjö, M Rantalainen, O Cloarec, JK Nicholson, E Holmes, and J Trygg. “OPLS discriminant analysis: combining the strengths of PLS-DA and SIMCA classification.” In: *J Chemom* 20.8-10 (2006), pp. 341–351. DOI: 10.1002/cem.1006.
- [52] MP Callao and I Ruisanchez. “An overview of multivariate qualitative methods for food fraud detection.” In: *Food Control* 86 (2018), pp. 283–293. DOI: 10.1016/j.foodcont.2017.11.034.
- [53] MP Marti, O Busto, and J Guasch. “Application of a headspace mass spectrometry system to the differentiation and classification of wines according to their origin, variety and ageing.” In: *J Chromatogr A* 1057.1-2 (2004), pp. 211–217. DOI: 10.1016/j.chroma.2004.08.143.
- [54] A Kenar, B Çiçek, FN Arslan, G Akin, SN Karuk Elmas, and I Yilmaz. “Electron impact-mass spectrometry fingerprinting and chemometrics for rapid assessment of authenticity of edible oils based on fatty acid profiling.” In: *Food Anal Methods* 12 (2019), pp. 1369–1381. DOI: 10.1007/s12161-019-01472-0.
- [55] J Rubert, O Lacina, M Zachariasova, and J Hajslova. “Saffron authentication based on liquid chromatography high resolution tandem mass spectrometry and multivariate data analysis.” In: *Food Chem* 204 (2016), pp. 201–209. DOI: 10.1016/j.foodchem.2016.01.003.

- [56] ME Karpuzcu, D Fairbairn, WA Arnold, BL Barber, E Kaufenberg, WC Koskinen, PJ Novak, PJ Rice, and DL Swackhamer. “Identifying sources of emerging organic contaminants in a mixed use watershed using principal components analysis.” In: *Environ Sci - Proc Imp* 16.10 (2014), pp. 2390–2399. DOI: 10.1039/C4EM00324A.
- [57] YE Corilo, DC Podgorski, AM McKenna, KL Lemkau, CM Reddy, AG Marshall, and RP Rodgers. “Oil Spill Source Identification by Principal Component Analysis of Electrospray Ionization Fourier Transform Ion Cyclotron Resonance Mass Spectra.” In: *Anal Chem* 85.19 (2013), pp. 9064–9069. DOI: 10.1021/ac401604u.
- [58] M Gaspari, KCM Verhoeckx, ER Verheij, and J van der Greef. “Integration of Two-Dimensional LCMS with Multivariate Statistics for Comparative Analysis of Proteomic Samples.” In: *Anal Chem* 78.7 (2006), pp. 2286–2296. DOI: 10.1021/ac052000t.
- [59] X Wang, MC Chambers, LJ Vega-Montoto, DM Bunk, SE Stein, and DL Tabb. “QC Metrics from CPTAC Raw LC-MS/MS Data Interpreted through Multivariate Statistics.” In: *Anal Chem* 86.5 (2014), pp. 2497–2509. DOI: 10.1021/ac4034455.
- [60] C Wang, H Kong, Y Guan, J Yang, J Gu, S Yang, and G Xu. “Plasma Phospholipid Metabolic Profiling and Biomarkers of Type 2 Diabetes Mellitus Based on High-Performance Liquid Chromatography/Electrospray Mass Spectrometry and Multivariate Statistical Analysis.” In: *Anal Chem* 77.13 (2005), pp. 4108–4116. DOI: 10.1021/ac0481001.
- [61] A Kiss, M Lucio, A Fildier, C Buisson, P Schmitt-Kopplin, and C Cren-Olivé. “Doping control using high and ultra-high resolution mass spectrometry based non-targeted metabolomics - a case study of salbutamol and budesonide abuse.” In: *PLoS One* 8.9 (2013), e74584. DOI: 10.1371/journal.pone.0074584.
- [62] H Tsugawa, Y Tsujimoto, M Arita, T Bamba, and E Fukusaki. “GC/MS based metabolomics: development of a data mining system for metabolite identification by using soft independent modeling of class analogy (SIMCA).” In: *BMC Bioinform* 12 (2011), pp. 131–144. DOI: 10.1186/1471-2105-12-131.
- [63] AL Dill, LS Eberlin, C Zheng, AB Costa, DR Ifa, L Cheng, TA Masterson, MO Koch, O Vitek, and RG Cooks. “Multivariate statistical differentiation of renal cell carcinomas based on lipidomic analysis by ambient ionization imaging mass spectrometry.” In: *Anal Bioanal Chem* 398 (2010), pp. 2969–2978. DOI: 10.1007/s00216-010-4259-6.
- [64] T Alexandrov. “MALDI imaging mass spectrometry: statistical data analysis and current computational challenges.” In: *BMC Bioinform* 13 (2012), S16. DOI: 10.1186/1471-2105-13-S16-S11.

- [65] FAP Peres and FS Fogliatto. “Variable selection methods in multivariate statistical process control: A systematic literature review.” In: *Comput Ind Eng* 115 (2018), pp. 603–619. DOI: 10.1016/j.cie.2017.12.006.
- [66] TA Anderson, CJ Salice, RA Erickson, ST McMurry, S.B Cox, and LM Smith. “Effects of landuse and precipitation on pesticides and water quality in playa lakes of the southern high plains.” In: *Chemosphere* 92.1 (2013), pp. 84–90. DOI: 10.1016/j.chemosphere.2013.02.054.
- [67] EM Thurman. “Amount of organic carbon in natural waters”. In: *Organic geochemistry of natural waters*. Dordrecht: Springer, 1985. Chap. 2, pp. 7–65. URL: https://link.springer.com/chapter/10.1007/978-94-009-5095-5_2.

5.3 Latest developments of SPIX - 3D approach

In this project, the photodegradation reactions resulted in multiple isomeric photoproducts; therefore, the chromatographic dimension was indispensable to characterize them accurately. To process them, the development of SPIX to handle three-dimensional datasets (GC-MS, LC-MS) started. It is only in its early development stages; the following section presents some of the preliminary data obtained from an LC-MS dataset.

A demo dataset was obtained from the LC-MS analysis of the same BIT photodegradation reaction; it contains four datapoints. This can be found when downloading the software (<http://spix.webpopix.org/benzisothiazolinone.html>). The data format is mzXML, but further developments will be done to extend it to different formats. This is an extensible markup language-based file format commonly used for proteomics datasets. The concept behind this approach was to obtain an image (Figure 5.3.1), in which m/z values are on the x-axis, the retention time on the y axis, and the colors will mark the m/z-retention time pairs where statistically significant changes occur over the course of a reaction. Again the threshold of m/z intensities which will be considered for data processing can be adjusted. For the easier readability of the data, the m/z scale is not linear, but only the values that undergo change will appear. The data is aligned considering both m/z values and retention times.

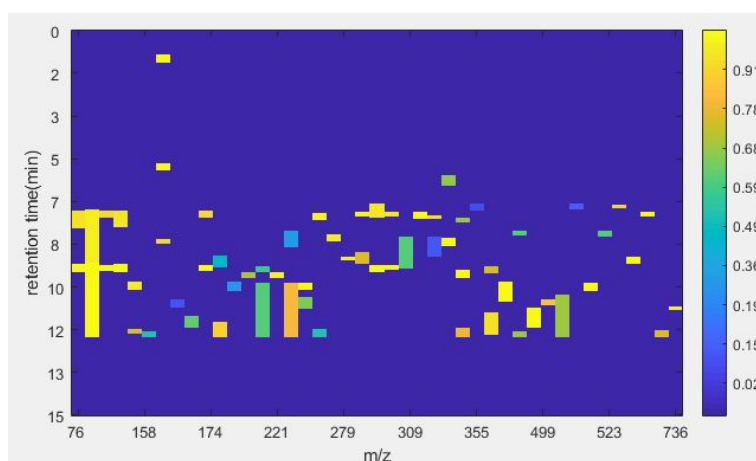


Figure 5.3.1: LC-MS dataset in SPIX with a threshold of 4.2×10^7

When considering the parent compound, a decaying pattern is obtained (Figure 5.3.2). The exponential models are the same as those used for 2D data processing; therefore, this appears as an A1 model (- -). There is also the possibility of polynomial modeling.

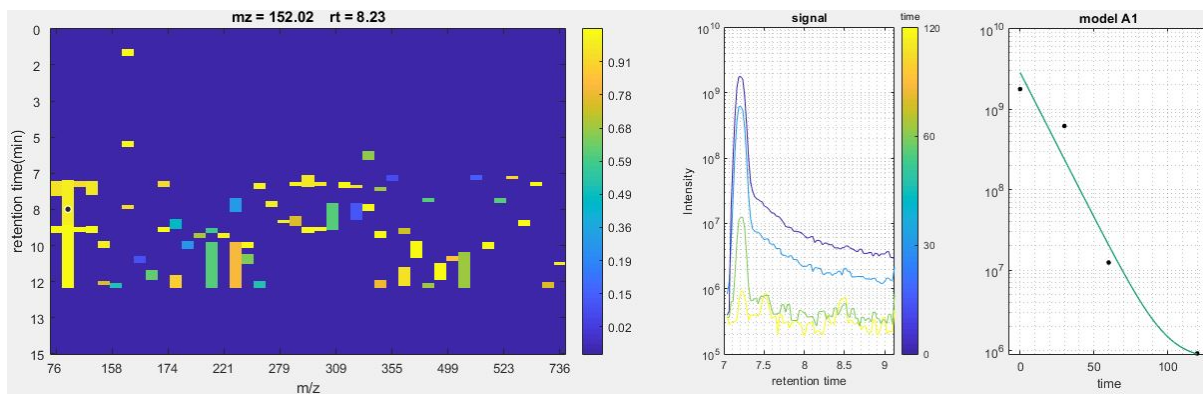


Figure 5.3.2: Modeling the behavior of the parent compound, exponential fit

Since the chromatographic separation allows the differentiation of isomers, the data processing will also achieve their separation. Therefore the isomer of the parent compound, which appears as a result of the irradiation, is detected and modeled (Figure 5.3.3). This corresponds to the model C1, with an increasing tendency, followed by a slight decrease in intensity.

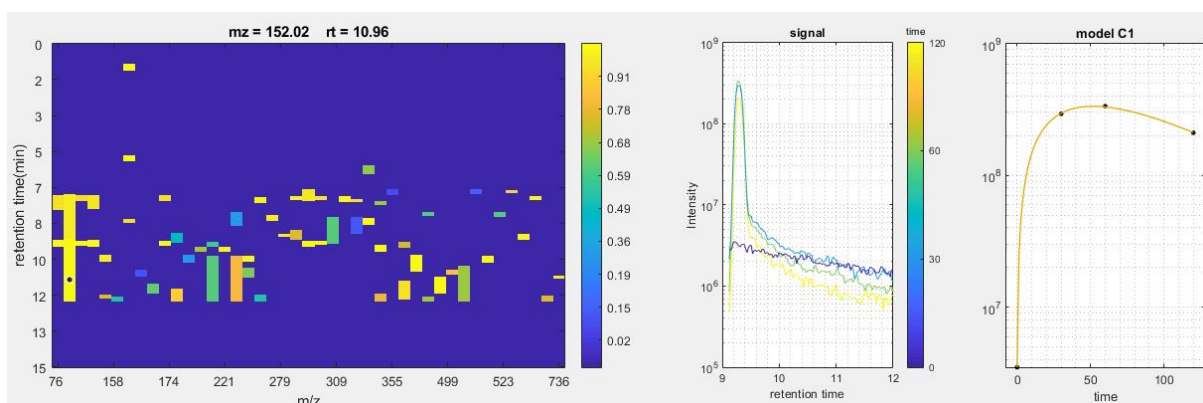


Figure 5.3.3: Modeling the behavior of an isomer of the parent compound, exponential fit

Considering that this was the first dataset processed with this approach, further improvements are envisaged in the future, consisting of evaluating datasets with more data points and improving the kinetic models since not all of them offer satisfactory fitting. It also shows the necessity for replicates as this first set of experiments used only one point for each condition. (Figure 5.3.4)

The relevant m/z -retention time pairs can be obtained by exporting the data, characterized by their statistical significance (Table 5.3.1). In this case, the p -values did not show satisfactory significance due to the limited number of data points. Using SPIX, almost all the peaks were found, which were previously identified using the modeling approach, except two isomers, resulting from the fact that their retention times were so close to each other that SPIX merged the two peaks during data alignment; this requires further

investigation.

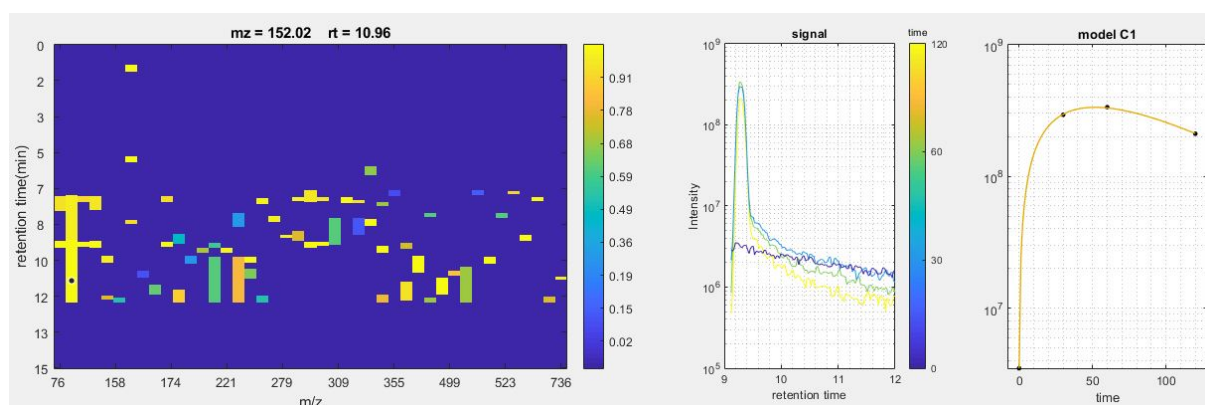


Figure 5.3.4: Modeling the behavior of a photoproduct, exponential fit

Table 5.3.1: Exporting the simulated data for the 3D dataset

m/z	retention time	r^2	p-value	model
122.096954	5.6	0.86616409	1	B2
138.05542	2.5	0.87899445	1	B2
138.05542	7.3	0.98948098	1	B2
152.017014	8.1	0.96231088	0.19413687	A1
152.017014	10.6	0.99998014	1	C1
168.011932	1.2	0.99695173	1	C1
168.011932	5.4	0.99880122	1	C1
168.011932	8.3	0.91619611	1	B2
202.017517	1.7	0.99822795	1	B2

The 3D approach is a useful complement to the previously developed 2D approach. It can be applied to a variety of datasets from different fields. It could provide a rapid scanning of vast amounts of samples to find statistically relevant information. Further features are planned, such as integrating multiple file formats and improving data alignment, which is still a general data processing difficulty in mass spectrometry. Overall developing, this software was instructive and provided a great insight into the challenges and necessity of interdisciplinary approaches.

Conclusions

In this project, advancements were achieved regarding the understanding of the fate of contaminants of emerging concern under photochemical processes. As a myriad of CECs exist that have an increasingly negative impact on the environment and human health, it is essential to work towards their mitigation. Water treatment technologies based on direct irradiation by light and advanced oxidation processes are promising abatement approaches. Efforts are made to use not only artificial UV irradiation but also irradiation by natural sunlight, which constitutes a renewable energy resource and is in line with attaining sustainability goals. However, upscaling remains a challenge due to the wide variety of contaminants in the presence of complex matrices. By studying AOPs in a pilot plant, it was shown that the optimization of these processes is challenging, and the choice of the treatment process should be tailored considering the influence of various parameters and the water composition. Ideally, mineralization of compounds should occur; however, this is almost never fully achieved, especially in the case of highly persistent chemicals. Since these are novel processes, it is essential to understand the associated physicochemical mechanisms, to avoid or minimize the formation of harmful by-products. The application of non-targeted analysis gives insight into understanding the efficiency and safety of the water treatment processes. This approach allowed the detection of halogenated disinfection by-products in the drinking water distributed in Turin area, as a result of a collaboration with Società Metropolitana Acque Torino S.p.A. (SMAT). Future work will be to repeat the sampling campaign and analysis, and optimize the treatment processes to minimize the formation of these potentially dangerous by-products.

In this study, photodegradation reactions were investigated. Although very powerful, photochemistry is still not very well understood due to unconventional activation energies and photochemical routes. This work aimed at improving their understanding, the ultimate goal being to predict photochemical reaction outcomes based on chemical functions. Advances in high-resolution mass spectrometry and data processing immensely helped in the assessment of molecular formulae and structures, even in complex mixtures. By using non-targeted analysis, a significant number of molecules could be detected. Through the modeling approach, the structures of detected photoproducts were tentatively assessed by the elucidation of fragmentation patterns; this helped in gaining expertise on photochemical degradation mechanisms. On the other hand, the laboratory-developed software, SPIX, provided a holistic overview of the changes occurring in a complex mixture during light irradiation. These statistical analyses are necessary to extract relevant information

from the generated large datasets. As an example from this project, the photodegradation of a pharmaceutical compound, maprotiline, was studied using the modeling approach in ultrapure water. This made possible the elucidation of photoproducts and perform risk assessment. When the compound was studied in secondary treated water, the approach involving ultrahigh-resolution DI-MS and data processing with SPIX, yielded highly relevant results, as the detection of photoproducts was facilitated by the provided kinetic models. The combination of the two approaches gave an in-depth understanding of the process in different matrices, and the complementarity of these techniques provided certitude in the results, both through detailed structural assessment by the modeling approach and relevant statistical information from the holistic approach.

After performing the photodegradation experiments and elucidating photoproducts, multiple toxicity testing should be carried out to follow the potential photo-induced toxic effects. This way, risks such as inducing antibiotic resistance in bacteria, accumulation of carcinogenic molecules, or transport of behavior-altering compounds into aquatic organisms could be decreased. In this project, a combination of *in silico* and *in vitro* toxicity tests was applied successfully to assess potentially hazardous molecules. The accuracy of *in silico* toxicity estimations increases due to the rapid development of computational methods and expanding databases; such testing constitutes a promising complementary approach to *in vivo* and *in vitro* ones. General protocols based on a combination of toxicity testing approaches should be implemented to achieve comparable and reproducible results in the field of environmental toxicity assessment.

As part of a collaboration with Dr. Claire Richard (Université Clermont Auvergne), a short-term future project includes continuing studying the interaction of natural organic matter with CECs. This is a promising research area that will help to understand both the transformations of CECs in the environment and the influence of NOM on water treatments. As NOM represents a highly complex mixture, SPIX will be an asset in data processing. It will help overcome already encountered analytical challenges produced by the high sensitivity of the matrix to various parameters, such as pH and concentration, by aiding in their optimization to achieve reproducibility. In the mid to long term, SPIX will be employed in various analytical areas. Our team considers applying it to aroma and fragrance authentication studies to find relevant differences when comparing counterfeits to original samples with strong intrinsic variability. Another planned application is the monitoring of metabolites of aquatic organisms, studied under controlled conditions and induced stress in an aquarium. This biological application will help in understanding and improving filtration systems. In a general perspective, SPIX may be used to monitor all types of chemical reactions – even unknown or unexpected ones – from the laboratory up to the industrial scale.

In conclusion, advances were accomplished in photochemistry, structural elucidation, risk assessment of photochemical processes, toxicity testing, and HRMS data analysis. This project showed that large-scale issues, such as the increasing number of contaminants of emerging concern, have a multi-level impact. To tackle complex problems by finding and applying innovative solutions, a close collaboration between various stakeholders is necessary, such as governments, researchers, and industries. The AQUAlity project showed that working together with other European teams brings cross-sectoral and multidisciplinary expertise, creative ideas, innovation, and fruitful scientific results. European scale projects are imperative to attain a sustainable future, protect the environment, and improve life quality. I am sincerely thankful to have had the opportunity to be part of such an ambitious project during three years and a half, and for all the gained experience from the valuable collaborations, both on a scientific and personal level.

Titre: Photodégradation de contaminants d'intérêt émergent en matrices environnementales: nouvelle approche holistique complémentaire à la modélisation en laboratoire

Mots clés: Spectrométrie de masse haute résolution, Produits de photodégradation, Tests in silico, Éluclidation structural, Procédés avancés d'oxydation

Résumé: Les contaminants d'intérêt émergent constituent une source importante de préoccupation en raison de leurs effets toxiques potentiels et de leur persistance dans l'environnement. Il est essentiel d'élaborer de nouvelles approches de traitement pour améliorer la qualité des eaux. Les procédés basés sur l'irradiation par la lumière sont très prometteurs. Il convient néanmoins de considérer la formation de photoproduits potentiels et la toxicité de ces derniers. Un des objectifs de ce projet était de comparer différentes approches pour étudier la photodégradation des CECs. Une approche de modélisation en laboratoire a d'abord été appliquée à cinq contaminants. La photolyse directe et certains procédés avancés d'oxydation ont été employés en conditions de laboratoire, ou à l'échelle d'une usine pilote dans des eaux usées traitées secondaires. La minéralisation des polluants étant rarement atteinte, des analyses non ciblées ont été réalisées sur un spectromètre de masse FT-ICR à très haute résolution. Cela a rendu possible l'identification précise des formules moléculaires alors que l'élucidation des structures

des photoproduits a été conduite par MS². Des calculs in silico ont été effectués à partir des structures des photoproduits pour évaluer leurs effets toxiques potentiels. Cette approche a permis d'évaluer le devenir des contaminants, de proposer et optimiser des procédés de photodégradation efficaces et d'élucider les mécanismes réactionnels associés. Parallèlement à la modélisation, une approche analytique non ciblée a été utilisée pour étudier des mélanges complexes. Le logiciel SPIX a été développé pour extraire les informations pertinentes de ces données complexes. Il permet de révéler l'évolution d'une série de conditions, proposant des modèles cinétiques associés. L'exportation de données statistiquement pertinentes et leur traitement ont été réalisés. L'approche holistique fournie par SPIX constitue un outil complémentaire aux approches de modélisation; il permet de détecter et de surveiller les réactions pertinentes dans des média très complexes et contribue significativement à réduire la subjectivité de l'opérateur.

Title: Photodegradation of contaminants of emerging concern in environmental matrices: a new holistic perspective to complete the laboratory modeling approach

Keywords: High-resolution mass spectrometry, Photodegradation products, In silico tests, Structural elucidation, Advanced oxidation processes

Abstract: Contaminants of emerging concern (CECs) show great environmental concern due to their potential toxic effect and persistence. Developing and understanding novel water treatment approaches is essential to improve water quality and protect the environment. Processes based on light irradiation are very promising in this way. It is of high interest to evaluate the formation of potential photoproducts and their related toxicity. The aim of this project was to apply different approaches to study the photodegradation of contaminants. Firstly, a laboratory modeling approach was applied to five contaminants. Direct photolysis and advanced oxidation processes, such as peroxide/UV, photocatalysis, photosensitizers, and Fenton reactions, were employed. They were either carried out under laboratory conditions or on a pilot plant scale in secondary treated wastewater to study the matrix effect. As mineralization is rarely achieved, LC-MS measurements were performed for the untargeted detection of photoproducts on an ultra-high-resolution FT-ICR mass spectrometer. Structural elucidation of numerous photoprod-

ucts was achieved owing to MS² experiments. Based on these structures, in silico toxicity calculations were performed to obtain information on their potential toxic effects. Through this approach, the scientific achievements include assessing the fate of contaminants, proposing and optimizing viable photodegradation processes, and elucidating photochemical reaction pathways. In parallel with the modeling approach, a non-targeted analytical approach was used to study complex mixtures. To better process complex MS datafiles, the SPIX software was developed. One of its features includes comparing a series of conditions, proposing kinetic models for each of them individually. The exportation of statistically relevant changes and further data processing was carried out. The holistic approach provided by SPIX constitutes a complementary tool to modeling approaches; it allows to detect and monitor relevant reactions in very complex media and contributes to reducing operator subjectivity during results interpretation.